



Université
de Toulouse

THÈSE

En vue de l'obtention du

DOCTORAT DE L'UNIVERSITÉ DE TOULOUSE

Délivré par **l'Institut Supérieur de l'Aéronautique et de l'Espace**
Spécialité : Génie mécanique

Présentée et soutenue par **Amir SHAHDIN**
le 23 juillet 2009

Surveillance vibratoire de l'endommagement dû à l'impact sur poutres en matériaux composites stratifiés, sandwiches et matériaux enchevêtrés par variations des paramètres modaux

**Monitoring of impact damage in composite laminate,
honeycomb sandwich and entangled sandwich beams
by modal parameter shifts**

JURY

M. Ménad Sidahmed, président
M. Frédéric Bos, rapporteur
M. Paul Cranga
M. Olivier Dorvaux
M. Yves Gourinat, directeur de thèse
M. Joseph Morlier, co-directeur de thèse
M. Hui-Ji Shi, rapporteur

École doctorale : **Mécanique, énergétique, génie civil et procédés**

Unité de recherche : **Équipe d'accueil ISAE DMSM**

Directeur de thèse : **M. Yves Gourinat**
Co-directeur de thèse : **M. Joseph Morlier**

[This page intentionally left blank]

ACKNOWLEDGMENTS

There are many people I would like to recognize for their help and support with my research. Without them, I would not have been able to accomplish this milestone so quickly with such satisfying results. I would like to thank profoundly my two advisors Prof. **Yves Gourinat** and Associate Prof. **Joseph Morlier** as they always believed in my abilities and provided whatever advice and resources necessary for me to accomplish my goals. Both of them spent countless hours meeting with me to discuss aspects of my research and working revisions of my various publications. This work would not have been possible without their help.

While not officially a member of my thesis committee, Associate Professors Christophe Bouvet, Bruno Castanié and Frédéric Lachaud provided as much technical support as anyone else during the past few years, and added much more meaning to my work. A special thanks also for the research engineers Michel Labarrère, Dr. Samuel Rivallant, Dr. Guilhem Michon and Dr. Elias Abi Adallah for teaching me from scratch about impact and vibration test techniques.

Next, I would like to acknowledge everyone who provided technical support during the manufacturing and testing processes. Big thanks to Guy Mirabel and Xavier Foulquier for teaching me almost everything I know about composite manufacturing, and Marc Chartrou, Thierry Duigou, Charlie Gilard and Joel Xuereb for providing invaluable assistance with testing and machining throughout my thesis. A special thanks goes to Laurent Mezeix and Associate Prof. Christophe Bouvet for introducing me to the wonderful world of entangled materials and for helping me out in every aspect of that work. Special thanks again to Associate Professors Frédéric Lachaud and Christophe Bouvet, Dr. Elias Abi Adallah and Julien Simon from Samtech, who spent much of their free time assisting me with the finite element modeling part of my thesis. Special thanks also to Serge Crézé, head of the laboratory for always providing me with useful advice. Another round of thanks for Marc Chartrou for helping me with the French translations of my manuscript.

A special thanks goes to research project students J. B. Lecaillon, A. de Nazelle, P. Jakob and G. Plever from Saint-Cyr l’Ecole for their help during the fabrication and testing of specimens and H. Niemann from TU Braunschweig for his brilliant support for the Topology Optimization part.

Many co-workers contributed to this work by helping with research, analysis, writing and providing support. Thank you Victorien Belloeil, Damien Guillon, Pierre Selva, Thibault Gouache, Matthieu Bizeul, Bernhard Broll, Boris Chermann, Charbel Bouery, Issam Tawk, Javier Toral Vazquez, Leonardo Sanchez, Pablo Navarro, Usman Zabit, Ahmad Akhtar Hayat, Agha Mujtaba, Muhammad Ilyas, Majid Shehzad, Rizwan Shaad and all the other labmates and friends who have given me wonderful advice, inspiration and friendship over the years.

Lastly, I need to thank all my loving family in Pakistan and abroad —Dad, Mom and Afi — who have always given me their support. I love you all.

Table of Contents

1 Chapter 1 : Introduction and Literature Review of Structural Health Monitoring (SHM) in Composites	13
1.1 Introduction to Structural Health Monitoring	13
1.2 Structural Health Monitoring in Smart Materials and Structures (Composite Materials)	15
1.3 Vibration-based Damage Detection Methods	18
1.4 Damage in Composite Materials	20
1.5 Damage Detection in Composites due to Change in Modal Parameters.....	22
1.5.1 Damage Detection Methods based on Frequency Changes	22
1.5.2 Damage Detection Methods based on Damping Changes	25
1.5.3 Damage Detection Methods based on Mode Shape Changes	29
1.5.4 Damage Detection Methods based on Finite Element Model	30
1.5.5 Damage Detection Methods based on Topology Optimization	33
1.6 Innovation in Composite Structures	34
1.6.1 Enhancements in the Damping Characteristics	35
1.6.2 Enhancements in the Impact Toughness	37
1.7 Conclusion of the First Chapter.....	39
2 Chapter 2: Analytical and Experimental Modal Analysis.....	40
2.1 System Identification.....	42
2.2 Single Degree of Freedom System.....	47
2.2.1 Basic Theory.....	47
2.2.2 Laplace Domain Theory	48
2.2.3 Analytical Models and Different Representations	50
2.2.4 Change of Physical Parameters	56
2.3 Experimental Modal Analysis	57
2.3.1 Types of Experimental Modal Testing	58
2.3.2 Types of Excitation Signals.....	60
2.3.3 Modal Parameter Estimation (Curve Fitting)	63
2.3.4 Correlation Tools.....	68
2.3.5 Sources of Lack of Precision in Modal Testing	71
2.3.6 Shaker Test Flow Diagram.....	71
2.4 Analytical Calculation of the FRF of a Free-Free Beam Excited at its Centre	72
2.5 Tracking of Poles for Damage Detection	75
2.6 Conclusion of the Second Chapter	77
3 Chapter 3 : Monitoring of Impact Damage in Composite Laminates by Shift in Modal Parameters	78
3.1 Theory of Laminated Composites	78
3.1.1 Nomenclature and General Composition	78
3.1.2 Modeling of Composite Properties and Behavior by Constitutive Laws	80
3.1.3 Material and Types of Composite Laminate Beams	81
3.2 Experimental Techniques	82
3.2.1 Vibration Tests	82
3.2.2 Impact Tests	85
3.3 Monitoring of Impact Damage for Composite Beams Clamped at Two Ends when Impacted.....	87

3.3.1	Significance of End Masses	87
3.3.2	Frequency and Damping Changes.....	87
3.3.3	Damage Index Variations.....	90
3.3.4	Comparison of Damping Ratio and Integral of the Resonance Peaks	91
3.3.5	Design of Experiments	92
3.4	Monitoring of Impact Damage for Composite Beams Clamped at all Four Ends when Impacted	94
3.4.1	Frequency and Damping Changes.....	94
3.4.2	Design of Experiments (DOE)	97
3.5	Conclusion of the Third Chapter	99

4 Chapter 4 : Study of Two Different Types of Damage in Honeycomb Sandwich Beams by Shift in Modal Parameters 100

4.1	Introduction to Sandwich Structures	100
4.1.1	Design Principle	100
4.1.2	Advantages and Disadvantages	102
4.1.3	Modes of Failure	102
4.2	Damage Monitoring in Honeycomb Sandwich Beams by Modal Parameter Shifts	104
4.2.1	Materials and Types of Honeycomb Sandwich Beams.....	104
4.2.2	Experimental Techniques	105
4.2.3	Significance of End-Masses	108
4.2.4	Estimation of Modal Parameters at the Undamaged State (UD).....	110
4.2.5	Effect of Impact Damage on Modal Parameters	110
4.2.6	Effect of Core-Only damage on Modal Parameters	113
4.2.7	Effect of Sine-Dwell Frequency Direction on Modal Parameters.....	116
4.2.8	Design of Experiments (DOE)	117
4.3	Conclusion of the Fourth Chapter	119

5 Chapter 5 : Static-Dynamic Characterization and Monitoring of Impact Damage in Entangled Sandwich Beams by Shift in Modal Parameters 121

5.1	Long Carbon Fiber Entangled Sandwich Beams by	121
5.1.1	Materials and Fabrication Procedure.....	121
5.1.2	Static Characterization of Long Carbon Entangled Sandwich Beams	124
5.1.3	Dynamic Characterization of Long Carbon Entangled Sandwich Beams	128
5.1.4	Impact Parameters of Carbon Entangled Sandwich Beams	130
5.1.5	Monitoring of Impact Damage in Long Carbon Entangled Sandwich Beams through Frequency and Damping Changes.....	132
5.1.6	Drawbacks of the Study on Long Carbon Fiber Entangled Sandwiches and Proposed Modifications	136
5.2	Damage Monitoring in Short Entangled Sandwich Beams by Modal Parameter Shifts	137
5.2.1	Materials and Fabrication Procedure.....	137
5.2.2	Static Characterization of Glass Sandwich Beams.....	139
5.2.3	Dynamic Characterization of Glass Sandwich Beams	143
5.2.4	Impact Parameters of Small Carbon and Glass Sandwich Beams	147
5.2.5	Monitoring of Impact Damage and the Evaluation of the Impact Toughness of Small Carbon and Glass Sandwich Beams through Frequency and Damping Changes .	149
5.2.6	Effect of Sine-Dwell Frequency Direction on Modal Parameters.....	155
5.2.7	Design of Experiments	157

5.3	Conclusion of the Fifth Chapter	159
6	Chapter 6 : Updating and Damage Detection in Composite Beams using Finite Element Analysis	161
6.1	Calculation of the Dynamic Response and Updating by Finite Element Methods	161
6.1.1	Dynamic Response Calculation by Finite Elements	161
6.1.2	Updating of the FE models for Experimental/Numerical Correlation	165
6.1.3	Updating Procedure on Composite Laminate Beams Impacted by Clamping Two Ends	172
6.1.4	Evaluation of the Degradation Factor with Impact Energy in Composite Laminate Beams Impacted by Clamping Two Ends	178
6.1.5	Updating Procedure on Composite Laminate Beams Impacted by Clamping all Four Ends	179
6.1.6	Evaluation of the Degradation Factor with Impact Energy in Composite Laminate Beams Impacted by Clamping all Four Ends	182
6.1.7	Updating Procedure on Long Honeycomb Sandwich Beams	183
6.1.8	Updating of Long Carbon Entangled Sandwich Beams.....	188
6.2	Damage Localization by Topology Optimization	191
6.2.1	Optimization Problem Formulation for damage Localization	191
6.2.2	Experimental Validation of Topology Optimization in Composites.....	197
6.3	Conclusion of the Sixth Chapter	199
7	Chapter 7 : Conclusion and Future Work	202
7.1	Overall Conclusion.....	202
7.2	Overall Comparison	208
7.3	Future Works and Perspectives	209
	Annex for Chapter 3.....	211
	Annex for Chapter 6.....	213
	References	227

General Introduction

The process of implementing a damage detection strategy for engineering structure is referred to as Structural Health Monitoring (SHM). The purpose of structural health monitoring systems is to provide information about the condition of a structure in terms of reliability and safety before the damage threatens the integrity of the structure. The improvement of safety seems to be a strong motivation, in particular after some spectacular accidents due to: i) unsatisfactory maintenance, for example, in the aeronautic field, the accident of Aloha Airlines (see Fig 1a) or, in the civil engineering field, the collapse of the Mianus River bridge; ii) ill-controlled manufacturing process, for example, the Injak bridge collapse (see Fig 1b).



Figure 1 Spectacular accidents have motivated the community to improve safety: a) the Aloha Airlines flight 243, April 29, 1988, due to corrosion insufficiently controlled by maintenance; b) the Injaka bridge collapse, July 1998, due to a poorly controlled construction process

So the diagnosis of the damage in structural systems requires an identification of the location and type of damage, as well as the quantification of the degree of damage. The SHM process involves the observation of a system over time using periodically sampled response

measurements from an array of sensors. The extraction of damage sensitive features from these measurements and the statistical analysis of these features are then used to determine the current state of system health. SHM essentially involves the embedding of a Non-Destructive Evaluation (NDE) into a structure to allow continuous remote monitoring for damage. There are several advantages to using a SHM system over traditional inspection cycles, such as reduced down time, elimination of component tear down inspections and the potential prevention of failure during operation. Structural health monitoring is a very vast domain and consists of five major steps:

- detection of damage in a structure
- localization of damage
- classification of the damage type
- quantification of damage severity
- prediction of the remaining service life of the structure

Due to the vastness of this subject, it is very difficult in a thesis to work on all the above mentioned five aspects. The scope of the work presented in this thesis concerns the first two steps of SHM i.e., detection and localization of damage. However we can approximately quantify and classify damage with equivalent stiffness changes by updating a damage model.

The thesis presents an experimental study coupled with finite element analysis on the effects of multi-site damage on the vibration response of laminated composite and composite sandwich beams. Vibrational modal analysis has been chosen as the non-destructive technique for detecting damage in the beam-type specimens. Vibration tests have been carried out by using burst random (broadband excitation) and sine dwell (single frequency excitation) excitations. The various types of test specimens have been impacted around the *Barely Visible Impact Damage* (BVID) limit by drop weight tests. The effectiveness of vibration-based damage detection is in case of those damages not visible by naked eye but reduce significantly the stiffness of the structure. The variation of modal parameters i.e., natural frequency, damping and mode shapes in the presence of impact damage is then studied.

The aim is to find that which of the parameters among natural frequency and damping ratios are more sensitive to impact damage in composite laminates and composite sandwich beams. The effect of mode shapes on impact damage is not studied as we have carried out vibration tests with a poor spatial resolution; our aim is to extract relatively reliable mode shapes for the purpose of identification of the type of mode i.e., bending mode or torsion mode. Based on this information damage detection algorithms shall be built in future to monitor damage in composite specimens. Furthermore, statistical analysis based on design of experiments is performed on the experimentally obtained modal parameters to find out the most significant design parameters. In the course of this thesis, an innovative sandwich known as entangled sandwich material has also been developed. The dynamic performance and impact toughness of entangled sandwich beams is evaluated and compared with standard sandwiches with honeycomb and foam cores. Finally finite element models are built to simulate the vibration tests in order to correlate the experimental results numerically. Impact damage in composite laminates and composite sandwiches is modeled by reducing the mechanical properties at the impacted zones, based on c-scan and radiography results.

Objectives of the Thesis

The main objectives of the presented thesis are

- Detection of low velocity impact damage in composite laminate and composite sandwich beams with the help of modal analysis which serves the purpose of a non-destructive technique for damage detection by taking into account a reliable baseline FE model
- Inducing damage in the test-beams by drop weight tests around the barely visible impact damage (BVID) so those damage that cannot be detected through visual inspection are made detectable by vibration testing
- Study the shift in modal parameters (natural frequency and damping) in the presence of impact damage, by studying several levels of damage
- Highlight the most sensitive modal parameter to impact damage among natural frequency and damping ratio in composite laminates and composite sandwich beams which shall help in future to built damage detection algorithms to monitor damage in composites
- Find the design parameter (for example impact energy and density of damage) that has the most significant effect on the experimentally obtained natural frequencies and damping ratios based on design of experiments
- Develop a new sandwich known as entangled sandwich material with an aim to enhance the damping capabilities and impact toughness of composite sandwich structures
- Perform vibration tests on sandwich beams with both broadband (burst random) and single frequency (sine-dwell) based testing to evaluate their effectiveness in the estimation of damping in the presence of damage
- Develop a Finite Element models that represent damaged composite beams in vibrations. These simplified damage models give us a degradation factor that can serve as a warning regarding structure safety
- Localize structural damage in composite beams by topology optimization

Based on the works of this thesis, the author has so far succeeded in publishing the following works:

International peer-reviewed journals (accepted):

- Shahdin A, Morlier J, Gourinat Y. Correlating low energy impact damage with changes in modal parameters: A preliminary study on composite beams. **Structural Health Monitoring** 2009, doi:10.1177/1475921709341007.

- Shahdin A, Mezeix L, Bouvet C, Morlier J, Gourinat Y. Fabrication and mechanical testing of a new sandwich structure with carbon fiber network core. **Journal of Sandwich Structures and Materials** 2009, doi: 10.1177/1099636208106070.
- Shahdin A, Mezeix L, Bouvet C, Morlier J, Gourinat Y. Fabrication and mechanical testing of glass fiber entangled sandwich beams: A comparison with honeycomb and foam sandwich beams. **Composite Structures** 2009;90(4):404-412.
- Shahdin A, Mezeix L, Bouvet C, Morlier J, Gourinat Y. Monitoring the effects of impact damages in carbon fiber entangled sandwich beams. **Engineering Structures** 2009, doi:10.1016/j.engstruct.2009.07.008.

International peer-reviewed journals (submitted):

- Shahdin A, Morlier J, Gourinat Y. Damage monitoring in sandwich beams by modal parameter shifts: A comparative study of burst random and sine-dwell testing. Submitted February 2009 in **Journal of Sound and Vibration**.
- Niemann H, Morlier J, Shahdin A, Gourinat Y. Damage Localization using Experimental Modal Parameters and Topology Optimization. Submitted July 2009 to **Mechanical Systems and Signal Processing**.

International conferences with proceedings:

- Shahdin A, Morlier J, Gourinat Y. Significance of low energy impact damage on modal parameters of composite beams by design of experiments. Open access on-line Journal of Physics Conference Series (MPSVA 2009, London).
- Shahdin A, Mezeix L, Bouvet C, Morlier J, Gourinat Y. Diagnosis of the fabrication process of a sandwich structure with fiber network core by vibration testing (Composites 2009, London).
- Shahdin A, Mezeix L, Bouvet C, Morlier J, Gourinat Y. Static and dynamic testing of glass fiber entangled sandwich beams: a comparison with honeycomb and foam sandwich beams (ICCS 15 Porto).

Significance of the Research Work

This thesis which correlates impact damage with modal parameters in composite laminates and composite sandwich materials has several interesting and novel aspects that are discussed separately below:

- The vibration tests have been performed by attaching steel masses at the ends of the composite beams in order to enhance the modal parameter shifts between the undamaged and the damaged test specimens.
- A novel damage detection tool known as Damage Index is introduced to study the changes in the modal parameters before and after impact. Damage index is based on the integral of the amplitudes of the frequency response functions (FRF) and therefore

estimates the phenomenon of dissipation in the test specimens. Therefore the aim of the damage index is to verify the damping ratio results estimated by the curve-fitting algorithms. As damping is a parameter difficult to estimate, so damage index gives us an additional tool for understanding the damping behavior of damaged composite beams.

- Vibration tests have been carried out with both burst random and sine dwell testing in order to find out that which of testing method gives a better estimation of damping in the presence of damage.
- Sine dwell testing which takes into account the effects of non-linearity unlike broadband excitation based testing, is done in both upwards and downwards frequency directions in order to detect structural non-linearities due to accumulation of damage in the test beams.
- A novel method using topology optimization design is used to localize damage in the composite laminate test beams. The aim is to verify numerically the c-scan results on the beams. Material is removed in the precise zones of the FE model in order to minimize the error between the experimental and numerical frequency response functions (FRFs), this way an equivalent damage is modeled. Thus topology optimization is a diagnostic tool (for all types of materials) and requires only the undamaged state for localization of damages.

Organization of the Thesis

The presented thesis is organized in six chapters.

The **first chapter** gives a brief introduction about the ever growing field of structural health monitoring emphasizing on the vibration-based damage detection methods to monitor the health of a structure. A comprehensive literature review is provided on the experimental and numerical damage detection methods based on modal parameter shifts. Damage in composites along with innovations concerning damping enhancement and impact toughness are also highlighted.

The **second chapter** gives the basics of mechanical vibrations focusing on the flexural vibration of beams. Damping and its measurement methods are discussed. Theoretical background on experimental modal analysis is the main emphasis of this chapter. Types of excitations, types of test set-ups for vibration testing and types of estimation methods are highlighted as well. Finally correlation tools are discussed used for updating a numerical model with respect to experimental results.

In the **third chapter**, vibration tests are carried out on damaged and undamaged laminate composite beams in order to study the effects of impact damage through shifts in modal parameters. The composite beams have been impacted by choosing two different boundary conditions i.e., by clamping them at two ends and by clamping them at all four ends, by keeping in view the BVID limit. Design of experiments is also carried out on the calculated natural frequencies to highlight the actor having the most significant effect on the modal parameters.

The **fourth chapter** deals with the monitoring of two different types of damages i.e., impact damage and core-only damage, in honeycomb sandwich beams with the help of modal parameters shifts.

The **fifth chapter** concerns a relatively new sandwich material known as entangled sandwich material. As this material is a newer one, so first of all static and dynamic characterization of entangled sandwich materials is performed, followed by monitoring of impact damage. Their mechanical behavior and impact toughness (uniquely based on decrease in natural frequency) is compared with standard sandwiches with honeycomb and foam cores. Design of experiments is also carried out to validate and further clarify the experimental results.

The **sixth chapter** deal with the Finite Element based updating and damage detection and is grouped in two parts. In the first part, FE models are developed that represent damaged composite beams in vibrations. The numerical results are compared with those obtained experimentally (Chapters 3 and 4) on the same beams. Updating is performed on the damaged zone in the FE models by reducing the material properties in order to improve the experimental/numerical correlation of the frequency response functions. These simplified damage models give us a degradation factor that can serve as a warning regarding structure safety. In the second part, a damage localization tool based on topology optimization is developed in order to locate damage accurately in composite laminate beams in order to correlate with the C-Scan results.

In the **seventh and last chapter**, an overall conclusion of the thesis is provided along with the propositions for the future work.

Chapter 1 : Introduction and Literature Review of Structural Health Monitoring (SHM) in Composites

1.1 Introduction to Structural Health Monitoring

Structural Health Monitoring (SHM) aims to give, at every moment during the life of a structure, a diagnosis of the “state” of the constituent materials, of the different parts, and of the full assembly of these parts constituting the structure as a whole. The state of the structure must remain in the domain specified in the design, although this can be altered by normal aging due to usage, by the action of the environment, and by accidental events. Thanks to the time-dimension of monitoring, which makes it possible to consider the full history database of the structure, and with the help of Usage Monitoring, it can also provide a prognosis (evolution of damage, residual life, etc.).

If we consider only the first function, the diagnosis, we could estimate that Structural Health Monitoring is a new and improved way to make a Non-Destructive Evaluation. This is partially true, but SHM is much more. It involves the integration of sensors, possibly smart materials, data transmission, computational power, and processing ability inside the structures. It makes it possible to reconsider the design of the structure and the full management of the structure itself and of the structure considered as a part of wider systems. This is schematically presented in Fig 1.1.

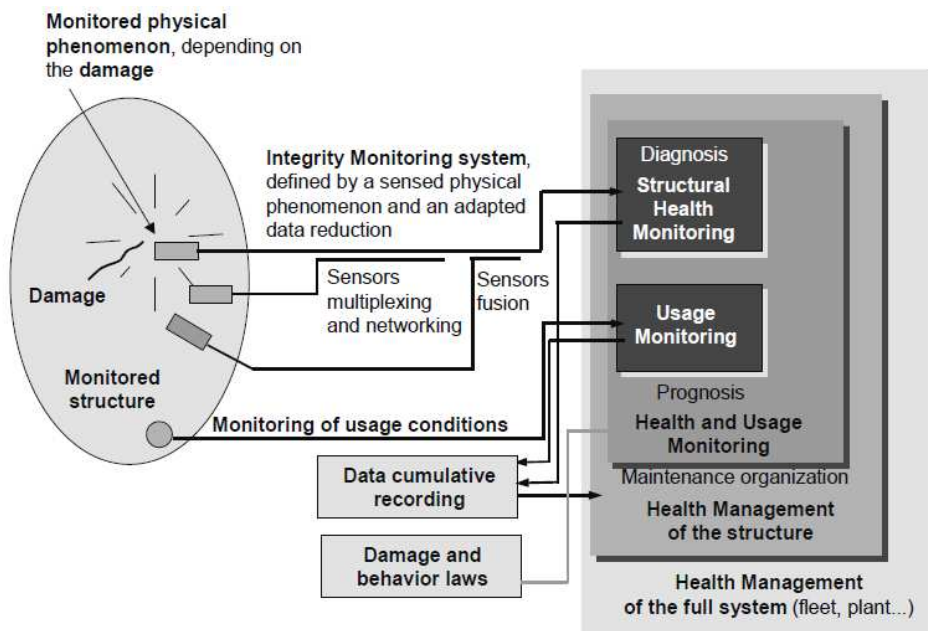


Figure 1.1 Principle and organization of a SHM system

In Figure 1.1, the organization of a typical SHM system is given in detail. The first part of the system, which corresponds to the structural integrity monitoring function, can be defined by:

- the type of physical phenomenon, closely related to the damage, which is monitored by the sensor
- the type of physical phenomenon that is used by the sensor to produce a signal (generally electric) sent to the acquisition and storage sub-system

Several sensors of the same type, constituting a network, can be multiplexed and their data merged with those from other types of sensors. Possibly, other sensors, monitoring the environmental conditions, make it possible to perform the usage monitoring function. The signal delivered by the integrity monitoring sub-system, in parallel with the previously registered data, is used by the controller to create a diagnostic.

Mixing the information of the integrity monitoring sub-system with that of the usage monitoring sub-system and with the knowledge based on damage mechanics and behavior laws makes it possible to determine the prognosis (residual life) and the health management of the structure (organization of maintenance, repair operations, etc.).

Finally, similar structure management systems related to other structures which constitute a type of super system (a fleet of aircraft, a group of power stations, etc.) make possible the health management of the super system. Of course, workable systems can be set up even if they are not as comprehensive as described here.

According to Farrar and Worden [1] and many other researchers too, structural damage detection can be divided into five levels:

1. detection of damage existence in a structure (Is damage present ?)
2. localization of damage (Where is the damage ?)
3. classification of the damage type (What kind of damage is this ?)
4. quantification of damage severity (How much damage has occurred ?)
5. prediction of the remaining service life of the structure (When will damage occur) ?

The “holy grail” of SHM may be thought of as the fifth level in the hierarchy, that of damage prognosis. There is a very limited amount of scientific literature available in this field. Damage prognosis is defined as the estimate of an engineered system’s remaining useful life [2]. This estimate is based on the output of models that develop behavioral predictions: by coupling information from usage monitoring; SHM; past, current and anticipated future environmental and operational conditions; the original design assumptions regarding loading and operational environments; and previous component and system level testing and maintenance. Also, ‘softer’ information such as user ‘feel’ for how the system is responding will be used to the greatest extent possible when developing damage prognosis solutions. In other words, damage prognosis attempts to forecast system performance by measuring the current state of the system (i.e. SHM), estimating the future loading environments for that system, and then predicting through simulation and past experience the remaining useful life of the system. It is important therefore to distinguish between usage monitoring and health monitoring.

Knowing the integrity of in-service structures on a continuous real-time basis is a very important objective for manufacturers, end-users and maintenance teams. In effect, SHM:

- allows an optimal use of the structure, a minimized downtime, and the avoidance of catastrophic failures
- gives the constructor an improvement in his products
- drastically changes the work organization of maintenance services

The economic motivation is stronger, principally for end-users. In effect, for structures with SHM systems, the envisaged benefits are constant maintenance costs and reliability, instead of increasing maintenance costs and decreasing reliability for classical structures without SHM as seen in Fig 1.2.

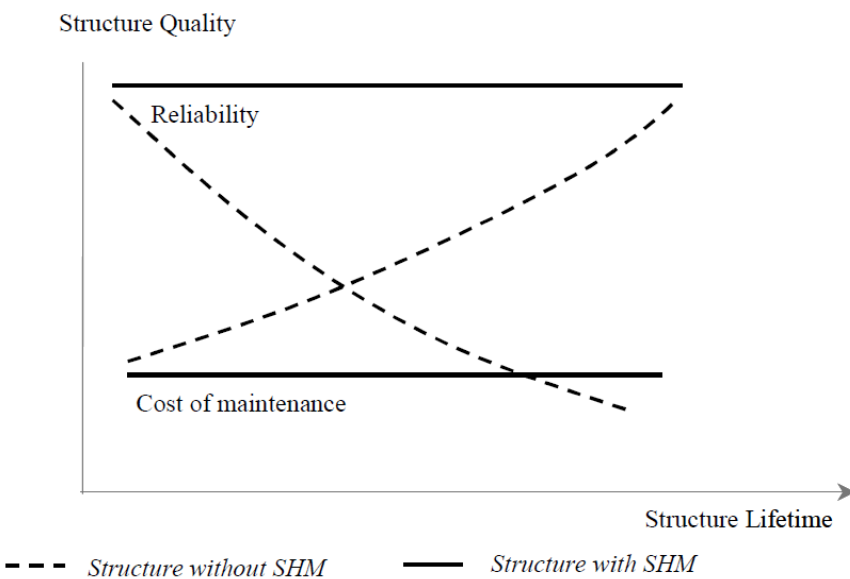


Figure 1.2 Benefit of SHM for end-users

1.2 Structural Health Monitoring in Smart Materials and Structures (Composite Materials)

Since the end of the 1980s, the concept of smart or intelligent materials and structures has become more and more present in the minds of engineers. These new ideas were particularly welcome in the fields of aerospace and civil engineering. In fact, the concept is presently one of the driving forces for innovation in all domains. The concept of Smart Materials/Structures (SMS) can be considered as a step in the general evolution of man-made objects as shown in Fig 1.3. There is a continuous trend from simple to complex in human production, starting from the use of homogeneous materials, supplied by nature and accepted with their natural properties, followed by multi-materials (in particular, composite materials) allowing us to create structures with properties adapted to specific uses. In fact, composite materials and multi-materials are replacing homogeneous materials in more and more structures. This is particularly true in the aeronautic domain.

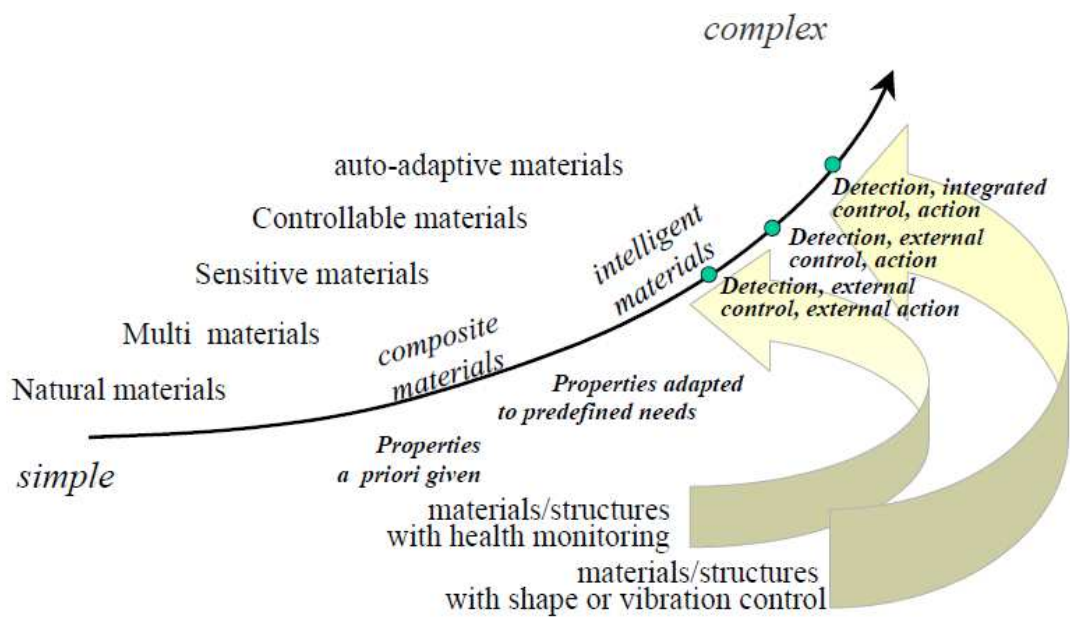


Figure 1.3 General evolution of materials/structures used by people, and the place of smart structures, including structures with SHM

For instance, composite parts are now currently used or envisaged for modern aircraft (see for instance in Fig 1.4, Boeing's 787 Dream-liner project, which has 50% of its structures made of composites). It is worth noting that this aircraft is the first one in which it is clearly planned to embed SHM systems, in particular systems for impact detection.

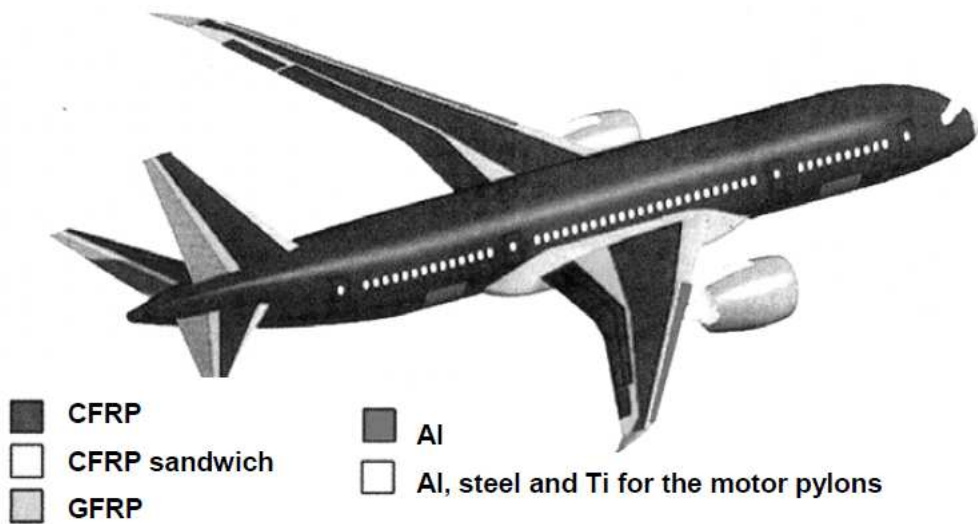


Figure 1.4 Example of the increasing importance of composites in civil aircraft: the 787 Dream-liner has 50% of its structure made of composites. For this aircraft, impact detection monitoring systems are envisaged for outer panels

The aim of using composites is to increase the stiffness and specific strength and to reduce the weight so it is advantageous to employ them in aerospace applications where the challenge is

to produce structures lighter and lighter. Safe and functional effectiveness of stressed composite structures can often depend on the retention of integrity of each of the different materials used in its manufacture. However damage in these structures may negate many of the benefits of sandwich construction. These materials are very different from metals with respect to their particular failure modes.

- composite laminates are susceptible to damage from a wide variety of sources which include fabrication stress, environmental cyclic loading, handling damage and foreign object impact damage. This may lead to the severe degradation of the mechanical behavior of structures due to loss of structural integrity.
- composite sandwiches are also prone to various types of damages. The face-sheets can be damaged through delamination and fiber breakage; the face-sheet and core interface region can be debonded and the core can be damaged through crushing and shear failure mechanisms.

Due to the complex nature of the composition of composites and composite sandwich materials, the damage is sometimes not visually apparent on the surface which is found to be quite detrimental to the load bearing capacities of sandwich structures underscoring the need for reliable damage detection techniques for composite structures. This is where structural health monitoring (SHM) comes into play. Usually damage introduces non-linearity in structures. The sources of non-linearity can be categorized as follows:

- material (small scale)
- geometric or constraint (medium and large scale)
- connectivity (all scales)
- damage inception and evolution (all scales)

In the scope of structural health monitoring (SHM), non-linearity can be exploited as follows:

- detection / characterization of non-linearity
- interrogation with non-linearity
- control / mitigation of non-linearity

At present, using non-destructive examination (NDE) method to detect damage status of engineering structures has become a hotspot and difficult issue. Recently, NDE technique is widely applied in industries, such as aeronautics aviation, space vehicle, power plant equipment, architecture, metallurgy and mechanical manufacture, etc. Generally, structural damage detection can be classified as local-damage detection [3] and global-damage detection.

Local-damage detection techniques refer to non-destructive testing (NDT) as CT scanning and ultrasonic, etc., because it is mainly used to detect local damage in structures, and it can determine damage existence and its location. Local damage detection methods utilize only data obtained from the damaged structure. Baseline data and theoretical models of the

undamaged structure are not used. These are the main advantages of local damage detection. For small and regular structures, such as pressure vessels, local damage detection is very effective. However, for the large and complicated structures in invisible or closed environments, it is very difficult to detect damage using local damage detection method. The engineers have to make on-site structural damage detection. Therefore, local damage detection methodology can only be used to detect some special components of a structure.

In order to detect damage throughout the whole structure, especially some large, complicated structures, a methodology called global vibration-based structural damage detection has been proposed.

1.3 Vibration-based Damage Detection Methods

In recent years, structural health monitoring (SHM) using vibration based damage detection has been rapidly expanding and has shown to be a feasible approach for detecting and locating damage. One way of damage detection is with the help of vibration testing, as the presence of damage effect the vibration characteristics of a structure (e.g., natural frequency, damping ratio and mode shape). The main idea behind this technique is that modal parameters i.e., frequencies, damping ratios and mode shapes change in a detectable manner due to loss of stiffness and mass. Comprehensive reviews on vibration-based damage detection methods have been presented by Zou et al. [4] on the model-dependent delamination identification methods for composite structures, and by Yan et al. [5], Doebling et al. [6], Sohn et al. [7] and Carden et al. [8] on general vibration-based damage detection methods.

The basic principle of vibration based damage detection can be explained as follows. Any structure can be considered as a dynamic system with stiffness, mass and damping. Once some damages emerge in the structures, the structural parameters will change, and the frequency response functions and modal parameters of the structural system will also change. This change of modal parameters can be taken as the signal of early damage occurrence in the structural system. Although vibration-based structural damage detection is a newly emergent research topic, its development can still be divided into traditional- and modern- type.

The traditional-type refers to detection method for structural damage by using only the structural characteristics, such as natural frequencies, modal damping, mode shapes, etc. These methods are among the earliest and most common, principally because they are simple to implement on any size structure. Structures can be excited by ambient energy, an external shaker or embedded actuators. Accelerometers and laser vibrometers can be used to monitor the structural dynamic responses. A variety of broadband excitation signals have been developed for making shaker measurements with FFT analyzers e.g., burst random, burst chirp etc. Since the FFT provides a spectrum over a broadband of frequencies, using a broadband excitation signal makes the measurement of broadband spectral measurements much faster than using sine dwell or swept sine excitations [9]. Despite the fact that sine dwell or swept sine modal testing requires large acquisition times, but they have the capability of detecting non linear structural dynamic behavior unlike the broadband excitations [10].

However, traditional-type methods generally require experimental modal analysis or transfer function measure, and this is very not convenient for online detection of structures in service because these experimental measures often need multifarious instrument or manual operation. They have three obvious disadvantages:

- they tend to depend more on experiments, especially the measurement of mode shape and damping. Thus, it is time-consuming and expensive, and these factors will not be adaptive to online damage detection for servicing structures
- when using traditional-type method to detect the location of structural damage, it is difficult to establish a universal methodology for various structures, and is more dependant on the properties of individual structures to be detected
- the traditional-type method is generally not sensitive to initial tiny damage in structures

The basics of traditional-type vibration based methods are illustrated in Fig 1.5.

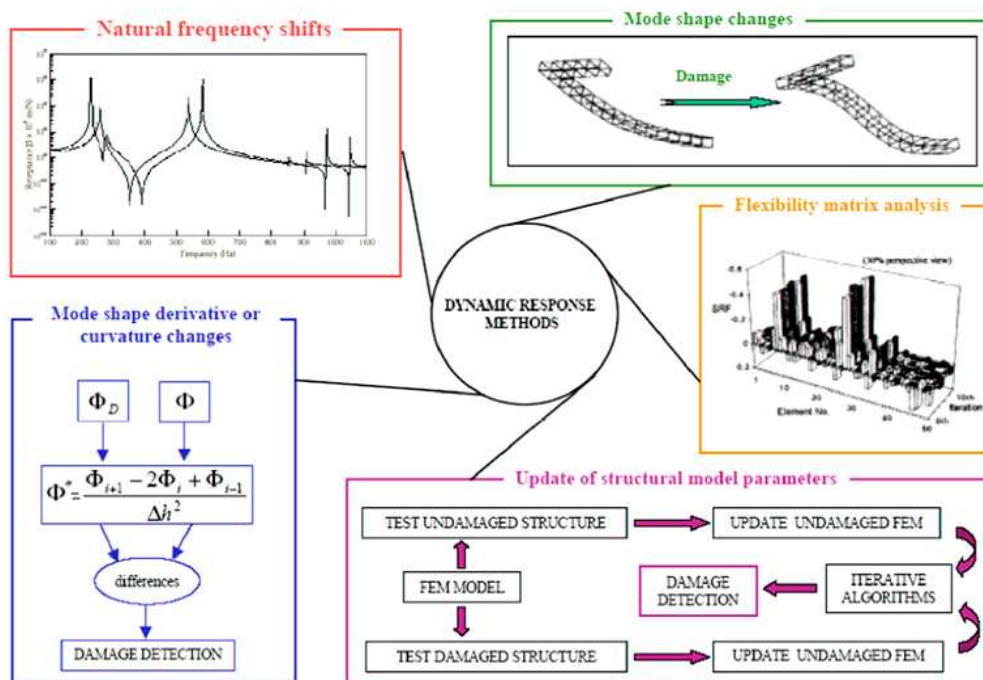


Figure 1.5 Methodology of traditional-type damage detection methods based on natural frequency shifts, mode shape changes, curvature changes along with update procedure of modal parameters

Several modern techniques e.g., statistical process control, neural networks, advanced signal processing, genetic algorithm, wavelet analysis etc., have been researched for detecting damage in composite materials, many of them showing the effectiveness of dynamic response measurements in monitoring the health of engineering structures [11-21]. These methods are generally classified as modern-type methods for damage detection. Of course, there are still several problems to be investigated and solved in the modern-type method, such as:

- this method has to rely on the environment excitation to the structures to be detected
- the measured signals are possibly contaminated by noise so that information from tiny damage in structures may be covered by the noise
- the selection and construction of the feature index of structural damage are very flexible and variable

The basic problems for structural damage detection are how to ascertain emergence, location and severity of structural damage using the given measured structural dynamic responses. In order to detect structural damage from structural dynamic response signals, the first problem is to select damage feature index to be constructed. The physical variable used to identify damage may be a global one, but the physical variable used to determine damage location is better to be a local one, and it should meet the following two requirements [23]:

- the variable must be sensitive to structural local-damage
- the variable must be monotone function of the location coordinate

Generally, determination of structural damage location is equivalent to determining a region, where the structural stiffness and loading capacity decreases using a measurable quantity. The key factor of vibration based damage detection is to establish the calculation model and to estimate the vibration parameter to be measured. Especially, the selection and sensitivity of the structural damage feature index will affect the final results and accuracy of structural damage detection [24].

1.4 Damage in Composite Materials

The use of composites and composite sandwich materials in structural components has increased dramatically in recent years by offering enormous potential and benefits to the aerospace industry and many other sectors. This is due to their specific properties like superior bending stiffness, low weight, excellent thermal insulation, acoustic damping, ease of machining, ease of forming, etc. An excellent over on composite materials and their applications has been provided by Gay and Hua [125]. There has been considerable research on the impact performance and damage development in carbon fiber composite materials and sandwich composite materials; see for example references [25-29]. As the composite materials are fabricated from different type of materials having different fiber orientations, therefore different type of damages and defect can be identified. The classification of these damages can be found in the scientific literature [30-32]. The damages are generally classified in two major types

- Damage due to fabrication
- In-service damages

Damages due to fabrication are due to porosity, micro-cracks, cutting of edges, surface scratches, external contaminations etc. The reasons of these damages can be machining problems, use of bad tools, dropping of tools during fabrication etc. In-service damages in composites are due to fatigue, environmental effects and impacts. The different types of impact damages classified by their appearance on the surface

- Surface damages e.g., scratches (Fig 1.6 a)
- Deep delamination followed by fissuration of matrix and rupture of fibers that can have a very considerable length that can be visually detected on the surface length (Fig 1.6 b-c-d)

- Damage penetrating the thickness e.g., fissures with and without delamination (Fig 1.6e) and holes containing delamination and different fissures on the edges (Fig 1.6 f)

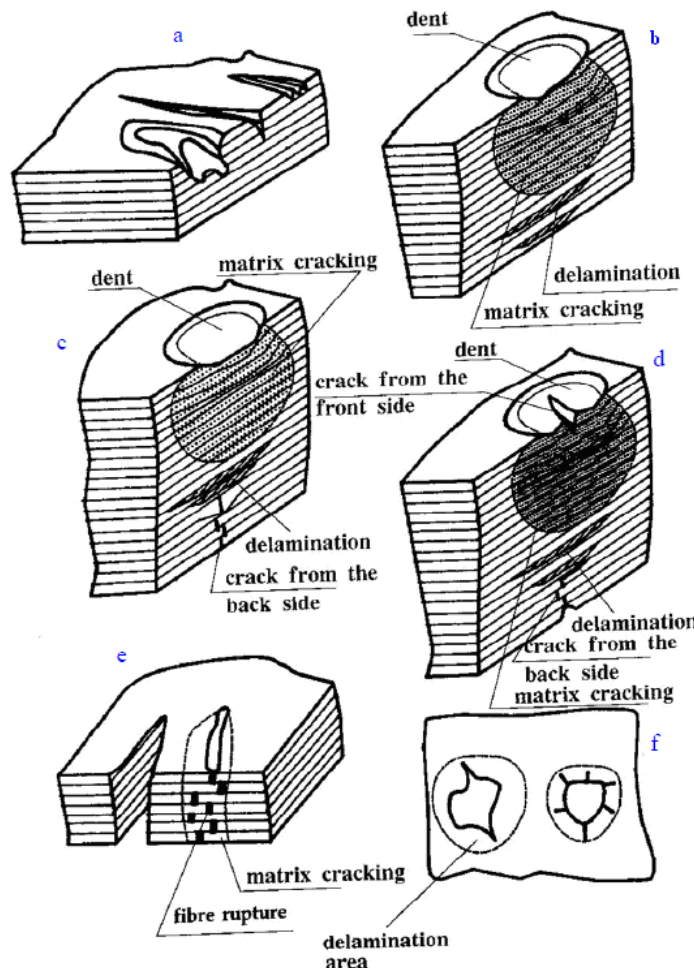


Figure 1.6 Classification of impact damage in composite materials (a) Surface Damages (b,c,d) Deep delamination followed by fissuration of matrix and rupture of fibers (e,f) holes with and without delamination [32]

For aeronautical structures, a field where this problem has been quite studied, the components have to undergo (i) low energy impacts caused by dropped tools or mishandling during assembly and maintenance, (ii) medium energy impacts caused in-service by foreign objects such as stones or birds, and (iii) in military aircraft, high energy impacts caused by weaponry projectiles. In a low energy impact (but high enough to produce damage), only a very small indentation will be seen on the impact surface. This level of damage is often referred to as barely visible impact damage (BVID).

BVID corresponds to the formation of an indentation on the surface of the structure that can be detected by detailed visual inspection and can lead to high damage. In the aeronautical domain, BVID corresponds to an indentation of 0.3 mm after relaxation, aging etc (according to Airbus certifications). In this study, it is decided to take 0.6-0.8 mm of penetration depth as detectability criterion just after the impact [27,33]. All the test specimens in this thesis have been damaged by drop weight impacts around the BVID limit.

Lastly, we shall put in evidence the different mechanisms of damage in composites due to impact. But first of all a brief synopsis of the different impact test methods present in scientific literature is given. The impact test techniques are divided in two parts depending upon the impact velocity.

- Low velocity impacts ($V \leq 10\text{m/s}$) that can be due to dropping of tools can be carried out by drop weight tests [27,33]
- Medium and high velocity impacts ($V \geq 10\text{m/s}$) that can be due to bird and ice impact etc, can be carried out by a Hopkinson bar or an impact gun [29].

Due to impact generally matrix breaks firsts creating micro-cracks in the structure followed by delamination between the plies. The different damage mechanisms in composites are explained in detail by Arbate [29], and are classified as

- Fissuration of matrix : includes the breakage fiber/matrix that appears parallel to the fibers as a result of traction, compression and shear
- Delamination : appears at the interfaces due to inter-laminar shear (Fig 1.6 b,c,d)
- Rupture of fibers: it occurs in traction, it is the standard rupture, or in compression which is due to buckling (Fig 1.6 e)

1.5 Damage Detection in Composites due to Change in Modal Parameters

The need to be able to detect damage in complex structures like composites has led to the development of a vast range of techniques, of which many are based upon structural vibration analysis. The presence of fissuration, delamination or rupture of fibers affects the vibration characteristics of a structure e.g., natural frequency, damping ratio and mode shape. There is an abundance of works in scientific literature that is related to damage detection through changes in modal parameters of composite structures, notably works of Kessler et al. [34], Della and Shu [35] and Yam et al. [36] give a detailed overview on the recent developments occurring in this subject. In addition, Montalvao et al. [37] reviewed the latest advances in structural health monitoring and damage detection with an emphasis on composite structures on the grounds that this class of materials currently has a wide range of engineering applications. The damage detection methods based on natural frequency, damping, mode shapes along with finite element and updating approaches are discussed separately below. Generally for diagnostic and monitoring purposes, we often need a reference, a base-line model. Therefore in this thesis, identification of damage is carried out by using the undamaged models (baseline models) for all the test-beams.

1.5.1 Damage Detection Methods based on Frequency Changes

Scientific literature is replete with damage detection methods based on natural frequency changes. A few of these references in relation with this thesis are explained briefly as follows:

Adams and Cawley [38] described a method of non-destructively assessing the integrity of structures using measurements of the structural natural frequencies. Experiments were carried

out on an aluminum plate and a cross-ply carbon-fiber-reinforced plastic plate. It was shown that how measurements made at a single point in the structure can be used to detect and locate damage. Results show an excellent agreement between the predicted and actual damage sites and a useful indication of the magnitude of the defect is obtained.

Kim and Hwang [39] studied the behavior of natural frequencies of honeycomb sandwich beams having debonding or delamination embedded between the face-layer laminates and honeycomb core. They compared these changes with a base-line (undamaged) model. By investigating the effect of the debonding extent on reduction in the flexural bending stiffness and on the natural frequencies, they concluded that increasing face-layer debonding progressively reduces the flexural bending stiffness of the beams.

Lestari and Qiao [40] carried out structural health monitoring on composite sandwich beams that are made of E-glass fiber and polyester resin, and the core consists of corrugated cells in a sinusoidal configuration (as seen in Fig 1.7). Damage identification was estimated from comparison of dynamic responses of healthy and damaged FRP sandwich beams. Artificial damage is created between the interface of core and face plate. Using piezo-electric smart sensors, dynamic response data is collected and the dynamic characteristics of a sandwich structure are extracted in order to evaluate the location and magnitude of the damage.

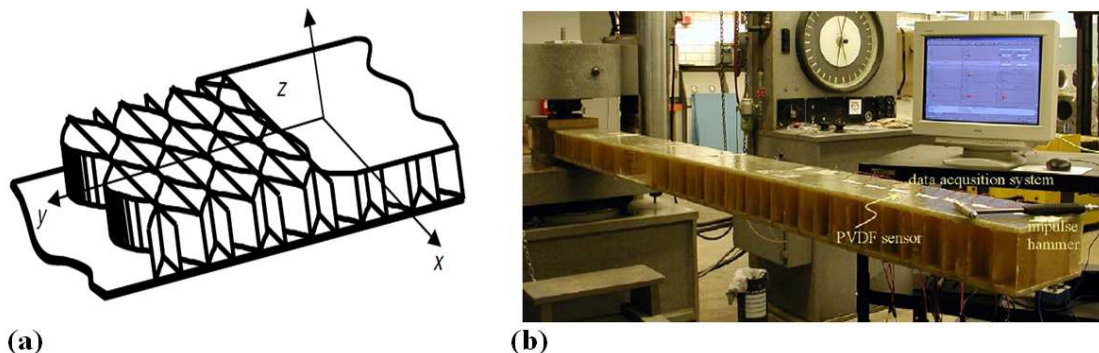


Figure 1.7 (a) Composite sandwich beams that are made of E-glass fiber and polyester resin, and the core consists of corrugated cells in a sinusoidal configuration (b) Vibration test set-up with the help of an impact hammer [40]

Yam and Cheng [41] conducted a study on the use of modal parameter analysis for damage detection in composite structures. Numerical and experimental investigation into the damage-induced changes of physical parameters has been carried out for multi-layer composites. The results showed that with the increase in delamination size the natural frequency decreases, by artificially creating a crack and then vibrating (exciting) the structure by placing an embedded actuator.

Arkaduiz [42] analyzed a laminated composite beam with a single closing delamination. The results showed that the presence of delamination reduces the natural frequencies of the beam. However, these changes are very small for short delaminations. Furthermore, it was found that delamination also influences the transverse displacements of the beam affecting their sizes and slopes. These changes are very sensitive to the delamination location and length.

Giannoccaro [43] discussed an experimental technique due to which fatigue strength can be correlated with modal parameters in composite specimens. The specimens were subjected to a

tensile fatigue load and a frequency of 10Hz. The results are shown in Fig 1.8. It can be seen that for all the six specimens there is a considerable shift towards the left in case of natural frequencies for around 50% of fatigue life and with the increase in damage (90% of fatigue life) there is a decrease in amplitude as well.

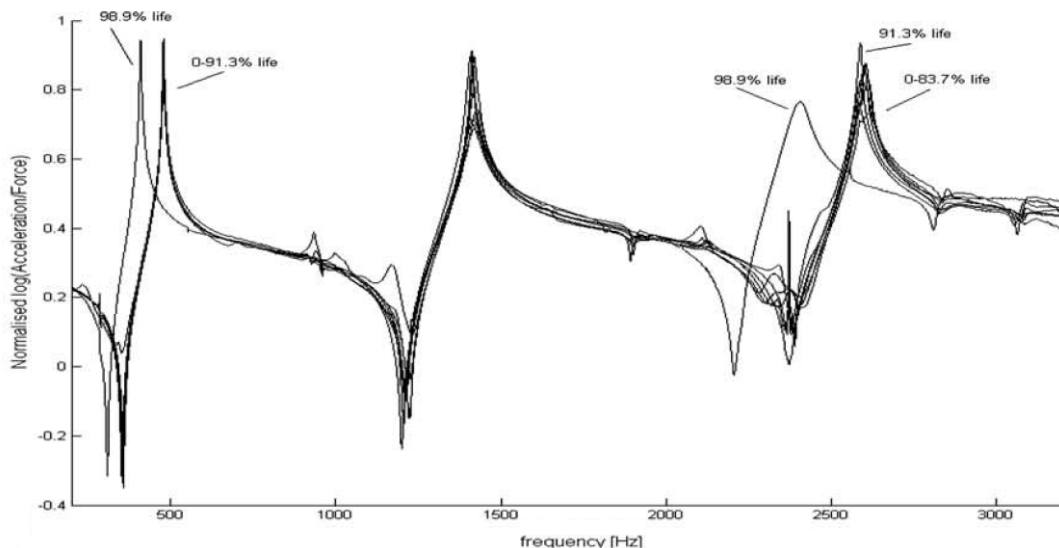


Figure 1.8 Shift in FRF towards the left coupled with a decrease in amplitude with an increase in damage [43]

Tracy and Pardoen [44] studied the effect of prescribed delamination on the natural frequencies of laminated beam specimens. Experimental modal analysis was used to measure the effect of delamination length on the first four frequencies of the simply supported test specimens. The experimental results were correlated with detailed finite element models as well as with simplified beam theory models. It is seen that delamination which covered one-third of the specimen length had a 20% effect on any of the first four frequencies. This kind of information is very important for damage detection.

Khoo et al. [45] employed different vibration techniques for detecting the presence and monitoring the presence of damage in structures. They presented a modal analysis technique by evaluating damage-sensitive parameters such as resonant pole shifts and mode shapes, residue and stiffness changes. They used resonant poles (s-plane) to identify the modes that exhibit relatively large pole shifts are believed to be affected by damage. The damaged region was identified by visual comparison of the deformation mode shapes before and after damage.

S.G. Mattson et al. [46] carried out damage detection based on residuals and discussed the phenomenon of false negatives. According to them, false negatives give no indication of damage when damage is present. Advantage of using the change of structural natural frequency to detect damage is its convenient measurement and high accuracy. Various methods of damage detection that use natural frequency information are reported in detail by Salawu in the reference [47]. The natural frequency is often not sensitive enough to the initial damage in structures. Usually, this method can only ascertain existence of large damage, but may not be able to give the damage location because the structural damage in different location may cause the same frequency change. In order to have an idea of the sensitivity of the experimental design factors on the modal parameters (natural frequency and damping), we have carried out design of experiments on the experimental results in this thesis.

Our works are principally derived from these above references. Vibration tests on pristine and damaged composite beams have been carried out by using burst random excitation [48]. The composite beams are impacted symmetrically with the help of a drop weight system by keeping in view the BVID limit. Results showed that with the accumulation of damage in the specimens, there is a decrease in natural frequency (Fig 1.9). It was also seen that the difference in natural frequencies between the damaged and the undamaged states is greater in case of the higher modes. A statistical analysis based on design of experiments is carried out on the experimentally obtained modal parameters, which showed the energy of impact as the design parameter having the most significant effect on the modal parameters.

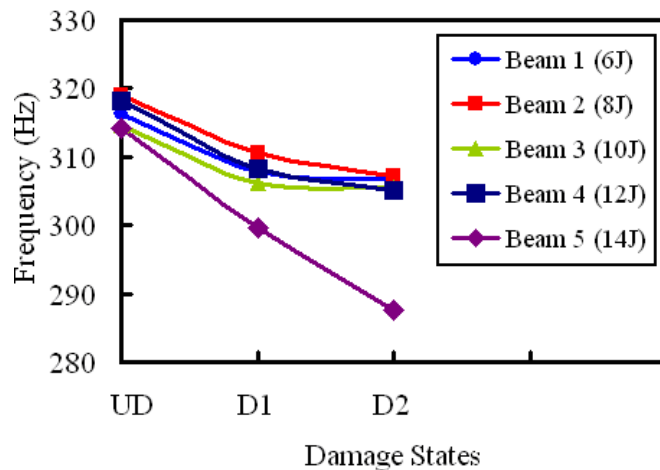


Figure 1.9 Decrease of natural frequency with an increase in damage in composite beams impacted at different energies [48]

1.5.2 Damage Detection Methods based on Damping Changes

In structures made of composite materials there seems to be a tendency to use damping as a damage indicator tool, as it tends to be more sensitive to damage than the stiffness variations, mainly when delamination is concerned. A part of our work in this thesis is to justify this tendency. The introduction of damage into a material generally results in an increase of damping, which is related to energy dissipation during dynamic excitation. When a delamination or debonding failure mode is concerned, friction between the interacting surfaces may occur for small bending deformations. As friction is an energy dissipation mechanism, it is reasonable to assume that damping may be used for SHM, when this type of damage is concerned. The main sources of internal damping in a composite material arise from micro-plastic and viscoelastic phenomena in the matrix together with the interface effects between the matrix and the reinforcement [49]. Summing up the above discussion, it can be said that damping due to damage is mainly of two types.

- Frictional damping due to slip in the unbound regions between fiber and matrix interface or delaminations
- Damping due to energy dissipation in the area of matrix cracks, broken fibers etc. Increase in damping due to matrix-fiber interface slip is reported to be very significant [50] and is more sensitive to damage than stiffness [51].

Therefore, damping has also been proposed as a potentially sensitive and attractive damage indicator though research works related to damping are far fewer in number than those on natural frequency because experimentally it is a parameter difficult to measure. A few experimental investigations on the effect of damage on composite damping are discussed briefly:

Saravacos and Hopkins [52] investigated the effects of delaminations on the dynamic characteristics of composite laminates especially damping, both experimentally and analytically. They developed a laminate theory in which the unknown kinematic perturbations induced by a delamination crack are treated as additional degrees of freedom. Based on this generalized laminate theory, an exact methodology was developed for predicting and relating the modal parameters with the delamination damage. These formulations were then encoded and integrated with micromechanical models to provide a unified computer code for the analysis of delaminated composite beams. Experiments were conducted on composite beams with a single delamination, and measured natural frequencies and modal damping were reported. The effect of delamination on the dynamic characteristics is very dependent on the laminate configuration. It was found that natural frequencies are rather insensitive to interfacial friction and for large delamination cracks, interfacial friction damping appears more important than natural frequency. Results showed that modal damping increases as the delamination grows bigger in the composite beam specimens (Fig. 1.10).

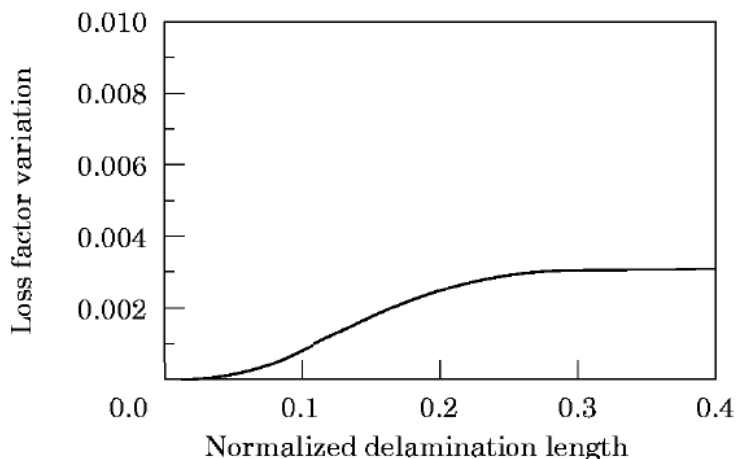


Figure 1.10 Increase in modal damping with an increase in the delamination length of a composite cantilever beam [52]

Montalvao et al. [53] proposed a novel method for the localization of delamination damage in quasi-isotropic in composite fiber reinforced plastic CFRP plates. They used the modal damping factor variation from a reference state (base-line undamaged model) to a damaged state as feature. They also made use of the modal strain shapes, described by mode shape function tool to spatially describe the local sensitivity to damage. The damage location was assessed by a Damping Damage Indicator Index, which provided a geometrical probability indication of the damage location. Damping variations were found to be more sensitive than stiffness variations for the CFRP plates as seen in Fig 1.11.

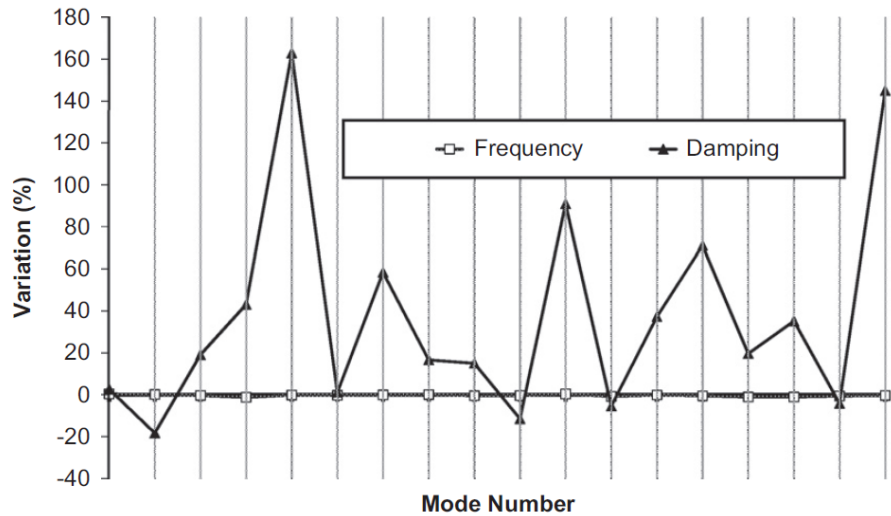


Figure 1.11 Natural frequency and modal damping factor shifts due to the presence of damage in CFRP plates, showing that damping variations are far more important than stiffness changes [53]

Gibson [54] discussed the use of modal vibration response measurements to characterize accurately the mechanical properties of fiber-reinforced composite materials and structures. He carried out impulse/frequency response tests in order to carryout on-line evaluation of full-scale composite components. Damage was induced by low-speed speed barrier crash tests of vehicles on which the hood-closure panels were mounted. It was concluded that damage generally causes the mean values of modal damping factors to change more than the modal frequencies as shown by the results in Fig 1.12.

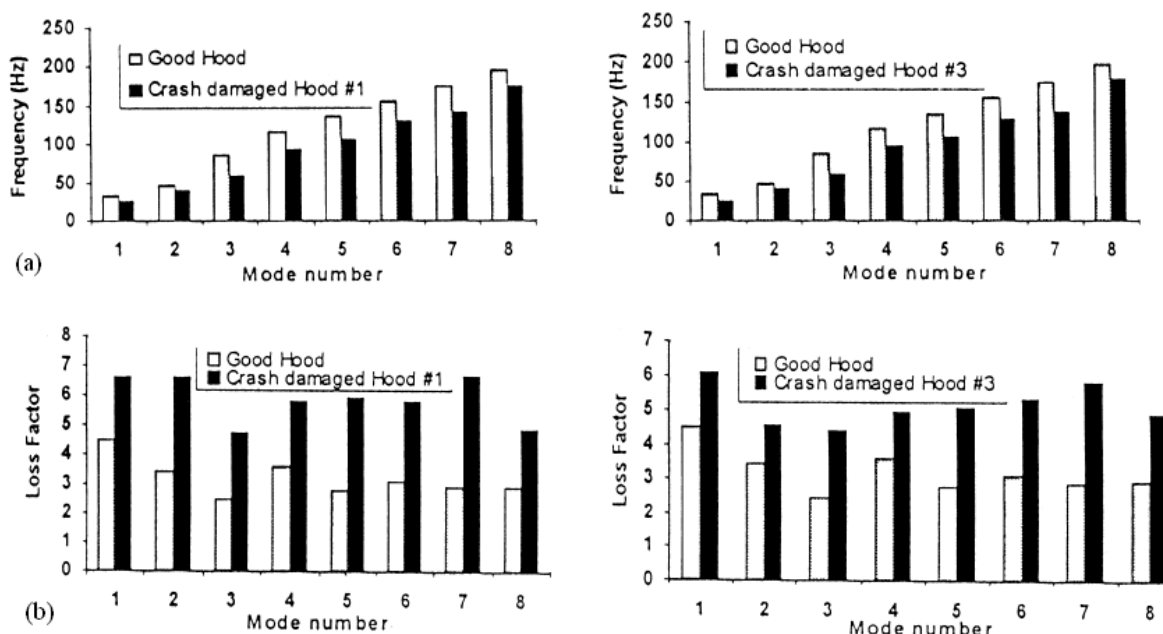


Figure 1.12 Comparison of (a) modal frequencies and (b) modal damping loss factors of composite automotive hood-closure panels with and without crash-induced damage [54]

Kyriazoglou et al. [55] explored the use of the specific damping capacity (SDC) for damage detection and localization in composite laminates. Results show SDC to be a sensitive technique for the detection of cracks in composite and woven laminates. Furthermore, the

resonant frequency, or value of dynamic flexural modulus, may be a useful technique to detect cracks in glass fiber reinforced laminates, although, the reduction may be quite small. However, for carbon fiber reinforced laminates, no detectable changes in the values of resonant frequency were found, whereas high changes in SDC were found.

Colakoglu [56] proposed a damping monitoring method that estimates damping factor by vibration excitations. By using this method, the damping factor as a function of stress amplitude and the number of fatigue cycles was determined experimentally in two different low carbon steels. It was found that the damping factor increased with the number of fatigue cycles. Furthermore, Zhang and Hartwig [57] recommended damping in the evaluation of damage process which seemed more sensitive than the natural frequencies. Similarly, Richardson and Mannan [58] found that the loss of stiffness in a structure corresponds to a decrease in natural frequency combined with an increase in damping.

In this thesis, based on shifts in damping, we propose two applications:

We propose to study the variations of modal parameters with impact damage in composite beams [59] with the help of changes in natural frequency, damping ratio and a novel damage detection parameter damage index (to be explained in detail later on). Results showed that with the accumulation of damage, a decrease in natural frequency accompanied by an increase in the damping ratio was observed in the s-plane (Fig 1.13). Damage index was also used as a damage indicator tool, which is based on the integral of the amplitudes of the frequency response functions (FRF) and therefore estimated the phenomenon of dissipation in composite beams. It was seen that damage index increased with the increase of damage and was used to verify the damping ratio results estimated by the curve-fitting algorithm, and served as an additional tool for understanding the damping behavior of damaged composite beams.

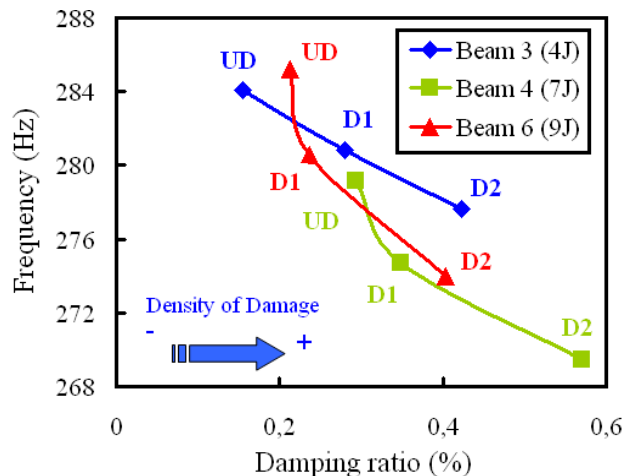


Figure 1.13 Variation of modal parameters in the complex s-plane showing a decrease in natural frequency coupled with an increase in damping as the density of damage increases in the composite beams [55]. UD is undamaged state; D1 is damage at 4 impact points and D2 is damage at 8 impact points.

We tested damaged honeycomb sandwich beams by burst random and sine dwell vibration testing [60], in order to compare that which testing method gives a more logical estimation of damping in the presence of damage, in terms of the theoretical shift in the s-plane. The honeycomb sandwich beams were damaged by two different ways i.e., by drop weight impacts and by piercing a hole all along the width in the honeycomb core (core-only damage).

Results showed that damping increased with an increase in impact damage (friction zone), whereas the effect of core-only damage on damping was negligible, as compared to impact damage. Furthermore, damping seemed to be more sensitive to damage than the natural frequency. Design of experiments showed that sine-dwell excitation based modal testing gives more reliable estimation of damping in the presence of damage as compared to burst random testing because it takes into account the effects of structural non-linearity.

1.5.3 Damage Detection Methods based on Mode Shape Changes

Another way to correlate damage with change in dynamic parameters is to use mode shapes. In the presented thesis, damage monitoring is principally based on shifts in natural frequency and damping. Variation of mode shapes in the presence of damage has not been dealt with in detail. However in order to give a detailed overview on the vibration-based damage detection, it has been thought necessary to provide a bit of literature review concerning mode shapes.

Works of Pandey et al. [61] can be cited as a first reference in this context. They proposed a parameter called curvature mode shape to identify and locate damage in a structure. By using a central difference approximation, curvature mode shapes were calculated from the displacement mode shapes. With the help of cantilever and a simply supported analytical beam models, they showed that the absolute changes in the curvature mode shapes are localized in the region of damage and hence they can be used to detect damage in a structure. The changes in the curvature mode shape increase with the increasing size of damage and this information can be used to obtain the amount of damage in the structure. The absolute differences between the curvature mode shapes of the intact and the damaged (element 13) cantilever beams are plotted in Figure 1.14. The maximum difference for each curvature mode shape occurs in the damaged region, which is between point 13 and 14 for this case.

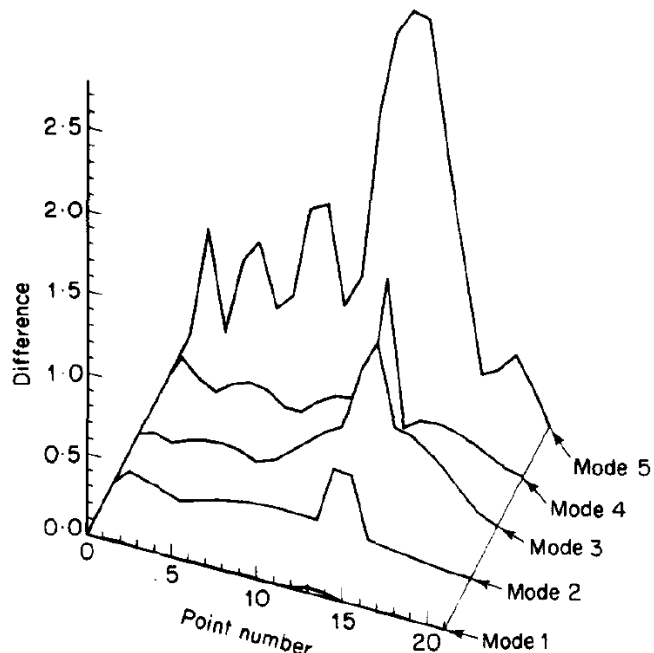


Figure 1.14 Absolute difference between the curvature mode shapes for the intact and the damaged (element 13) cantilever [61] - Maximum difference occurs in the damaged region, which is between point 13 and 14

Kim et al. [62] also proposed a methodology to non-destructively locate and estimate the size of damage in structures using a few natural frequencies. First, a frequency-based damage detection (FBDD) method is outlined. A damage-localization algorithm to locate damage from changes in natural frequencies and a damage-sizing algorithm to estimate crack-size from natural frequency perturbation are formulated. Next, a mode-shape-based damage detection (MBDD) method is outlined. A damage index algorithm to localize and estimate the severity of damage from monitoring changes in modal strain energy is formulated. The FBDD method and the MBDD method are evaluated for several damage scenarios. The result of the analyses indicates that the FBDD method and the MBDD method correctly localize the damage and accurately estimate the sizes of the cracks simulated in the test beam.

Salawu and Williams [63] evaluated the performance of the curvature mode shape method and the mode shape relative difference method. They found that their performance when using experimental data was not very satisfactory. The results showed that the procedures were unsatisfactory in predicting the most severe damage case, and were unable to satisfactorily differentiate between damage cases with close degrees of severity.

Dong et al. [64] carried out a systematic analytical and experimental study to correlate the crack of a beam with changes in its modal parameters. The sensitivity to both crack location and crack size was developed for each modal parameter. They examined a parameter which is based on the change in the strain mode shape and another one that depends on natural frequency. The reason to use the strain modes in finite element model updating is that the sensitivity of the strain mode shapes is larger than the sensitivity of the displacement mode shapes. Strain based equation of motion is needed to calculate strain mode shapes from analytical model. The authors showed that the strain eigen-parameter is more sensitive to the size of the crack than the frequency eigen-parameter.

1.5.4 Damage Detection Methods based on Finite Element Model

As physical testing usually demands a high financial and time effort, it is nowadays desirable to run numerical simulations prior to experimental testing as much as possible. In this context finite element analysis always plays a major role. Furthermore, most industrial used finite element codes already contain reliable algorithms for modal parameter estimation and give reliable results depending on a suitable modeling of the physical problem.

Numerical simulations by the finite element methods have been used in most of the literature review presented in the preceding sections. Changes in vibration parameters, such as frequencies and mode shapes of beams, plates, even rather complicated truss and bridge structures, were investigated for different types, sizes, and locations of structural defects by finite element vibration analysis. Conclusive points from these investigations are

- the natural frequencies of a degraded structure will usually decrease due to the loss in stiffness caused by the presence of damage
- the higher mode frequencies and mode shapes are more sensitive to damage than the lower mode frequencies but it is difficult to reconstruct reliable high frequency mode shapes

Zhang and Yang [153] reviewed the recent advances of the finite element analysis of composite laminated plates based on various lamination theories, with the focus on the free vibration and dynamics, buckling and post-buckling analysis, geometric nonlinearity and large deformation analysis and failure and damage analysis of composite laminated plates, are reviewed in this paper. The development of buckling and post-buckling analysis under material nonlinearity and thermal effects are emphasized and in the failure analysis, the concentration is especially on the advances of the first-ply failure analysis. Based on the author's investigation, it has been found that the research on the following aspects of the composite laminated plates is relatively limited and may attract more interests in the future research.

- Material nonlinearity effects on structural behavior of composite laminates
- Failure and damage analysis under viscoelastic effects such as thermal and creep
- Failure and damage analysis under cyclic loading
- Micromechanical approach for damage analysis
- Analysis of the damage evolution in composite laminates
- Multi-scale modeling of crack initiation, propagation and overall structural failure

Yam et al [65] presented a new method for the prediction of delamination location in multilayer composite plates by carrying out numerical and experimental investigations into the delamination-induced changes of modal parameters. Numerical analysis showed that an intrinsic connection exists between delamination location and the changes of modal parameters. The effect of delamination location on delamination induced variation of mode-shape is consistent with that of natural frequency. Numerical simulations provided a good explanation for damping increase due to delamination, i.e., the energy dissipation is mostly induced by the interfacial slip across the delamination and the tendency of penetration between the upper and lower surfaces in the delamination region. The results of this study showed that the location of internal delamination in multilayer composite plate can be estimated using a combination of measured modal damping change with computed modal strain energy distribution. The proposed method has attractive application to damage detection of composites, especially for smart structures because of their inherent ability to provide excitation to the structure without requiring much additional equipment.

Yan et al. [66] presented an improved method for establishing a dynamic model of a laminated composite vessel with small damage. The method proposed has two steps: (1) directly meshing structure and ignoring existence of structural damage, (2) for those elements in position of structural damage, their element stiffness are adjusted to simulate structural damage. The improved method can greatly decrease the number of required elements for modeling small structural damage, so that the efficiency of dynamic analysis for damaged structures can be increased.

Yang et al. [67] simulated and studied free-free flexural vibrations of composite beams with different levels of defects, by using finite-element analysis. Two types of defects were considered (Fig 1.15). The first one is a complete void in the epoxy layer and the second one is a delamination between the adhesive layer and composite. A void was simulated by

deleting the elements in its place. A delamination was developed by creating a pair of nodes with the same coordinates but different node numbers and then lining them up to form the contact boundaries and element edges for the composite and the adhesive.

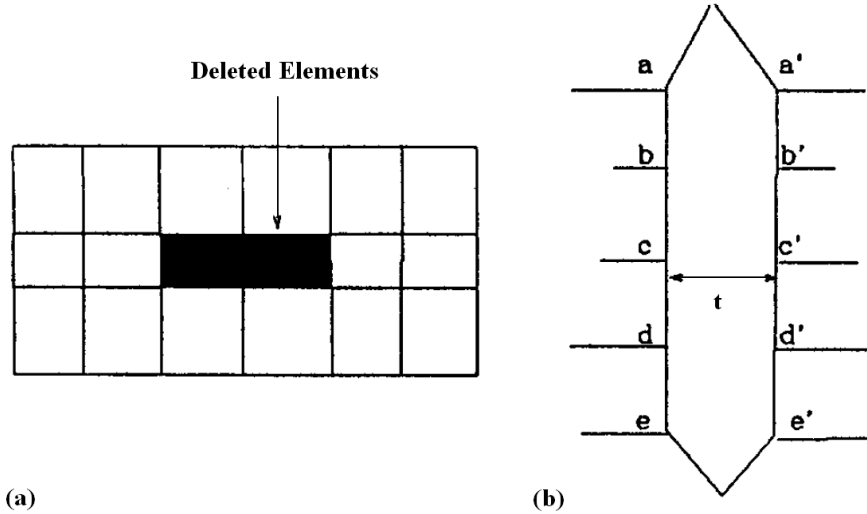


Figure 1.15 Mesh formation defect (a) elements are deleted to form a void (b) $t = 0$ to form a delamination [67]

Kessler et al. [34] performed a 2-D finite element analysis to determine the frequency response of graphite/epoxy composite specimens in order to compare with experimentally obtained results. Damage was modeled by altering the extension and bending stiffness matrices either in specific regions. The models accurately predicted the response of the specimens at low frequencies, but coalescence (merging) of higher frequency modes makes mode-dependent damage detection difficult for structural applications.

Teughels et al. [69] investigated a new global optimization method named coupled local minimizers (CLM). In CLM the average objective function value of multiple design vectors is minimized, subjected to pairwise synchronization constraints. This is done with the augmented Lagrangian method, which they implemented with a Newton-based algorithm, in order to maximize the convergence rate. In order to generalize the problem, the objective function and the synchronization constraints are normalized. The CLM method is successfully applied to a test function containing several local minima. CLM is used for FE model updating. The correct damage pattern of a beam is identified with this method by comparing the experimental and numerical results in Fig 1.16.

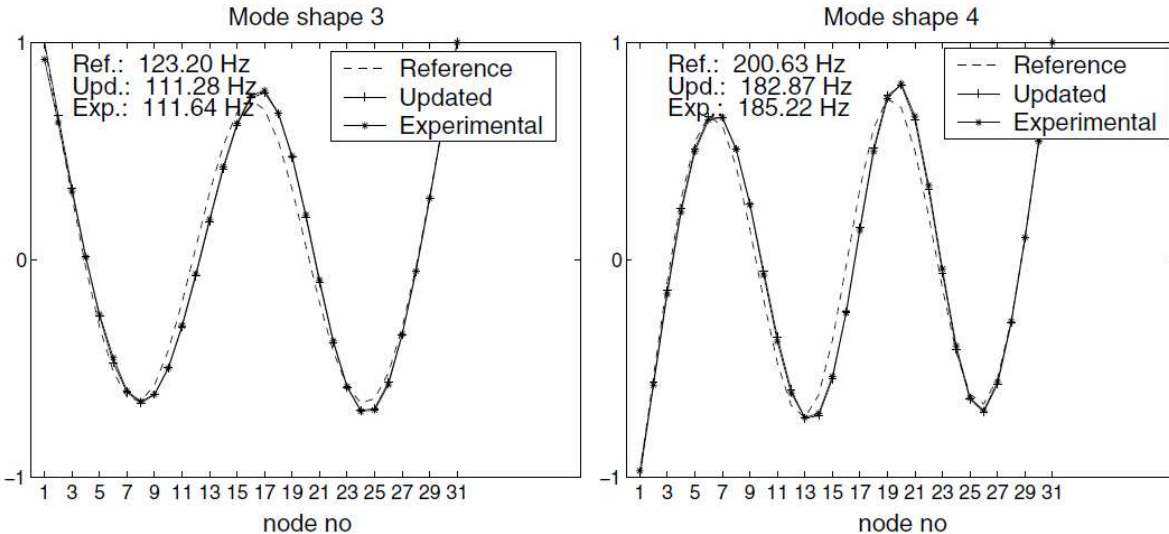


Figure 1.16 Comparison of the experimental (damaged state) and numerical (reference and updated) bending mode shapes, the updated and experimental results show a good correlation [69]

Several other papers in scientific literature have documented the use of a combination of the modal analysis and frequency domain methods to detect various damages, coupled with finite elements or analytical models.

Hou and Jeronimidis [68] simulated free vibrations of undamaged and damaged composite laminates by using layered orthotropic plate elements in order to simulate the experimental results. The relative sensitivity of the damaged plates to transverse cracking and delamination was developed. The transverse cracking damage was simulated by a local reduction of E_1 , E_2 , G_{12} and Poisson's ratio, whereas delamination in composite plates was modeled by putting the elastic properties of matrix layers locally equal to zero. The authors concluded that sometimes changing the geometrical properties of the structures by damage makes the structures stiffer and increases the resonant frequencies. They found that the phenomenon of local thickening difficult to simulate numerically and this should be kept in mind while developing NDT methods based on natural frequencies.

The aim of our work based on Finite Elements is to build a numerical model of the test-beams in order to simulate their dynamic response for both the undamaged (base-line) and the damaged cases. The FE approach is then coupled with an updating methodology to find a good experimental / numerical correlation. These works are presented in Chapter 6.

1.5.5 Damage Detection Methods based on Topology Optimization

In using finite element models for damage detection, either few elements or only a part of a structure was considered as the damaged region, but neither the total number of elements nor an entire structure. The small-region damage assumption is valid only when the information on the candidate damaged area is available. This limitation may be overcome by the use of the topology design method for damage identification because this method has been used to design an entire structure. The topology design method was originally developed to find an optimal material distribution of a structure having the minimum compliance or maximum eigen-values [70,71].

Subjected to specific constraints and penalizations, an optimal structure can be found by iteratively changing the stiffness of selected elements and deleting elements with low stiffness. In recent years this method has been expanded to fit a lot of different problems [72]. Amongst these are also formulations for matching eigen-values or frequency response function data [73]. This knowledge has been implemented in MSC. Nastran and structural topology optimization is now possible using the implemented optimization libraries [74].

A new approach, using the stiffness related topology optimization variables for localizing damages has been carried out by Lee et al. [75]. Since it has been shown that damage causes changes in modal parameters, therefore Lee et al. formulated a topology design based formulation for the detection of damage, where both resonances and anti-resonances are used as the damage indication modal parameters. An idea to progressively reduce the candidate damaged elements is also developed to improve the accuracy and efficiency of the proposed method.

The topology optimization formulation for damage localization described in this thesis is based on the works of Lee et al, which are implemented in Nastran for general diagnosis purpose. We apply this method to locate damage in composite beams i.e., validate the ultrasound (C-Scan) results. This damage localization part of the thesis is carried out with the help of a research project student Hanno Niemann from TU Braunschweig.

1.6 Innovation in Composite Structures

The main part of this thesis concerns damage detection in composite laminates and composite sandwiches. Standard sandwiches with honeycomb and foam cores have been tested for this purpose, but the main focus is on a new sandwich material with randomly placed carbon fibers in the core. This new sandwich material is also known as entangled sandwich material. The aim of developing this material is to study its dynamic characteristics (especially damping) and impact toughness in comparison with standard sandwiches having honeycomb and foam cores. As fabrications norms of this new sandwich are not defined as such, therefore entangled sandwich materials have been fabricated with the help a PhD student Laurent Mezeix from CIRIMAT Toulouse. First a general introduction about innovations in composite sandwich structures is given, followed by literature survey related to novel enhancements in damping and impact toughness.

Composites structures are used more and more in aerospace and automobile structures, since they offer great energy absorption potential without significant weight penalties [125]. With the help of some innovative measures, the properties of these composites can be further enhanced without sacrificing rigidity and toughness. In recent years, several investigators have considered a number of innovative ideas in order to improve the mechanical performance of composite sandwich structures.

But the majority of these works present in scientific literature are related with the improvement of the mechanical properties (in particular the longitudinal Young's modulus and the transverse shear modulus) and the impact toughness (energy absorption characteristics) of sandwich structures. Though works related to the enhancement in damping in sandwich structures are relatively few in number as compared to those on enhancement in mechanical properties and impact toughness. Enhancements in damping and impact toughness in composite materials (based on vibration test results only) shall be discussed separately as

considerable experimental work has been carried out in this thesis regarding these two enhancements.

1.6.1 Enhancements in the Damping Characteristics

The importance of material damping in the design process has increased in recent years as the control of noise and vibration in high precision, high performance structures and machines has become more of a concern. In polymeric composites, the fiber contributes to the stiffness and the damping is enhanced owing to the internal friction within the constituents and interfacial slip at the fiber/matrix interfaces. At the same time, polymer composites researchers have focused more attention on damping as a design variable and the experimental characterization of damping in composites and their constituents [76-78].

A comprehensive overview on the status of research on damping in fiber-reinforced composite materials and structures with emphasis on polymer composites has been presented by Chandra et al. [79]. Their paper presents damping studies involving macro-mechanical, micro-mechanical and viscoelastic approaches. Some important works related to improved damping models for thick laminates, improvement of laminate damping and optimization for damping in fiber-reinforced composites/structures are critically reviewed.

A way of increasing damping in sandwich materials is by putting a viscoelastic layer as core between the two laminates [80-82]. Yim et al. [83] studied the damping behavior of a 0° laminated sandwich composite cantilever beam inserted with a viscoelastic layer. Gacem et al. [84] improved damping in thin multilayer sandwich plates having five layers composed of elastomer and steel by submitting the structure to shear vibrations under a compression preload. With the advancement of technology in electro-rheological (ER) materials, their applicability to sandwich structures has been increased significantly due to their merits such as variable stiffness and damping properties [85]. The vibration analysis of a sandwich plate with a constrained layer and electro-rheological (ER) fluid as core has been investigated by Yeh and Chen [86]. Basic configuration for viscoelastic/ER sandwich material is shown in Fig 1.17 below.

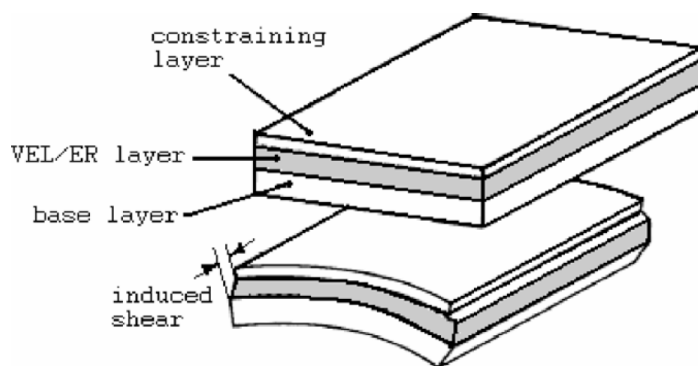


Figure 1.17 Basic configuration for viscoelastic/ER sandwich material (constrained treatment) for enhanced damping characteristics [85]

Jueng and Aref [87] also investigated the feasibility of a combined composite damping material system. In this new configuration, they used two different styles of composite materials. One is a polymer honeycomb material and the other is a solid viscoelastic material. The honeycomb material is helpful to enhance the stiffness of the entire structure, and the

solid viscoelastic will provide more energy dissipation properties in the multilayer panel systems when subjected to in-plane shear loading. These advanced polymer matrix composite (PMC) systems are also addressed for seismic retrofitting of steel frames [88]. Damping layer in sandwich structures can be made of any suitable material which provides the vibration damping function. Damping can be promoted in sandwich structures by using rubber-type cores made of butyl rubber or natural rubber, plastics such as polyvinyl chloride (PVC), adhesives of various polymer materials including epoxy-based materials, silicones, polyurethane etc [89,90]. A 3MTM VHBTM structural glazing tape is also used as damping layer in sandwich structures [91].

These advancements have led to the need for developing materials possessing better damping characteristics. Entangled materials are made from natural materials (wool, cotton etc) as well as artificial ones (carbon, steel, glass, etc.) and are quickly becoming of widespread use as sound absorbers [92]. Bonded metal entangled materials offer advantages for use as heat exchanger [93] or insulation [94]. These materials possess low relative density, high porosity and are cost-effective. Recently, a novel type of sandwich has been developed with bonded metallic fibers as core material [95-99]. This material presents attractive combination of properties like high specific stiffness, good damping capacity and energy absorption.

Entangled materials with carbon fibers have also been studied as core material [100]. Entangled materials with cross-linked carbon fibers present many advantages as core materials i.e., open porosity, multifunctional material or the possibility to weave electric or control cables on core material. Mezeix et al. [101] studied the mechanical behavior of entangled materials in compression. Mechanical testing has also been carried out on specimens made of wood fibers [102], glass fibers [103] and various matted fibers [104]. There are also some works in the literature related to 3D modeling of wood based fibrous networks based on X-ray tomography and image analysis [105]. Unfortunately, only a few works can be found in the scientific literature devoted to the mechanical testing of entangled sandwich materials, and no scientific literature can be found related to the vibration testing of entangled sandwich materials or even simple entangled materials.

As shown by the previous references, enhanced sandwich structures with better damping characteristics exist, but so far in this thesis, our work deals only with the static and dynamic characterization of glass entangled sandwich specimens and their comparison with standard honeycomb and foam sandwiches. Comparison with enhanced sandwich structures e.g., honeycomb sandwiches with viscoelastic layer, etc is not in the scope of this work and shall be duly considered in future.

In this thesis, with an aim to find a sandwich with enhanced damping characteristics, Shahdin et al. [106,107] fabricated and mechanically tested entangled sandwich beams with both carbon and glass fibers as cores and skins. The compression and bending test results showed that these entangled sandwich specimens have a relatively low compressive and shear modulus as compared to standard sandwiches with honeycomb and foam cores. The advantage of the vibration testing is to diagnose the variability of the fabrication process and to verify experimentally the potentially good damping characteristics of the fiber network sandwich specimens. Vibration tests demonstrate the presence of high damping in the entangled sandwich specimens making them suitable for specific applications like the inner paneling of a helicopter cabin, even if the structural strength of this material is on the lower side. Furthermore, the vibration tests showed (Fig 1.18) that entangled sandwich specimens possess in average 150 % higher damping ratios and on the average 20 dB lower vibratory levels than the honeycomb and foam sandwich beams.

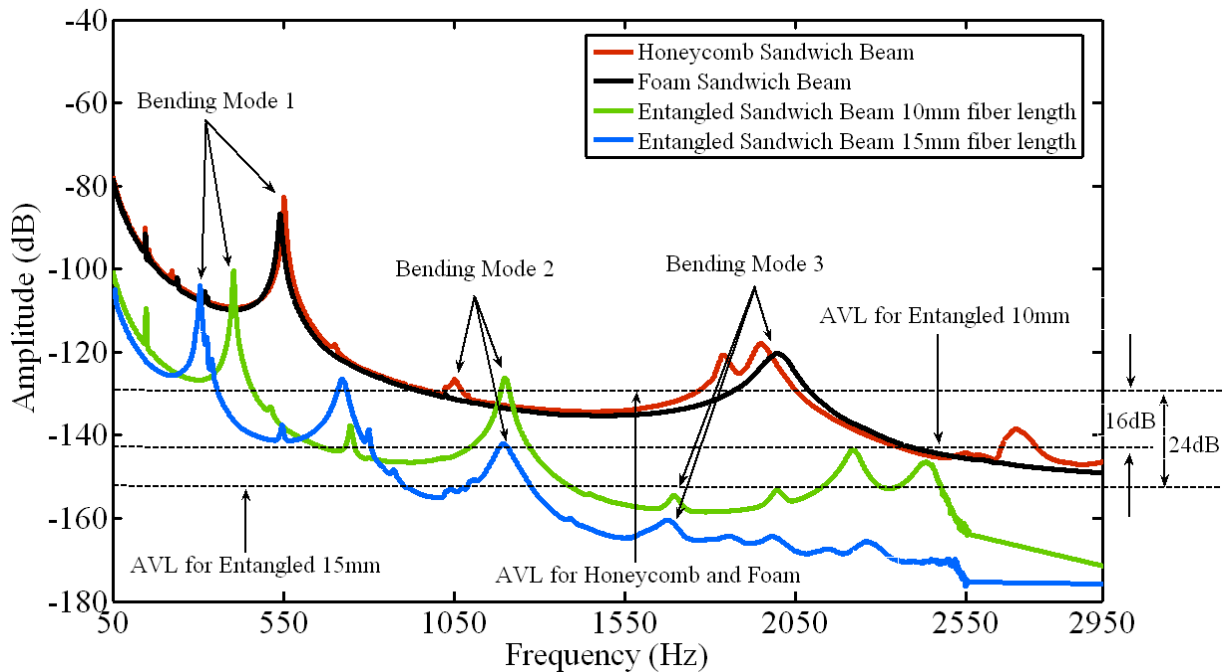


Figure 1.18 Comparison of the Sum of Frequency Response Function (FRF) for the honeycomb, foam and entangled sandwich specimens with the average vibratory level [107]

1.6.2 Enhancements in the Impact Toughness

Several novel sandwiches have been developed in scientific literature with a view to enhance the impact toughness. A few similar developments are discussed briefly as follows:

Wang [108] conducted dynamic cushioning tests by free drop and shock absorption principle on paper honeycomb structures in order to study the effect of impact behavior. Experimental results showed that the thickness of length and honeycomb cell-wall have a great effect on its cushioning properties. Increasing the relative density of paper honeycomb can improve the energy absorption ability of the sandwich panels.

Yoo and Chang [109] fabricated egg-box shaped energy absorbing structures made of fabric composites to find out the compressive characteristics and energy absorbing capacity. From the test results it was found that the foam filled composite egg-box panels had good energy absorption capacity with smooth stress-strain curves which resembles the ideal energy absorber.

Sandwich structures with various light weight cores have also been extensively studied. In a study by Li and Jones [110], low velocity impact response of hybrid syntactic foam with rubber latex coated micro-balloons sandwiched between two facesheets was studied. It was found that compared to the core which consists of pure epoxy or just the syntactic foam without rubber coating, the impact energy absorbed by rubberized syntactic foam core was much higher. In another study the syntactic foam was modified by using crumb rubber [111]. The impact tolerance of the structure was found to increase with the increase in the rubber content of the core.

Torre and Kenny [112] reported the development of new type of sandwich construction which consisted of skins made from a glass fiber phenolic matrix composite laminate and a core formed by an internal corrugated structure of the same laminate used for the faces filled by a phenolic foam to improve crashworthiness for transport applications. The corrugated sandwich panels showed better performance in terms of impact energy absorbing properties and strength as compared to traditional sandwich structures.

Grid stiffened structures are found to have higher impact resistance and the delamination and crack propagation occurring in these structures is less compared to laminated composite panels [113]. Low velocity impact tests were conducted by Hosur et al. [114] on integrated core sandwich composite samples which show that skin thickness and composition of skin plays a significant role in the impact response of these structures. Hollow core panels having varying thickness of rib were also prepared and the response when subjected to low velocity impact was observed and it was found that these cores provided greater impact resistance due to additional energy absorption mechanisms [115].

The author would like to highlight the fact that all of these novel materials, fabricated to enhance the impact resistance are mostly composite materials i.e., consisting of fibers and a matrix. In case of entangled sandwich materials, the concept of matrix does not exist as such. The fibers are vaporized by the resin and not immersed in the resin. Unfortunately, little scientific literature can be found related to impact testing of entangled sandwich materials. One work that can be cited in this regard is that of Dean et al [98]. Their paper documents an experimental and numerical study of energy absorption in lightweight sandwich panels with entangled stainless steel fiber cores. The results show that the sandwich panel absorbs 40% more energy than the two separated face plates.

In this thesis, the entangled sandwich beams tested previously will be evaluated for their impact toughness as well [116]. Evaluation of impact toughness is uniquely based on vibration test results i.e., decrease in natural frequency. Due to the lack of available literature on the behavior of entangled sandwich materials due to impact damage, a simple case of symmetrical impacts is studied. Two types of entangled sandwich specimens (heavy and light) are studied in this section. The light specimens have 2.5 times less resin than the heavy ones. The impact energies are chosen in such a way that the heavy and light specimens have the same level of damage. Vibration test results prove that the light specimens having better damping characteristics but they are more sensitive to impact damage than the heavy ones. Therefore, while selecting the application of these light entangled sandwich materials, their sensitivity to impact damage should be taken into consideration. Further in this thesis, this work has been carried a bit further and the impact toughness of carbon and glass entangled sandwich beams is compared with classical sandwich materials with honeycomb and foam cores.

The impact toughness of entangled sandwich beams in this thesis is evaluated by the decrease in natural frequency (global parameter of a structure) which signifies loss of rigidity. The author wants to clarify here, that impact toughness is only studied through vibration tests and the classical procedure used for determining the impact toughness i.e., compression after impact (CAI) has not been implemented as it is outside the scope of our work.

1.7 Conclusion of the First Chapter

The first chapter gives a literature review on the vibration based damage detection techniques based on traditional type methods. The emphasis of damage detection in this thesis is on composite and composite sandwich beams. A brief but comprehensive literature review is provided regarding **damage detection by changes in natural frequency, damping** and mode shapes from both the experimental and numerical point of view. Furthermore, a few works related to enhancements in damping and impact toughness characteristics in composites are also highlighted.

Literature review showed that impact damage in composite beams leads to

- **a decrease in natural frequency (loss of rigidity)**
- **an increase in damping (increase of friction zone)**

These two trends shall be the main criterions for studying the effect of impact damage in the composite laminate and composite sandwich beams during the experimental part of this thesis.

In our work, by carrying out a good number of vibration tests on different types of materials we have a lot of statistical data e.g., 33 frequency response functions for each test-beam for each state, a frequency band of 0-2500 Hz, 4 bending modes, extracted modal parameters, different densities of damage and levels of impact energy etc. In order to take into account all this data by studying the influence of various parameters on the extracted modal parameters (frequency and damping), we have used Design of Experiments (DOE), which is a powerful analysis tool for **highlighting the influence of key parameters** that affect an experimental process.

Chapter 2: Analytical and Experimental Modal Analysis

Today's engineers are faced with many complex noise and vibration problems associated with the design and troubleshooting of structures. Never before have structures had so many constraints, such as legislative, cost, and durability, imposed upon them. Because of these constraints, present day structures are typically more complex in terms of design and materials. Therefore, the engineering that goes into these structures must be more exact than ever before. The structural analyst must design with accurate and realistic models and the experimentalist must be able to accurately define a structure's dynamic response to specified input forces.

Recently, tools have been developed to assist the structural engineer in these areas. The analyst now uses sophisticated finite element programs, such as Nastran, to aid in the understanding and the design of structures. The experimentalist has sophisticated digital signal analysis equipment that aids him in quantifying and understanding a structure's dynamic and input forces. This part is commonly known as experimental modal analysis (EMA).

The major point of this chapter is to show how frequency response function (FRF) measurements are related to the structure's mode shapes and vibrational frequencies. This overall objective will be accomplished by building a mathematical foundation from the analytical and experimental point of view. This chapter is divided into three main sections:

System identification: This is a widely used approach to characterize a physical process in a quantified way. In modal analysis terms, this is also known as vibration signal analysis.

Single degree of freedom system: This system will be used as a means for defining some standard terminologies in order to help the readers to grasp with relative ease the basic theoretical aspects of this thesis. Detailed explanation on the fundamentals and applications of vibrations can be found in a multitude of technical books, for example by De Silva in reference [117].

Experimental modal analysis: Theoretical background on experimental modal analysis is discussed briefly. Types of excitations, types of test set-ups for vibration testing and types of estimation methods are highlighted as well. Finally correlation tools are discussed used for updating a numerical model with respect to experimental results.

Basic Assumption of this Thesis

Before proceeding, the basic assumptions must be established before the theory on which this thesis is based can be developed. The first assumption is that the structure is a mechanical system whose dynamics may be represented by a set of linear, second order, differential equations. The second assumption is that the structure during the test can be considered as time invariant. This assumption implies that the coefficients in the linear, second order, differential equations are constants and do not vary with time. The third assumption is that the structure is observable. While this may seem trivial, this means that the system characteristics that are affecting the dynamics can be measured and that there are sufficient sensors to adequately describe the input-output characteristics of the system.

It appears that damping which is a phenomenon of dissipation in structural aerospace materials (metallic and composites) is not well represented by the three assumptions previously discussed. The friction (between components and around defects) makes the peak unsymmetrical around resonance frequency and induces a significant part of the vibrating irreversibility, consequently making the model non-linear. The damping ratios encountered in this thesis are relatively low (except in certain cases with entangled sandwich materials) which truncate the resonance modes with a $1/2\zeta$ equivalent quality factor. At this point of resonance, the excitation compensates exactly the cyclic dissipation (the modal sine motion being then independent, with constant mechanical energy) [151]. Thus, this linear approach can be used for diagnosing impact damage in complex materials (composites). The important points of our approach are given as follows:

- The system is linear in the range of amplitudes under consideration
- The damping is considered proportional
- The method of modal superposition is chosen for the solution
- Condition of reciprocity is assumed

This approach can be applied to a multi degree of freedom system (MDOF) as well, which can then be decomposed into several single degree of freedom systems (SDOF) by modal decomposition. Fig 2.1 shows an example of a simple cantilever beam (3 DOF) excited at its tip by a pulse, decomposed to three SDOF systems by modal superposition, which can then be treated separately.

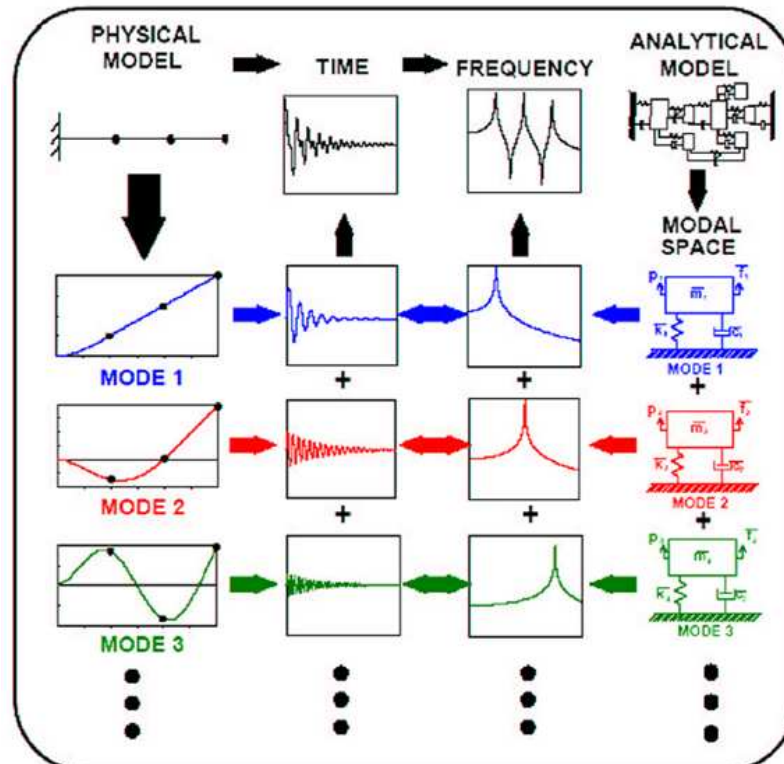


Figure 2.1 An example of a cantilever beam showing the decomposition of a 3 DOF system to three separate SDOF systems [122]

2.1 System Identification

System identification helps us to characterize a physical process in a quantified way. The object of this quantification is that it reveals information about the process and accounts for its behavior, and also it allows us to predict its behavior in future environments. The physical processes could be anything, e.g. vehicles (land, sea, and air), electronic devices, sensors and actuators, biomedical processes, etc. In essence what we do is simply to watch what ‘a physical system’ does. This is of course totally useless if the system is ‘asleep’ and so we rely on some form of activation to get it going – in which case it is logical to watch (and measure) the particular activation and measure some characteristic of the behavior (or response) of the system. A very comprehensive overview regarding the fundamentals of signal processing for vibration engineers has been given by Shi and Hammond in reference [154].

Having got this far let us simplify things even further to a single activator (input) and a single response (output) as shown in Fig 2.2.

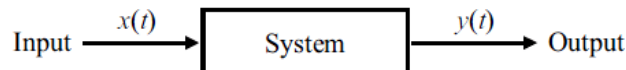


Figure 2.2 A single activator (input) and a single response (output) system [119]

It is now convenient to think of the activator $x(t)$ and the response $y(t)$ as time histories. For example, $x(t)$ may denote a voltage, the system may be a loudspeaker and $y(t)$ the pressure at some point in a room. However, this time history model is just one possible scenario. The activator x may denote the intensity of an image, the system is an optical device and y may be a transformed image. Our emphasis will be on the time history model generally within a sound and vibration context.

The box marked ‘System’ is a convenient catch-all term for phenomena of great variety and complexity. From the outset, we shall impose major constraints on what the box represents, specifically systems that are **linear** and **time invariant**. These systems are known as a linear time-invariant (LTI) systems i.e., the system is unaffected by time and is linear if and only if the input signal produces the same output signal. A time-invariant system may be illustrated as in Fig 2.3, such that if the input is shifted by t_0 , then the response will also be shifted by the same amount of time.

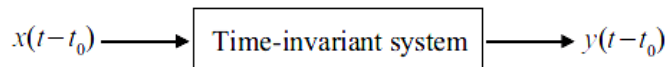


Figure 2.3 Property of a time-invariant system [119]

To solve many engineering problems, the response of a linear time invariant system to some input signal is needed. If the input signal can be broken up into simple signals and the system response to these simple signals is known, then it can be predicted how the system behavior. Therefore anything that can break a signal down into its constituent parts would be very useful. One such tool is the **Fourier series**. In applications related to vibrations, the Fourier transform is typically thought of as decomposing a signal into its component frequencies and

their amplitudes. This tool helps to navigate between the time and the frequency domains. The frequency domain tends to be more useful than the time domain because mathematics is simpler in the frequency domain. One immediate advantage of the Fourier Transform is that through its use, differential operations (differentiation and integration) in the time domain are converted into simpler algebraic operations (multiplication and division). The following example shall clarify the above statements

If we have a continuous signal $x(t) = A \sin(\omega_0 t)$ and we take the continuous Fourier transform to find its frequency content we get is two impulses in the frequency domain at the frequency of the sine wave as shown in Fig 2.4.

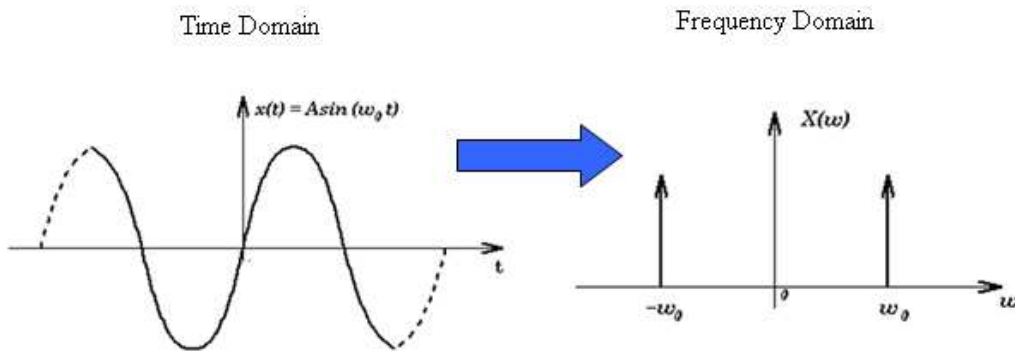


Figure 2.4 Representation of a signal in time and frequency domains [120]

The above example deals with only continuous signals, so what to do if discrete signals are encountered? This is where sampling comes into play. Sampling simply means recording a signal. The only way that a computer can handle a continuous (analog) signal is by sampling it. To improve the resolution of discrete signals, first thing we want is to sample them. This is equivalent to multiplying the time signal by a series of impulses $c(t)$ as shown in Fig 2.5.

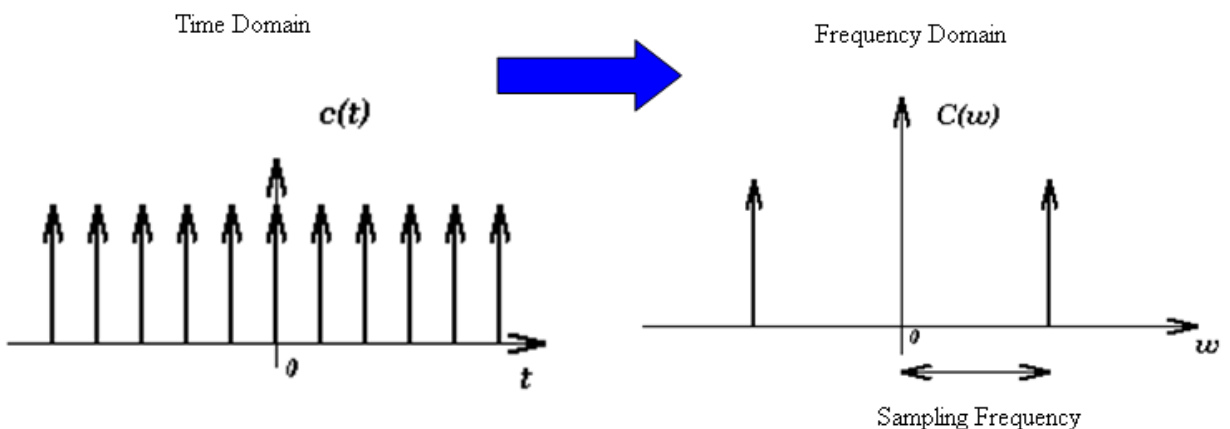


Figure 2.5 Multiplying the time signal by a series of impulses $c(t)$ which has the frequency response of the series of impulses [120]

However this can lead to aliasing distortion, which is an error that can enter into computation in both the time and the domain frequency domain, depending on the domain in which the results are presented. In vibration signal analysis, a sufficiently small sample step should be chosen in order to reduce aliasing distortion in the frequency domain, depending on the frequency of interest in the analyzed signal. This means that a continuous signal must be discretely sampled at least twice the frequency of the highest frequency in the signal. The

sampling frequency has to be at least twice the maximum frequency in the continuous signal, that is the absolute maximum frequency, not just the twice the maximum frequency. This fact is known as **Shannon's Sampling Theorem**, and the limiting cut off frequency is called the **Nyquist Frequency**.

In digital processing of vibration signals, sampled signals are truncated to eliminate less significant parts. The effect of direct truncation of a signal $x(t)$ on its Fourier Spectrum is shown in Fig 2.6. In the time domain, truncation is accomplished by multiplying $x(t)$ by the boxcar function $b(t)$. This is equivalent to a convolution in the frequency domain explained later on. This introduces ripples (side lobes) into the side spectrum. The resulting error is known as the leakage or truncation error. Similar leakage effects arise in the time domain. The truncation error can be reduced by suppressing the side lobes which requires modification of the truncation function (window) from the boxcar shape $b(t)$ to a more desirable shape.

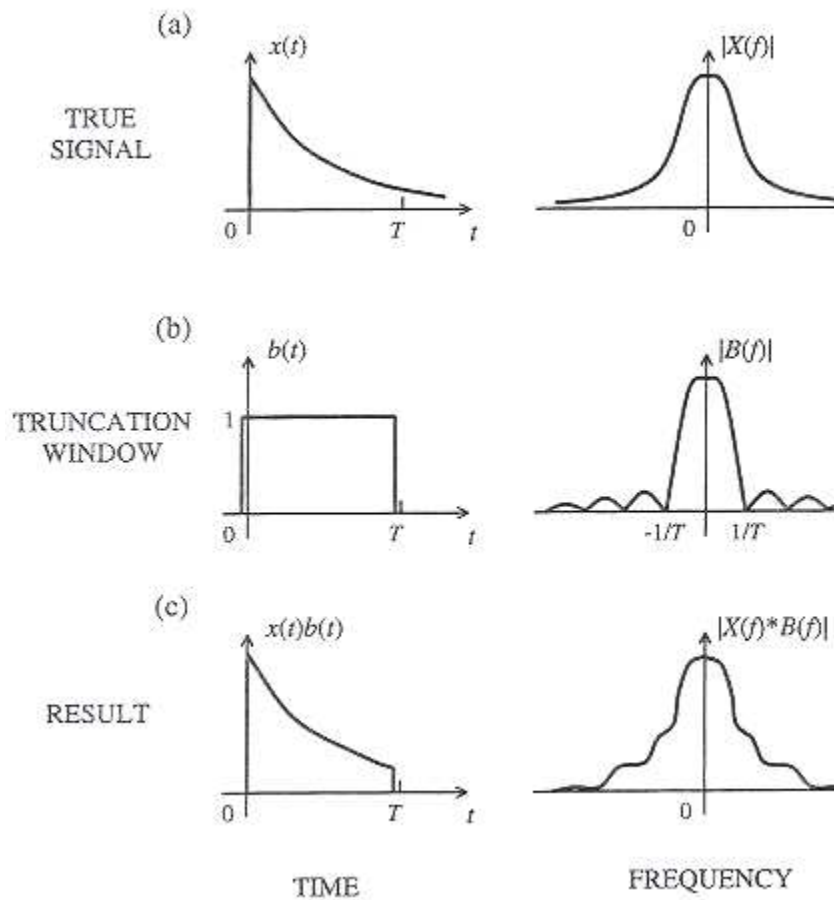


Figure 2.6 Illustration of truncation error: (a) signal and its frequency spectrum; (b) a rectangular (boxcar) window and its frequency spectrum; and (c) truncated signal and its frequency spectrum [117]

Window functions other than the boxcar functions are widely used to suppress the side lobes (leakage error). A graphical comparison of commonly used window types is given in Fig 2.7. Hanning windows are very popular in practical applications. A related window is the Hamming window, which is simply a Hanning window with rectangular cutoffs at the two ends. In Figure (2.7b), one observes that the frequency domain weight of each window varies with the frequency range of interest. Characteristics of the signal that is being analyzed and

also the nature of the system that generates the signal should be considered in choosing an appropriate truncation window. Hanning window is recommended for use with lightly damped system.

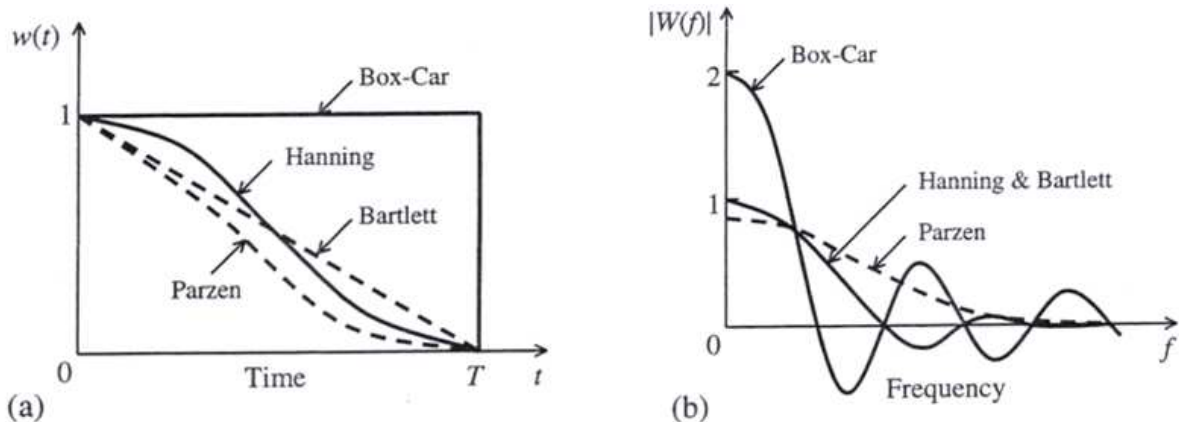


Figure 2.7 Some common window functions: (a) time domain function, and (b) frequency spectrum [117]

The time-invariant system is normally described by a particular feature, namely their response to an ideal impulse and their corresponding behavior is then the impulse response. We shall denote this by the symbol $h(t)$. Because the system is linear, therefore this rather ‘abstract’ notion turns out to be very useful in predicting the response of the system to any arbitrary input. This is expressed by the convolution of input $x(t)$ and system $h(t)$ sometimes abbreviated as

$$y(t) = h(t) * x(t) \quad (2.1)$$

where ‘*’ denotes the convolution operation. Expressed in this form the system box is filled with the characterization $h(t)$ and the (mathematical) mapping or transformation from the input $x(t)$ to the response $y(t)$ is the convolution integral.

System identification now becomes the problem of measuring $x(t)$ and $y(t)$ and deducing the impulse response function $h(t)$. Since we have three quantitative terms in the relationship (2.1), but assuming that we know two of them, then, in principle at least, we should be able to find the third. Life becomes considerably easier if we apply a transformation that maps the convolution expression to a multiplication. One such transformation is the Fourier transform as discussed above. Taking the Fourier transform of the convolution in Equation (2.1) produces

$$Y(f) = H(f) \times X(f) \quad (2.2)$$

where f denotes frequency, and $X(f)$, $H(f)$ and $Y(f)$ are the transforms of $x(t)$, $h(t)$ and $y(t)$. This achieves the unraveling of the input–output relationship as a straightforward multiplication in the frequency domain. In this form the system is characterized by the quantity $H(f)$ which is called the system frequency response function (FRF). The problem of ‘system identification’ now becomes the calculation of $H(f)$: that is, divide $Y(f)$ by $X(f)$, i.e. divide the Fourier transform of the output by the Fourier transform of the input. If the Laplace transform is taken, then by a similar argument as for the Fourier transform, it becomes

$$Y(s) = H(s)X(s) \quad (2.3)$$

where $s = j\omega$ and $\omega = 2\pi f$

The ratio $Y(s)/X(s) = H(s)$ is called the transfer function of the system. The relationships between the impulse response function, the frequency response function and the transfer function are depicted in Fig 2.8. Note that $H(\omega)$ can be obtained by $H(s)$ on the imaginary axis in the s -plane (shown ahead in Fig), i.e. the Fourier transform can be considered as the Laplace transform taking the values on the imaginary axis only.

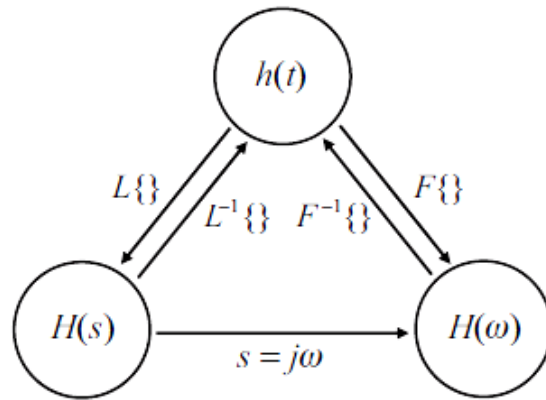


Figure 2.8 Relationship between $h(t)$, $H(\omega)$ and $H(s)$ [120]

Reality interferes in the form of ‘uncertainty’. The measurements $x(t)$ and $y(t)$ are often not measured perfectly – disturbances or ‘noise’ contaminates them – in which case the result of dividing two transforms of contaminated signals will be of limited and dubious value.

This is where ‘optimization’ comes in. We try and find a relationship between $x(t)$ and $y(t)$ that seeks a ‘systematic’ link between the data points which suppresses the effects of the unwanted disturbances. The procedure we use to obtain this fit is seen in Fig 2.9 where the slope of the straight line is adjusted until the match to the data seems best.

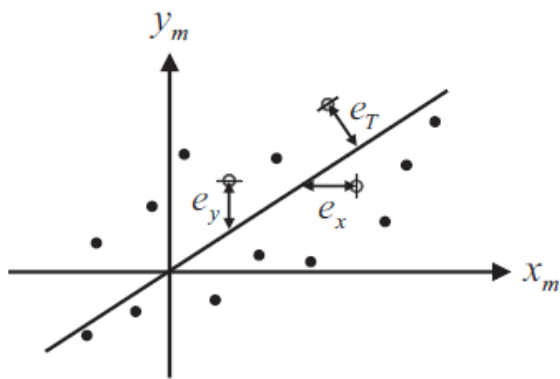


Figure 2.9 A linear fit to the measured data x_m and y_m [120]

Just a reminder that the major aim of this chapter is to show how frequency response function (FRF) measurements are related to the structure’s natural frequencies and damping. As it has

been explained that how the frequency response function is identified in a physical system and in the end it is a ratio of the Fourier transform of the output to the Fourier transform of the input, now a basic example of a single degree of freedom system will be used to define some standard terminologies.

2.2 Single Degree of Freedom System

2.2.1 Basic Theory

The general mathematical representation of a single degree of freedom system is expressed using Newton's second law in Equation 2.4, and is represented schematically in Fig 2.10.

$$M\ddot{x}(t) + C\dot{x}(t) + Kx(t) = f(t) \quad (2.4)$$

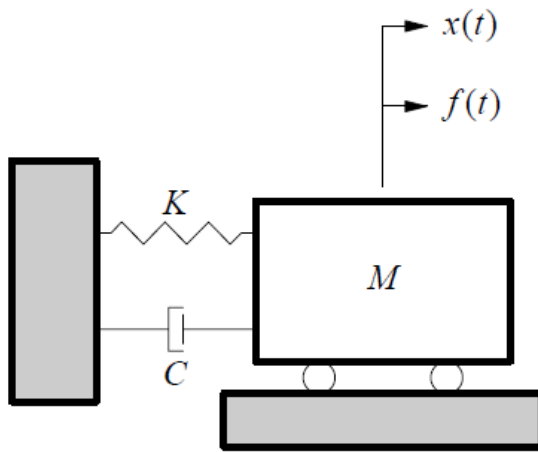


Figure 2.10 Single Degree of Freedom System [117]

Equation 2.4 is a linear, time invariant, second order differential equation, where \$x\$ is considered as the displacement of the mass. The total solution to this problem involves two parts as follows:

$$x(t) = x_c(t) + x_p(t)$$

where,

$$x_c(t) = \text{Transient portion}$$

$$x_p(t) = \text{Steady state portion}$$

By setting \$f(t)=0\$ the homogeneous (transient) form of Equation 2.4 can be solved

$$M\ddot{x}(t) + C\dot{x}(t) + Kx(t) = 0 \quad (2.5)$$

From differential equation theory, the solution can be assumed to be of the form $x_c(t) = Xe^{st}$, where s is a constant to be determined. Taking appropriate derivatives and substituting into Equation 2.5 yields:

$$(Ms^2 + Cs + K)Xe^{st} = 0$$

Thus, for a non-trivial solution ($Xe^{st} \neq 0$):

$$s^2 + (C/M)s + (K/M) = 0 \quad (2.6)$$

Equation 2.6 is the system's characteristic equation, whose roots λ_1 and λ_2 (λ = system pole) are:

$$\lambda_{1,2} = -\frac{C}{2M} \pm \sqrt{\left(\frac{C}{2M}\right)^2 - \left(\frac{K}{M}\right)}$$

Thus the homogeneous solution of Equation 2.4 is:

$$x_c(t) = X_1 e^{\lambda_1 t} + X_2 e^{\lambda_2 t}$$

where X_1 and X_2 are constants determined from the initial conditions imposed on the system at $t = 0$. The particular solution (steady state) is a function of the form of the forcing function. If the forcing function is a pure sine wave of a single frequency, the response will also be a sine wave of the same frequency.

2.2.2 Laplace Domain Theory

Equation 2.4 is the time domain representation of the system in Fig 2.9. An equivalent equation of motion may be determined for the Laplace or s domain. This representation has the advantage of converting a differential equation to an algebraic equation. This is accomplished by taking the Laplace transform of Equation 2.4, thus:

$$L\{M\ddot{x} + C\dot{x} + Kx\} = M(s^2 X(s) - sx(0) - \dot{x}(0)) + C(sX(s) - x(0)) + KX(s)$$

$$L\{M\ddot{x} + C\dot{x} + Kx\} = (Ms^2 + Cs + K)X(s) - Msx(0) - M\dot{x}(0) - Cx(0)$$

$$L\{f(t)\} = F(s)$$

Thus Equation 2.4 becomes:

$$[Ms^2 + Cs + K]X(s) = F(s) + (Ms + C)x(0) + M\dot{x}(0) \quad (2.7)$$

where

$x(0)$ is the initial displacement at time $t = 0$

$\dot{x}(0)$ is the initial velocity at time $t = 0$

If the initial conditions are zero, then Equation 2.10 becomes

$$[Ms^2 + Cs + K]X(s) = F(s) \quad (2.8)$$

Let $B(s) = Ms^2 + Cs + K$. $B(s)$ is referred to as the system impedance. Then Equation 2.8 becomes:

$$B(s)X(s) = F(s) \quad (2.9)$$

Equation 2.9 is an equivalent representation of Equation 2.4 in the Laplace domain. The Laplace domain (s domain) can be thought of as complex frequency ($s = \sigma + j\omega$). Therefore, the quantities in Equation 2.9 can be thought of as follows:

$F(s)$ - Laplace domain (complex frequency) representation of the forcing function $f(t)$

$X(s)$ - Laplace domain (complex frequency) representation of the system response $x(t)$

Equation 2.12 states that the system response $X(s)$ is directly related to the system forcing function $F(s)$ through the quantity $B(s)$. If the system forcing function $F(s)$ and its response $X(s)$ are known; $B(s)$ can be calculated. That is:

$$B(s) = \frac{F(s)}{X(s)}$$

More frequently one would like to know what the system response is going to be due to a known input $F(s)$, or:

$$X(s) = \frac{F(s)}{B(s)} \quad (2.10)$$

By defining $H(s) = \frac{1}{B(s)}$, Equation 2.10 becomes :

$$X(s) = H(s)F(s) \quad (2.11)$$

The quantity $H(s)$ is known as the system transfer function as discussed in the previous section, but the difference being that this time we will be in terms of modal parameters that describe a system dynamically. In other words, a transfer function relates the Laplace transform of the system input to the Laplace transform of the system response. From Equations 2.8 and 2.11, the transfer function can be defined as follows by assuming the initial conditions to be zero.

$$H(s) = \frac{X(s)}{F(s)} = \frac{1/M}{s^2 + (C/M)s + (K/M)} \quad (2.12)$$

The denominator term is referred to as the system characteristic equation. The roots of the characteristic equation are:

$$\lambda_{1,2} = -\frac{C}{2M} \pm \sqrt{\left(\frac{C}{2M}\right)^2 - \left(\frac{K}{M}\right)}$$
(2.13)

Note that the above definition of the transfer function establishes a form of an analytical model that can be used to describe the transfer function. This analytical model involves a numerator and denominator polynomial with scalar coefficients. For the single degree of freedom case, the numerator polynomial is zero-th order and the denominator polynomial is second order.

2.2.3 Analytical Models and Different Representations

Before dwelling into the analytical models and the different types of representations, first of all some basic terms related to damping will be provided.

Critical Damping

Critical damping C_c is defined as being the damping which reduces the radical in the characteristic equation to zero.

$$(C_c / 2M)^2 - (K / M) = 0$$

$$(C_c / 2M) = \sqrt{K / M} = \Omega_1$$

$C_c = 2M\Omega_1$ = critical damping coefficient

Ω_1 = undamped natural frequency (rad/s)

Fraction of Critical Damping – Damping Ratio (Zeta)

The fraction of critical damping or damping ratio, ζ , is the ratio of the actual system damping to the critical system damping.

$$\zeta_1 = C/C_c$$

The roots of characteristic Equation 2.13 can now be written as:

$$\lambda_{1,2} = \left(-\zeta_1 \pm \sqrt{\zeta_1^2 - 1}\right)\Omega_1$$
(2.14 a)

$$\lambda_{1,2} = \left(-\zeta_1 \pm \sqrt{\zeta_1^2 - 1}\right)\Omega_1$$
(2.14 b)

Systems can be classified depending on their damping ratios. That is:

- Over-damped system: $\zeta_1 > 1$
- Critically damped system: $\zeta_1 = 1$
- Under-damped system: $\zeta_1 < 1$

Further details and the time domain responses of these three systems are easily available in scientific literature [117,122]

For most real structures, unless active damping systems are present, the damping ratio is rarely greater than ten percent. For this reason, all further discussion will be restricted to under-damped systems $\zeta_1 < 1$. For an under-damped system, the roots of the characteristic equation can be written as:

$$\lambda_{1,2} = \sigma_1 \pm j\omega_1$$

where:

$$\sigma_1 = \text{damping ratio}$$

$$\omega_1 = \text{damped natural frequency}$$

Laplace Plane (s-Plane) Representation

Note that for this case λ_2 is always the complex conjugate of λ_1 . Therefore, the λ_2 notation will be replaced in further equations by λ_1^* . Using Equation 2.14 the above parameters can be related to the damping ratio (ζ_1) and the undamped natural frequency (Ω_1) as follows:

$$\zeta_1 = -\frac{\sigma_1}{\omega_1^2 + \sigma_1^2}$$

$$\sigma_1 = -\zeta_1 \Omega_1$$

$$\Omega_1 = \sqrt{\omega_1^2 + \sigma_1^2}$$

The transfer function $H(s)$ can now be rewritten as a product of the roots (in factored) form as follows:

$$H(s) = \frac{1/M}{(s - \lambda_1)(s - \lambda_1^*)} \quad (2.15)$$

where:

$$\lambda = \text{complex conjugate pole of the transfer function}$$

$$\lambda_1 = \sigma_1 + j\omega_1$$

$$\lambda_1^* = \sigma_1 - j\omega_1$$

The poles of the single degree of freedom system can also be viewed, looking down on the s-plane as shown in Fig 2.11:

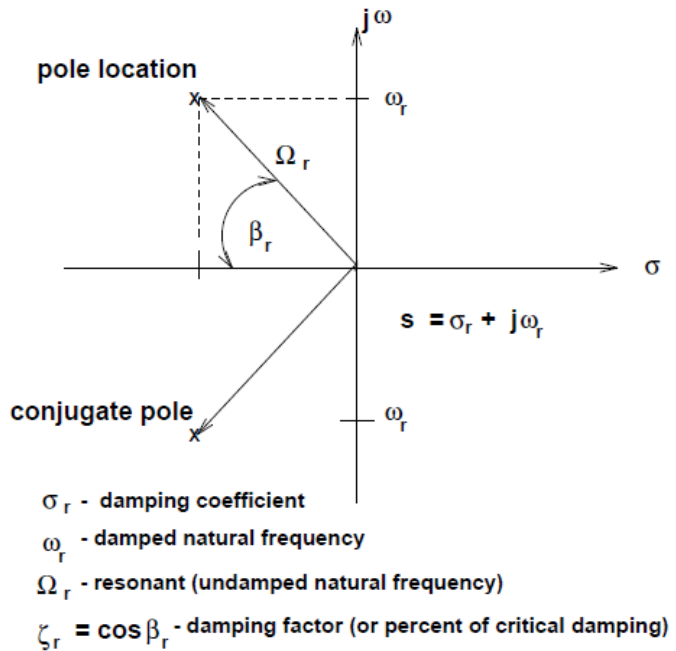


Figure 2.11 *s*-plane (Laplace Plane) pole location [118]

Analytical Model: Scalar Polynomial

One popular method of representing the transfer function involves a scalar polynomial representation in the numerator and denominator. For the single degree of freedom case, this is very simple concept that is directly based upon the physical characteristics (M,C,K) of the system. Generalizing Equation (2.12) yields:

$$H(s) = \frac{\beta_0}{a_2(s)^2 + a_1(s)^1 + a_0(s)^0} \quad (2.16)$$

This can be rewritten:

$$H(s) = \frac{\beta_0}{\sum_{k=0}^2 a_k(s)^k} \quad (2.17)$$

This model serves as the basis for many modal parameter estimation methods and is a common formulation utilized in control theory applications.

Analytical Model : Partial Fraction

The concept of residues can now be discussed in terms of the partial fraction expansion of the transfer function equation. This is just one common approach to determining the residues. Another popular method involves a polynomial representation in the numerator and denominator. Equation 2.15 can be expressed in terms of partial fractions:

$$H(s) = \frac{1/M}{(s - \lambda_1)(s - \lambda_1^*)} = \frac{c_1}{(s - \lambda_1)} + \frac{c_2}{(s - \lambda_1^*)} \quad (2.18)$$

The residues of the transfer function are defined as being the constants c_1 and c_2 . The terminology and development of residues comes from the evaluation of analytic functions in complex analysis. As will be shown later, the residues of the transfer function are directly related to the amplitude of the impulse response function. The constants c_1 and c_2 (residues) can be found by multiplying both sides of Equation 2.15 by $(s - \lambda_1)$ and evaluating the result at $s = \lambda_1$. Thus:

$$\left. \frac{1/M}{(s - \lambda_1^*)} \right|_{s=\lambda_1} = c_1 + \left[\frac{c_2(s - \lambda_1)}{(s - \lambda_1^*)} \right]_{s=\lambda_1}$$

$$\frac{1/M}{(\lambda_1 - \lambda_1^*)} = c_1$$

Thus:

$$c_1 = \frac{1/M}{(\sigma_1 + j\omega_1) - (\sigma_1 - j\omega_1)} = \frac{1/M}{j2\omega_1} = A_1$$

Similarly:

$$c_2 = \frac{1/M}{-j2\omega_1} = A_1^*$$

In general, for a multiple degree of freedom system, the residue A_1 can be a complex quantity. But, as shown for a single degree of freedom system A_1 is purely imaginary.

Therefore:

$$H(s) = \frac{A_1}{(s - \lambda_1)} + \frac{A_1^*}{(s - \lambda_1^*)} \quad (2.19)$$

Frequency Response Function Representation

The frequency response function is the transfer function (surface) evaluated along the $j\omega$ (frequency) axis. Thus, from the previously derived equations:

Polynomial Model

$$H(s)|_{s=j\omega} = H(\omega) = \frac{\beta_0}{a_2(j\omega)^2 + a_1(j\omega)^1 + a_0(j\omega)^0} \quad (2.20 \text{ a})$$

Partial Fraction Model

$$\begin{aligned}
 H(s)|_{s=j\omega} &= H(\omega) = \frac{A_1}{(j\omega - \lambda_1)} + \frac{A_1^*}{(j\omega - \lambda_1^*)} \\
 H(\omega) &= \frac{A_1}{(j\omega - \sigma_1 - j\omega_1)} + \frac{A_1^*}{(j\omega - \sigma_1 + j\omega_1)} \\
 H(\omega) &= \frac{A_1}{j(\omega - \omega_1) - \sigma_1} + \frac{A_1^*}{j(\omega + \omega_1) - \sigma_1}
 \end{aligned} \tag{2.20 b}$$

From an experimental point of view, when one talks about measuring a transfer function, the frequency response function is actually being measured. The value of the frequency response function at the damped natural frequency of the system is:

$$H(\omega_1) = -\frac{A_1}{\sigma_1} + \frac{A_1^*}{j2\omega_1 - \sigma_1} \tag{2.21}$$

which can be approximated as:

$$H(\omega_1) = -\frac{A_1}{\sigma_1}$$

The second term on the right of Equation 2.21 approaches zero as ω_1 gets large. In other words, the contribution of the negative frequency portion of the frequency response function is negligible. Therefore, many single degree of freedom models are represented as:

$$H(\omega) \approx \frac{A_1}{(j\omega - \lambda_1)} \tag{2.22}$$

Another way of interpreting Equation 2.20 is that the value of the transfer function, for a single degree of freedom system, at a particular frequency (ω) is a function of the residue, damping, and damped natural frequency.

Impulse Response Function Representation

The impulse response function of the single degree of freedom system can be determined from Equation 2.20 assuming that the initial conditions are zero and that $F(s) = 1$ for a system impulse. Thus:

$$X(s) = \frac{A_1}{(s - \lambda_1)} + \frac{A_1^*}{(s - \lambda_1^*)}$$

$$x(t) = L^{-1}\{X(s)\}$$

$$x(t) = A_1 e^{\lambda_1 t} + A_1 * e^{\lambda_1 * t} = h(t) \text{ = impulse response}$$

$$x(t) = e^{\sigma_1 t} [A_1 e^{j\omega_1 t} + A_1 e^{-j\omega_1 t}] e^{j\omega_1 t}$$

Thus, using Euler's formula for $e^{j\omega_1 t}$ and $e^{-j\omega_1 t}$, the residue A_1 controls the initial amplitude of the impulse response, the real part of the pole is the decay rate and the imaginary part of the pole is the frequency of oscillation. Fig 2.12 and Fig 2.13 illustrate the frequency response and impulse response functions respectively, for a single degree of freedom system.

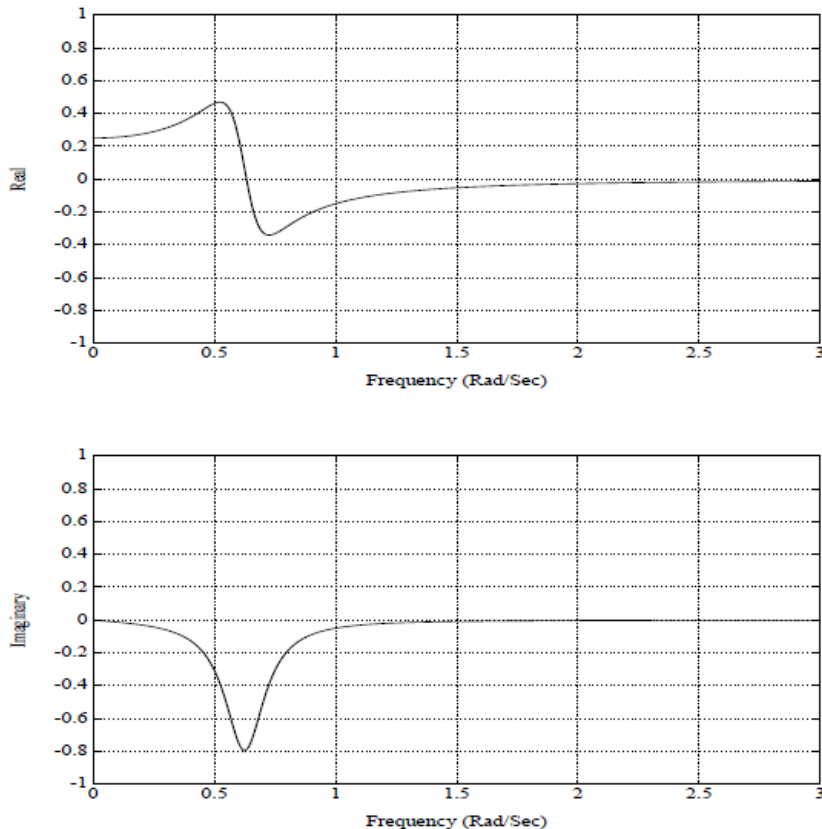


Figure 2.12 Frequency response function (SDOF) with the real and imaginary part [117]

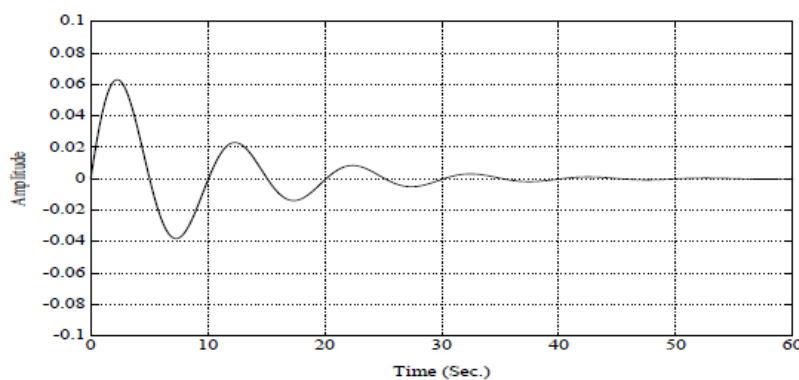


Figure 2.13 Impulse response function (SDOF) [117]

2.2.4 Change of Physical Parameters

While it is not always possible to alter the physical parameter (mass, stiffness and/or damping) of a system and is very difficult to practically alter one physical parameter (mass, for example) without altering another physical parameter (stiffness, for example), it is still important to understand how a change in physical parameter will affect the system characteristics. Figures (2.14), (2.15) and (2.16) show how the frequency response function will be affected due to change in one physical parameter at a time.

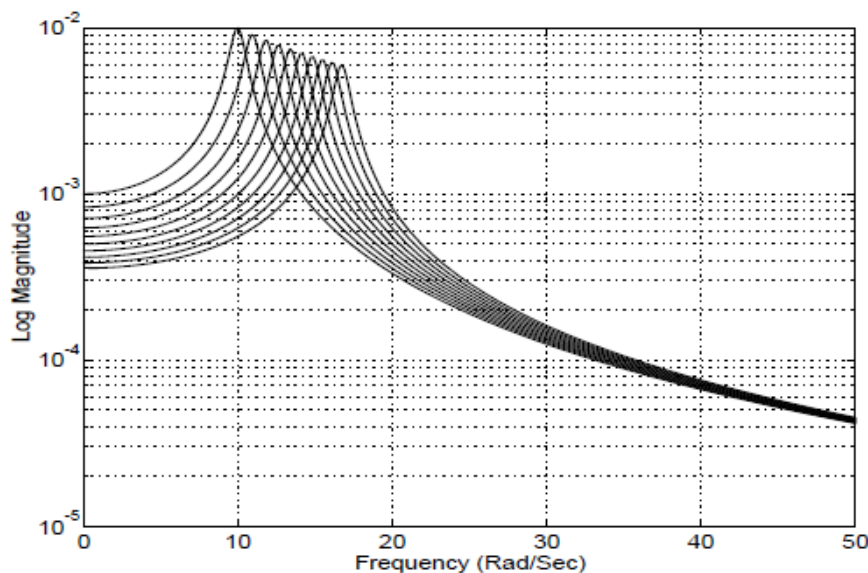


Figure 2.14 Change of stiffness (SDOF) [120]

Note that a change in stiffness affects both the resonant frequency as well as the system characteristic at low frequency. This dominance of stiffness at low frequency is the reason that this region of the frequency response function is known as the stiffness, or more accurately, compliance line.

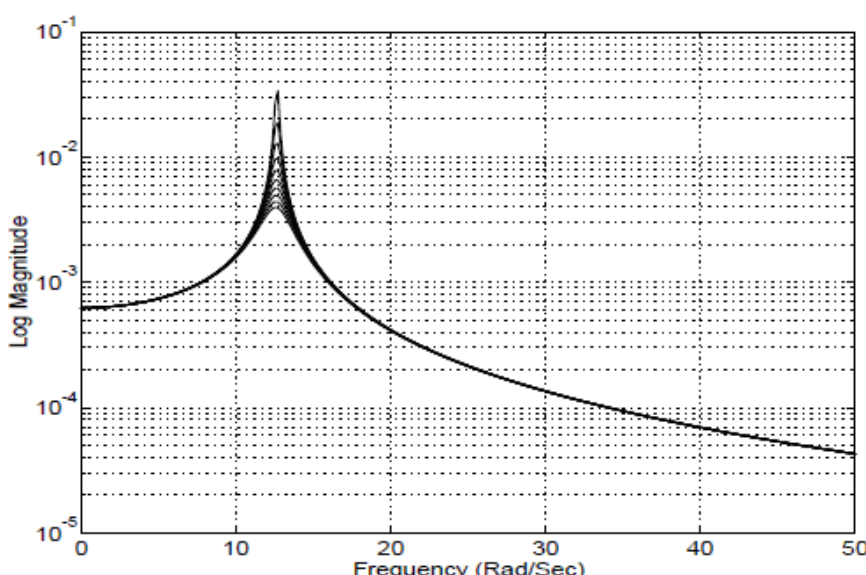


Figure 2.15 Change of damping (SDOF) [120]

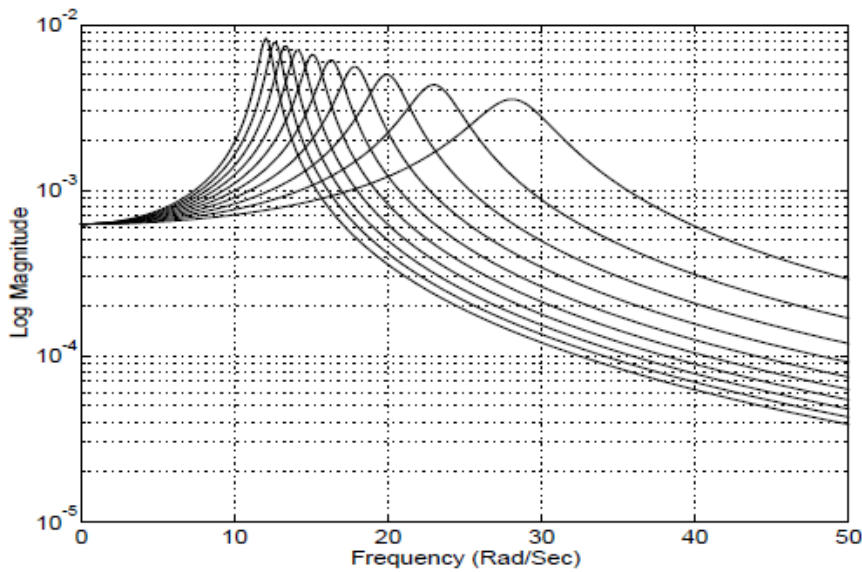


Figure 2.16 Change of mass (SDOF) [120]

Note that a change in mass affects both the resonant frequency as well as the system characteristic at high frequency. This dominance of mass at high frequency is the reason that this region of the frequency response function is known as the mass line. Also note that as the mass changes, the apparent damping (sharpness of the resonant frequency) changes accordingly. A change in mass affects both the resonant frequency, the system characteristic

$$\text{at high frequency as well as the fraction of critical damping } \zeta_1 = \frac{C}{C_c} = \frac{C}{2M\Omega_1}.$$

2.3 Experimental Modal Analysis

Experimental modal analysis is the process of determining the modal parameters (frequencies, damping factors, modal vectors and modal scaling) of a linear, time invariant system by way of an experimental approach. The modal parameters may be determined by analytical means, such as finite element analysis, and one of the common reasons for experimental modal analysis is the verification/correction of the results of the analytical approach (model updating). Often, though, an analytical model does not exist and the modal parameters determined experimentally serve as the model for future evaluations such as structural modifications. Predominately, experimental modal analysis is used to explain a dynamics problem, vibration or acoustic that is not obvious from intuition, analytical models, or previous similar experience. It is important to remember that most vibration and/or acoustic problems are a function of both the forcing functions (and initial conditions) and the system characteristics described by the modal parameters. Modal analysis alone is not the answer to the whole problem but is often an important part of the process. Likewise, many vibration and/or acoustic problems fall outside of the assumptions associated with modal analysis (linear superposition as considered in our work). For these situations, modal analysis may not be the right approach and an analysis that focuses on the specific characteristics of the problem will be more useful. Experimental modal analysis is useful in the following domains with regards to vibrations

- Design of Mechanical Systems
- Diagnosis of Mechanical Systems

- Control of Mechanical Systems

The typical steps of experimental modal analysis are shown in Fig 2.17.

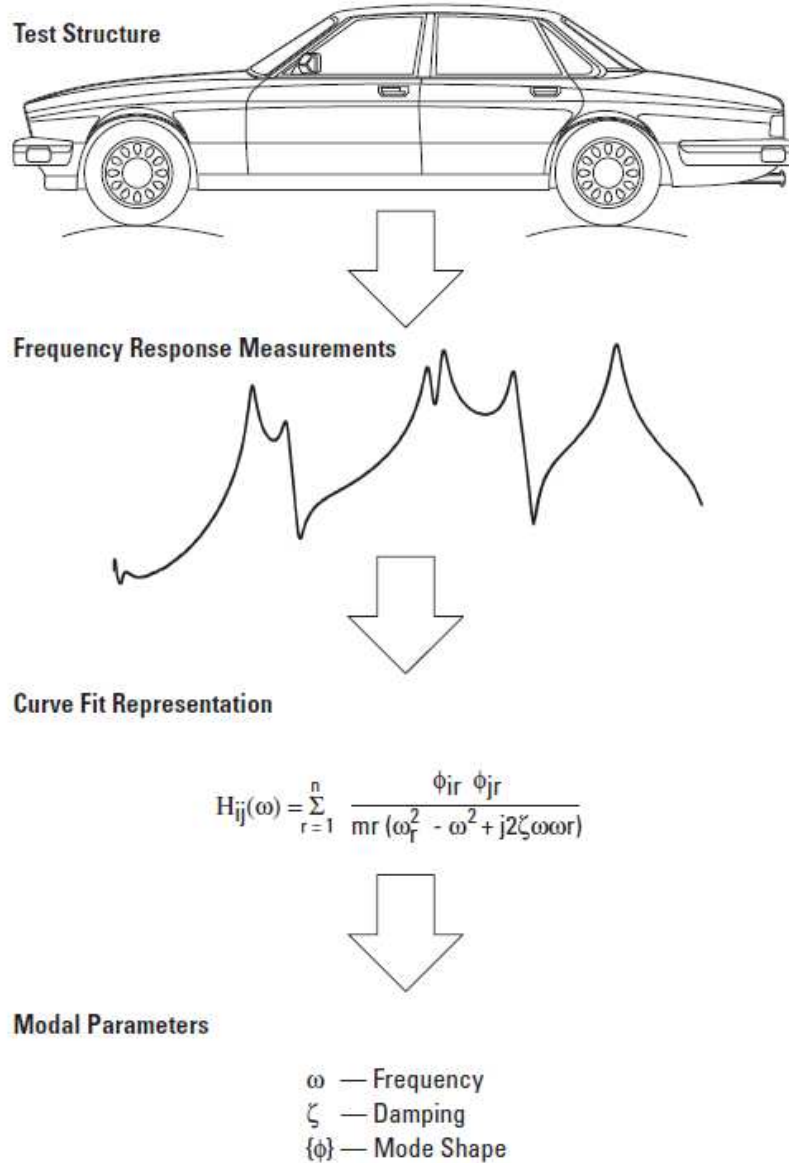


Figure 2.17 Typical flow of an experimental modal analysis [119] - Aim is to extract the modal parameters from Frequency Response Functions obtained through experiments

2.3.1 Types of Experimental Modal Testing

The basic methodology of a modal test is very simple. First the structure to be tested is excited with the help of ambient energy, an external shaker or embedded actuators. Next the response of that structure is measured by using accelerometers, velocity-meters or laser vibrometers in order to monitor the structural dynamic responses. The experimental modal testing can be classified into two main types:

Impact Testing

Impact testing is a fast, convenient and low cost way of finding the modes of machines and structures. Impact testing is depicted in Fig 2.18. In impact testing, the output is fixed and FRFs are measured for multiple inputs, this corresponds to measuring elements from a single row of the FRF matrix. To perform impact test, an impact hammer with a load cell attached to its head is used to measure the impact force. Accelerometers are employed to measure the response acceleration at various measurement points. A multi-channel FFT analyzer is used to compute the frequency response functions. A curve-fitting algorithm integrated in the data acquisition software is used to estimate the modal parameters from experimentally obtained frequency response functions.

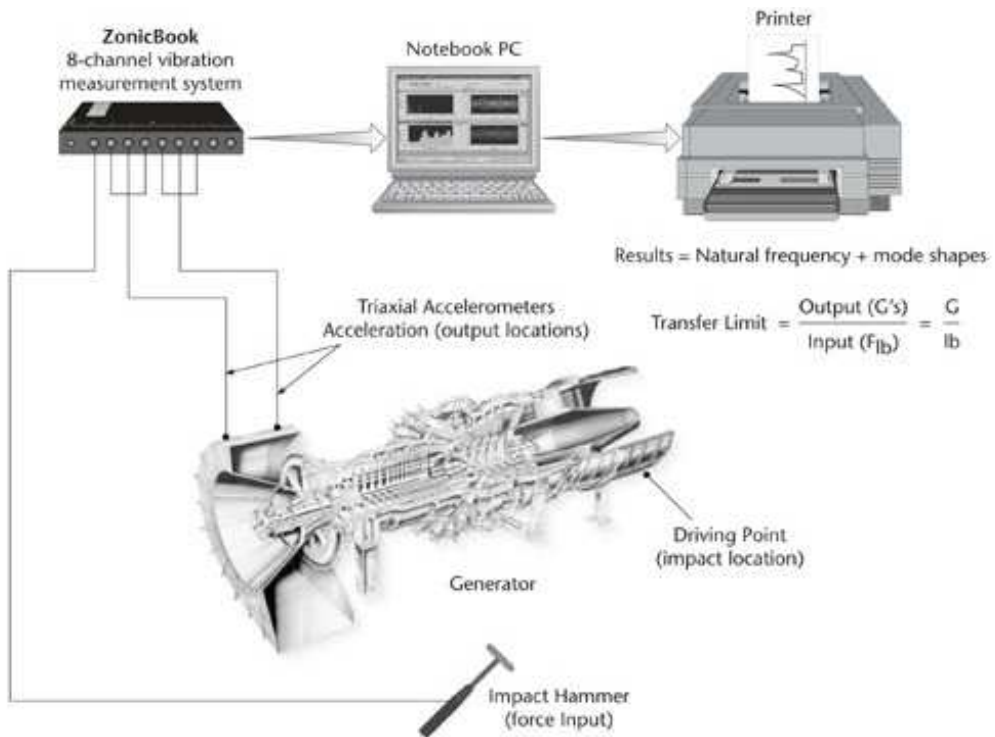


Figure 2.18 Impact testing procedure [122] - Excitation is provided at multiple points by an impact hammer and the response is measured with the help of accelerometers

The drawbacks of impact testing are that all structures cannot be impact tested e.g., structures with delicate surfaces, or because of its limited frequency range and low energy density over a wide spectrum, the impacting force is not sufficient to adequately excite the modes of interest.

Shaker Testing

Another way of dynamically testing mechanical structures is with the help of one or more shakers. A shaker is usually attached to the structure using a stinger (long slender rod), so that the shaker will only impart force to the structure along the axis of the stinger, the axis of force measurement. A load cell is then attached between the structure and the stinger to measure the excitation force. Common types of shakers are electro-dynamic and hydraulic shakers. A typical shaker test is shown in Fig 2.19.

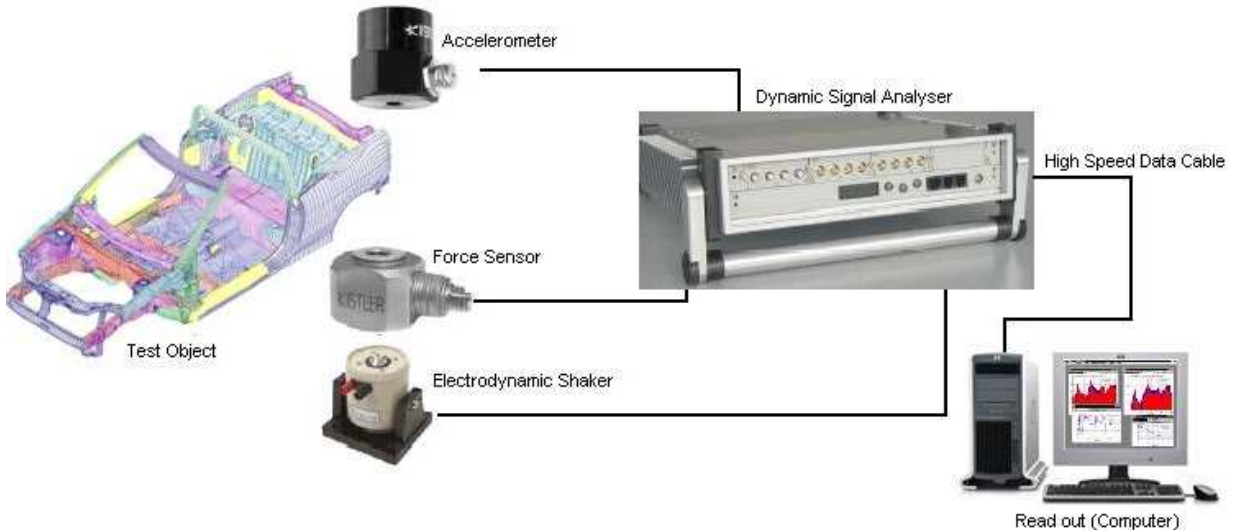


Figure 2.19 Shaker Test Set-up [122] - Excitation is provided at a single point by a shaker and response is measured at multiple points with the help of accelerometers

The vibration tests in this thesis are based on shaker testing. The beam-type test specimens are excited at their centers by a shaker, and the response is measured at multiple points by a high performance laser vibrometer. The experimental procedure is explained in detail in chapter 3 in Section 3.2.

2.3.2 Types of Excitation Signals

Excitation signals in vibration testing can be categorized into three main categories as shown in Table 2.1.

Table 2.1 Categories of excitation functions that can be used in modal analysis [118]

Periodic Excitation	Random Excitation	Transient Excitation
Stepped Sine (Sine-Dwell)	True Random	Burst Sine
Slow Sine Sweep	Burst Random (White Noise)	Burst Random
Periodic	Narrow Band Random	Chirp
Pseudo Random		Impulse
Periodic random		

Details on all these types of excitations can be found easily in scientific literature [117-122]. The authors will only explain those excitations (burst random and sine-dwell) that have been used for carrying out vibration testing.

Burst Random Excitation

Burst random excitation has the combined advantages of both pure random and pseudo random testing. Its signals are leakage free and use with spectrum averaging removes non-linearity from the frequency response functions. It consists of short sections of an underlying continuous signal followed by a period of zero input. The duration of burst is selected to allow the damping out of the response by the end of the measurement period (to avoid leakage errors). A burst random excitation signal along with its response is shown in Fig 2.20.

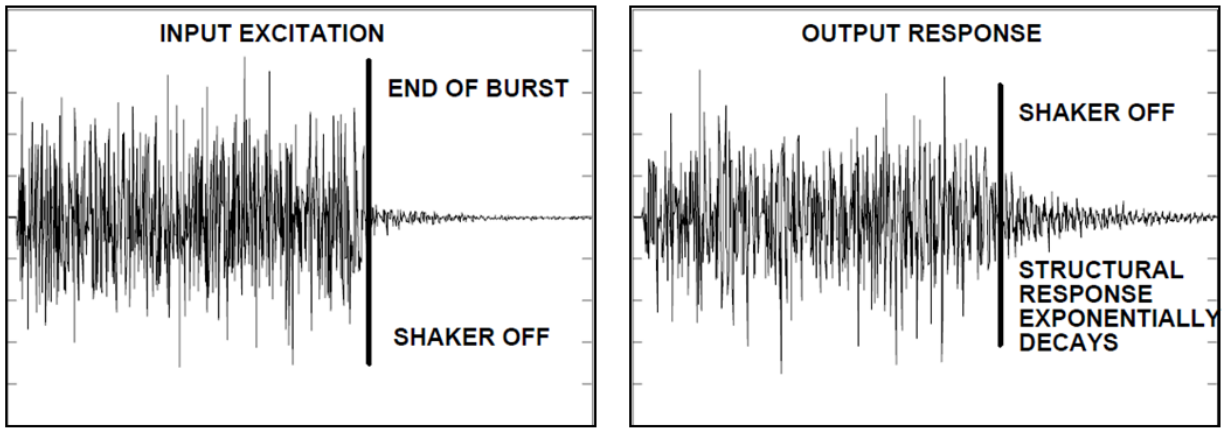


Figure 2.20 Burst random excitation signal and its response in the time domain – Burst random excitation signal is one of the two excitation signals used for the vibration tests in this thesis

Sine-Dwell Excitation

Sine dwell is the discrete version of a sine sweep. The frequency is not varied continuously, but is incremented by discrete amount at discrete time points i.e., step-by-step variation of the frequency of the excitation signal. This is shown graphically in Fig 2.21.

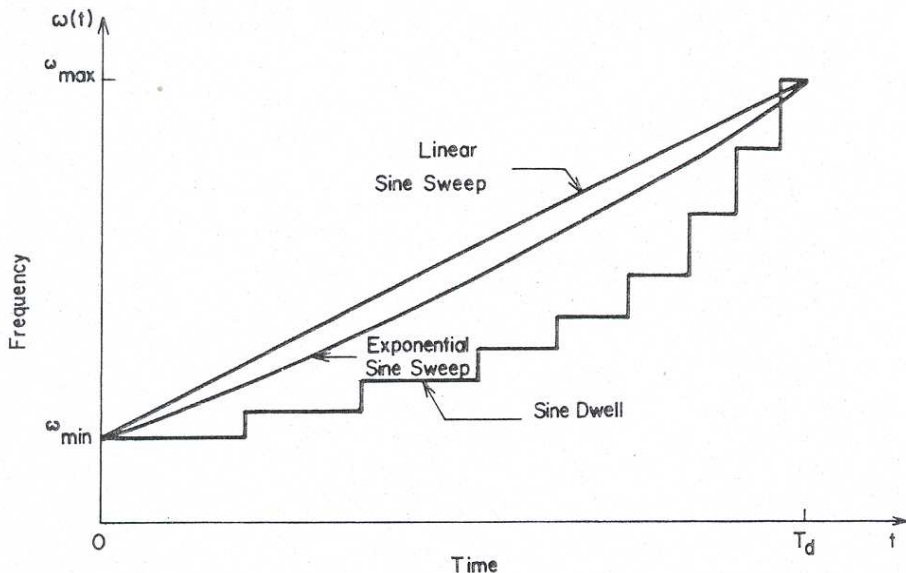


Figure 2.21 Frequency variations in some periodic excitation signals [117]

With sine-dwell excitation, it is necessary to ensure steady-state conditions before the measurements are made. The extent of the unwanted transient response will depend on:

- the proximity of a natural frequency
- the lightness of the damping
- the abruptness of the changeover

The major advantage of sine-dwell excitation over burst random is that it takes into account the effects of non-linearity [10], which enhances the quality and robustness of measurements on structures in the presence of damage. On the other hand, large acquisition times are a drawback of sine-dwell testing. To rectify the problem of lengthy measurements, small fine sweeps are localized around the resonances of interest and rapid coarse sweeps with large frequency increments are carried out for the less important portions of the frequency response functions (FRF) as shown in Fig 2.22.

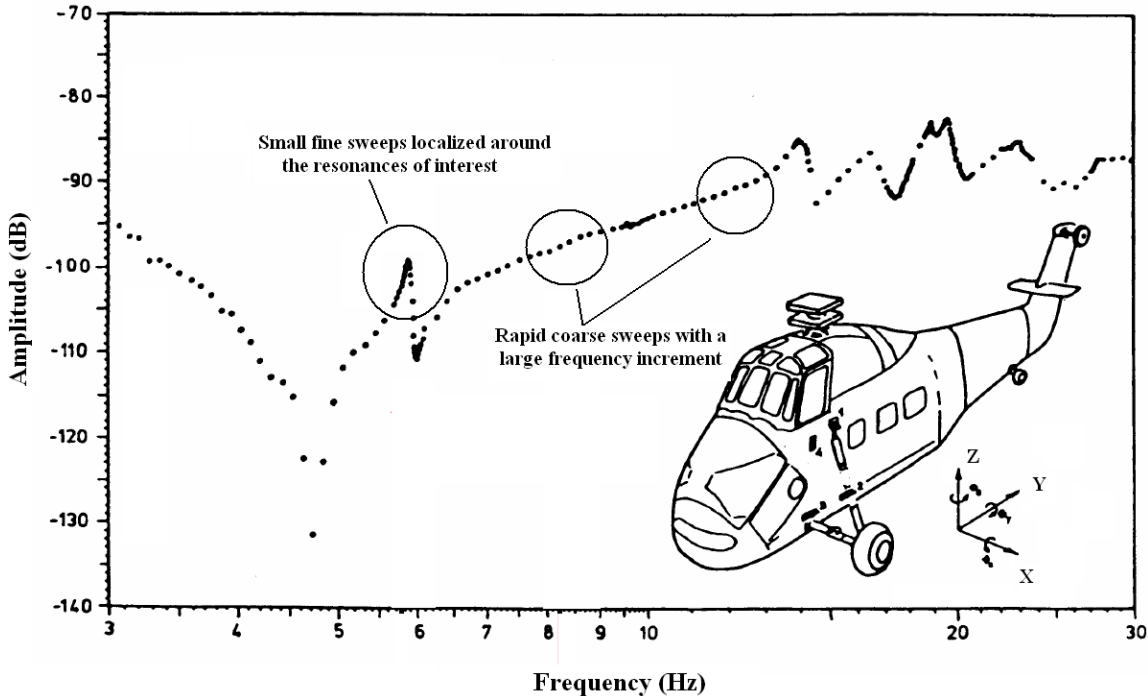


Figure 2.22 Sine dwell testing methodology i.e., fine sweeps around resonance and coarse sweeps for the rest [122]

A summary of the commonly used excitations in vibration testing is provided in Table 2.2.

Table 2.2 Summary of excitation functions with those highlighted that have been used for experimental modal analysis in this thesis [118]

	Sine Dwell	True random	Pseudo random	Fast sine	Burst Sine	Burst random
Minimize Leakage	No	No	Yes	Yes	Yes	Yes
Signal to noise ration	Very High	Fair	Fair	High	High	Fair
RMS to peak ratio	High	Fair	Fair	High	High	Fair
Test Measurement Time	Very Long	Long	Short	Long	Short	Short
Controlled Frequency Content	Yes	Yes*	Yes*	Yes*	Yes*	Yes*
Controlled Amplitude Content	Yes	No	Yes*	Yes*	Yes*	No
Removes Distortion	No	Yes	No	No	No	Yes
Characterize Nonlinearity	Yes	No	No	Yes	Yes	No

* Requires additional equipment or hardware

The two types of excitations used for vibration testing in the experimental part of this thesis are sine dwell and burst random excitations. The obvious advantage of burst random

excitation is its short measurement times [9] while sine-dwell excitation's main advantage is that it takes into account structural non-linearity [10].

2.3.3 Modal Parameter Estimation (Curve Fitting)

Curve-fitting is probably the most difficult part of the whole experimental modal analysis process for most people. Actually, it is better to refer to it as *modal parameter estimation*. The aim is to extract modal parameters (frequency, damping and mode shapes) from measured data. In general, curve fitting requires three steps:

- Determine how many modes k are represented in the data
- Estimate a pole $\lambda_i = \sigma_i + j\omega_i$ for each mode to obtain the damped natural frequency ω_i and damping ratio σ_i
- Estimate residues A_i for each mode in order to calculate the mode shape

It is important to know when to use a SDOF or MDOF technique. Fig 2.23 shows a variety of different situations for a two DOF system. Fig 2.23a shows modes that are well separate with very light damping. These types of modes can be approximated with a SDOF fit. However, Fig 2.23b shows modes that there is some overlap from one mode to the next which may not be correctly compensated with a SDOF fit. It is likely that a MDOF fit may need to be employed for these two modes.

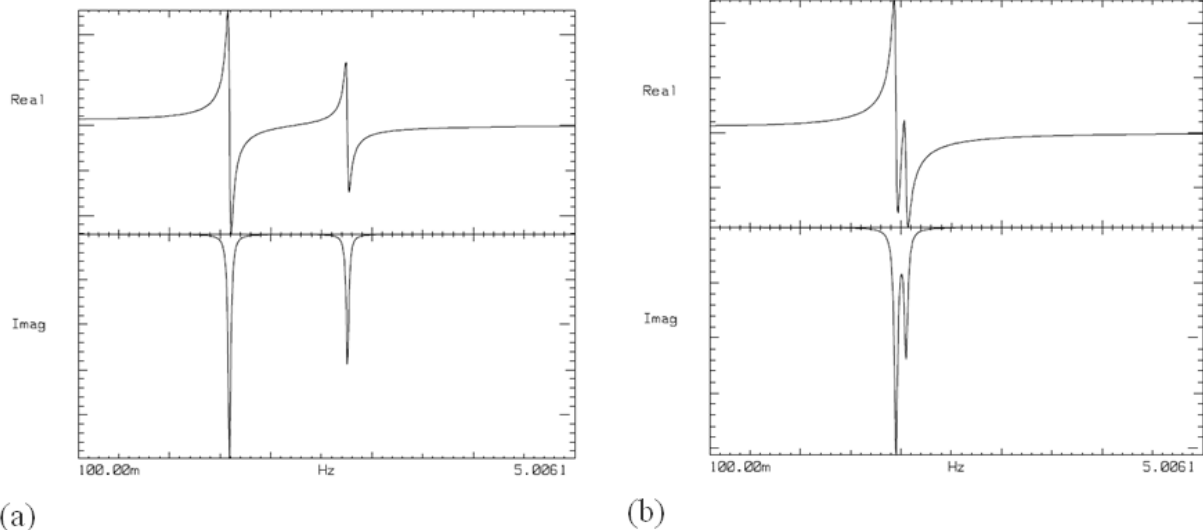


Figure 2.23 Different situations for a two DOF system having light damping (a) Modes well separated (b) Coupled modes [118]

The modal identification methods can generally be classified in the following three ways:

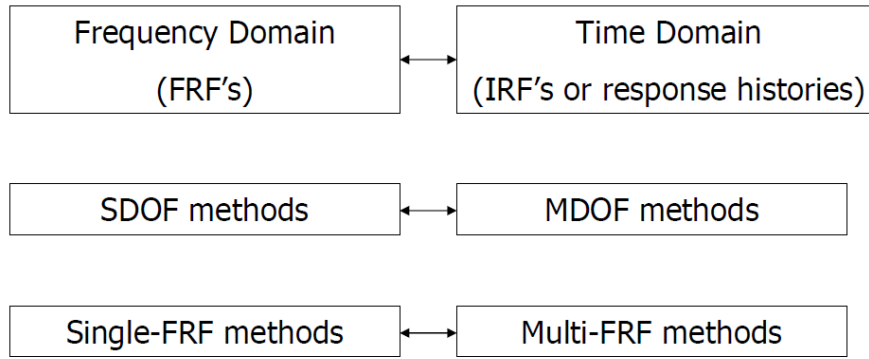


Figure 2.24 Classification of the three main types of modal parameter estimation categories [120]

We shall base further discussions on curve fitting by explaining separately SDOF and MDOF methods

SDOF Modal Estimation (Curve Fitting) Methods

The analytical models have been presented previously, now the estimation of parameters from the partial fraction in case of a SDOF is shown.

Assuming that a lightly damped single degree of freedom (SDOF) system is being evaluated, the parameters needed for a partial fraction model can be quickly estimated directly from the measured frequency response function. While this approach is based upon a SDOF system, as long as the modal frequencies are not too close together, the method can be used for multiple degree of freedom (MDOF) systems as well.

Starting with the partial fraction model formulation of a SDOF frequency response function

$$H(\omega) = \frac{A_1}{(j\omega - \lambda_1)} + \frac{A_1^*}{(j\omega - \lambda_1^*)} \quad (2.23)$$

only the poles λ_1 and the residuals A_1 must be estimated. Since $\lambda_1 = \sigma_1 + j\omega_1$, the estimation process begins by estimating ω_1 . The damped natural frequency ω_1 is estimated in one of three ways:

- the frequency where the magnitude of the FRF reaches a maximum.
- the frequency where the real part of the FRF crosses zero.
- the frequency where the imaginary part of the FRF reaches a relative minima (or maxima).

Once the damped natural frequency ω_1 has been estimated, the real part of the modal frequency, the damping factor σ_1 , can be estimated. The damping factor σ_1 can be estimated by using the **half-power bandwidth** method. This method uses the data from the FRF in the region of the resonance frequency to estimate the fraction of critical damping from the following formula:

$$\zeta_1 = \frac{\omega_b^2 - \omega_a^2}{(2\omega_1)^2} \quad (2.24)$$

In the above equation, ω_1 is the damped natural frequency as previously estimated. ω_a is the frequency, below ω_1 , where the magnitude is 0.707 of the peak magnitude of the FRF. This corresponds to a half power point. ω_b is the frequency, above ω_1 , where the magnitude is 0.707 of the peak magnitude of the FRF. This also corresponds to a half power point.

For lightly damped systems, the above equation can be approximated by the following:

$$\zeta_1 = \frac{\omega_b - \omega_a}{2\omega_1} \quad (2.25)$$

Once ζ_1 is estimated, the damping factor σ_1 can be obtained from the following equation.

$$\sigma_1 = -\zeta_1 \Omega_1 \quad (2.26)$$

Again, assuming that the system is lightly damped, $\Omega_1 \approx \omega_1$, the damping factor can be estimated from the following equation:

$$\sigma_1 = -\zeta_1 \omega_1 \quad (2.27)$$

Once the modal frequency λ_i has been estimated, the residue A_i can be estimated by evaluating the partial fraction model at a specific frequency. If the specific frequency is chosen to be ω_1 , the following result is obtained.

$$H(\omega_1) = \frac{A_i}{(j\omega_1 - \sigma_1 - j\omega_1)} + \frac{A_i^*}{(j\omega_1 - \sigma_1 + j\omega_1)} \quad (2.28)$$

$$H(\omega_1) = \frac{A_i}{(-\sigma_1)} + \frac{A_i^*}{(2j\omega_1 - \sigma_1)} \quad (2.29)$$

As long as ω_1 is not too small, the above equation can be approximated by:

$$H(\omega_1) \approx \frac{A_i}{(-\sigma_1)} \quad (2.30)$$

Therefore, the residue A_i can be estimated from the following relationship:

$$A_i \approx (-\sigma_1)H(\omega_1) \quad (2.31)$$

In the above relationship, $H(\omega_1)$ is very close to being a purely imaginary value for the displacement over force FRF. This means that the residue A_1 will be very close to a purely imaginary value as well. An example of the estimated modal parameters is shown in Fig 2.25.

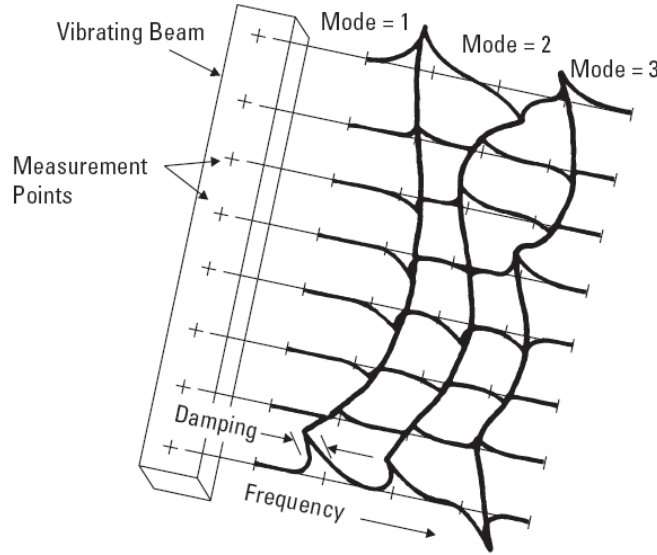


Figure 2.25 Concepts of modal parameters – Damping, frequency same at each measurement point - Mode Shape obtained from the imaginary part of the FRF [118]

The generally used methods used for estimating the modal parameters from a SDOF system are

- Peak Amplitude Method (Peak-Picking)
- Circle Fit Method

The author would however like to mention the concept of residual terms as shown in Fig 2.26.

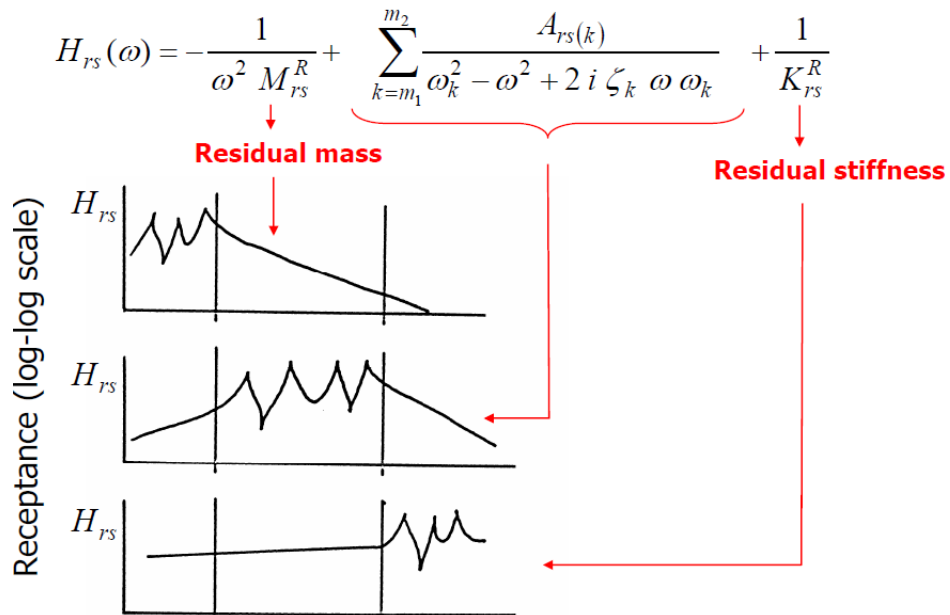


Figure 2.26 Contribution of low, medium and high frequency modes which help to obtain a superior quality of the reconstructed FRFs [120]

It is important to take into account the influence of modes which exist outside the frequency range of measurement to have a better correlation of the experimental and reconstructed frequency response functions (FRFs).

MDOF Modal Estimation (Curve Fitting) Methods

The most commonly used MDOF based modal estimation methods are

- Least Squares Complex Exponential (LSCE) – It is a time domain technique and globally estimates the modal parameters of several modes simultaneously.
- Least Squares Frequency Domain (LFSD) – It is a frequency domain technique and provides a global estimate of the poles and residues for the complex modes.

The estimation methods used for curve fitting in this thesis are Polymax and Polyreference. Polymax algorithm is used in case of burst random and Polyreference algorithm is used for sine-dwell testing. Polymax and Polyreference are enhanced versions of the least-squares complex frequency-domain (LSCF) estimation method. Both Polymax and Polyreference estimators function with the help of a **stability diagram**.

In modal analysis, a stability diagram is an important tool that is often used to assist the user in separating physical poles from mathematical ones. A stabilization chart is obtained by repeating the analysis for increasing model order n of Equation 2.32.

$$[H(\omega)] = \sum_{k=1}^N \left[\frac{A_1}{(j\omega - \lambda_1)} + \frac{A_1 *}{(j\omega - \lambda_1 *)} \right] \quad (2.32)$$

where:

$$\text{complex conjugate poles} = \lambda_1 = \sigma_1 \pm j\omega_1 \text{ and residues} = A_1$$

For each model order, the poles are calculated from the estimated denominator coefficients. The stable poles (i.e. the poles with a negative real part) are then presented graphically in ascending model order in a so-called “stability diagram” (Fig 2.27). Estimated poles corresponding to physically relevant system modes tend to appear for each estimation order at nearly identical locations, while the so-called mathematical poles, i.e. poles resulting from the mathematical solution of the normal equations but meaningless with respect to the physical interpretation, tend to jump around. These mathematical poles are mainly due to the presence of noise on the measurements.

The order of the mathematical model is shown on the right vertical end of the stability diagram (Fig 2.27). The poles are typically plotted on top of a Mode Indicator Function (shown in blue in Fig 2.27) which is used to help determine the number of modes in a set of experimental data [122]. A stability diagram has two advantages:

- It helps the user determine how many modes are really contained in a frequency band
- By displaying a stable pole estimate for several model sizes, it confirms that the estimate is correct

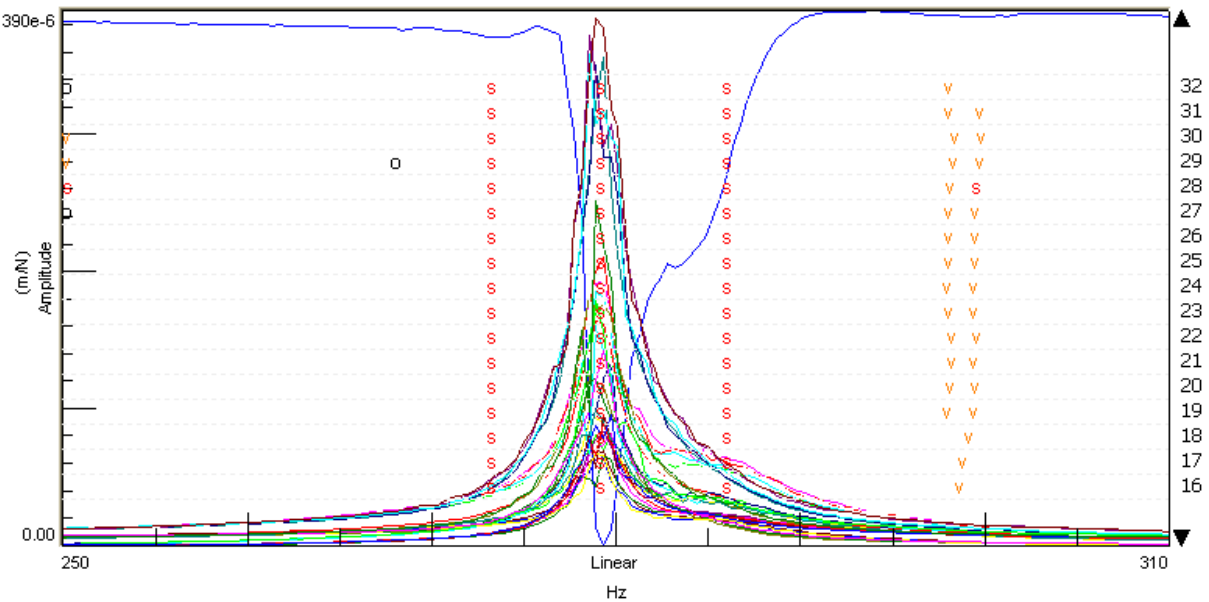


Figure 2.27 Stability diagram for parameter estimation showing different symbols which indicate whether the mode is stable or not [122] along with the mode indicator function (MIF) in blue

The signification of the different symbols on the stability diagram is given in Table 2.3.

Table 2.3 Signification of the symbols used in a stability diagram [119]

Symbol	Description
o	The pole is not stable
f	The frequency of the pole does not change within the tolerances
d	The damping and frequency of the pole does not change within the tolerances
v	The pole vector does not change within the tolerances
s	Both frequency, damping and vector are stable within the tolerances

2.3.4 Correlation Tools

The main aim of correlation tools is

- Visual inspection experimental / calculated mode-shapes
- Visual inspection of regenerated / predicted FRFs
- Use of mathematical tools

It is often necessary to validate Finite Element Analysis (FEM) results with measured data from a modal test [123,124]. This correlation method is generally an iterative process and involves two major steps (Fig 2.28):

- First, the modal parameters, both frequencies and mode shapes are compared and the differences quantified.
- Second, adjustments and modifications are made, usually to the finite element model in order to achieve a better experimental / numerical correlation.

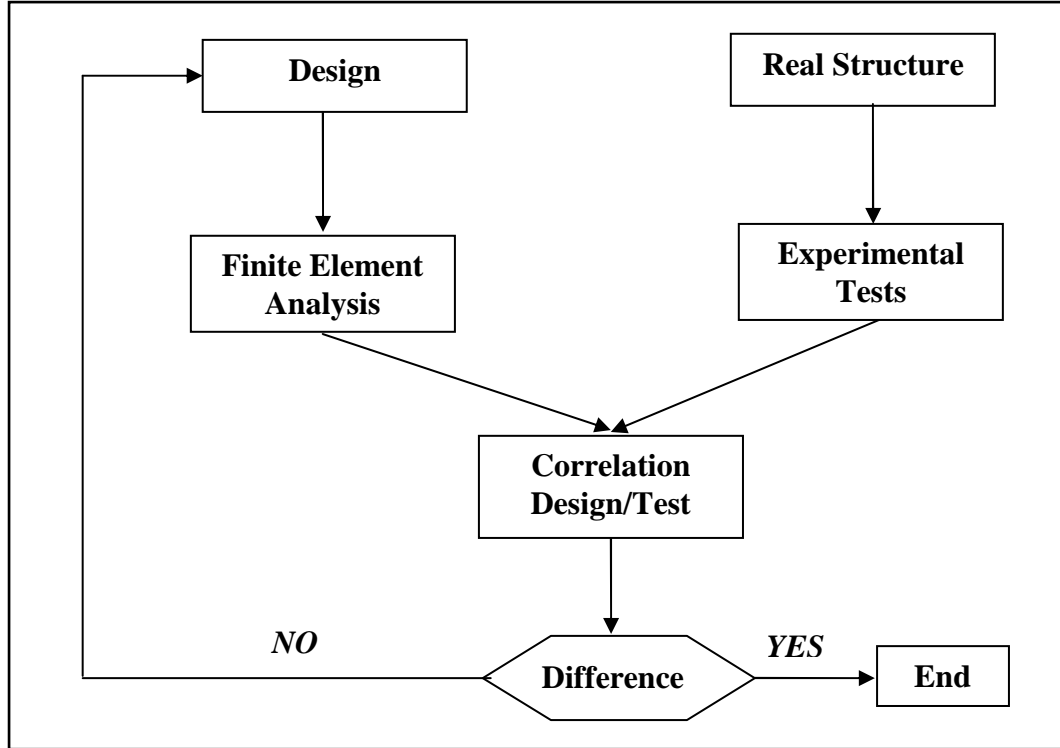


Figure 2.28 Flow Chart of a basic experimental / numerical correlation procedure [124]

Some commonly used mathematical correlation tools based on modal parameters are:

Comparisons of Natural Frequencies (NFD)

The simplest comparison for linear dynamic systems is based on natural frequencies. The NFD (Natural Frequency Difference) is defined by

$$NFD(i, j) = \frac{\omega_{\text{exp}i} - \omega_j}{\max(\omega_{\text{exp}i}, \omega_j)} \quad (2.33)$$

Where $\omega_{\text{exp}i}$ is the experimental pulsation of mode i and ω_j is the numerical pulsation of mode j .

Correlation of Mode Shapes (MAC)

MAC (Modal Assurance Criterion) is the most commonly used experimental-numerical correlation tool due to its ease of use. For two mode shapes defined, one experimental and numerical, MAC the correlation coefficient is defined by

$$MAC(i, j) = \frac{|\{\phi_{\text{exp}_i}\}^T - \{\phi_j\}|^2}{|\{\phi_{\text{exp}_i}\}^T - \{\phi_{\text{exp}_i}\}| |\{\phi_j\}^T - \{\phi_j\}|} \quad (2.34)$$

where $\{\phi_{\text{exp}_i}\}$ is the experimental mode shape and $\{\phi_j\}$ is the mode shape obtained numerically for the mode j . A perfect correlation between two modes means that the value MAC is equal to 1 (i.e., 100%). A correlation is deemed poor if the MAC is inferior to 70%.

Today, most computer systems routinely utilize colour to present magnitude data like MAC using a 2D or 3D plot as shown in Figures 2.29 a and b. It is important to remember, however, that MAC is a discrete calculation and what appears as a colour contour plot really only represents the discrete mode to mode comparison.

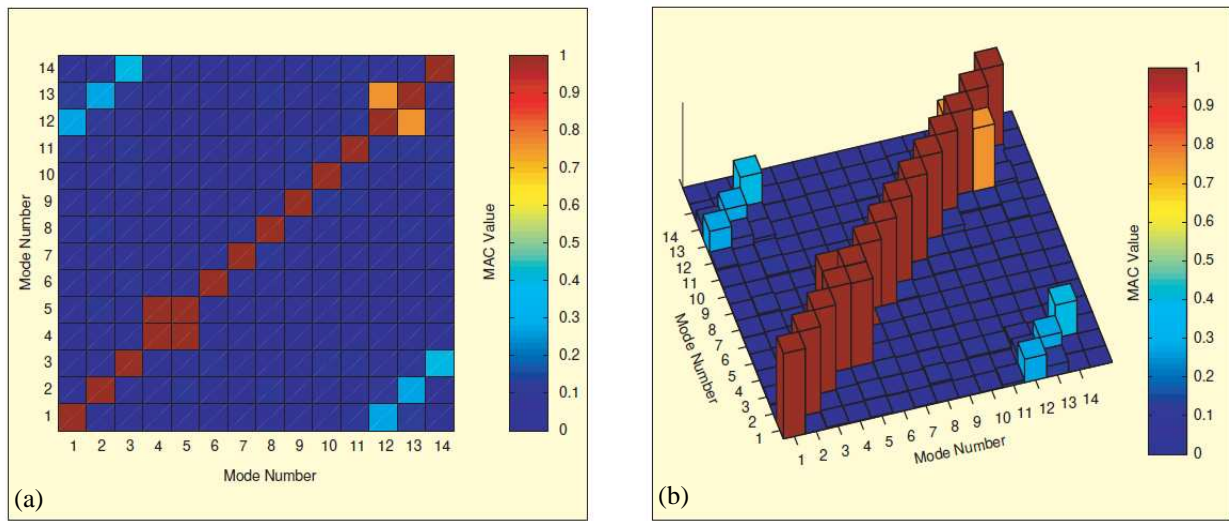


Figure 2.29 (a) 2-D (b) 3-D presentation of MAC values [124]

Comparison of Loss Factors (LFD)

LFD (Loss Factor Difference) is a comparison between the loss factors, with the help of which loss factors to be updated are calculated. LFD is calculated as follows

$$LFD(i, j) = \frac{\eta_{\text{exp}_i} - \eta_j}{\max(\eta_{\text{exp}_i}, \eta_j)} \quad (2.35)$$

Where η_{exp_i} is the experimentally measured loss factor for the mode I , and η_j is the loss factor calculated numerically for the mode j .

Comparisons of Frequency Response Functions (FRF)

The majority of correlation techniques employ the use of mode shapes, in which MAC is the most well known criterion. The direct comparison between the calculated and the measured FRFs is less developed but is more interesting than the correlation of mode shapes, because the experimental FRFs are more easily obtained. In order to calculate the difference between

the frequency responses calculated experimentally and numerically, various criterions can be used, e.g., FRAC (Frequency response assurance criterion), FDAC (Frequency domain assurance criterion). Two other criterions are SAC (Signature Assurance Criterion) and LAC (Local Assurance Criterion) to correlate a pair of FRFs. Detailed explanation on these methods can be found in references [123,124].

2.3.5 Sources of Lack of Precision in Modal Testing

The sources of a lack of precision in modal testing procedure [122] can be categorized in three groups:

Experimental Data Acquisition Errors

- Mass loading effect of transducers
- Shaker-structure interaction
- Supporting of the structure
- Measuring enough points on the structure
- Measuring enough Degrees of Freedom

Signal Processing Errors

- Leakage
- Aliasing
- Effect of window functions
- Effect of Discrete Fourier Transform
- Effect of averaging

Modal Analysis Errors

- Circle-Fit Modal Analysis
- Line-Fit Modal Analysis
- Global-Fit Modal Analysis

The main concern of this research is the first category of the sources of a lack of precision, namely experimental data acquisition errors and especially mechanical errors which demand particular attention in order to provide input data of high-quality which are required for the next stages.

2.3.6 Shaker Test Flow Diagram

Shaker testing has been briefly explained previously. Some further details on shaker testing are provided as the experiments presented further in this thesis are based on shaker testing. For shaker testing, the excitation of the shaker is measured at the lowest channel of the acquisition system. The response transducers are measured in the remaining channels of the data acquisition system. Depending on the excitation type triggering will vary. Burst random excitations start from a signal source or force trigger.

In addition, sometimes a pre-trigger delay is specified for burst random excitations. To minimize the leakage effects, Hanning windows are used in case of burst random excitations.

As discussed before, the time captured data must be transformed to frequency domain using the FFT and the transform algorithm. The measurement process for shaker testing is explained in the flow diagram in Fig 2.30.

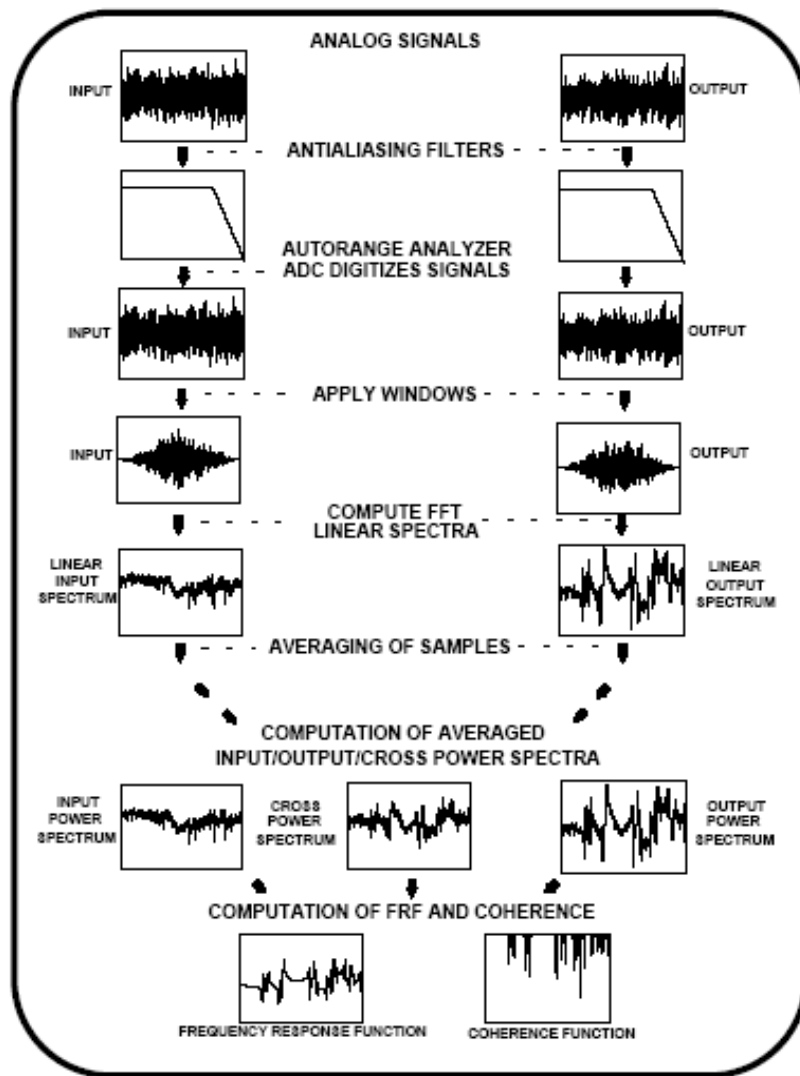


Figure 2.30 Shaker test flow diagram showing the whole cycle from the time of measurements to curve fitting for a burst random excitation with averaging [122]

2.4 Analytical Calculation of the FRF of a Free-Free Beam Excited at its Centre

The experimental set-up for vibration tests used in this thesis is that of a free-free beam excited at its center, based on Oberst method [22] as shown in Fig 2.31. The Oberst method states that a free-free beam excited at its center has the same dynamical behavior as that of a half length cantilever beam. Frequency Response Function (FRF) can be calculated analytically for a free-free beam excited harmonically at its centre by using the following procedure.

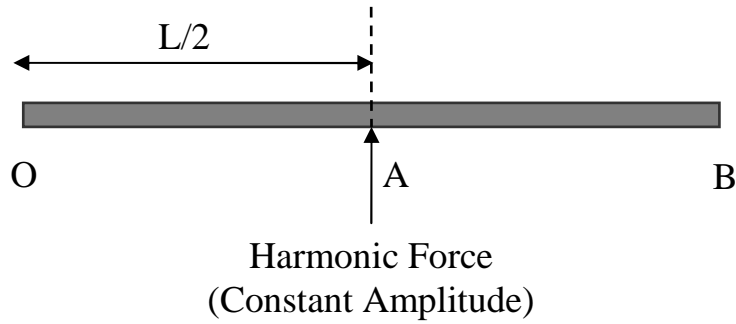


Figure 2.31 Free-Free beam excited harmonically at its centre (Oberst Beam)

Definition of Beam Parameters

The beam has the following parameters,

L = Length of the beam

b = breadth of the beam

d = height of the beam

$S = b \cdot d$ = area of the cross-section

ρ = mass per unit volume

E = Young's Modulus

$I = \frac{bd^3}{12}$ = Moment of Inertia

$\omega = 2\pi f$ = Circular frequency

f = frequency

T_y = Shearing force

M_z = Bending moment

The characteristic equation of dynamic response is given by

$$V(x, t) = f(x)g(t) \quad (2.36)$$

The components $f(x)$ and $g(t)$ are

$$f(x) = A_1 \cos \Omega X + A_2 \sin \Omega X + A_3 \operatorname{ch} \Omega X + A_4 \operatorname{sh} \Omega X \quad (2.37)$$

$$g(t) = \cos(\omega t + \phi) \quad (2.38)$$

Putting the above two Equations in Equation 2.36,

$$V(x, t) = [A_1 \cos \Omega X + A_2 \sin \Omega X + A_3 \operatorname{ch} \Omega X + A_4 \operatorname{sh} \Omega X] \cos(\omega t + \Phi) \quad (2.39)$$

where:

A_1, A_2, A_3 and A_4 are constants, and are required to be found for the calculation of dynamic response.

$$\text{Pulsation} = \Omega^4 = \frac{\rho S}{EI} \omega^2 \quad (2.40)$$

The equations of Bresse are as follows:

$$EIV'' - M_z = 0 \quad (2.41)$$

$$EIV''' + T_y = 0 \quad (2.42)$$

Application of Boundary Conditions

Now boundary conditions shall be applied at the two ends of the beam in order to calculate the four constants A_1, A_2, A_3 and A_4 .

At O ($x = 0$):

$$\text{Shearing Force} = T_y = 0$$

Putting this condition in Equation 2.42, gives

$$V'''(0, t) = 0 \text{ and consequently}$$

$$f'''(0) = 0$$

Putting the above two results in Equation 2.39, we get

$$A_2 = A_4$$

$$\text{Bending Moment} = M_z = 0$$

Putting this condition in Equation 2.41, we have

$$V''(0, t) = 0 \text{ and consequently}$$

$$f''(0) = 0$$

Similarly as for the previous condition, by putting this condition in Equation 2.39, we obtain the following relation for the constants

$$A_1 = A_3$$

At A ($x = L/2$), the beam is considered clamped as there is a displacement imposed

$$\text{The imposed displacement at A} = V\left(\frac{L}{2}, t\right) = V_o \cos(\Omega t)$$

$$\text{The rotation at A} = V'\left(\frac{L}{2}, t\right) = 0$$

Putting these two conditions in the characteristic equation of dynamic response in Equation 2.39 in order to calculate the remaining two constants

$$A_1 = \frac{V_o (ch(\Omega L/2) + \cos(\Omega L/2))}{2(1 + ch(\Omega L/2)\cos(\Omega L/2))}$$

$$A_2 = -\frac{V_o (sh(\Omega L/2) - \sin(\Omega L/2))}{2(1 + ch(\Omega L/2)\cos(\Omega L/2))}$$

Calculation of Dynamic Response and Frequency Response Function

Putting the values of the four calculated constants A_1 , A_2 , A_3 and A_4 , in the characteristic equation of dynamic response in Equation 2.39, we get

$$V(x,t) = \left[\frac{[ch(\Omega L/2) + \cos(\Omega L/2)]}{2[1 + ch(\Omega L/2)\cos(\Omega L/2)]} [ch(\Omega x) + \cos(\Omega x)] - \frac{[sh(\Omega L/2) - \sin(\Omega L/2)]}{2[1 + ch(\Omega L/2)\cos(\Omega L/2)]} [sh(\Omega x) + \sin(\Omega x)] \right] \cos(\omega t + \Phi)$$

The ratio of the dynamic response to the imposed movement yields the Frequency Response Function which is given by

$$H(x, \omega) = \left[\frac{[ch(\Omega L/2) + \cos(\Omega L/2)]}{2[1 + ch(\Omega L/2)\cos(\Omega L/2)]} [ch(\Omega x) + \cos(\Omega x)] - \frac{[sh(\Omega L/2) - \sin(\Omega L/2)]}{2[1 + ch(\Omega L/2)\cos(\Omega L/2)]} [sh(\Omega x) + \sin(\Omega x)] \right]$$

In this thesis some of the beam-specimens have been tested with end masses, so in order to calculate the analytical solution for a cantilever beam with end-masses, the same procedure is followed by modifying the two boundary conditions in Equations 2.41 and 2.42.

2.5 Tracking of Poles for Damage Detection

So far in this chapter, the author has presented briefly the analytical and experimental aspects of experimental modal analysis. The author now would like to correlate all this information with the main subject of the thesis i.e., monitoring of impact damage due to shift in modal parameters.

As discussed previously, modal parameter estimation is a special case of system identification where the a priori model of the system is known to be in the form of modal parameters. The identification process consists of estimating the modal parameters from frequency response function (FRF) measurements. Modal identification uses numerical techniques to separate the contributions of individual modes of vibration in measurements such as frequency response functions. Each term of the FRF matrix can be represented in terms of pole location and a mode shape. The FRF matrix model is represented mathematically by:

$$[H(\omega)] = \sum_{k=1}^N \left[\frac{A(k)}{(j\omega(k) - \lambda(k))} + \frac{A(k)^*}{(j\omega(k) - \lambda(k)^*)} \right] \quad (2.43)$$

The numerator $A(k)$ is the residue of the FRF and is a function of the product between mode shape components at all points. The denominator gives the modal frequency and modal damping (second term in Equation (2.43) is the complex conjugate term). The poles $\lambda(k)$, are the roots that satisfy this equation and are related to modal frequency and damping as follows:

$$\lambda(k) = \sigma(k) + j\omega(k) \quad (2.44)$$

The magnitude of each pole is the undamped natural frequency (Ω). The undamped natural frequency (ω) and the modal damping (σ) are related to mass, stiffness and damping as follows: given by

$$\Omega = \sqrt{\omega^2 + \sigma(k)^2} = \sqrt{\frac{K}{M}} \quad (2.45)$$

$$2\sigma(k) = \frac{C}{M} \quad (2.46)$$

The effect of physical properties on poles in the complex s-plane is illustrated in Fig 2.32.

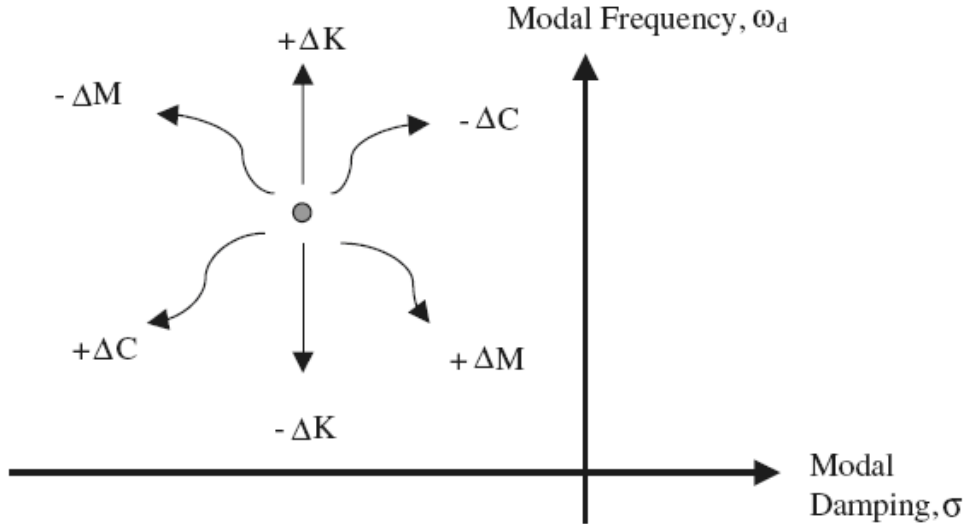


Figure 2.32 Movement of pole due to mass stiffness and damping effect [60]

From Fig 2.31, it can be observed that a change in stiffness affects only the frequency, while changes in mass and structural damping affect both modal damped frequency (ω) and modal damping (σ).

The primary interest of this thesis is to study the decrease in the modal damped frequency (ω) and the increase in modal damping (σ) due to damage in the composite specimens [40,60].

2.6 Conclusion of the Second Chapter

The major point of this chapter is to show how frequency response function (FRF) measurements are related to the structure's mode shapes and vibrational frequencies. Theoretical background on experimental modal analysis is the main emphasis of this chapter. Types of excitations, types of test set-ups for vibration testing and types of estimation methods are highlighted as well. Finally correlation tools are discussed used for updating a numerical model with respect to experimental results. This chapter is divided into three main sections:

System identification: This is a widely used approach to characterize a physical process in a quantified way. In modal analysis terms, this is also known as vibration signal analysis.

Single degree of freedom system: This system will be used as a means for defining some standard terminologies in order to help the readers to grasp with relative ease the **basic theoretical aspects of this thesis**. Detailed explanation on the fundamentals and applications of vibrations can be found in a multitude of technical books, for example by De Silva in reference [117].

Experimental modal analysis: Theoretical background on experimental modal analysis is discussed briefly. Types of excitations, types of test set-ups for vibration testing and types of estimation methods are highlighted as well. Finally correlation tools are discussed used for updating a numerical model with respect to experimental results.

Chapter 3 : Monitoring of Impact Damage in Composite Laminates by Shift in Modal Parameters

This chapter focuses on the correlation of modal parameters and impact damage in composite laminate beams from an experimental point of view. Two batches of composite laminate beams having different impact boundary conditions are studied. First a brief theory of composite laminates is presented followed by the experiment details and discussions.

3.1 Theory of Laminated Composites

A composite material is a combination of two distinct materials that are generally called the matrix and the reinforcement [125]. They have often complementary properties, that when combined have complementary physical properties different from their constituents. The mechanical role of the matrix is normally to provide cohesion between the different elements of the reinforcement and thus play the role of ‘cement’ by assuring a minimum of homogeneity between the two constituents. In the majority of composite materials, the mechanical properties are essentially given by the reinforcements, in such a way that the rate of reinforcement in the matrix as well as the quality of the interface reinforcement/matrix defines the mechanical properties of the composite materials. The reinforcement can be used in different forms, e.g., long fibers, short fibers, spheres and even in the form of complex fiber sheets.

3.1.1 Nomenclature and General Composition

Nowadays a large number of composites are employed in various walks of life, thus making it impossible to treat them all equally as their properties vary enormously from one to the other. However, it is possible to distinguish some families of composites by the types of matrix and reinforcement used. From an industrial point of view, the most widely used composites are those having polymer matrix and long fibers (simple or woven). Most commonly used fibers nowadays are those made of glass because of them being cheap and cost effective, as well as carbon and aramide fibers for specific applications.

Table 3.1 Types of matrices used in commonly used composites [125]

Type of Matrix	Examples	Properties
Polymer	Epoxy resin, polyester,	Materials having thermoplastic and thermo hardening properties, low resistance to temperature, light and easily mountable, generally ductile.
Metal	Aluminum, Magnesium and Tungsten	Materials produced in foundry or by metallurgy of powders at high fusion temperatures, having good intrinsic mechanical resistance, high average density, generally ductile but sometimes fragile
Ceramic	Carbure of Silicium (SiC)	Materials produced by fusing powders at high temperatures of operation at high density, but fragile.

A composite material is called stratified if it is a combination of sequentially oriented layers having certain thicknesses and made of different materials. A layer of composite material is normally known as a ply. The type of a stratified composite material is usually defined by the orientation sequence of its plies. For example, a stratify of type $(90^0, 0^0)_{2s}$ is made up of 8 plies as follows, two group of plies at 90^0 and 0^0 then by symmetry of two groups of plies of 0^0 and 90^0 . The advantage of stratified composites is to create materials having mechanical properties oriented in an optimal manner in order to bear in a better way the structural loads.

Table 3.2 Types of reinforcements used in commonly used composites [125]

Type of Reinforcement	Properties	Commonly used Matrices
Fibers or palettes of glass	Glass fibers of type E or R of different diameters, in the form of fabric or bobbin, at low cost, at average density and at average mechanical properties	Polymers: polyester, resin, epoxy, thermoplastics
Carbon fibers	Fibers obtained by carbonization of polymers, mostly in the form of pre-impregnated fabric or bobbin, at medium to high cost depending upon the quality, low density, excellent rigidity and rupture limit, machining normally difficult but possible with tools made of diamond or hard metal	Polymers : resin, epoxy, PEKK etc.
Aramid fibers (Kevlar)	Polymer fibers, often in the form of fabric or pre-impregnated sheets, sometimes a combination of aramide-carbon fibers, low density, medium to high rigidity, high tenacity and resilience, very difficult to cut and machine.	Polymers : resin, epoxy, PEKK etc.
High tenacity polypropylene fibers	Polymer fibers, in fabric or in pre-impregnated form, low density, low to medium rigidity, high tenacity and resilience, very difficult to cut and machine.	Polymers : resin, epoxy, polyester etc
Aluminum oxide fibers	Fibers having very high rigidity and rupture limit, high density, high cost and at very high temperature limit	Metals: aluminum, magnesium and ceramic

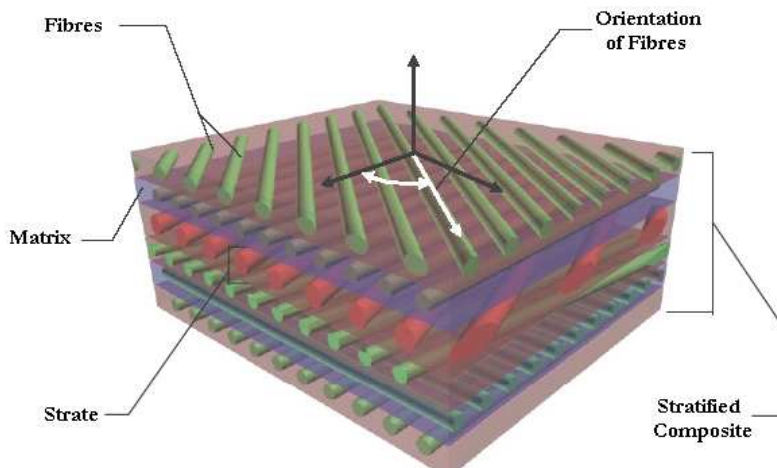


Figure 3.1 Nomenclature of stratified composites [125]

3.1.2 Modeling of Composite Properties and Behavior by Constitutive Laws

One of the essential properties of composite materials is direction dependence of their mechanical properties. In fact, these materials do not possess at all the same properties in the direction of reinforcements (fibers) than in the direction perpendicular to the reinforcements (fibers). These types of properties or behavior are often modeled by an elastic-orthotropic law. This law enables to represent a material whose elastic mechanical properties are dependent on the three orthogonal principal directions. With help of this law, unidirectional composites, fabric composites and also more isotropic materials like reinforced plastics can be successfully modeled. The law representing the behavior of an elastic-orthotropic material can be written mathematically as [125]:

$$\begin{bmatrix} \sigma_{11} \\ \sigma_{22} \\ \sigma_{33} \\ \sigma_{23} \\ \sigma_{31} \\ \sigma_{12} \end{bmatrix} = \begin{bmatrix} \overline{C_{11}} & \overline{C_{12}} & \overline{C_{13}} & 0 & 0 & 0 \\ \overline{C_{12}} & \overline{C_{22}} & \overline{C_{23}} & 0 & 0 & 0 \\ \overline{C_{13}} & \overline{C_{23}} & \overline{C_{33}} & 0 & 0 & 0 \\ 0 & 0 & 0 & \overline{C_{44}} & 0 & 0 \\ 0 & 0 & 0 & 0 & \overline{C_{55}} & 0 \\ 0 & 0 & 0 & 0 & 0 & \overline{C_{66}} \end{bmatrix} \begin{bmatrix} \epsilon_{11} \\ \epsilon_{22} \\ \epsilon_{33} \\ 2\epsilon_{23} \\ 2\epsilon_{31} \\ 2\epsilon_{12} \end{bmatrix} \quad (3.1)$$

where,

$$\overline{C_{11}} = \frac{1 - v_{23}v_{32}}{E_2 E_3 \Delta}; \quad \overline{C_{12}} = \frac{v_{21} + v_{31}v_{23}}{E_2 E_3 \Delta} = \frac{v_{12} + v_{32}v_{13}}{E_1 E_3 \Delta}; \quad \overline{C_{13}} = \frac{v_{31} + v_{21}v_{32}}{E_2 E_3 \Delta} = \frac{v_{13} + v_{12}v_{23}}{E_1 E_2 \Delta}$$

$$\overline{C_{22}} = \frac{1 - v_{13}v_{31}}{E_1 E_3 \Delta}; \quad \overline{C_{23}} = \frac{v_{32} + v_{12}v_{31}}{E_1 E_3 \Delta} = \frac{v_{23} + v_{21}v_{13}}{E_1 E_2 \Delta}; \quad \overline{C_{33}} = \frac{1 - v_{12}v_{21}}{E_1 E_2 \Delta}$$

$$\overline{C_{44}} = G_{23}, \quad \overline{C_{55}} = G_{31}, \quad \overline{C_{66}} = G_{12}$$

$$\Delta = \frac{1 - v_{12}v_{21} - v_{23}v_{32} - v_{13}v_{31} - 2v_{21}v_{32}v_{13}}{E_1 E_2 E_3}$$

$$v_{ji} = \frac{E_j}{E_i} v_{ij} \quad (\text{for } i,j = 1,2,3)$$

where the different variables are defined as :

σ_{ij} : nominal stress tensor represented in vector form

ϵ_{ij} : infinite deformation tensor represented in vector form

\overline{C}_{ij} : tensor of linear orthotropic elasticity expressed in matrix form in the principal direction coordinate system of the material

E_i : elastic modulus in the principal direction i

v_{ij} : poisson ratio in the direction j for a traction in the direction i

G_{ij} : shearing modulus in the i,j plane

It can be seen that in order to define a material by the law presented above, ten constitutive parameters have to be determined, three elastic modulii, three coefficients of poisson ratio, three shearing modulii and the density of the material. It should be noted that the elastic-

orthotropic model is generally a model of unidirectional composites, often considered as transverse isotropic. A transverse isotropic model is obtained by making the following the assumptions:

- E_2 and E_3 are equal to the transverse modulus of elasticity E_t , E_1 being equal to the longitudinal modulus of elasticity E_L in the principal direction (of the fibers).
- G_{12} and G_{23} are equal to the shearing modulus G_{LT} between the principal direction and the transverse plane, G_{23} being equal to the shearing modulus G_{TT} in the transverse plane.
- ν_{12} and ν_{23} are equal to the poisson coefficient ν_{LT} between the principal and transverse directions, ν_{23} being equal to the poisson coefficient ν_{TT} in the transverse plane.

A unidirectional transotropic composite material can be described by six constants: E_L , E_T , G_{LT} , G_{TT} , ν_{LT} and ν_{TT} . However, due to fabrication processes of composite materials are such that, it is hard to consider a unidirectional composite material completely transotropic. For plate and shell structures, the constants required to characterize an orthotropic material are E_1 , E_2 , G_{12} , G_{23} , G_{31} and ν_{12} . Infact, the classical hypothesis of plates and shells imposes both the transverse incompressibility and the absence of transverse traction/compression. These assumptions thus nullify the presence of Modulus of Elasticity E_3 in the thickness as well as the Poisson ratio's ν_{13} and ν_{23} associated to the transverse deformation. Further details on the different theories of stratified composites can be found abundantly in scientific literature, especially by Gay and Hua on the designs and applications of composite structures [125].

3.1.3 Material and Types of Composite Laminate Beams

Resin-containing carbon-fiber/epoxy prepgs of T300/914 is used to fabricate the beam-type test specimens. The material is supplied by Hexcel composites and the physical properties are set out in Table 3.3 [137]. The specimens are processed in a press. The curing cycle of the laminates is 2h at 180°C with a warming-up cycle of 0.5h at 135°C. The laminates are cut into beams using a diamond wheel cutter, following the ASTM D3039/D3470 standards.

Table 3.3 Physical properties of carbon/epoxy prepgs T300/914 [137]

Properties	Symbol	Value
Young's modulus in fiber direction	E_1	144000 MPa
Young's modulus in transverse direction	E_2	10000 MPa
Shear Modulus	G_{12}	4200 MPa
Poisson ratio	$\nu_{12}, \nu_{23}, \nu_{31}$	0.25, 0.3, 0.017
Volume density	ρ	1550 kg/m ³

Composite laminate beams having two different thicknesses are tested. The first ones have a thickness of 1.04 mm having 8 plies and are discussed under the name of Type-1 beams, whereas the others have a thickness of 3.12 mm having 24 plies and are described as Type-2 beams. The geometric configurations and lay-up of these two types of beams are listed in Table 3.4. The lay-up is chosen as such, in which the delamination is demonstrated as having a more profound effects on the dynamic characteristics [52].

Table 3.4 Geometry and lay-up of the two types of composite laminate beams

Type-1 Beams		Type-2 Beams	
Length	480 mm	Length	480 mm
Width	50 mm	Width	50 mm
Thickness	1.04 mm	Thickness	3.12 mm
Number of layers (plies)	8	Number of layers (plies)	24
Thickness of each ply	0.125 mm	Thickness of each ply	0.125 mm
Lay-up	[0/90/45/-45]s	Lay-up	[(0/90/45/-45) ₃]s

The vibration tests are carried out with two steel masses attached at the ends. The aim of putting these masses at the ends is to enhance the difference in the modal parameters between the undamaged and the damaged test specimens [20,59]. The dimensions of these end masses for specimens of Type-1 and Type-2 are listed in Table 3.5.

Table 3.5 Dimensions of the end masses for the two types of composite test specimens

End Masses for Type-1 Beams		End Masses for Type-2 Beams	
Length	50 mm	Length	50 mm
Width	12 mm	Width	30 mm
Thickness	8 mm	Thickness	10 mm
Material	Steel	Material	Steel

3.2 Experimental Techniques

The experimental part of this thesis consists principally of two types of experiments. Vibrations tests for measuring the dynamic characteristics of the beam-type specimens and impact tests in order to create damage in them. The experimental procedure for these two types of tests is discussed separately.

3.2.1 Vibration Tests

The experimental equipment used for vibration testing is shown in Fig. 3.2. The experimental set-up is that of a free-free beam excited at its center, based on Oberst method [19]. The Oberst method states that a free-free beam excited at its center has the same dynamical behavior as that of a half length cantilever beam. The test specimen is placed at its center on a B&K force sensor (type 8200) which is then assembled on a shaker supplied by Prodera having a maximum force of 100 N. However the force sensor is not capable of measuring reliable response below 5 Hz. A fixation system is used to place the test specimens on the force sensor. The fixation is glued to the test specimens with a HBM X60 rapid adhesive. The response displacements are measured with the help of a non-contact and high precision Laser Vibrometer OFV-505 provided by Polytec. The shaker, force sensor and the laser vibrometer are manipulated with the help of a data acquisition system supplied by LMS Test Lab for burst random testing and Ideas Test (B&K) for sine dwell testing. Two types of data acquisition systems are used for different types of vibration testing in this thesis.

- LMS Test Lab system is used principally for burst random excitations which are averaged 10 times for each measurement point. Burst random excitation is a broadband type excitation signal. 50% burst percentage is used for burst random

excitation. Normally burst random excitations are leakage free but the first author after trying different window functions found out that by putting Hanning windows on both the excitation and response signals, better quality signals FRFs are obtained. The signal is averaged 10 times for each measurement point and the frequency band chosen is 0-2650Hz. A disadvantage of burst random excitation is that it does not take into account the effects of non-linearity, because it is not possible to differentiate between the linear and non-linear effects due to the mixing of all the frequencies. Modal parameter estimation is carried out with the help of Polymax.

- Ideas Test System (B&K) is used for sine dwell testing. Sine-dwell excitation is the discrete version of sine sweep. The frequency is not varied continuously, but is incremented by discrete amounts at discrete time points. The advantage of sine-dwell testing is its capability of detecting non linear structural dynamic behavior unlike the broadband excitations. As sine dwell testing requires larger acquisition times, so instead of studying the whole frequency band [0-2650 Hz], acquisition is carried out only around the first four bending modes previously identified by burst random testing by keeping the same resolution. Extraction of modal parameters is done by using Polyreference.

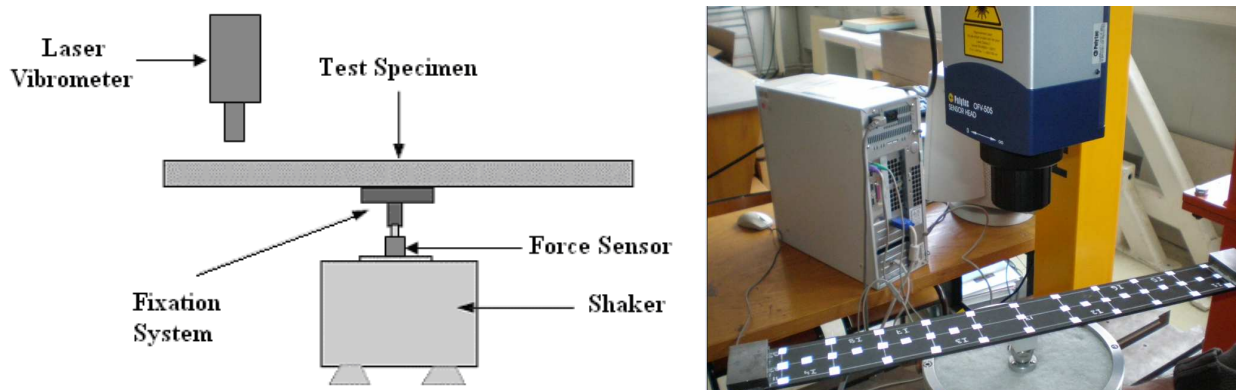


Figure 3.2 Diagram of the experimental set-up for the vibration tests

All of the test-beams in thesis have not been tested by each of these two systems. So for each set of test-beams, the type of excitation signal and type of data acquisition system shall be mentioned. The center of the test specimens is excited at Point 17 as shown in Fig. 3.3. Each sandwich specimen is tested with two types of excitations i.e., burst random and sine dwell. For both the testing systems (LMS and B&K), the resolution is kept 0.25 Hz to allow a good shape of the resonance peaks at low frequency range and to have a reliable comparison of modal parameters between the two systems. Response is measured at 27 points that are symmetrically spaced in three rows along the length of the beam to have reliable identifiable mode shapes. The level of the excitation signal for both the excitations is chosen as 1N which is kept fixed during all the vibration tests conducted in this thesis. With the help of LMS by using burst random excitation, we have the advantage of having in quick time the overall dynamic (modal) response of our structure if we are mostly concerned with frequency and mode shapes. In addition, this broadband type of testing helps us identify the modes that we can use later on for sine-dwell testing. However if we need precise damping measurements then sine-dwell testing becomes inevitable but the problem with it is the lengthy acquisition times.

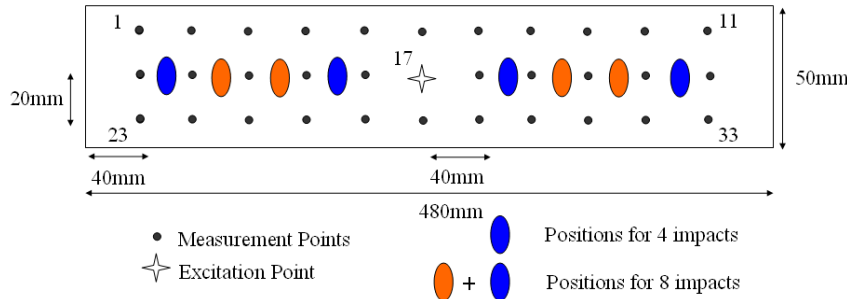


Figure 3.3 Composite test-beams with location of damage, excitation and measurement points

The modal parameters are extracted with the help of Polymax and Polyreference, integrated in the data acquisition systems, for burst random and sine-dwell testing respectively. The Polymax estimation method used by LMS acquisition system is a new non-iterative frequency domain parameter estimation method based on weighted least squares approach. This Polymax least-squares complex frequency domain method is implemented in a very similar way as the industry standard Polyreference used by B&K system, which is a time domain least squares frequency domain method. Both of these methods work in similar fashion as follows (discussed briefly in Section 2.3.3):

- Firstly all the 27 FRFs are sort of superimposed along with a FRF sum. Limited frequency band estimation is then performed by taking each resonance separately.
- For accurate assessment of damping, a frequency interval of ± 20 Hz is chosen for each resonance peak for both Polymax and Polyreference, because by changing the frequency interval damping values can be affected.
- In the next step the stability diagram is constructed containing the poles i.e., frequency, damping information. For each mathematical model order, the poles are calculated from the estimated denominator coefficients of Equation 3. The order of the mathematical model is shown on the right vertical end of the stability diagram. For reliable damping measurement, that value of pole should be chosen which displays a stable value for several model orders and if possible for each mode the value of poles should be chosen at the same model order to ensure that there is minimum uncertainty while comparing the damping values between different damage states.

One of the specific advantages of these two techniques lies in the very stable identification of the system poles and participation factors as a function of the specified system order, leading to easy-to-interpret stabilization diagrams. This implies a potential for automating the method and to apply it to "difficult" estimation cases such as high-order and/or highly damped systems with large modal overlap. As discussed previously, both Polymax and Polyreference are based on least-squares complex optimization methods, so both of them calculate the optimal pole value (frequency and damping) based on the 27 measurement points. We do not have access to the average values, variances or standard deviations for the 27 FRFs as the estimated modal parameters are the results of an optimized process. The reference [155] explains these two estimators in detail. So from the above discussion it can be said that both Polymax and Polyreference methods work in similar fashion, so the difference in the resulting modal parameters if it is the case, is due to the difference in excitations than due to the different estimation methods.

The composite beams have three states. First one is the undamaged state (UD), the second is the damage state due to 4 impacts (D1) and the third is the damage state due to 8 impacts (D2). Vibration tests are carried out after each of these three states. A simple case is studied where the impact points are chosen as such that the damage is symmetric on both sides of the two axes of symmetry.

3.2.2 Impact Tests

The composite laminate beams are damaged by drop weight impacts around the barely visible impact damage limit (BVID), in order to simulate damage by foreign impact objects such as stones or birds. The majority of these beams are impacted below the BVID limit because the effectiveness of vibration testing is for the damages not visible on the beam surface. The impact tests are carried out by a drop weight system as shown in Fig. 3.4 a, and a detailed cut away of the drop assembly is shown in Fig. 3.4 b.

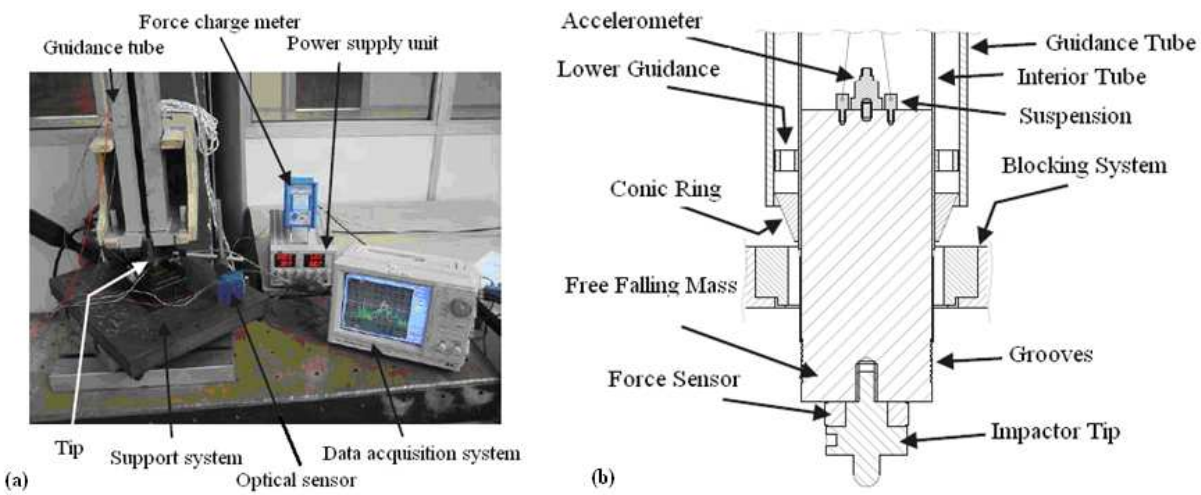


Fig. 3.4 (a) Arrangement of the test equipment for the impact test (b) Detailed cutaway of the drop assembly, the guidance tube and the blocking system

The impactor tip has a hemispherical head with a diameter of 12.7 mm. A force sensor (type 9051A) provided by Kistler is placed between the impactor tip and the free falling mass of 2 kg. The impact velocity is measured with the help of an optic sensor. The combined weight of the impact head, freefalling mass, force sensor and the accelerometer is 2.03 kg. In the calculation of impact height, a factor of 1.1 is used to compensate for the losses due to friction between the guidance tube and the drop assembly. Further details on the impact test methodology of this drop tower can be found in the references [27,33]. The composite beams have been impacted by choosing two different boundary conditions i.e., by clamping them at two ends and by clamping them at all four ends.

Impact Tests by Clamping Two Ends

A set of composite laminate beams have been impacted by clamping two sides of the beam. The beams are clamped at the two shorter ends by supports. The impact parameters for the composite laminate beams impacted this way are provided in Table 3.6. All the seven composite beams presented in Table 3.6 have been impacted below the BVID limit. As discussed previously, the detectability criterion for BVID corresponds to an average indentation (average of the indentation by measuring in different direction by a compass) of

0.6 mm measured just after impact [27,33]. For the composite beams 4-7, the indentation depth measured just after the impact is approximately in the range of 0.15 to 0.35 mm. For the beams 2-3, the indentation depth is below 0.1 mm.

Table 3.6 Impact test parameters for composite laminate beams by clamping two ends

Beam No.	Thickness (mm)	Impact Energy (J)	Height (mm)	Velocity of impact (m/s)
1	1.04	2.5	138	1.59
2	3.12	3	166	1.74
3	3.12	4	221	1.98
4	3.12	7	387	2.64
5	3.12	8	442	2.83
6	3.12	9	498	3.07
7	3.12	10	553	3.24

The impact parameters (Table 3.6) show that the impact energies can be classified into two major groups. A low impact energy group comprising of impact energies of 3J and 4J, and a high impact energy group with impact energies from 7J to 10J.

Impact Tests by Clamping all Four Ends

The next set of composite laminate beams have been impacted by clamping all four sides of the beam. The size of the impact window is 80 x 40 mm² which allows all the impact points to have the same boundary conditions. The impact parameters for the five composite beams impacted by clamping all four ends are given in Table 3.7. Beam 3 impacted at 10 J giving an initial indentation depth of 0.55 mm that shall be considered as the BVID limit. Two of the five specimens are impacted with an impact energy (6 and 8 J) below the BVID limit in order to study the damage that is not visible by naked eye, and two (12 and 14 J) above BVID.

Table 3.7 Impact test parameters for composite laminate beams by clamping all four ends

Beam No	Energy of Impact (J)	Height (mm)	Velocity of impact (m/s)
1	6	331.8	2.49
2	8	442.3	2.76
3	10 (BVID)	552.9	3.12
4	12	663.5	3.52
5	14	774.1	3.84

Beam 3 impacted at 10 J by clamping all four ends had an initial indentation depth of 0.55 mm, whereas Beam 7 impacted at 10 J by clamping two ends had 0.35 mm of damage depth. So it can be concluded that the boundary conditions of the test specimen at the time of impact play an important role in the level of damage induced to the specimen. In case of clamping at two ends, the beam moved a bit when impacted so the impact energy was not totally transferred to the beam resulting in less damage as compared to the case when the beams were clamped at all ends.

For the sake of clarity, the variation of modal parameters with impact damage in composite laminate beams shall be studied separately for the two clamping conditions.

3.3 Monitoring of Impact Damage for Composite Beams Clamped at Two Ends when Impacted

The shift in modal parameters due to impact damage in composite beams presented in Table 3.6 shall be studied in this section. The vibrations tests are carried out on composite beams by LMS Test Lab using burst random excitation.

3.3.1 Significance of End Masses

As discussed before, the end masses are placed to enhance the difference between the modal parameters for the undamaged and the damaged cases. In order to verify this, vibration tests are carried out on Beam 1, tested in the intact condition (UD), first without end masses and then with the end masses. Then it is impacted at 2.5J first at 4 points (D1) and then at 8 points (D2). After each of these two series of impacts on Beam 1, vibration tests are again carried out both with and without masses. A comparison of the frequency response functions for the measurement point 5 of Beam 1 with and without end masses is shown in Fig 3.5.

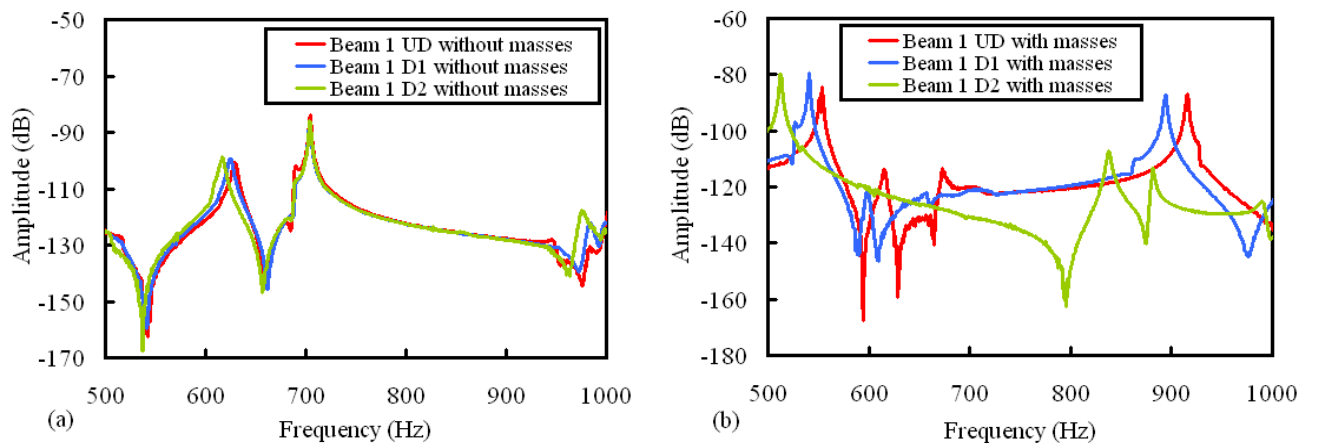


Figure 3.5 Comparison of frequency response functions (FRF) of Beam 1 at measurement point 5 for the states UD (undamaged), D1 (damaged at 4 impact points) and D2 (damaged at 8 impact points) for (a) Beam 1 without end masses and (b) Beam 1 with end masses

From Fig 3.5, it is clear that the difference in the damped modal frequencies before and after impact is greater for the case with end masses. The disadvantage of Type-1 beams (1.04 mm thickness) is that, the maximum energy for which they can be impacted is 5 J. Above this energy level, the impactor tip penetrates the specimens creating severe damage (creating a hole). The aim of the impact tests is to damage locally the test specimens instead of damaging them globally. Therefore, vibration test results ahead in this chapter concern only Type-2 specimens (3.12 mm thickness).

3.3.2 Frequency and Damping Changes

Frequency and damping changes are studied with the help of bending modes as they have the largest amplitudes for the type of test configuration presented in this thesis. The first three bending mode shapes of the composite beam calculated by the Polymax method integrated in LMS Test Lab are shown in Fig 3.6.

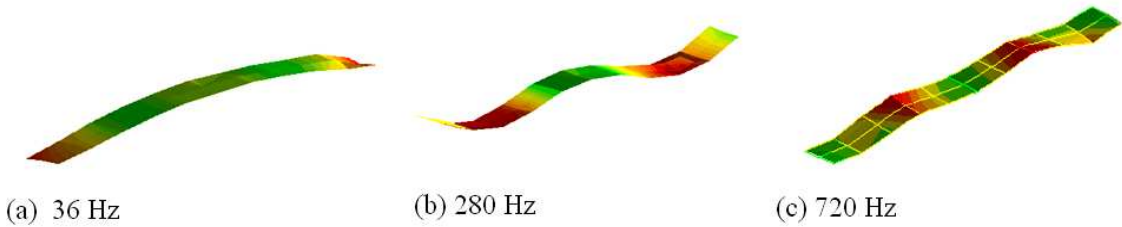


Figure 3.6 Mode shapes of composite beam calculated by the Polymax method (a) first bending, (b) second bending and (c) third bending

In this section the first bending mode is not studied, because the difference in the damped natural frequencies between the damaged states (D1 and D2) and undamaged state (UD) for the first mode is very small. For the 2nd and 3rd bending modes, the variation of damped natural frequency as a function of the undamaged (UD) and the two damage states (D1 and D2) is presented in Fig 3.7.

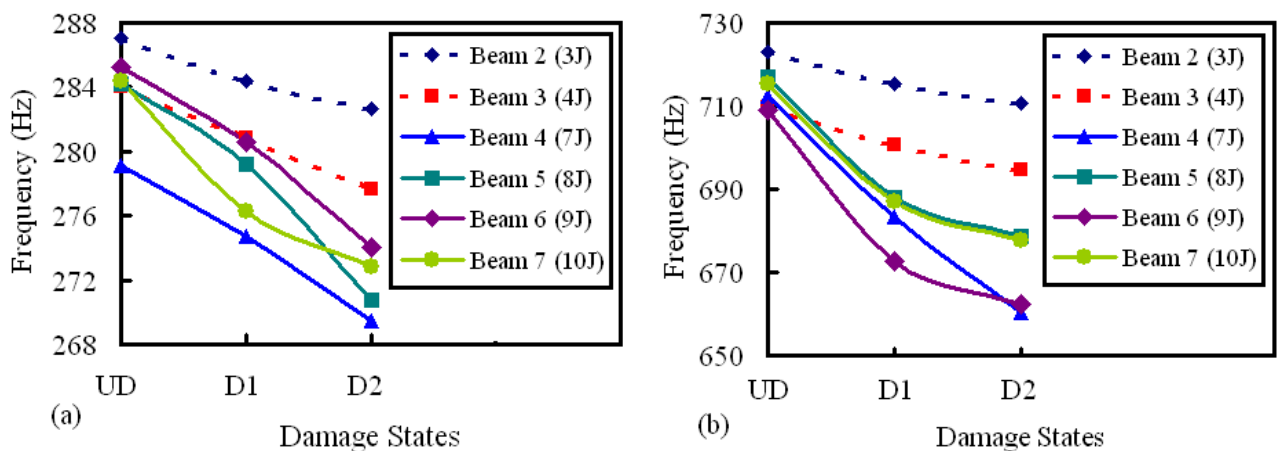


Figure 3.7 Variation of damped natural frequencies with damage states for (a) 2nd bending mode and (b) 3rd bending mode: UD is undamaged state, D1 is damaged at 4 points of impact and D2 is damaged at 8 points of impacts, for six levels of impact energy for beams clamped at two ends for the impact tests

As discussed before in Section 2.7, that damage in the specimens prompts a decrease in natural frequencies so from Figure 8, it is clear that the decrease in the natural frequencies in case of the high energy group (7, 8, 9 and 10J) is more prominent than that for the low energy group (3J and 4J). Beam 4 for the second bending mode (Figure 3.7a), has a natural frequency lower than that of the other beams for the undamaged case (UD) but this is not the case for the third bending mode (Figure 3.7b). This anomaly outlines the inherent possibility of false negatives which can arise due to boundary conditions and gives no indication of damage when it is present as discussed in the reference [46].

The shift in the natural frequencies between the undamaged and the damaged cases is more prominent at higher frequencies. This is evident in Fig 3.8, which shows a comparison of the sum of the frequency response functions for Beam 7 (impacted at 10J) for the undamaged case (UD), damaged at 4 points (D1) and damaged at 8 points (D2). The sum of the FRF can be compared as for each beam 33 symmetric measurement points have been chosen and the eight impact points are also symmetric on both sides of the two major axes of symmetry.

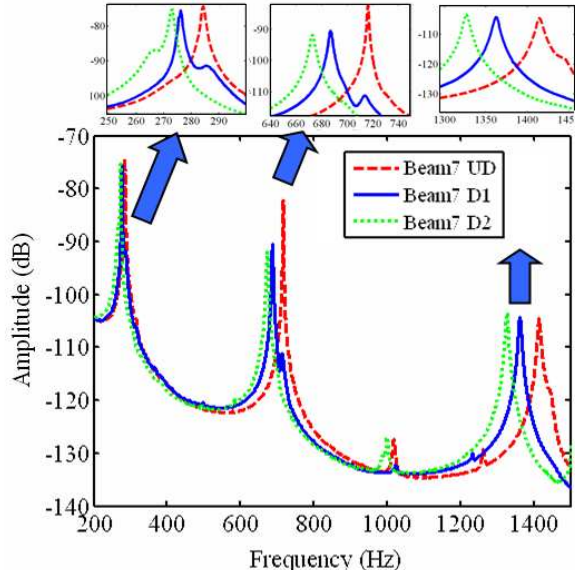


Figure 3.8 Comparison of the sum of the frequency response functions for Beam 7 for the undamaged case (UD), damaged at 4 points (D1) and damaged at 8 points (D2)

The variation of damped natural frequencies with damping ratios (shift in the s-plane) for the Beams 3, 4 and 6 for the 2nd and 3rd bending modes is plotted in Fig 3.9.

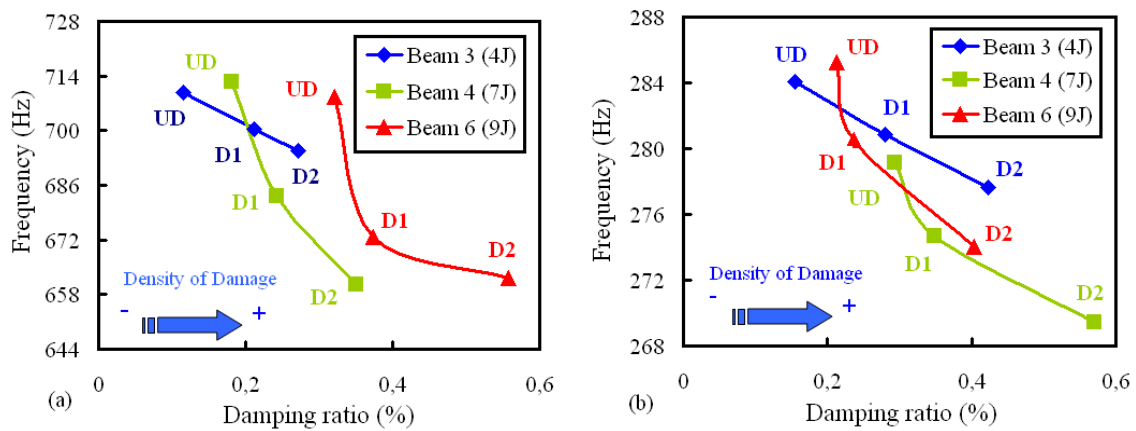


Figure 3.9 Variation of natural frequencies with damping ratio, for an increase in density of damage, for (a) 2nd bending mode and (b) 3rd bending mode, for Beam 3 (4J), Beam 4 (7J), Beam 6 (9J), where (UD) is undamaged state, (D1) damaged at 4 impact points and (D2) damaged at 8 impact points

Fig 3.9 shows that damping increases whereas the frequency decreases with the increase in damage. The increase in damping is more prominent in specimens impacted at 7J and 9J (Beam 4 and 6) as compared to 4J (Beam 3). So it can be said that the variation of damping ratio validates the theoretical reasoning presented in Section 2.7.

In scientific literature, several works underlined that the damping change ratios are more prominent than the frequency change ratios. In case of Beam 6 (9J), the average change in natural frequency (between the damaged and the undamaged cases) for the first four bending modes is 3.5 % whereas in case of damping ratios this average change is as high as 23 % (Annex Tables 3.A and 3.B). Therefore, use of damping as a damage indicator tool instead of stiffness might prove more fruitful.

3.3.3 Damage Index Variations

Another way to explain the changes in modal parameters due to damage is with the help of a Damage Index (DI), as explained in reference [21,59]. The first step is to calculate the integral (I_x) of the amplitude of the frequency response functions (FRF) over a defined frequency range (interval) as follows:

$$I_x = \int_{f_k-int}^{f_k+int} |H(\omega)| d\omega \quad (3.2)$$

where $H(\omega)$ is the frequency response function matrix obtained experimentally, (f_k) is the damped resonant frequency and (int) means the frequency interval chosen.

In the second step, the Damage Index is calculated by taking the percentage difference between the integrals of the resonance peaks of the FRF at the damaged and the undamaged states. In this study, there are two damaged states (D1 and D2) and one undamaged state (UD). So the two damage indices are calculated as follows:

$$\text{Damage Index for states D1 and UD} = DI4 = \left| \frac{I_x^{4\text{Damaged}} - I_x^{\text{Undamaged}}}{I_x^{\text{Undamaged}}} \right| \times 100 \quad (3.3)$$

$$\text{Damage Index for states D2 and UD} = DI8 = \left| \frac{I_x^{8\text{Damaged}} - I_x^{\text{Undamaged}}}{I_x^{\text{Undamaged}}} \right| \times 100 \quad (3.4)$$

where $I_x^{\text{Undamaged}}$, $I_x^{4\text{Damaged}}$ and $I_x^{8\text{Damaged}}$ are the integrals of the resonance peaks of the FRF for the undamaged state (UD), damage state D1 (damaged at 4 points) and damage state D2 (damaged at 8 points) respectively.

For our work, a frequency interval of $\pm 20\text{Hz}$ (Fig 3.10) is chosen to calculate the integral of the resonance peaks of the FRF. In order to verify the robustness of this method, similar calculations have been carried out on frequency intervals of $\pm 10\text{Hz}$ and $\pm 40\text{Hz}$ as well. It has been observed that if the intervals are changed, the values of the integral (I_x) are different but the damage index always gives the same results being a ratio.

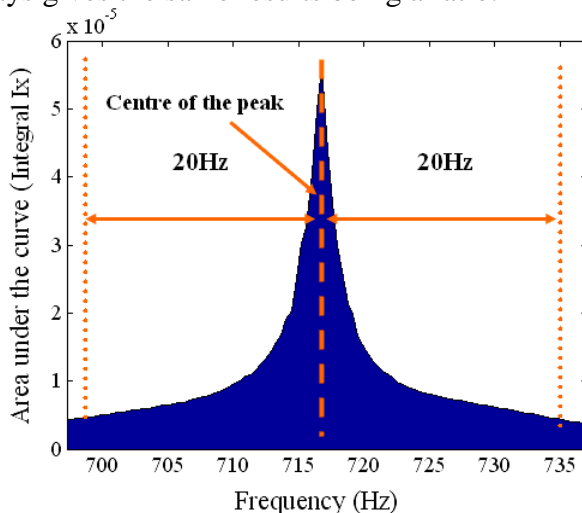


Figure 3.10 Methodology for the calculation of integral I_x (area under the curve)

The percentage increase in damage index is the percentage difference of DI8 and DI4 based on Equations (3.3) and (3.4) and is calculated as follows:

$$\% \text{ increase in damage index} = \left[\left(\frac{DI8 - DI4}{DI8} \right) \times 100 \right] \quad (3.5)$$

The damage index variation is explained in Fig 3.11 by plotting the percentage increase in damage index calculated from Equation (3.5) as a function of the first four bending modes.

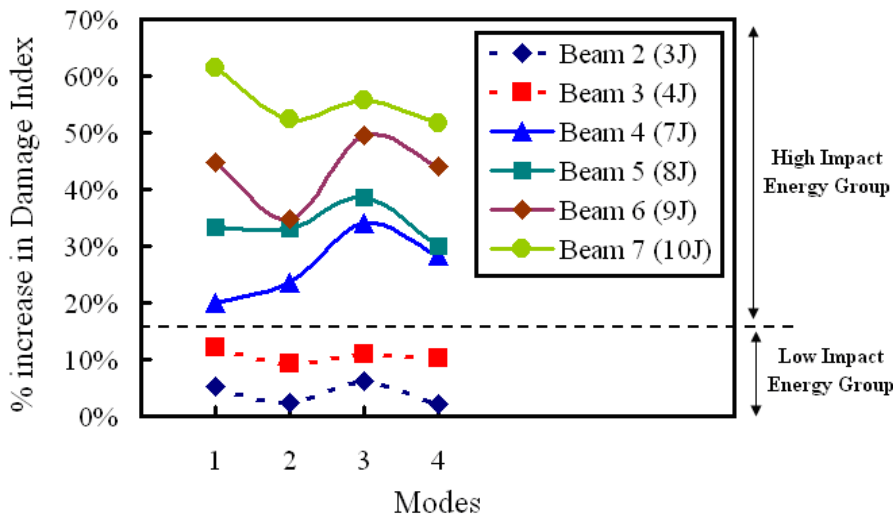


Figure 3.11 Variation of percentage of increase in Damage Index as a function of modes for the six Type-2 composite beams impacted by clamping two ends

Fig 3.11 shows that in case of the low energy impact group (3J and 4J), the percentage increase in damage index is between 2% to 13%. But in the cases of high impact energies (7, 8, 9 and 10J), this percentage ranges from 20% to 60%. Therefore, there is a clear increase in damage index with the rise in impact energy levels which corresponds to damage accumulation in the composite beam specimens.

3.3.4 Comparison of Damping Ratio and Integral of the Resonance Peaks

A comparison between the damping ratio and the integral of the resonance peaks (I_x) is carried out because they both describe the shape of the peak in the frequency response. The damping ratio and the integral (I_x) calculated by Equation (3.2) plotted as a function of damped natural frequency for the 2nd and 3rd bending modes, for the Beams 3, 4 and 6 is shown in Fig 3.12. This type of graph is also known as the s-plane as discussed in Section 2.7. The direction of the increase of damage is represented by the increase in marker size for each plot. The smallest marker size represents the undamaged state (UD), the medium damage at 4 points (D1) and the largest damage at 8 points (D2).

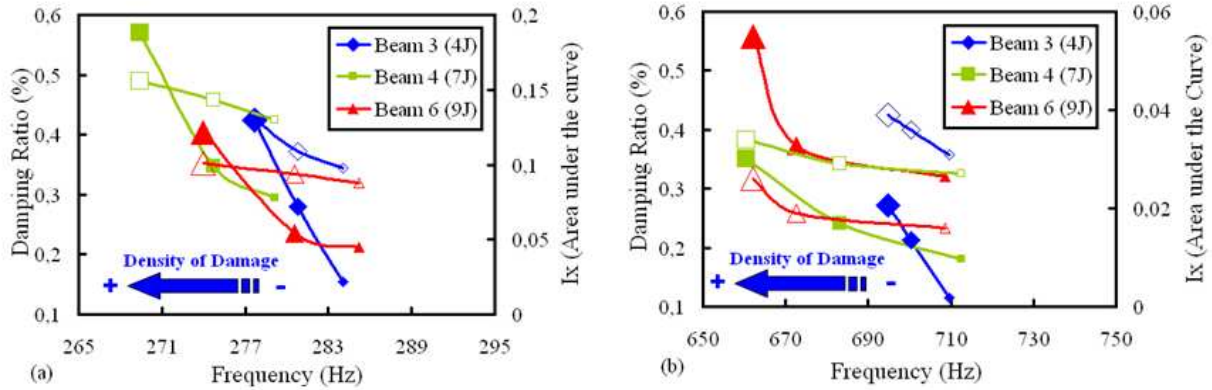


Figure 3.12 Variation of Damping ratio and Integral (I_x) as a function of frequency for (a) second bending mode (b) third bending mode for Beam 3 (4J), Beam 4 (7J), Beam 6 (9J). Damping ratio—◆—(4J), —■—(7J)—▲—(9J). Integral—◇—(4J), —□—(7J) and —△—(9J).

It can be seen from Fig 3.12, that the variation of damping ratio and the integral of the amplitudes of the resonance peaks (I_x) show similar behavior for the same beam specimen which is not surprising because they both describe the form of the resonance peaks. For the other three Type-2 beams (Beam 2, 5 and 7), the damping ratios estimated by the Polymax method are not stable because they do not show an increase with the increase in damage in the specimens. On the other hand, the integral (I_x) values for these three beams (Beam 2, 5 and 7) increase with the increase in damage in the specimens. This variation of the integral (I_x) with the increase in damage for Beam 2, 3 and 5 for the 2nd and 3rd bending modes is plotted in Fig 3.13. As both damping ratio and damage index (based on the integral I_x) explain the same phenomenon, therefore the reason for introducing the Damage Index (DI) parameter is to verify the damping ratio results estimated by Polymax which are not stable for the case of Beam 2, 3 and 5. In using DI, an additional tool is introduced for understanding the damping behavior of damaged composite beams.

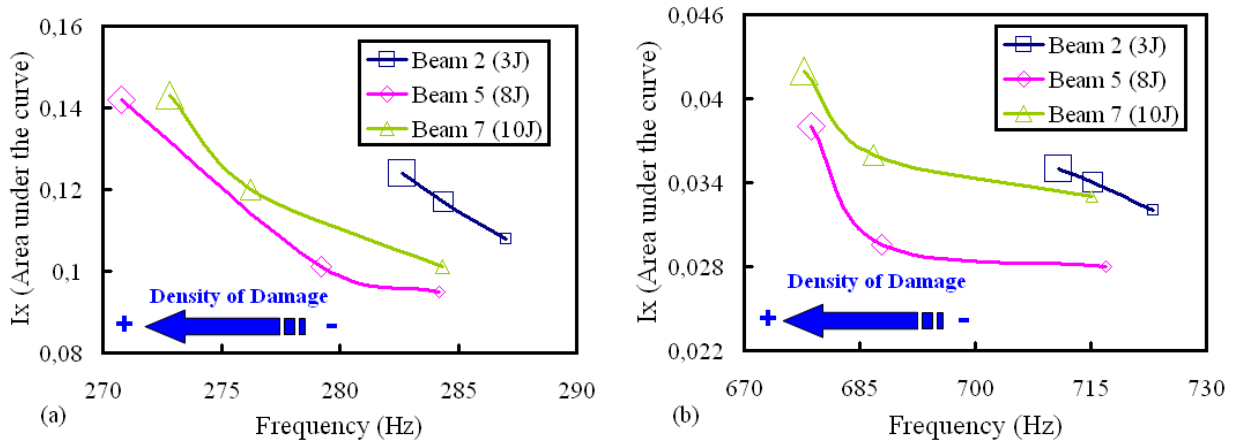


Figure 3.13 Variation of Damping ratio and Integral (I_x) as a function of frequency for (a) second bending mode (b) third bending mode for Beam 2 (3J), Beam 5 (8J), Beam 7 (10J)

3.3.5 Design of Experiments

Design of experiments is a powerful analysis tool for modeling and analyzing the different factors which affect an experimental process and the output of that process [140]. This study

is carried out on the six Type-2 composite beams impacted by clamping two ends. The aim is to identify the factors which have the most significant effect on the experimental results (natural frequencies). These design factors along with their respective levels are given in Table 3.8. By keeping in view the levels of the two factors, a 6x3 full factorial design is chosen. The results of the design of experiments are shown with the help of leverage plots in Fig 3.14.

Table 3.8 Design parameters for the design of experiments and levels for each factor

Design Factors		Levels for each Factor					
Density of Damage	UD (undamaged)	D1 (4 impacts)			D2 (8 impacts)		
Energy of Impact	3 J	4 J	7 J	8 J	9 J	10 J	

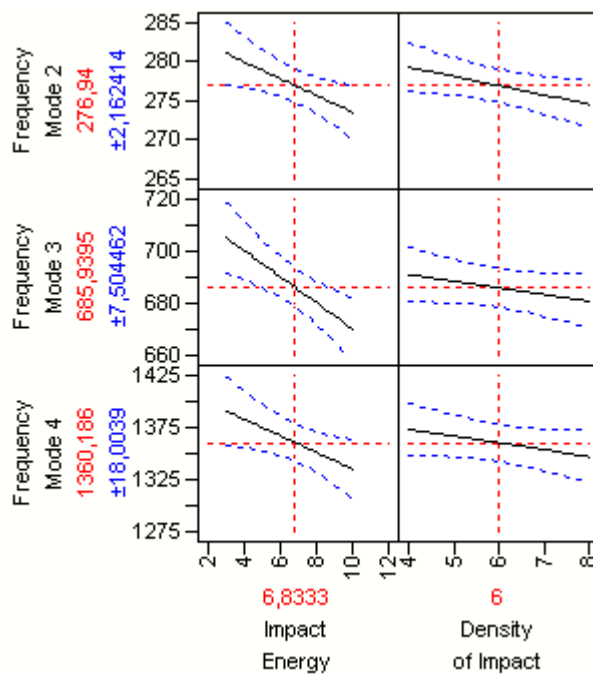


Figure 3.14 Results of Design of Experiments (Leverage plots with confidence curves)

The leverage plots are shown with confidence curves in dotted blue with their respective values in blue on the y axis. The horizontal red dotted line shows the current predicted value of each Y variable for the current values of the X variables. The black lines show the prediction trace. If the confidence curves cross the horizontal red lines, then the effect of that factor is said to be significant on the results. If the confidence curves are asymptotic to the horizontal line then the effect of the factors is marginally significant and finally if the confidence region between the curves contains the horizontal line then the effect is said to be insignificant. The results shown in Fig 3.14 prove that the effects of impact energy are significant on the natural frequencies for the 2nd, 3rd and 4th bending modes. The effects of the density of impact are partially significant on these modes as compared to the impact energy. However, these two factors have no influence on the natural frequency of the first bending mode because the frequency shift between the damaged and the undamaged cases is insignificant.

3.4 Monitoring of Impact Damage for Composite Beams Clamped at all Four Ends when Impacted

Monitoring of impact damage by shift in modal parameters is carried out on composite beams presented in Table 3.7 by clamping all four ends. The vibrations tests are carried out on composite beams by LMS Test Lab using burst random excitation. The major difference from the previous set of tests on composite beams is that vibration tests are carried out by gluing small reflecting stickers at the measurement points as shown in Fig 3.2. These stickers help in reflecting better the vibrometer laser beam thus rendering the measurements much less noisier as compared to the tests in section carried without stickers.

3.4.1 Frequency and Damping Changes

Frequency and damping changes are studied with the help of the first four bending modes as they have the largest amplitudes for the type of test configuration presented in this thesis. As discussed previously, delamination induced damage in composites leads to an increase in damping and a decrease in natural frequency. This effect is more significant in the high frequency range [38]. This fact is verified by our experimental results which show that the difference in natural frequencies between the damaged (D1 and D2) and the undamaged state (UD) for the first mode is very small. But this difference in frequencies increases for the higher modes. For the 2nd and 3rd bending modes, the variation of natural frequency as a function of the undamaged (UD) and the two damage states (D1 and D2) is presented in Fig 3.15.

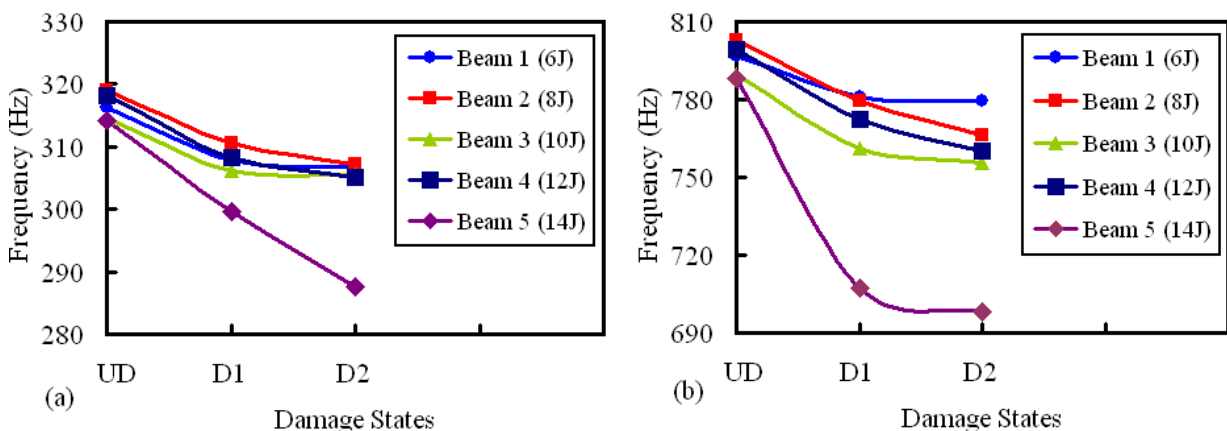


Figure 3.15 Variation of damped natural frequencies with damage states for (a) 2nd bending mode and (b) 3rd bending mode: UD is the undamaged state, D1 is the damaged state at four impact points and D2 is the damaged state at eight impact points

Fig 3.15 (a) and (b) show that the decrease in natural frequencies with the increase in damage is more significant in case of the higher impact energies as observed in Section 3.3.2. In case of Beams 1-4, the trend of decrease in frequency with damage is relatively small, but the trend increases consistently with the damage. It can be concluded that the four beams (Beams 1-4) remain relatively intact and do not possess a large amount of damage. However, Beam 5 damaged at impact energy of 14 J, which induced damage well above the BVID limit, has a more significant change in frequencies as compared to the other beams. This fact is also evident in Table 3.9, which compares the change in natural frequencies between the undamaged and the damaged states. Similar results are obtained for the 4th bending mode.

The damping ratios estimated by Polymax from burst random testing for the five composite beams impacted by clamping at four ends are shown in Fig 3.16. Fig 3.15 and Fig 3.16 show a slight discrepancy between the modal parameters at the undamaged state. This anomaly outlines the inherent possibility of false negatives as discussed in Section 3.3.2.

It can be seen from the results in Fig 3.16 that the damping ratio increases with increase in damage in the five beams except for Mode 2 (Fig 3.16 b). Furthermore, the change in damping ratios between the three states (UD, D1 and D2) for Beams (1-4) is very small for the 2nd and 3rd bending modes (Fig 3.16 b and 3.16 c). However unlike natural frequencies, the increase in damping ratio between the damaged and the undamaged states is not always consistent with the impact energy level, due to the complex nature of damping and the difficulties in its estimation. But in case of Mode 4 (Fig 3.16 d), damping ratio exhibits quasi linear dependence on the energy of impact.

The damping ratio results for the set of composite beams presented in this section are more coherent as compared to those presented in Section 3.3.2. The main reason for achieving better damping results is that the measurements are more noise free due to use of reflecting stickers. As damping is a more complex parameter estimate, so it is more affected by the quantity of noise in the measurements as compared to natural frequency.

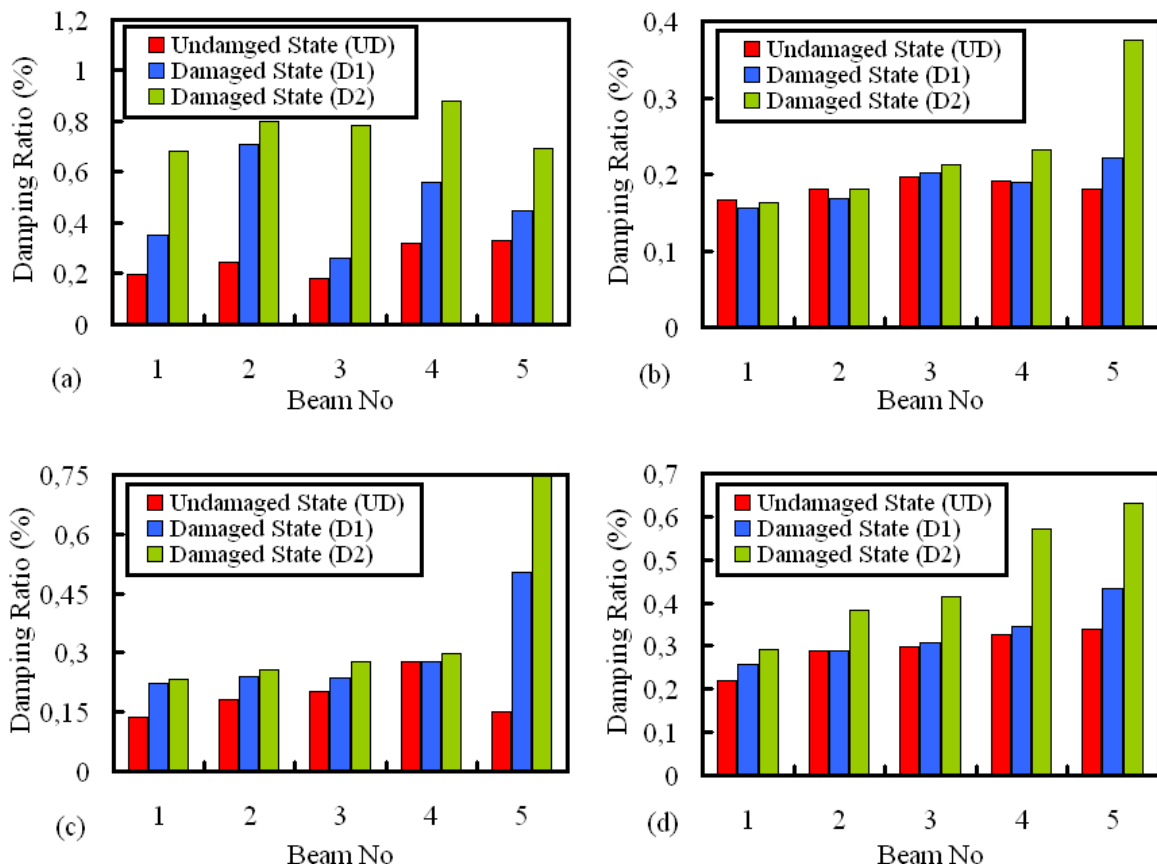


Figure 3.16 Variation of damping ratios (%) estimated by Polymax for the five composite beams for (a) 1st bending mode (b) 2nd bending mode (c) 3rd bending mode and (d) 4th bending mode, where 'UD' is the undamaged state, 'D1' is the damaged state at four points and 'D2' is the damaged state at eight points

Furthermore, the modal parameter results underline the fact that the damping change ratios are more prominent than the frequency change ratios. In case of Beam 5 impacted at 14 J, the average change in natural frequency (between the damaged and the undamaged cases) for the first four bending modes is 8% whereas in case of damping ratios this average change is as high as 78% (Tables 3.9 and 3.10). So it is reasonable to assume that damping may be used instead of natural frequency as a damage indicator tool for structural health monitoring purposes. However, the fact that damping is a parameter that is relatively difficult to estimate as compared to natural frequency has to be taken into account.

Table 3.9 Frequency change ratios (%) between the undamaged (UD) and the two damaged states (D1 and D2) for the five composite beams impacted by clamping all four ends

Beam No	Between States	Mode 1	Mode 2	Mode 3	Mode 4
Beam 1 6J	UD & D1 UD & D2	3.6 4.6	2.6 3.0	2.0 2.1	1.9 2.3
Beam 2 8J	UD & D1 UD & D2	6.1 6.6	2.7 3.7	2.9 4.6	2.6 5.9
Beam 3 10J	UD & D1 UD & D2	4.8 5.5	2.6 2.8	3.6 4.1	7.2 7.7
Beam 4 12J	UD & D1 UD & D2	3.4 5.1	3.1 4.0	3.4 4.9	3.4 4.5
Beam 5 14J	UD & D1 UD & D2	4.1 7.4	4.6 8.4	10.6 11.1	4.4 11.7

Table 3.10 Damping change ratios (%) between the undamaged (UD) and the two damaged states (D1 and D2) for the five composite beams impacted by clamping all four ends

Beam No	Between States	Mode 1	Mode 2	Mode 3	Mode 4
Beam 1 6J	UD & D1 UD & D2	76.5 240.5	-6.5 -2.9	64.7 70.5	16.8 33.1
Beam 2 8J	UD & D1 UD & D2	10.7 19.5	-6.6 -0.5	31.6 29.0	229.5 77.0
Beam 3 10J	UD & D1 UD & D2	44.6 77.2	2.5 7.9	17.2 26.7	3.0 28.2
Beam 4 12J	UD & D1 UD & D2	42.9 175.6	-1.5 20.3	0.7 7.2	4.6 74.0
Beam 5 14J	UD & D1 UD & D2	35.1 52.3	23.3 52.1	234.7 82.2	80.0 61.9

For certain measurement points, damage in the composite beams distorts the shape of the resonance peaks and sometimes there is an appearance of twin peaks instead of one in the frequency response functions (FRF) as shown in Fig 3.17

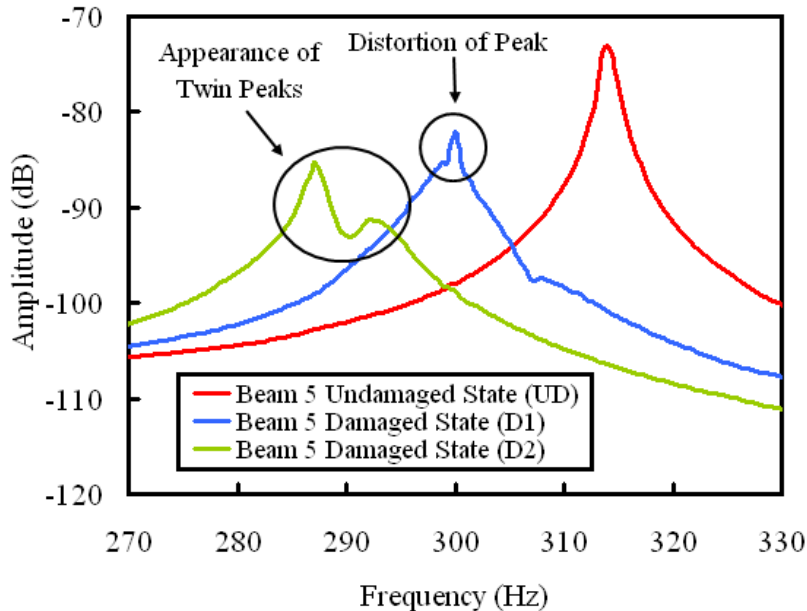


Figure 3.17 Comparison of the shapes of the FRF at point 2 for Beam 5 for (UD) is the undamaged state, (D1) is the damaged state at four impact points and (D2) is the damaged state at eight impact points

Damage Index calculations give similar results as in case of previous set of composite beams (Section 3.3.3). In case of the composite beams impacted by clamping all four ends, it can be seen from Annex Fig 3.B that damage index increases with the rise in impact energy levels which corresponds to damage accumulation in the composite beam specimens. Similarly the variation of damped natural frequencies with damping ratios (shift in the s-plane) for the composite beams impacted by clamping all four ends is plotted in Annex Fig 3.A and gives similar results as compared to the results shown in Section 3.3.2.

3.4.2 Design of Experiments (DOE)

In Section 3.3.5, design of experiments on the composite beams impacted by clamping two sides was carried out only on the natural frequency as the damping ratio results were less reliable due to noisy measurements. For the present set of composite beams, relatively better damping ratio results are obtained so the statistical study is carried out on both natural frequencies and damping ratios estimated by burst random excitation, with an aim to identify the factors which have the most significant effect on the experimentally obtained modal parameters.

The two factors chosen for the design of experiments are the energy of impact (*IE*) and the density of damage (*DD*). For the energy of impact there are five levels (6, 8, 10, 12, 14J) and for the density of damage there are three levels (undamaged state, damage at 4 impact points and damage at 8 impact point). By keeping in view the levels of the two factors, a 5 x 3 full factorial design is chosen. The linear regression model associated with a 5 x 3 full factorial design, based on the two variables discussed above is expressed as follows:

$$Y = a_0 + a_1 \cdot (IE) + a_2 \cdot (DD) + a_3 \cdot (IE) \cdot (DD) + E \quad (3.6)$$

In Equation 3.6, coefficients represent model constants (a_i) that are the contribution of independent variables on the response. E is the random error term representing the effects of uncontrolled variables, i.e., not included in the model. The model constants (a_i) are determined by multi-linear regression analysis and are assumed to be normally distributed. The error is assumed to be random and normally distributed. These constants (a_i) are obtained with 90% confidence level. The significance of each variable on a given response (modal parameters in our case) is investigated using t test values based on Student's distribution. The t ratio is the ratio of the parameter estimate (constants) to its standard deviation. A t ratio greater than 2 in absolute value is a common rule of thumb for judging significance of the variable. The derived constants (a_i) and t ratios for the natural frequencies and the damping ratios are presented in (Tables 3.11 and 3.12). The t ratios greater than 2 are marked in bold in (Tables 3.11 and 3.12). Negative values of the model constants and t ratios indicate that the response decreases with the increase in the value of the parameter. In our case, this is most of the times true for the natural frequencies (Table 3.11) as they decrease with the increase in damage in the specimens.

Table 3.11 Coefficients and t ratios for the natural frequencies (Hz)

	Mode 1		Mode 2		Mode 3		Mode 4	
Term	Constants (a_i)	t ratio						
IE	0.122	0.66	-7.66	-5.06	-38.91	-6.29	-53.69	-10.33
DD	-0.532	-4.09	-2.36	-2.57	-4.52	-1.03	-30.73	-7.93
IE x DD	-0.278	-1.51	-2.48	-1.64	-2.17	-0.35	-24.03	-4.39

Table 3.12 Coefficients and t ratios for damping ratios (%) estimated by Polymax (burst random testing)

	Mode 1		Mode 2		Mode 3		Mode 4	
Term	Constants (a_i)	t ratio						
IE	0.014	0.20	0.063	4.36	0.186	2.83	0.126	9.80
DD	0.151	3.00	0.026	2.20	0.043	0.92	0.066	7.64
IE x DD	0.007	0.10	0.008	1.26	0.016	1.03	0.046	1.74

By comparing the t ratios for the energy of impact (IE) and the density of damage (DD) in (Tables 3.11 and 3.12), it can be seen that the energy of impact has a more significant effect on the modal parameters than the density of damage for the 2nd, 3rd and 4th bending modes. However, the density of damage is a more significant factor for the first bending mode. The second order interaction term (IE x DD) is in the majority of the cases insignificant as well.

From the design of experiments, it can be concluded that the energy of impact (IE) is the most significant factor on the natural frequencies and damping ratios (estimated by Polymax method with burst random excitation) for the 2nd, 3rd and 4th bending modes. These design of experiments results validate those found previously in Section 3.3.5.

3.5 Conclusion of the Third Chapter

Vibration tests have been carried out on pristine and damaged composite laminate beams. The composite beams have been impacted by choosing two different boundary conditions i.e., by **clamping them at two ends** and by **clamping them at all four ends**, by keeping in view the BVID limit. The aim is not to make a comparison between the variations of modal parameters for the two impact boundary conditions. At the start of the thesis, the fixation system available only provided the opportunity to impact the beams by clamping two ends. It was observed that the beams were not properly held and so for the next lot of composite laminate beams, the fixation system was modified so that impacts by clamping all four ends can be done. However it was observed that if impacted at the same energy, beam clamped at two ends had lesser damage than the beam clamped at four ends. Results for the two lots of beams are presented to give a better validation of the variations of modal parameters with impact damage in composite laminate beams.

Results show that with the accumulation of damage in the specimens, there is a **decrease in natural frequency accompanied by an increase in damping ratio**. Results show that damping ratio is a more sensitive parameter for damage detection than the natural frequency. Better and noise free vibration test results are obtained by **gluing reflecting stickers** on the measurement points. **Energy of impact** is highlighted as the factor having the most significant effect on the modal parameters by carrying out design of experiments on the experimental data.

Chapter 4 : Study of Two Different Types of Damage in Honeycomb Sandwich Beams by Shift in Modal Parameters

4.1 Introduction to Sandwich Structures

Sandwich structures are commonly used in aerospace and automobile structures, since they offer great energy absorption potential and increase the flexural inertia without significant weight penalties. The purpose of the core is to maintain the distance between the laminates and to sustain shear deformations. By varying the core, the thickness and the material of the face sheet of the sandwich structures, it is possible to obtain various properties and desired performance [126-129]. Examples of widely used laminate materials are glass reinforced plastic (GRP) and carbon fiber. There are many wide varieties of core materials currently in use. Among them, honeycomb, foam, balsa and corrugated cores are the most widely used. Usually honeycomb cores are made of aluminum or of composite materials: Nomex, glass thermoplastic or glass-phenolic. The other most commonly used core materials are expanded foams, which are often thermoset to achieve reasonably high thermal tolerance, though thermoplastic foams and aluminum foam are also used. For the bonding of laminate and core materials, normally two types of adhesive bonding are commonly employed in sandwich construction, i.e., co-curing and secondary bonding.

Characterization of sandwich materials has been carried out in detail in scientific literature. The determination of the sandwich material behavior under crushing loads and the measurements of the ductile fracture limits is normally done with the help of compression tests [130,131]. Typically, cores are the weakest part of sandwich structures and they fail due to shear. Understanding the shear strength properties of sandwich core plays an important role in the design of sandwich structures subjected to flexural loading [132,133]. Therefore, 3-point bending tests are often performed to find the flexural and shear rigidities of sandwich beams [134-136].

4.1.1 Design Principle

The design principle of sandwich composite materials is based on the concept of I-beams. These types of structures get their structural efficiency, as most part of the material is situated in the flanges, which are located far from the centre (neutral axis). Correspondingly, the rigid plates in the sandwich replace the flanges of the I-beam and the core does the web's function. From a functional point of view, both structures have the same behavior (I-beam and sandwich beam Fig 4.1). However if the compositions of both these forms are considered, it shall be seen that the I-beam is made of classical materials and the sandwich type is made of materials intrinsically and mechanically different.

The core resists the shear loads, increases the stiffness of the structure by holding the facing skins apart, and improving on the I-beam, it gives continuous support to the flanges or facing skins to produce a uniformly stiffened panel. The core-to-skin adhesive rigidly joins the sandwich components and allows them to act as one unit with a high torsional and bending rigidity. The outside rigid plates of sandwich structure are called skins or faces, and the material used in the middle is known as core. Fig 4.1 also shows a sandwich structure with position of its constituents.

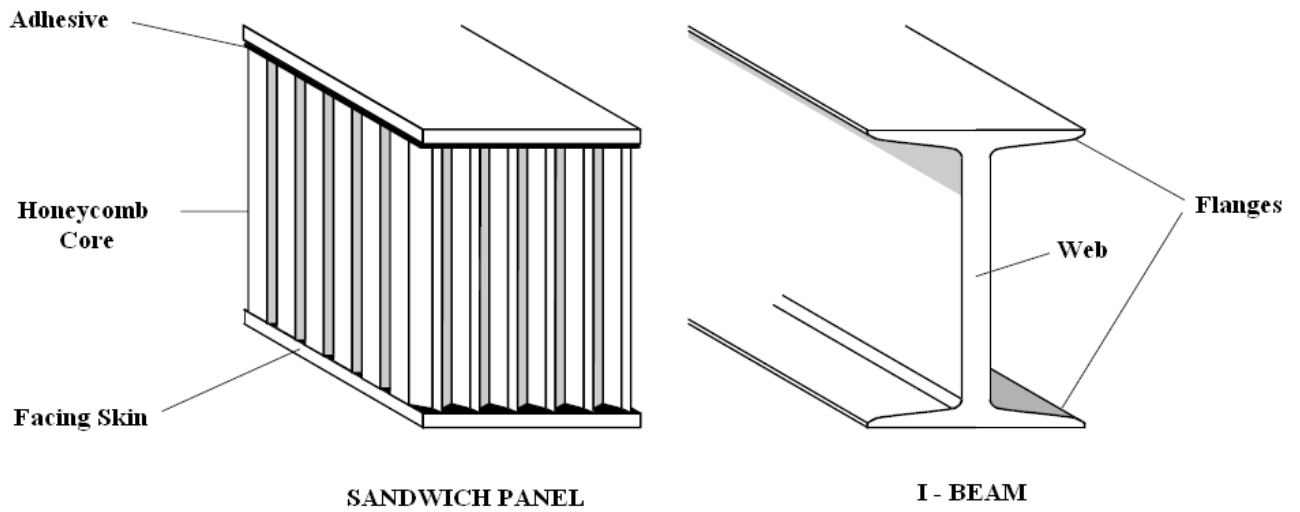


Figure 4.1 I-Beam and sandwich composite beam with its constituents

The skins act together to form an efficient stress couple or resisting moment counteracting the external bending moment. The core resists shear and stabilize the faces against buckling. The adhesive between the faces and the core must be strong enough to resist the shear and tensile stresses set up between them. These loads and stresses imposed on a sandwich panel are shown in Fig 4.2.

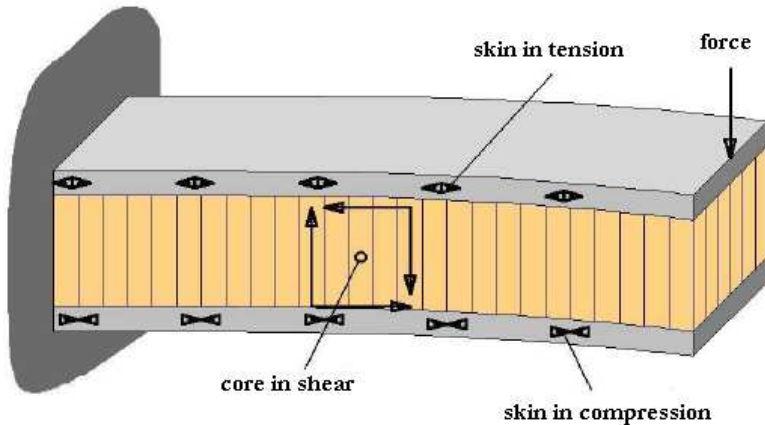


Figure 4.2 Loads and stresses in a sandwich beam under flexural load

The deflection of a sandwich panel is made of bending and shears components. The bending deflection is dependent on the relative tensile and compressive modulus of the skin materials and the shear deflection is dependant on the shear modulus of the core. Therefore,

$$\text{Total Deflection} = \text{Bending Deflection} + \text{Shear Deflection}$$

The skin and core definition besides other related vocabulary are formally described in the ASTM norms [C274-99]. A compilation of the norms applicable to the sandwich structures is presented in [128].

4.1.2 Advantages and Disadvantages

The main aim of sandwich structures is that they are light and stiff resulting in an extremely high flexural stiffness to weight ratios and widely used in mechanical structures such as airplanes and ships. The design flexibility offered by these and other composite configurations is obviously quite attractive to designers, and the potential now exists to design not only the structure but also the structural material itself. In marine structures, carbon fiber epoxy skins with polyurethane foam panels are being used. The common properties for the skin materials in a sandwich are:

- High stiffness giving high flexural stiffness
- High tensile and compressive strength
- Impact resistance
- Surface finish
- Environmental resistance
- Wear resistance

The disadvantage, however, is that composite materials present challenges for design, maintenance and repair over metallic parts since they tend to fail by combined failure modes [127,128].

4.1.3 Modes of Failure

Furthermore, damage detection in composite sandwiches is much more difficult due to the anisotropy of the material, the conductivity of the fibers, the insulation properties of the matrix and the fact that much of the damage often occurs beneath the top surface of the laminate. There principal modes of failure of composite sandwiches are:

The skin and core materials should be able to withstand the tensile, compressive and shear stresses induced by the design load. The skin to core adhesive must be capable of transferring the shear stresses between skin and core.

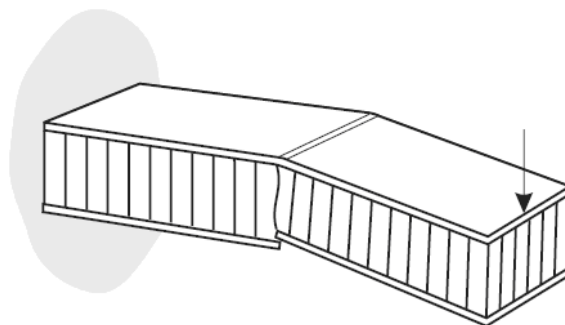


Figure 4.3 Skin compression failure due to end loading

The sandwich panel should have sufficient bending and shear stiffness to prevent excessive deflection.

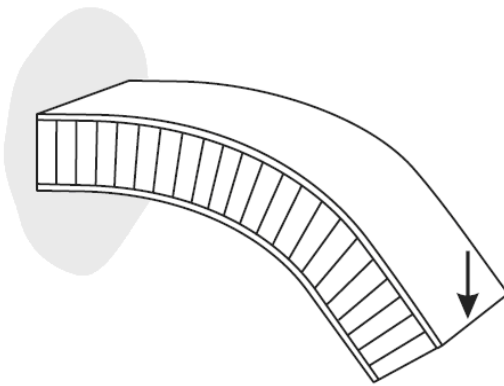


Figure 4.4 Excessive deflection due to larger end load

The core thickness and shear modulus must be adequate to prevent the panel from buckling under end compression loads.

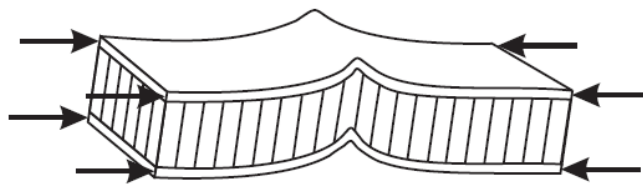


Figure 4.5 Panel buckling

The core thickness and shear modulus must be adequate to prevent the core from prematurely failing in shear under end compression loads.

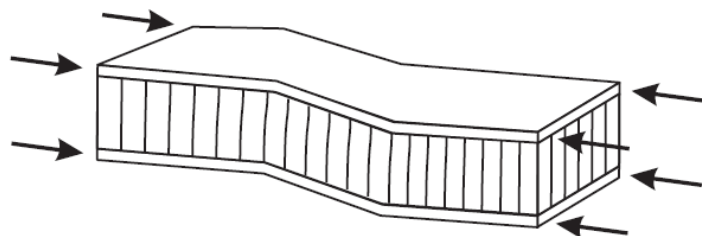


Figure 4.6 Shear crimping

The compressive modulus of the facing skin and the core compression strength must both be high enough to prevent skin wrinkling failure.

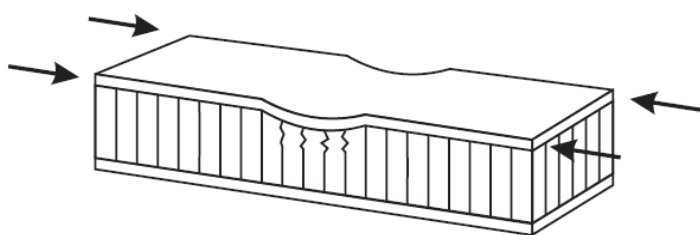


Figure 4.7 Skin wrinkling

For a given skin material, the core cell size must be small enough to prevent intra cell buckling.

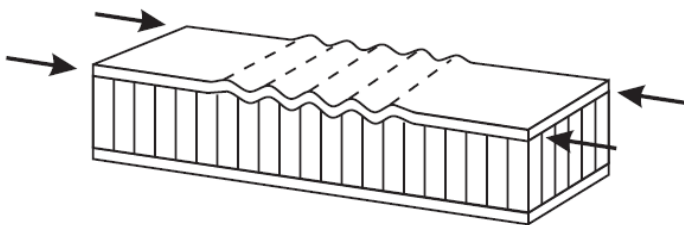


Figure 4.8 Intra cell buckling

Design, construction and mechanical application of sandwich structures are explained in detail by Allen [127] and Zenkert [128]. In addition, other types of failures can occur in the laminated composite (face sheet) such as fiber breaking, debonding, matrix micro-cracking and delamination.

The aim of this chapter is to monitor two different types of damages (impact and core-only damages) by shifts in modal parameters in honeycomb sandwich beams.

4.2 Damage Monitoring in Honeycomb Sandwich Beams by Modal Parameter Shifts

4.2.1 Materials and Types of Honeycomb Sandwich Beams

Resin-containing carbon-fiber/epoxy prepgs of T700/M21 is used to fabricate the skin materials [138]. The material is supplied by Hexcel composites, the physical properties are set out in Table 4.1. The upper and lower skins consist of four plies each with a stacking sequence of [0/90/90/0]. The thickness of each ply is 0.125mm.

Table 4.1 Physical properties of carbon/epoxy prepgs T700/M21as skin material [138]

Properties	Value
Young's modulus in fiber direction (E_1)	125000 MPa
Young's modulus in transverse direction (E_2)	9000 MPa
Shear Modulus (G_{12})	5000 MPa
Poisson Ratio (ν_{12})	0.4
Volume density (ρ)	1550 kg/m ³

The core material is honeycomb and can be selected from a wide range of metallic and non-metallic honeycomb cores. The honeycomb sandwich beams in this thesis are made of Nomex-aramid honeycomb core (HRH 10) supplied by Hexcel composites [139]. The honeycomb core has a nominal cell size of 6.5 mm and a core thickness of 10 mm. Mechanical properties of the honeycomb core is listed in Table 4.2. The sandwich beam specimens are fabricated using an autoclave and an aluminum mold. The skin and the core are

cured simultaneously in order to have an excellent bond. The final dimensions of the six identical honeycomb sandwich beams used in this thesis are 480 x 50 x 11 mm.

Table 4.2 Properties of Honeycomb core (Hexel-aramid)

Properties	Value
Cell size	6.5 mm
Density	31 kg/m ³
Compressive strength	0.896 MPa
Compressive modulus	75.8 MPa
Shear strength in longitudinal direction (σ_{xz})	0.65 MPa
Shear modulus in longitudinal direction (G_{xz})	29 MPa
Shear strength in width direction (σ_{yz})	0.31 MPa
Shear modulus in width direction (G_{yz})	13.8 MPa

The vibration tests are carried out with two steel masses (50 x 25 x 5 mm) attached at the ends [20,55,57].

4.2.2 Experimental Techniques

Vibration and impact tests shall be carried out on the fabricated honeycomb sandwich beams by following the same procedure as of the composite laminate beams in Chapter 3 in Section 3.2.1. Vibration tests shall be carried out by both burst random and sine-dwell excitations by using LMS Test Lab and Ideas B&K System respectively, as discussed in Section 3.2.1.

In case of the impact tests, the apparatus explained in Section 3.2.2 shall be employed. Impact tests shall only be done by clamping all four ends of the beam-type specimens. A schematic of the honeycomb sandwich beam with the locations of damages, measurement and excitation points are shown in Fig 4.9.

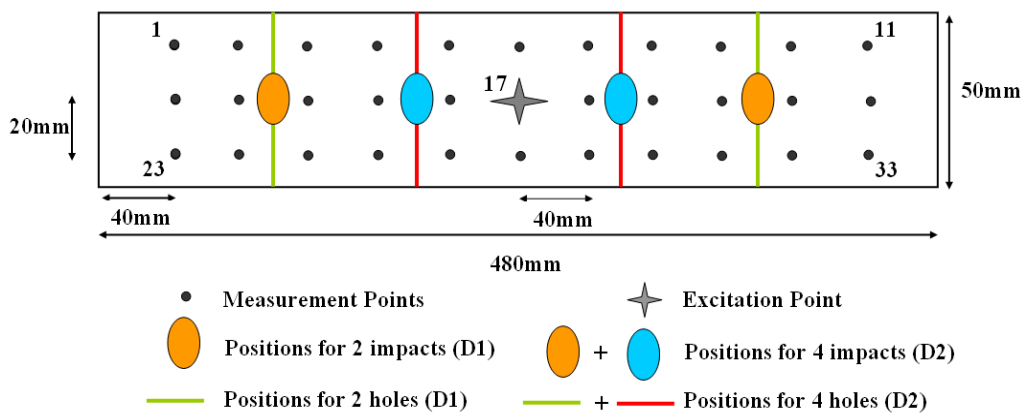


Figure 4.9 Sandwich test beams with location of impact damage, core-only damage (holes), excitation and measurement points

The six honeycomb sandwich beams are also impacted by taking into account the barely visible impact damage limit (BVID). Just to remind the readers, that BVID limit corresponds

to 0.6-0.8 mm of indentation depth, measured just after the impact. Four of the six sandwich beams are impacted symmetrically at four points with the same impact energy, as shown in Fig. 4.9. However in honeycomb sandwich beams, it is difficult to induce the same amount of damage at different points in the same specimen, even if it is impacted with the same energy i.e., impacting at the honeycomb cell center and at the corner leads to different damages. Therefore, it is not possible to have the same density of damage in honeycomb sandwich specimens at all the different impact points. This phenomenon of the dispersion of damage in honeycomb cores is shown schematically in Fig 4.10.

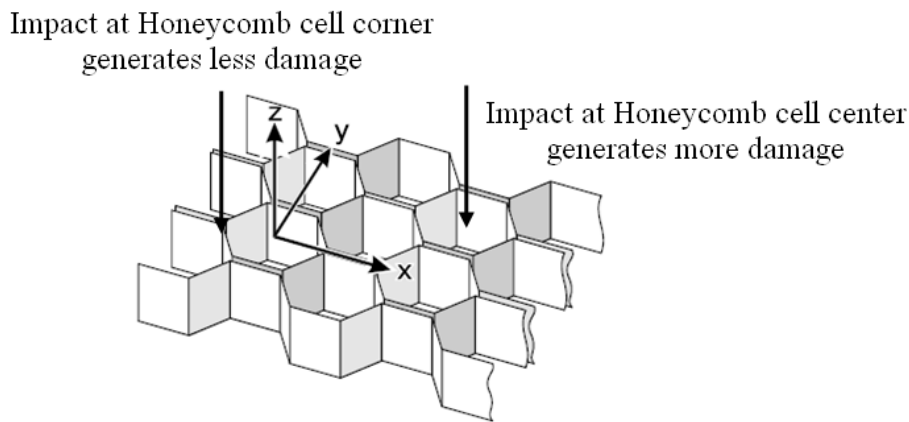


Figure 4.10 Schematic of a Honeycomb core showing the reason of dispersion of impact damage, due to impact at the same energy on a cell center or a cell corner

The first two honeycomb sandwich beams (H1 and H2) are impacted at 4J that produces a very small damage (not measurable by NDT methods) which is not visible on the surface. The reason for having the same impact energy for these two beams is to study the effect of end masses i.e., H1 is without and H2 is with end masses. The next honeycomb beam (H3) is impacted at 6J, which produces an indentation depth from 0.1 to 0.3 mm at the four impact points. However, the greatest dispersion in damage is seen in the honeycomb beam H4 which is impacted at 8J as shown in Fig. 4.11.

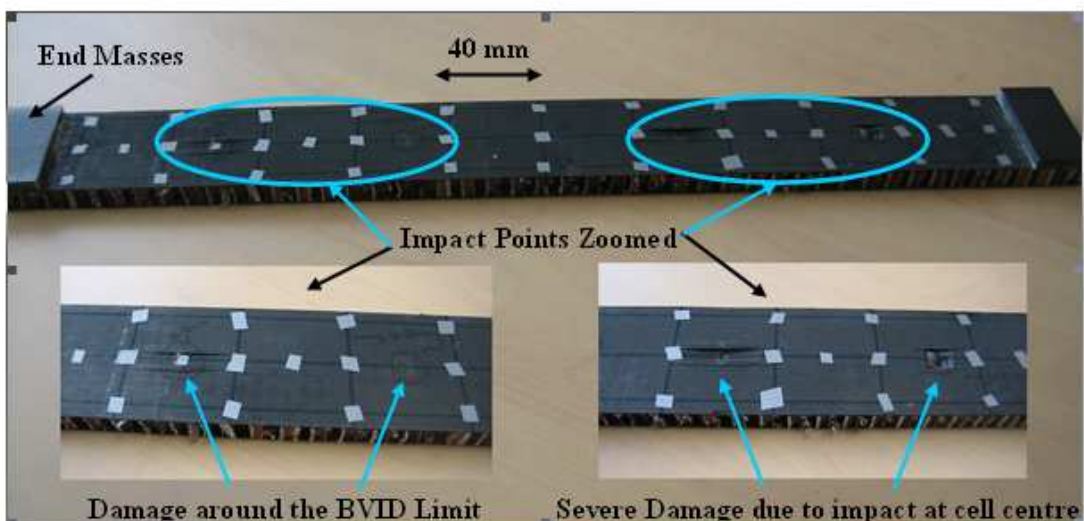


Figure 4.11 Dispersion of damage at the four impact points in case of honeycomb beam H4 impacted at impact energy of 8J

The damage depth for two impact points at one side of the beam is approximately 0.7 mm which corresponds to the BVID limit. But at the two impact points on the other end of the beam, the impactor head has induced severe damage due to impact at honeycomb cell center. This phenomenon introduces asymmetry in the beams and highlights the difficulty in inducing a global symmetric damage. The impact parameters for these four sandwich beams are listed in Table 4.3.

Table 4.3 Impact parameters for honeycomb beams

Honeycomb Beam Name	Energy of Impact (J)	Height (mm)	Indentation just after impact (mm)	Velocity of impact Measured (m/s)
H1 (without end-masses)	4	221.2	Very small damage	1.98
H2 (with end-masses)	4	221.2	Very small damage	1.98
H3 (with end-masses)	6	331.8	0.1 - 0.3	2.49
H4 (with end-masses)	8	442.3	0.7 – 3.0	2.83

The data obtained during the drop weigh impact tests carried out on the honeycomb beams (H2, H3 and H4) is shown in Fig 4.12. The impact test data for the honeycomb beams (H1 and H2) is similar as they are impacted with the same energy.

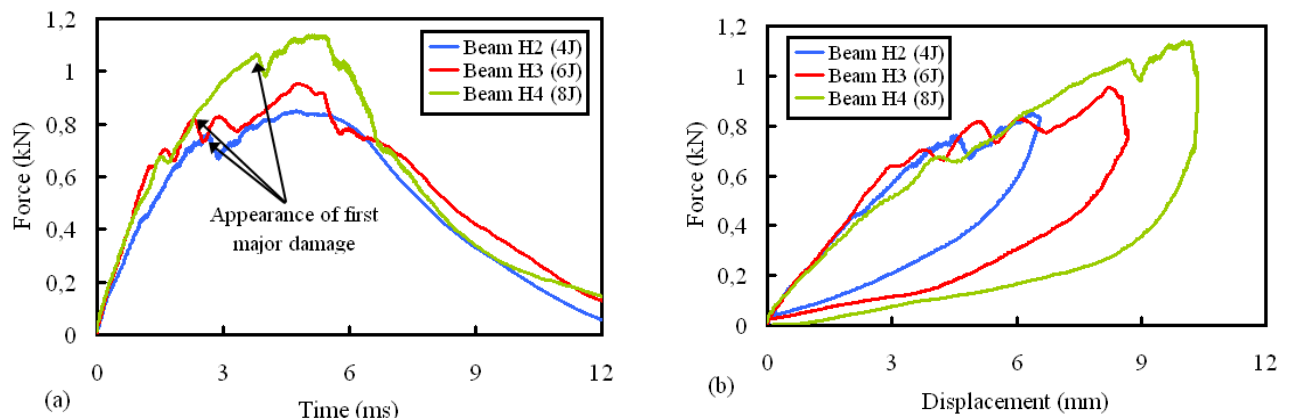


Figure 4.12 Impact test data (a) force-time (b) force-displacement

Four similar impacts have been performed on each specimen. However, in order to clarify these plots, only one impact test result for each specimen is plotted. All the impact curves presented in Fig 4.12 are filtered at 15 kHz. These curves, representative of all performed impact tests, are very classic in the literature [28,29]. In Fig. 4.12 a, the impact forces are drawn as a function of time. These curves are globally smooth and almost sinusoidal at low impact energy, with little oscillation due to natural frequencies of the panel. They show an important force signal fall followed by oscillations which is characteristic of delamination onset i.e., the appearance of first major damage in the sandwich beams. This is also evident in the force-displacement plot (Fig 4.12 b). The evolution of the peak force signal for the three beams (H2, H3 and H4) shows a logical increase with the increase in the impact energy.

As discussed previously, the second way of inducing damage is by piercing a hole all along the width in the honeycomb core by a hand drill. This type of damage can be referred to as core-only damage. In case of the honeycomb beams (H5) and (H6), approximately 5 mm and 10 mm diameter holes are pierced all along the width at the same positions as the impact

points as shown in Fig 4.10. For the 5 mm holes (Beam H5), some honeycomb material is present between the hole and the skins, however in case of 10 mm holes (Beam H6), no honeycomb material is present between the damage and the skin (Fig 4.13). The aim of inducing core-only damage is to check that whether this type of damage induces the same effect on the modal parameters as the impact damage. This will help us in future to develop dedicated algorithms based on shift in modal parameters to detect these kinds of damages (impact and core-only damage) in sandwich structures.

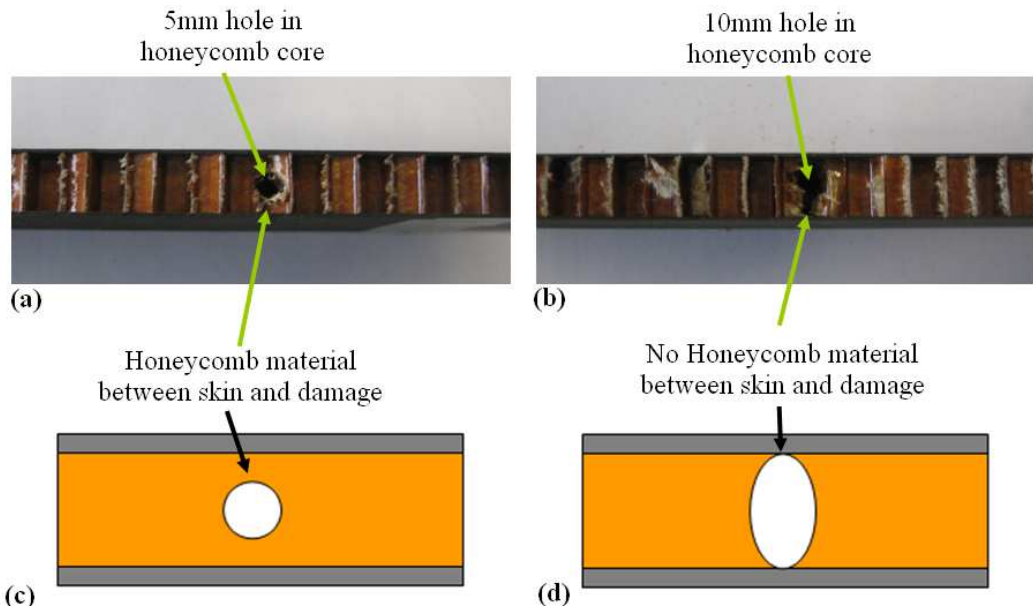


Figure 4.13 Cross-section view of test beams showing the holes pierced in the honeycomb core all along the width (a) 5 mm diameter hole for honeycomb beam H5, (b) approximately 10 mm diameter hole for honeycomb beam H6. Schematic view explaining presence and absence of material between the damage and the skin (c) 5 mm diameter hole for honeycomb beam H5, (d) approximately 10 mm diameter hole for honeycomb beam H6.

The sandwich beams have three states. First one is the undamaged state (UD), the second is the damage state due to two impacts or two holes (D1) and the third is the damage state due to four impacts or four holes (D2). Vibration tests are carried out on the six sandwich beams after each of these three states. For the instance, a simple case with symmetric impacts is chosen. If satisfactory results are obtained, then asymmetric damage shall be studied in the future.

4.2.3 Significance of End-Masses

Vibration tests are carried out on honeycomb sandwich beams (H1 without end-masses) and (H2 with end masses). First these beams are tested in the undamaged condition (UD), then these two beams are impacted at 4 J first at 2 points (D1) and then at 4 points (D2). Vibration tests are carried out again after each of these two series of impacts. The effect of end-masses on the modal parameters can be elaborated by studying the frequency and the damping change ratios between the undamaged (UD) and the two damaged cases (D1 and D2) for the honeycomb sandwich beams (H1 without end-masses) and (H2 with end-masses) for both burst random (BR) and sine dwell (SD) testing, presented in Table 4.4. The percentage change in frequency and damping ratios between the undamaged and the damaged cases is calculated with the help of Equations 4.1 and 4.2.

$$\text{Change in frequency between UD and D1, } (\Delta f) = \frac{f_{UD}(k) - f_{D1}(k)}{f_{UD}(k)} \quad (4.1)$$

$$\text{Change in damping between UD and D1, } (\Delta \zeta) = \frac{\zeta_{D1}(k) - \zeta_{UD}(k)}{\zeta_{UD}(k)} \quad (4.2)$$

where $f_{UD}(k)$ is the damped natural frequency for the undamaged specimen for the k_{th} mode and $f_{D1}(k)$ is the damped natural frequency for the specimen damaged at two impact points (D1) for the k_{th} mode. Nomenclature in case of Eq. 4.2 is the same.

From Tables 4.4, it can be said that on the whole the changes in frequency and damping ratios are more prominent in case of the beam H2 with end masses. A closer examination of the results reveals that by adding end-masses, the damping ratios seem to be affected more as compared to the natural frequencies. We can say that the end-masses increase the effect of shearing forces which causes an increase in friction in the material, consequently leading to a higher change in damping ratios as compared to natural frequencies. Table 4.4 shows that by putting end-masses, the change in natural frequency (between the undamaged and the damaged cases) is increased by around 3 %. In the case of damping ratios, this increase is as high as 93 %. It can be said that the damping ratios are more affected by the end-masses as compared to the natural frequencies. Therefore, the rest of the honeycomb sandwich beams (H2 to H6) except beam H1 in this section have been tested with end-masses.

It can also be noticed that the change in damping ratios is greater in case of sine dwell testing, because the damping ratio estimated by sine-dwell testing is always higher in case of the two damaged states (D1 and D2) as compared to the burst random testing (also seen in Fig 4.17). Theoretically, damping should increase with damage in the specimen, and as sine-dwell testing takes into account the effects of non-linearity due to damage, therefore the estimation of damping by sine-dwell testing is normally higher than that of burst random testing which does not takes into account the effects of structural non-linearity.

Table 4.4 Frequency and damping change ratios (%) between the undamaged (UD) and the two damaged states (D1 and D2) for the honeycomb sandwich beams (H1 without end-masses) and (H2 with end-masses) for both burst random (BR) and sine dwell (SD) testing

Natural Frequency Change Ratios (%)								
Beam Name	States	Mode 1		Mode 2		Mode 3		Mode 4
H1 (4J)	UD and D1	BR	SD	BR	SD	BR	SD	BR
	UD and D2	5.9	6.2	9.1	9.6	10.7	10.8	8.3
No end-masses	UD and D2	12.2	12.8	16.6	16.4	14.3	14.5	14.9
H2 (4J)	UD and D1	8.3	8.7	9.5	9.0	13.5	13.6	12.7
With end-masses	UD and D2	13.6	14.2	19.8	20.2	16.0	16.7	17.7
Damping Change Ratios (%)								
H1 (4J)	UD and D1	BR	SD	BR	SD	BR	SD	BR
	UD and D2	14.9	124.6	38.2	125.3	21.5	73.1	6.94
No end-masses	UD and D2	132.5	153.4	56.2	188.7	19.8	153.2	17.7
H2 (4J)	UD and D1	21.1	4.2	92.5	159.9	44.8	102.9	12.1
With end-masses	UD and D2	574.5	752.7	127.0	294.4	64.9	135.8	-10.9
								242.7

4.2.4 Estimation of Modal Parameters at the Undamaged State (UD)

The honeycomb sandwich beams are first tested at the undamaged state. As five of the beams with end-masses (H2 to H6) have the same geometrical and material configuration, so they must possess similar values of natural frequencies and damping ratios at the undamaged state (UD). In order to have a clear picture, the average values of natural frequencies and damping ratios for the first four bending modes for the five honeycomb sandwich beams (H2 to H6) with both burst random and sine dwell testing are plotted in Fig 4.14.

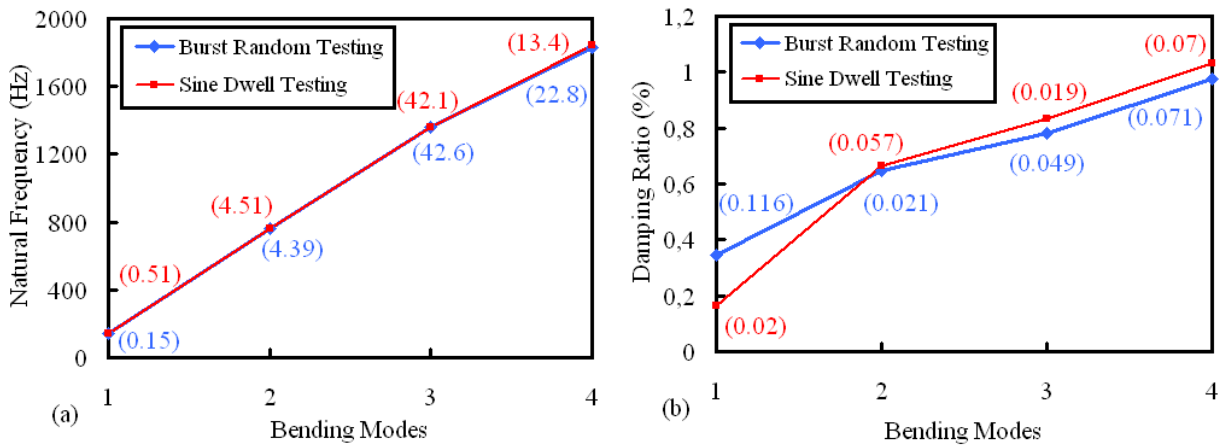


Fig 4.14 Average values of modal parameters (a) natural frequency, (b) damping ratio for the first four bending modes for the five honeycomb sandwich beams (H2 to H6) with both burst random and sine dwell testing. The standard deviation of the modal parameters for each mode is represented in blue for burst random and in red for sine dwell testing

The standard deviation associated with each average value is also represented for both burst random and sine dwell testing. In case of natural frequencies, the two types of testing, give similar results at the undamaged states as shown by the standard deviation values. However the dispersion at the 3rd bending mode for the natural frequency is a bit on the higher side, which is due to the fact that the beam H5 at the 3rd bending mode has a natural frequency of 1429 Hz whereas the average for the other four beams is 1338 Hz. This anomaly outlines the inherent possibility of false negatives which can arise due to boundary conditions and gives no indication of damage when it is present as discussed in the reference [46] and in Section 3.3.2.

In case of damping ratios, the results at the undamaged state give a good comparison as well for the two types of testing with small standard deviation values. However the exception in case of the damping ratios is the 1st bending mode for burst random testing which has a high standard deviation value of 0.116 (Fig 4.14 b). This is because of the honeycomb beam H2, which has a damping ratio of 0.161 % for the 1st bending mode, whereas the average damping ratio for the other four beams estimated by burst random testing is 0.389 %. This dispersion is not present in case of sine dwell testing, so this result gives us a first indication that the sine dwell testing might be better suited for damping estimation.

4.2.5 Effect of Impact Damage on Modal Parameters

The variation of natural frequency and damping ratio due to impact damage is studied for the honeycomb beams (H2, H3 and H4) with end-masses for the first four bending modes.

Frequency and damping ratios are the global parameters of the specimen, and are extracted from high quality measurements on the 33 measurement points. The modal parameters (natural frequency and damping) help in monitoring globally the health of a specimen. For the first four bending modes, the variation of damped natural frequency as a function of the undamaged (UD) and the two damage states (D1,D2) for the honeycomb beams (H2, H3, H4) for both burst random (BR) and sine-dwell (SD) testing is presented in Fig 4.15.

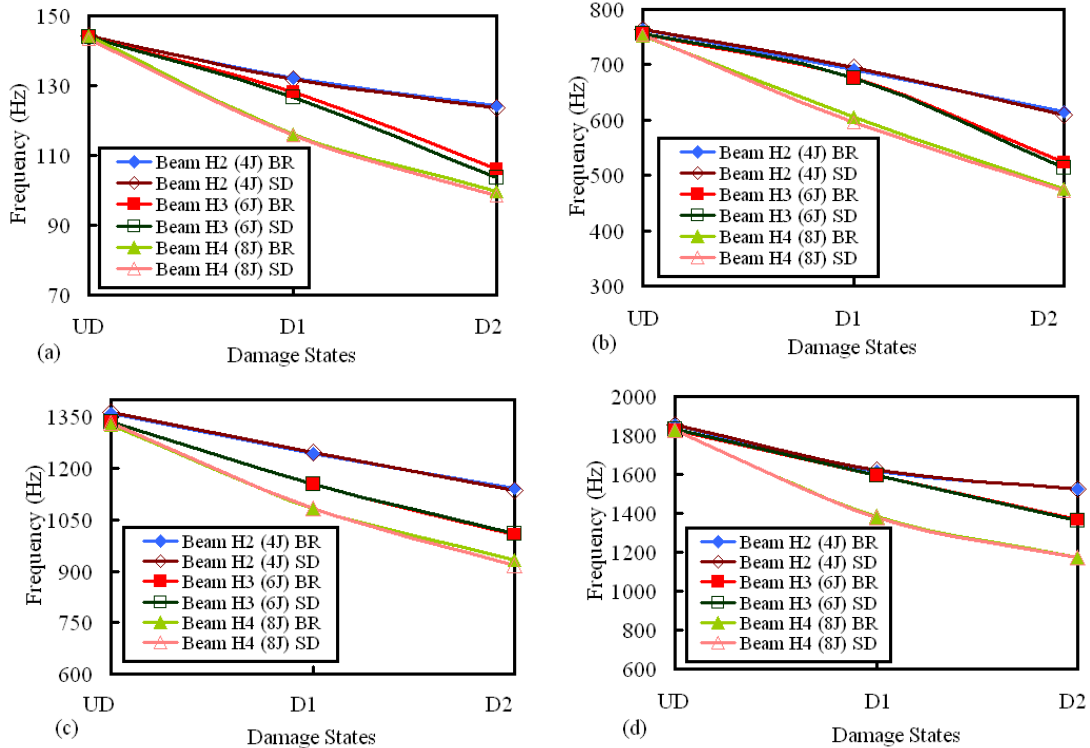


Figure 4.15 Variation of damped natural frequencies with damage states for (a) 1st bending mode, (b) 2nd bending mode, (c) 3rd bending mode and (d) 4th bending mode: UD is undamaged state, D1 is damaged at 2 impact points and D2 is damaged at 4 impact points, for the honeycomb beams (H2, H3 and H4) for burst random (BR) and sine-dwell (SD) testing, showing good correlation between BR and SD

As discussed before in Section 2.7, that damage in the specimens prompts a decrease in natural frequencies. So from Fig 4.15, it is clear that the decrease in the natural frequencies for the three honeycomb beams is more prominent in case of the beam H4 impacted at 8J. In case of natural frequencies, both burst random and sine-dwell testing give similar results. But the interesting fact is that, even for beam H2 impacted at 4 J which does not produce a visible damage on the surface, the average change in frequency for the first four bending modes between the undamaged and the damaged cases is 14 %, which proves that the beam H2 has a notable loss of rigidity without any signs of damage on the beam surface. It is particularly in these cases that vibration testing becomes a very useful tool for structural health monitoring.

It is noticed that in case of honeycomb beams H3 and H4 impacted at 6 and 8 J respectively, the level of damage is not the same on both sides of the beams as it depends on whether the honeycomb cell center or corner is impacted as discussed previously and shown in Fig 4.11. So this asymmetric damage leads to distortion of the resonance peaks or the appearance of twin peaks instead of one. This is evident in Fig 4.16, which shows a comparison of the sum

of the frequency response functions (FRF), estimated by burst random testing, for the honeycomb sandwich beams (H2, H3 and H4) for the undamaged case (UD), damaged at 2 points (D1) and damaged at 4 points (D2) for the 2nd bending mode. The sum of the FRF can be compared as for each sandwich beam 33 symmetric measurement points have been chosen that are symmetric on both sides of the two major axes of symmetry.

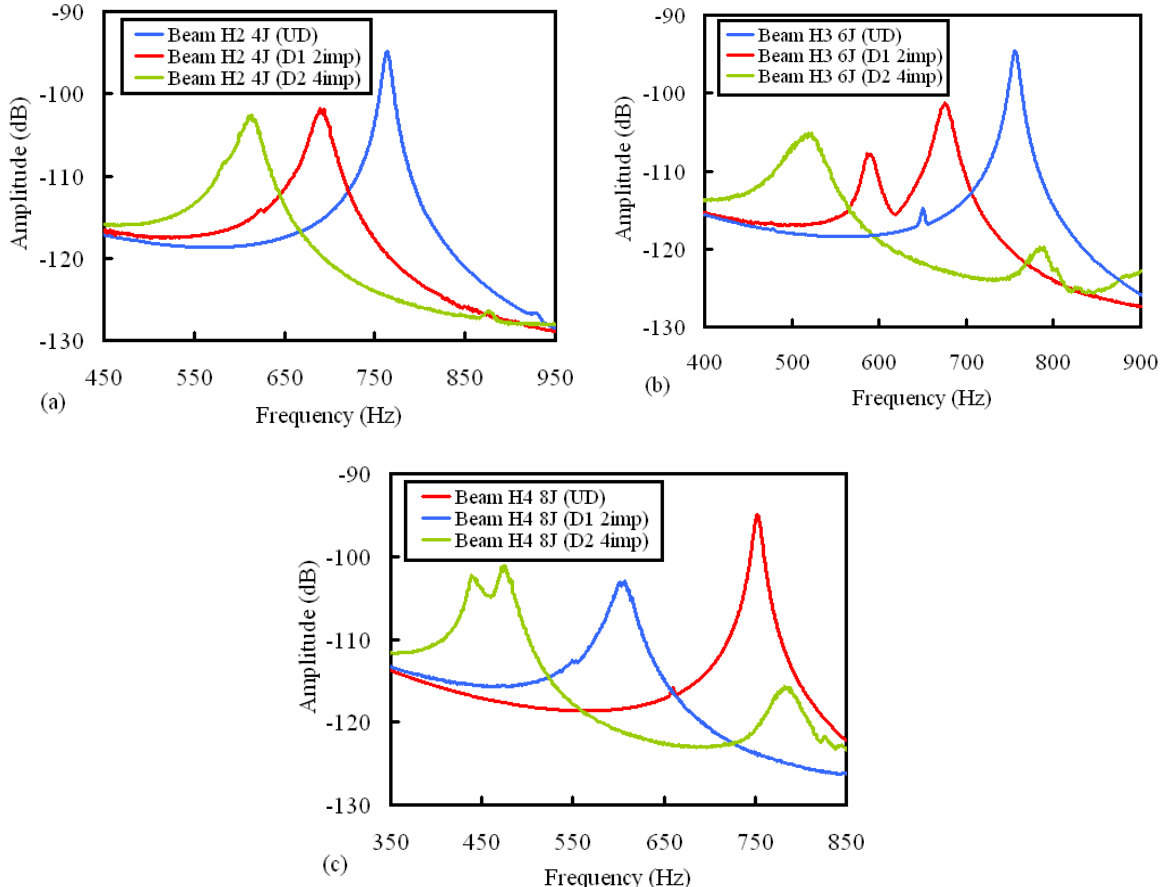


Figure 4.16 Comparison of the sum of the frequency response functions estimated by burst random testing for the undamaged case (UD), damaged at 2 points (D1) and damaged at 4 points (D2) for the 2nd bending mode for honeycomb beams (a) H2 damaged at 4J (b) H3 damaged at 6J (c) H4 damaged at 8J

Fig 4.16a shows that the resonance peaks for the beam H2 impacted at 4J are pretty much intact even for the damaged cases, showing that on the whole the beam is lightly damaged. But for the beams H3 and H4, as the damage level increases and with the addition of the asymmetric distribution of damage as discussed previously, the shape of peaks becomes distorted. This distortion of peaks does not affect the estimation of natural frequencies as such, as shown in Fig 4.15 i.e., both burst random and sine-dwell testing give similar natural frequency results in the presence of damage. However, for the estimation of damping ratios for the damage states D1 and D2, there is a notable difference between the results of burst random and sine dwell testing as shown in Fig 4.17.

It can be seen in Fig 4.17 that in general the damping increases with the increase in damage in the sandwich beams. However, in case of burst random testing, for the beam H2 for the 4th bending mode (Fig. 4.17 d) and for the beam H4 for the 1st bending mode (Fig. 4.17 a) the damping does not increase with damage. However sine dwell testing shows a logical increase

of damping for these beams. Furthermore, the estimation of damping by sine-dwell testing for the damage state (D2) is always notably higher as compared to burst random testing with the exception of the beam H3 for the 1st bending mode. It confirms the fact that sine dwell testing is more capable of detecting non linear structural dynamic behavior (due to accumulation of high damage as in state D2) unlike the broadband excitations [10].

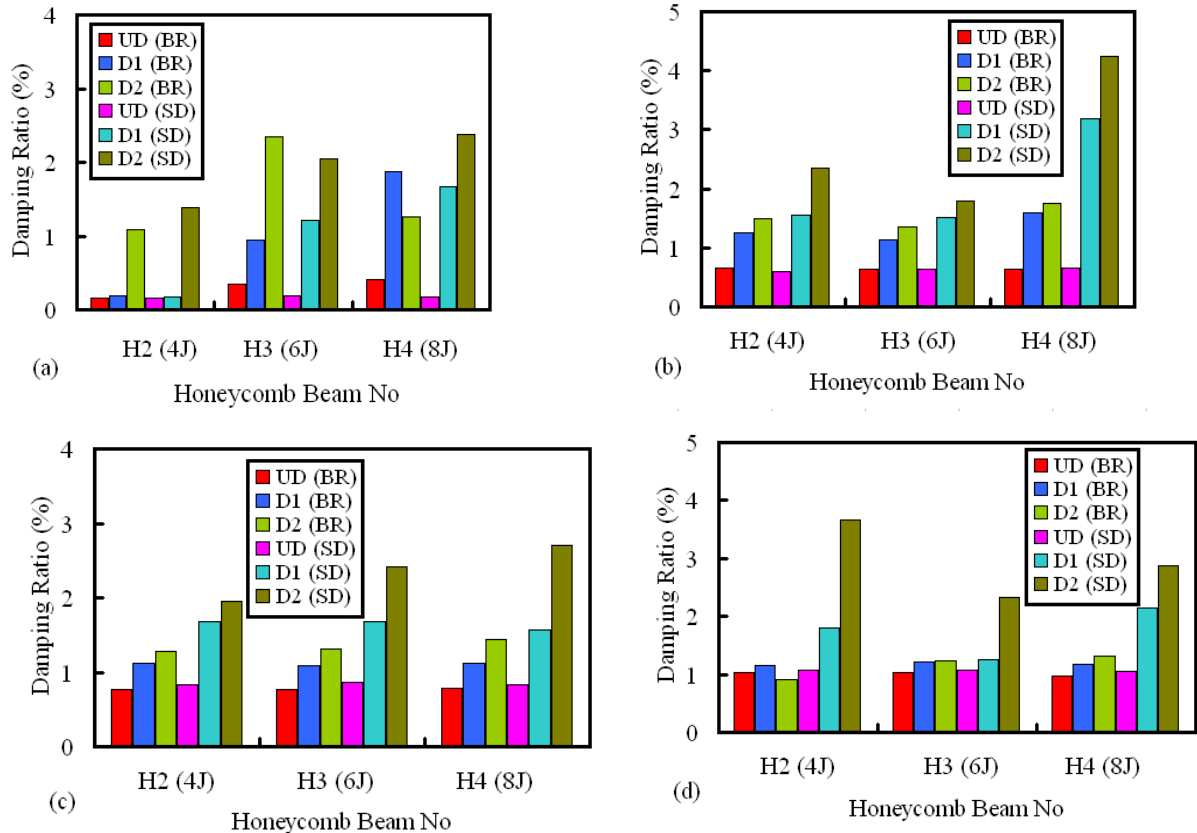


Figure 4.17 Variation of damping ratio with damage states for (a) 1st bending mode, (b) 2nd bending mode, (c) 3rd bending mode and (d) 4th bending mode: UD is undamaged state, D1 is damaged at 2 impact points and D2 is damaged at 4 impact points, for the honeycomb beams (H2, H3 and H4) for both burst random (BR) and sine-dwell (SD) testing

4.2.6 Effect of Core-Only damage on Modal Parameters

As discussed previously, in case of the honeycomb beams (H5) and (H6), approximately 5 mm and 10 m diameter holes are pierced all along the width at the same positions as the impact points. The aim of inducing core-only damage is to see that whether this type of damage induces the same effect on the modal parameters as the impact damage. The effect of core-only damage on the natural frequency and damping is studied similarly as the impact damage and is shown in Fig 4.18 and Fig 4.19.

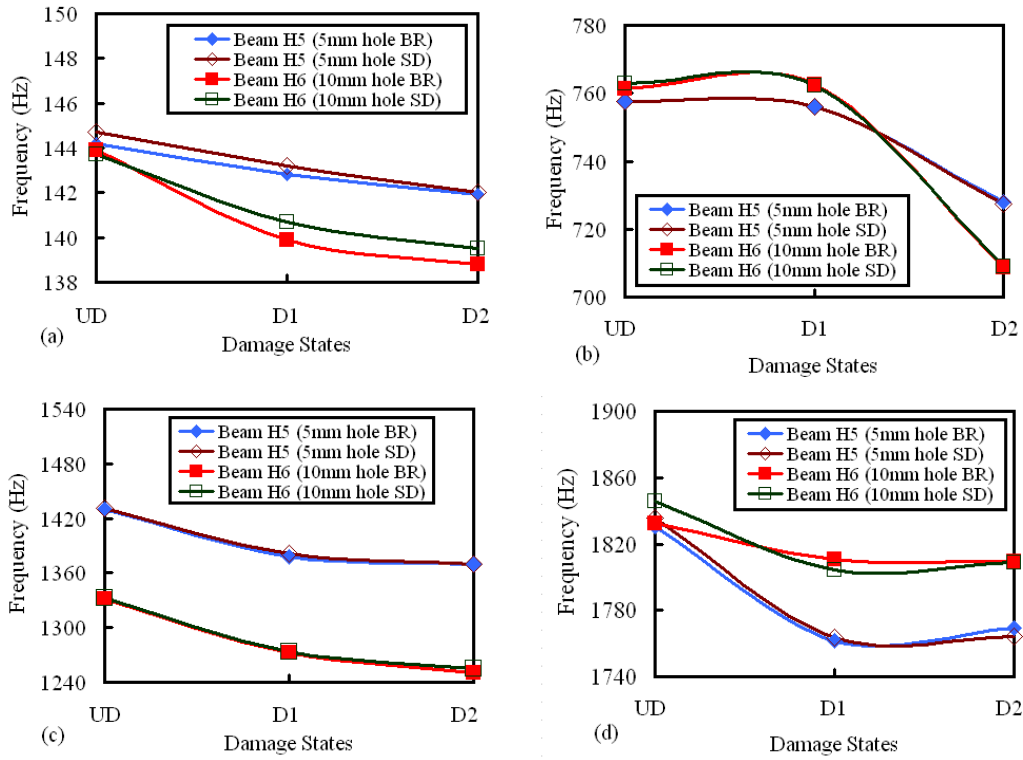


Figure 4.18 Variation of damped natural frequencies with damage states for (a) 1st bending mode, (b) 2nd bending mode, (c) 3rd bending mode and (d) 4th bending mode: UD is undamaged state, D1 is damaged at 2 points and D2 is damaged at 4 points, for the honeycomb beams (H5 and H6) for both burst random (BR) and sine-dwell (SD) testing

Fig 4.18 shows that the core-only damage induces a smaller change in natural frequencies as compared to the impact damage. The change in frequencies between the damaged states and the undamaged state is below 7 % for both the honeycomb beams H5 and H6 as shown by the frequency change ratios in Table 4.5. Both burst random and sine-dwell testing give relatively similar results for natural frequencies with the exception of beam H5 for the 4th bending mode.

However, it is interesting to note in Fig 4.19 (b-d) that there is no remarkable change in damping ratios for the beams H5 and H6 in the presence of core-only damage, with the exception of the damping for the 1st bending mode estimated by burst random testing for both beams H5 and H6. Whether the damping increases or decreases with damage, the change in damping ratio is generally very small between the undamaged (UD) and the damaged cases (D1 and D2). So it can be concluded that the core-only damage does not reduce much the stiffness (lesser number of friction zones) of the honeycomb sandwich beams as compared to the impact damage. As the change in modal parameters is slight for the core-only damage, so it shall be more difficult to carryout core-only damage detection with the help of modal parameter changes.

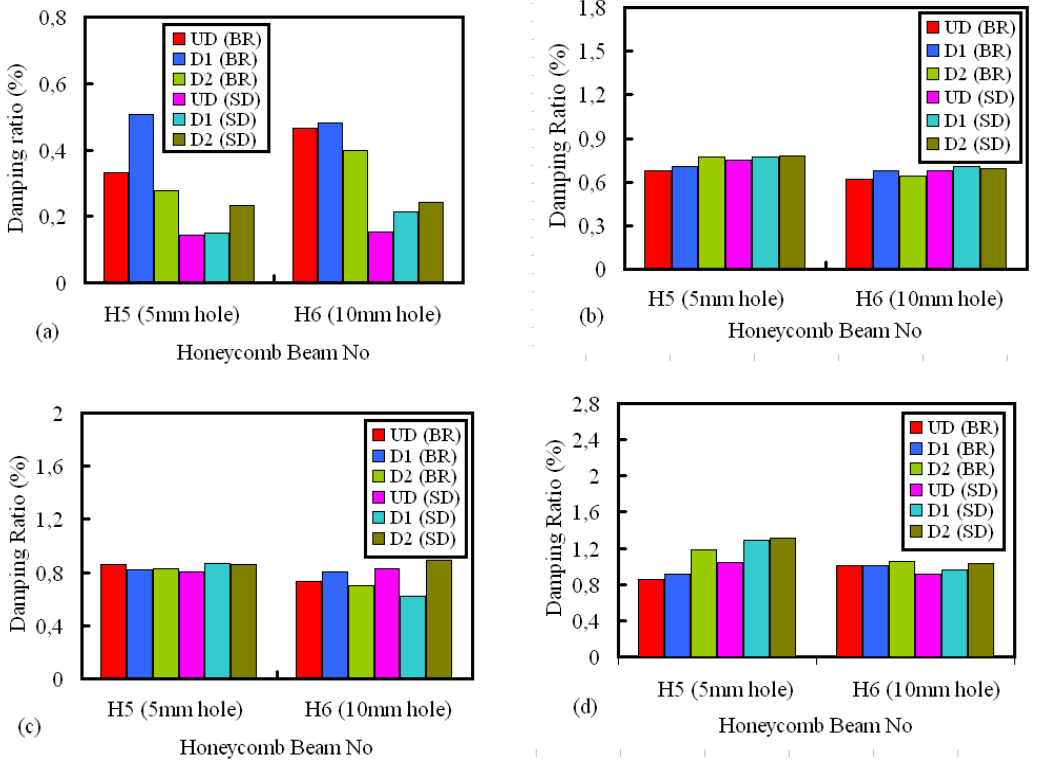


Figure 4.19 Variation of damping ratios with damage states for (a) 1st bending mode, (b) 2nd bending mode, (c) 3rd bending mode and (d) 4th bending mode: for the honeycomb beams (H5 and H6) for both burst random (BR) and sine-dwell (SD) testing

The effect of impact and core-only damage on the frequencies and damping ratios can be further elaborated by studying the frequency and the damping change ratios between the undamaged (UD) and the damaged cases (D1 and D2) for the impact damaged beams H3 and H4 and for the core-only damaged beams H5 and H6 in Tables 4.5 and 4.6. Same procedure as explained in Section 4.2.3 is followed. It can be clearly seen that the change in modal parameters is by far more prominent in case of the impact damaged beams (H3 and H4). Furthermore, the results in Tables 4.5 and 4.6 underline the fact that the damping change ratios are more prominent than the frequency change ratios. The maximum damping change ratio is 668 % whereas the maximum frequency change ratio is 38 %.

As discussed previously, the damping change ratio estimated by sine-dwell testing is higher as compared to burst random testing. It can be concluded from the above results that damping seems more sensitive to damage than the natural frequency variations in case of honeycomb sandwich beams. So it is reasonable to assume that damping may be used instead of natural frequency as a damage indicator tool for structural health monitoring purposes. However, the fact that damping is a parameter that is relatively difficult to estimate as compared to natural frequency has to be taken into account [142].

Table 4.5 Frequency change ratios (%) between the undamaged (UD) and the two damaged states (D1 and D2) for the impact damaged honeycomb beams (H3, H4) and the core-only damaged honeycomb beams (H5, H6) for both burst random (BR) and sine-dwell (SD) testing

Beam. No	States	Mode 1		Mode 2		Mode 3		Mode 4	
		BR	SD	BR	SD	BR	SD	BR	SD
H3 (6J)	UD and D1	10.9	11.5	10.5	10.7	13.6	13.6	12.7	12.7
	UD and D2	26.3	28.8	30.8	32.1	24.5	24.4	25.3	25.6
H4 (8J)	UD and D1	19.4	19.2	19.5	20.9	18.3	18.6	24.3	24.5
	BVID	UD and D2	30.8	31.8	36.7	37.3	29.7	31.1	35.7
H5	UD and D1	0.9	1.0	0.2	0.2	3.5	3.4	3.7	3.9
	5mm hole	UD and D2	1.6	1.8	3.8	3.9	4.1	4.2	3.3
H6	UD and D1	2.7	2.0	-0.1	0.09	4.4	4.4	1.1	2.2
	10mm hole	UD and D2	3.5	2.9	6.9	7.8	6.0	5.8	1.2
									1.9

Table 4.6 Damping change ratios (%) between the undamaged (UD) and the two damaged states (D1 and D2) for the impact damaged honeycomb beams (H3, H4) and the core-only damaged honeycomb beams (H5, H6) for both burst random (BR) and sine-dwell (SD) testing

Beam. No	States	Mode 1		Mode 2		Mode 3		Mode 4	
		BR	SD	BR	SD	BR	SD	BR	SD
H3 (6J)	UD and D1	175.1	531.7	78.4	137.2	41.8	95.8	18.4	16.6
	UD and D2	677.1	668.2	113.6	179.7	72.7	181.5	19.8	23.2
H4 (8J)	UD and D1	348.4	539.5	146.7	388.2	42.8	88.3	22.1	104.6
	BVID	UD and D2	200.7	124.5	172.6	549.4	83.2	226.6	35.6
H5	UD and D1	53.4	6.3	3.8	3.0	-5.1	7.8	6.4	22.7
	5mm hole	UD and D2	-16.3	64.7	14.6	4.5	-3.4	6.8	38.1
H6	UD and D1	3.22	40.1	9.3	4.2	10.5	-25.2	0.1	4.83
	10mm hole	UD and D2	-14.8	59.8	2.5	1.7	-3.7	7.46	5.6
									12.6

4.2.7 Effect of Sine-Dwell Frequency Direction on Modal Parameters

The aim of carrying out sine dwell testing in both up and down frequency directions is to be able to detect structural non-linearities in the damaged honeycomb beams. In literature it has been shown that frequency response functions (FRF) vary for the different sweep directions [10]. In this section, the effect of sweep directions is studied only for the beams with the highest level of damage i.e., impact damaged beams H3 and H4 for the damage state (D2) as presented in Table 4.7.

Table 4.7 Comparison of natural frequency and damping ratios for both up and down sine-dwell frequency directions for the honeycomb beams H3 and H4 for the damage state (D2)

Beam .No	Sine Dwell Direction	Natural Frequency (Hz)				Damping ratio (%)			
		Mode1	Mode 2	Mode3	Mode 4	Mode1	Mode 2	Mode 3	Mode 4
H3 (6J)	Up	97.5	499.5	1010.1	1374.0	2.05	1.79	2.42	1.33
D2 (4imp)	Down	98.8	499.1	1010.2	1378.6	2.73	1.83	2.36	1.00
H4 (8J)	Up	98.4	471.9	918.4	1172.2	2.38	4.24	2.71	2.86
D2 (4imp)	Down	98.1	467.7	921.8	1175.7	2.46	4.63	2.99	2.90

Table 4.7 shows the presence of nonlinear behavior in the honeycombs beams H3 and H4, as the natural frequencies and damping ratios show a slight discrepancy when tested in the increasing and decreasing frequency order. This is also shown graphically in Fig 4.20 by plotting the frequency response functions from sine-dwell sweeps upwards and downwards in frequency. It is observed that in the presence of non-linearity, there is always a change in amplitude coupled with a slight shift in frequencies.

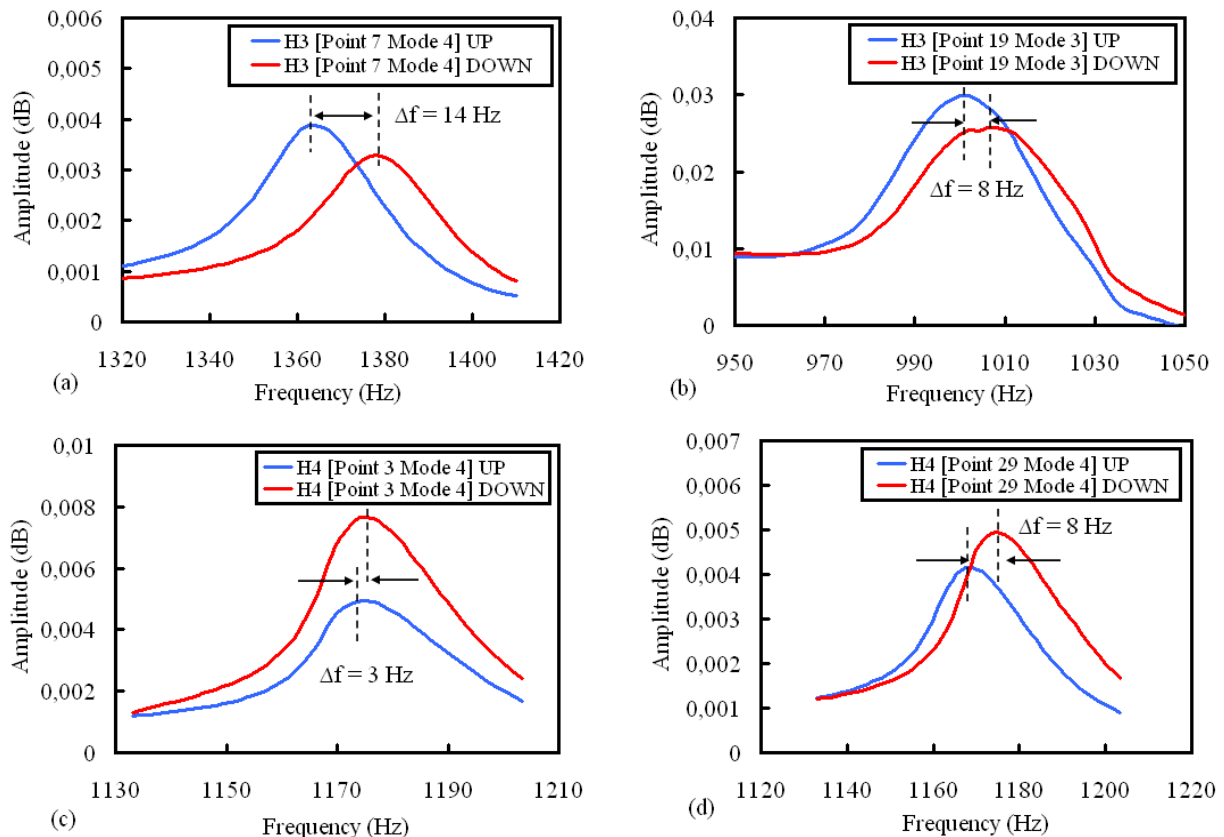


Figure 4.20 FRFs from sine-dwell sweeps upwards and downwards in frequency honeycomb beams (a) H3 Point 7 M4 (b) H3 Point 19 M3 (c) H4 Point 3 M4 (d) H4 Point 29 M4

4.2.8 Design of Experiments (DOE)

This study is carried out on the modal parameters (natural frequency and damping ratio) of the three impact damaged sandwich beams with end-masses (H2, H3 and H4) tested by both burst random and sine-dwell testing as compared in Section 3.3.5 and Section 3.4.2. The aim is to find out that which testing method gives a relatively more reliable estimation of damping in the presence of damage i.e., damping increases with the increase of damage in the specimen [60]. The design of experiments shall also help us identify the factors which have the most significant effect on the experimentally obtained modal parameters.

The two factors chosen for the design of experiments are the energy of impact (IE) and the density of damage (DD). For the energy of impact there are three levels (4, 6 and 8J) and for the density of damage there are also three levels (the undamaged state (UD), damage at 2 impact points (D1) and damage at 4 impact point (D2)). By keeping in view the levels of the two factors, a full factorial design is chosen. The linear regression model used to represent the

interaction between the design variables, associated with the full factorial design, based on the two variables discussed above is expressed as follows:

$$Y = a_0 + a_1.(IE) + a_2.(DD) + a_3.(IE).(DD) + E \quad (4.3)$$

In Equation 4.3, coefficients represent model constants (a_i) that are the contribution of independent variables on the response. E is the random error term representing the effects of uncontrolled variables, i.e., not included in the model. The model constants (a_i) are determined by multi-linear regression analysis and are assumed to be normally distributed. The error is assumed to be random and normally distributed. These constants (a_i) are obtained with 90% confidence level. The significance of each variable on a given response (modal parameters in our case) is investigated using t test values based on Student's distribution. The t ratio is the ratio of the parameter estimate (constants) to its standard deviation. A t ratio greater than 2 in absolute value is a common rule of thumb for judging significance of the variable.

The constants (a_i) and t ratios for the natural frequencies and the damping ratios estimated by burst random testing are presented in Tables 4.8 and 4.9. Negative values of the model constants and t ratios indicate that the response decreases with the increase in the value of the parameter. In our case, this is most of the times true for the natural frequencies as they decrease with the increase in damage in the specimens.

Table 4.8 Coefficients and t ratios for the natural frequencies (Hz) estimated by burst random testing

Term	Mode 1		Mode 2		Mode 3		Mode 4	
	Constants (a_i)	t ratio						
IE	-3.35	-5.53	-19.59	-6.42	-33.46	-7.49	-51.19	-4.55
DD	-8.51	-14.05	-54.98	-18.02	-78.49	-17.57	-120.4	-10.70
IE x DD	-1.55	-4.18	-7.95	-4.25	-10.99	-4.02	-20.21	-2.94

Table 4.9 Coefficients and t ratios for damping ratios (%) estimated by burst random testing

Term	Mode 1		Mode 2		Mode 3		Mode 4	
	Constants (a_i)	t ratio						
IE	0.175	1.49	0.049	1.11	0.015	1.74	0.029	1.62
DD	0.313	2.68	0.541	3.83	0.381	13.58	0.036	2.01
IE x DD	-0.005	-0.08	0.017	0.65	0.009	1.76	0.028	2.58

By comparing the t ratios for the energy of impact (IE) and the density of damage (DD) in Tables 4.8 and 4.9, it can be seen that the density of damage (DD) has a more significant effect on the modal parameters than the impact energy (IE) for the first four bending modes. The second order interaction term (IE x DD) is more significant in case of the natural frequencies as compared to the damping ratios. Similar results are observed in case of sine-dwell testing. The design of experiment results based on the modal parameters estimated by sine-dwell testing is laid out in Tables 4.10 and 4.11.

Table 4.10 Coefficients and t ratios for the natural frequencies (Hz) estimated by sine-dwell testing

Term	Mode 1		Mode 2		Mode 3		Mode 4	
	Constants (a_i)	t ratio						
IE	-3.52	-3.36	-20.7	-4.77	-34.1	-8.95	-51.98	-4.63
DD	-9.33	-8.91	-57.8	-13.30	-80.6	-21.14	-121.3	-10.8
IE x DD	-1.52	-2.38	-7.93	-2.98	-11.5	-4.94	-20.3	-2.96

Table 4.11 Coefficients and t ratios for damping ratios (%) estimated by sine-dwell testing

Term	Mode 1		Mode 2		Mode 3		Mode 4	
	Constants (a_i)	t ratio						
IE	0.208	3.57	0.300	2.13	0.053	1.90	-0.039	-0.39
DD	0.441	7.56	0.221	5.02	0.142	16.09	0.472	4.59
IE x DD	0.061	1.71	0.114	1.33	0.047	2.75	-0.049	-0.78

Sine-dwell testing also proves the significance of density of damage (*DD*) as the parameter that has the most significant effect on the results. If the t ratios for the damping ratios estimated by burst random and sine-dwell testing are compared in Tables 4.9 and 4.11, it can be seen that the two factors (*IE and DD*) have higher t ratios in case of the damping ratios estimated by sine-dwell testing. So from the results, it can be said that sine-dwell testing gives a relatively more reliable estimation of damping in the presence of damage as compared to burst random testing. Although the main disadvantage of sine-dwell testing is the lengthy acquisition times as compared to broadband excitations, but if quality damping estimations are required then sine-dwell excitation based vibration testing becomes indispensable.

4.3 Conclusion of the Fourth Chapter

In this chapter damage monitoring has been carried out on honeycomb sandwich beams damaged in two different ways (impact damage and core-only damage). Vibration tests have been carried out on pristine and damaged long honeycomb sandwich beams using burst random and **sine dwell excitations** in order to compare that which testing method gives a relatively more reliable estimation of damping in the presence of damage, because damping is much harder to estimate as compared to natural frequency.

Vibration tests are carried out by placing steel masses at the two ends of the sandwich beams in order to enhance the shift between the modal parameters between the undamaged and the damaged cases. The six long honeycomb sandwich beams tested in this chapter are damaged in two different ways. The first four are damaged by **drop weight impacts** around the barely visible impact damage limit (BVID), in order to simulate damage by foreign impact objects such as stones or birds. The other two are damaged by **piercing a hole** all along the width in the honeycomb core by a hand drill (core-only damage), simulating mishandling during assembly and maintenance.

Results show that with the accumulation of damage in the specimens, there is a **decrease in natural frequency accompanied by an increase in damping ratio**. The impact of core-only damage seems feeble on the modal parameters as compared to impact damage. Furthermore, damping seems to be more sensitive to damage than the natural frequency. So it is reasonable

to assume that damping may be used instead of natural frequency as a damage indicator tool for structural health monitoring purposes. **Presence of non-linearity** in the impacted sandwich beams is proved by carrying out **sine-dwell testing upwards and downwards in frequency**. It is observed that in the presence of non-linearity, there is always a change in amplitude coupled with a slight shift in frequencies in the FRFs. Design of experiments carried out on the extracted modal parameters show highlighted **density of damage** as the factor having the most significant effect on the modal parameters, and prove that sine-dwell excitation based modal testing **gives more reliable estimation of damping** in the presence of damage as compared to burst random testing.

Chapter 5 : Static-Dynamic Characterization and Monitoring of Impact Damage in Entangled Sandwich Beams by Shift in Modal Parameters

A good part of the experimental work of this thesis concerns entangled sandwich materials. A literature review on these materials has been presented previously in Section 1.4.1. The aim of fabricating and testing these sandwich materials is to verify whether they can be used as potential dampers and sound absorbers in specific applications like the inner paneling of a helicopter, where structural strength is not the primary requirement.

The impact toughness of entangled sandwich beams is also evaluated by the decrease in natural frequency (global parameter of a structure) which signifies loss of rigidity. The author wants to clarify here, that impact toughness is only studied through vibration tests and the classical procedure used for determining the impact toughness i.e., compression after impact (CAI) has not been implemented as it is outside the scope of this work. Nonetheless, impact toughness based on decrease in natural frequency and monitoring of impact damage by shift in modal parameters (damage detectability) are closely related.

As the entangled sandwich materials are a relatively new breed, hence we need to explain a bit in detail the fabrication process and their static and dynamic characterization before talking about damage monitoring due to shift in modal parameters. In general, two types of entangled sandwich beams have been tested in this thesis.

- Long carbon fiber entangled sandwich beams (480mm length)
- Short carbon/glass fiber entangled sandwich beams (250mm length)

5.1 Long Carbon Fiber Entangled Sandwich Beams by

5.1.1 Materials and Fabrication Procedure

The core of the entangled sandwich beams consists of carbon fibers (HTS-5631) that are made of a yarn of standard carbon filaments having a diameter of 7 μm . The length of the carbon fibers is 10 mm and their elastic modulus is 240 GPa. The fibers are provided by the company Toho-Tenax. For the cross-linking of carbon fibers, epoxy resin is used. The epoxy resin SR 8100 and injection hardener SD 8824 are used provided by Sicomin. All the test specimens presented in the section are carefully weighed using Mettler balance. A better vaporization is achieved if the resin is heated up to 35°C before being sprayed on the carbon fibers. This allows the mixture of resin and hardener to become less viscous. Prepregs of T700-M21 are used as skins as in case of honeycomb sandwich beams in Section 4.2.1. Their properties are given in Table 4.1.

The fabrication of entangled sandwich specimens is often a tedious and complex process. As these types of materials are still mostly in the research phase, so as such standard fabrication processes do not exist. The fabrication procedure used in this thesis is the one developed by Mezeix et al. [100,101]. For the carbon entangled beams used in this thesis, approximately 900 g of fibers of 10 mm length are cut manually. The carbon fibers are then treated in a

solution of dichloromethane for 24 hours and are then cleaned for 2 hours in methanol. These uncoated carbon fibers are then separated by a blow of compressed air. The mixture of resin and hardener is then sprayed on the separated carbon fibers by a spray paint gun. In case of larger test specimens, the volume of carbon fibers is large, so with the current technology it is not easy to spray the resin equally on the carbon fibers. The fibers impregnated by the resin are then placed in the mold between the two skins of unidirectional composites. In order to polymerize the fiber network sandwich specimens, the mold is then heated in an oven up to 180°C for two hours in a press. The thickness of the entangled sandwich specimen core is 10 mm and that of each skin is 0.5 mm. The types of carbon entangled sandwich specimens used are shown in Figure 5.1 and their specifications are provided in Table 5.1.

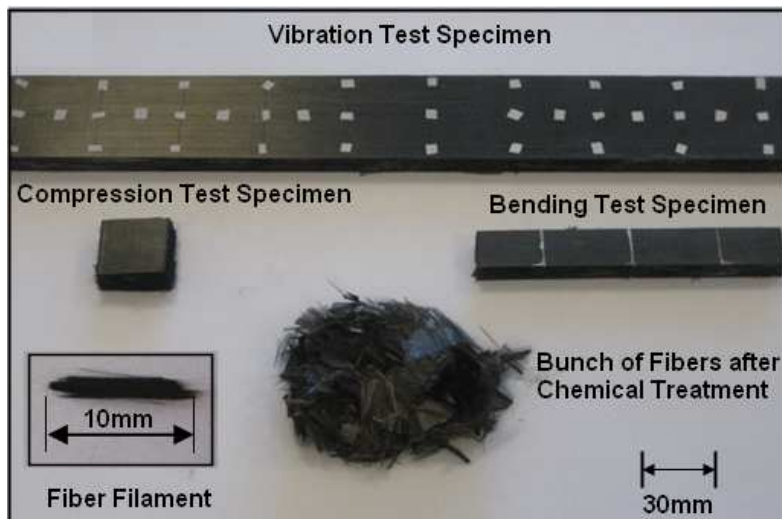


Figure 5.1 Core material and carbon entangled sandwich test specimens

Table 5.1 Types of carbon entangled sandwich specimens

	Compression Tests	Bending Tests	Vibration Tests
Length (mm)	30	140	480
Width (mm)	30	20	50
Core Thickness (mm)	10	10	10
Skin Thickness (mm)	1	1	1

In order to verify the process of fabrication, a single test specimen is fabricated first by using a small mold (510 x 65 x 11 mm) with a fiber core density of 100 kg/m³. This specimen showed that 100 kg/m³ fiber core density is relatively insufficient for a volume of 480 x 50 x 10 mm³, as there are places in the core of the sandwich beam that lack sufficient quantity of fibers. So for the next specimen, a fiber core density of 150 kg/m³ is chosen. As compared to the previous specimen (fiber core density of 100 kg/m³), the specimen with 150 kg/m³ fiber core density has a far better fiber distribution. Finally a test specimen with a fiber core density of 200 kg/m³ is fabricated by using the same small mold. It is seen that a fiber density of 200 kg/m³ for the core is on the higher side and it is not possible to close the mold properly. So for the fabrication of the next batch of specimens, a fiber core density of 150 kg/m³ is chosen.

In the next step a larger mold (510 x 250 x 11 mm) is used to produce multiple test specimens having the same characteristics. First the large mold is used to fabricate four relatively identical test specimens referred to as heavy specimens in the thesis. The average composition

of these four heavy test specimens is presented in Table 5.2. Next, the same large mold is used to produce relatively lighter specimens. They have approximately 25 g less mixture of resin and hardener than the previously produced heavier specimens. These specimens shall be referred to as light specimens in future discussions (Table 5.2). The ratio of the mixture of resin and hardener in the heavy specimens is approximately 2.5 times more than that of the light specimens.

Table 5.2 Composition of vibration test specimens having fiber core density of 150 kg/m^3 fabricated from the small and large mold (Average of four specimens)

Density	150 kg/m^3 (Light)	150 kg/m^3 (Heavy)
Weight of Fibers	39 g	39 g
Weight of Resin & Hardener	18 g	43 g
Weight of Skin (Upper + Lower)	38 g	38 g
Total Weight of Specimen	95 g	120 g

The difference in resin between the heavy and light specimens can also be observed with the help of a scanning electron microscope (SEM). Fig 5.2 shows SEM observations on heavy and light specimens. In case of the heavy specimen (Fig 5.2a), the resin can be seen all along the length of the fibers and is seldom in the form of droplets. On the other hand, for the light specimen (Fig 5.2b), droplets of resin can be seen at the fiber joints but the presence of resin along the fiber lengths is negligible.

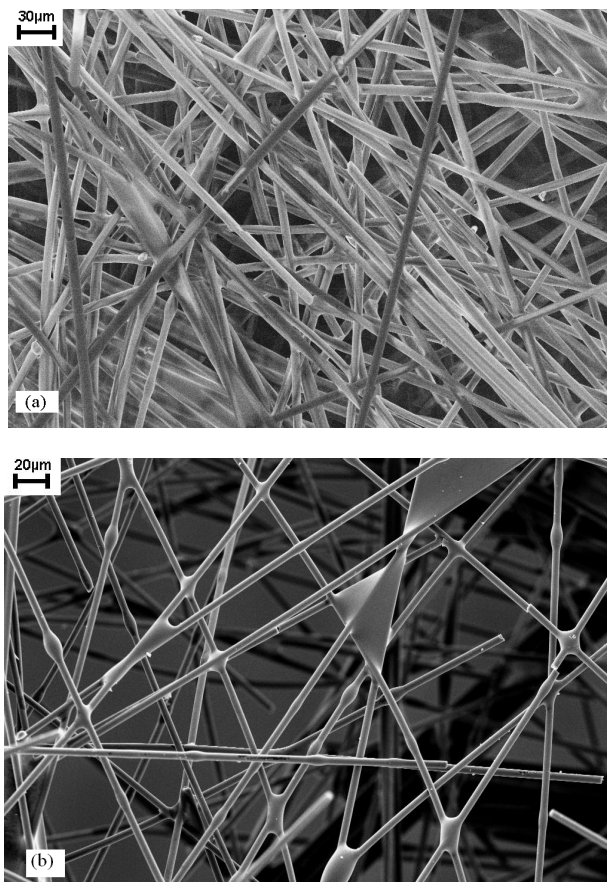


Figure 5.2 Scanning Electron Microscope SEM observations (a) heavy specimen, resin can be seen all along the length (b) light specimen, resin mostly at the fiber joints

5.1.2 Static Characterization of Long Carbon Entangled Sandwich Beams

As entangled materials are a new type of sandwich materials so it is required to characterize these new materials statically. For this reason, compression and bending tests are carried out on the carbon entangled sandwich specimens to find their elastic and shear modulus. These two tests with their results are discussed separately:

Compression Tests

The quasi-static compressive response of the sandwich fiber network test specimens are measured in 100 kN Instron machine. The aim is to calculate the elastic modulus. Both light and heavy compression test specimens are tested. The specimen size chosen for the compression tests is 30 x 30 x 11 mm [143]. The test specimens are placed between the moveable and the fixed plate as shown in Fig 5.3. The displacement of the machine is used to measure the displacement of the test-specimen. As the entangled materials are not very rigid, therefore a relatively small force is applied to compress the entangled sandwich materials. As the force is small, so it is safe to assume that the displacement of the machine is same as the displacement of the specimen.

The applied velocity of $v_o = 2 \text{ mm/min}$ corresponds to a nominal strain rate of $\dot{\epsilon} = 3 \times 10^{-3}/\text{s}$ at the beginning of the test. The maximum applied load is 20 kN corresponding to 22.2 MPa. To analyze the experimental results, the following definitions for the true strain and stress are used.

$$\text{Strain, } \varepsilon = \ln\left(\frac{h}{h_o}\right) \quad (5.1)$$

$$\text{Stress, } \sigma = \frac{F}{S} \quad (5.2)$$

where h is the height during compression, h_o is the initial height of the sample, S is the area during compression. S_o is the initial area and F is the applied force. In our case, the area S varies very little during the compression tests, so it is assumed that $S = S_o$. No lateral displacement of the test-specimen is observed during the compression tests and the section remains constant. So it can be concluded that there are no barreling effects.

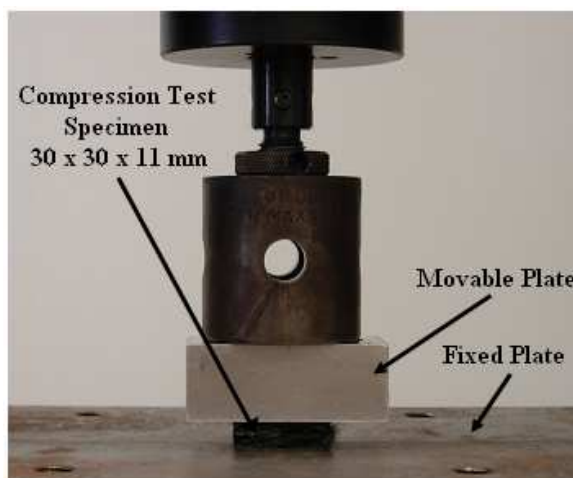


Figure 5.3 Test Specimen between the fixed and moveable plate during compression test

Fig 5.4 compares the results of the compression tests carried out on the two heavy and two light specimens. As explained previously, the fiber core density of all the four compression test specimens is 150 kg/m^3 . The ratio of resin and hardener in the heavy specimens is 2.5 times than that in the light ones.

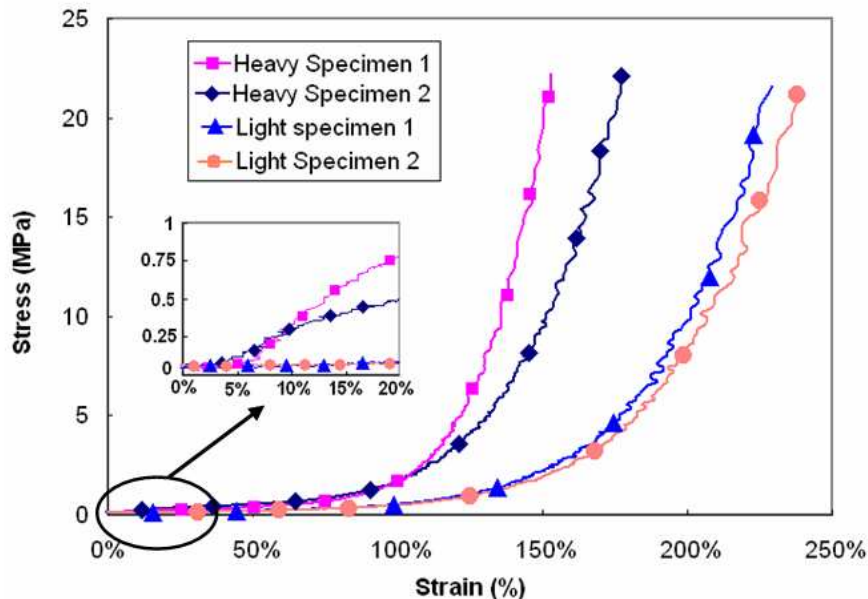


Figure 5.4 Compression stress/strain curves for the heavy and light fiber network sandwich specimens (150kg/m^3 fiber density). The zoomed view shows the linear-elastic phase used for calculating the elastic modulus

From the graph (Fig 5.4), it can be noticed that there is a good reproducibility of compression tests carried out on the two types of fiber network sandwich specimens. In case of the heavy specimens, compression curves move from the right to the left and the densification starts for smaller strains (100 % for the heavy specimens). The extra resin in the heavy specimens results in better cross-linking of the fibers and increases the initial stiffness of the material which is evident by the linear elastic phase which is quite prominent (zoomed view in Fig 5.4). The heavy specimens show a linear-elastic behavior up to around 0.8 MPa. The calculation of the elastic modulus is based on the linear-elastic part of the curves as shown in the zoomed view in Fig 5.4. Even if the stress-strain curves shown are highly non-linear, there is a linear-elastic part in case of the heavy specimens. The elastic modulus is calculated by measuring the slope of this linear-elastic part as explained in the ASTM standard in reference [144]. The average elastic modulus for the two heavy specimens is around 1.4 MPa.

However in case of the light specimens, one has to compress longer in order to achieve densification (strain around 160 %) as they are less rigid as compared to the heavy specimens due to the lack of resin. The linear elastic phase is non-existent in case of the light specimens so the calculation of the elastic modulus is not possible. Unloading has not been performed to reveal the effects of plasticity because it is not in the scope of this work. The authors are mainly interested in the linear-elastic part in order to calculate the elastic modulus which shall be used in future for the modeling of the entangled sandwich beams.

Bending Tests

In order to measure the shear modulus of the test specimens, three point bending tests are carried out on the heavy and light bending test specimens on a 10 kN Instron machine. As discussed previously, these specimens are fabricated from the large mold and have 150 kg/m^3 fiber core density. The dimension of these test specimens are $140 \times 20 \times 11 \text{ mm}$ and the distance between the two supports is 80 mm, the choice of which is based on the three-point bending tests carried out in detail in reference [143]. The applied velocity is $v_o = 1 \text{ mm/min}$ and the maximum applied load is 100 N. Round steel bars or pipes are used as supports having a diameter of 6 mm which is not less than one half the core thickness (5 mm) and not greater than 1.5 times the sandwich thickness as per ASTM standards [132]. The three point bending test is shown in Fig 5.5.

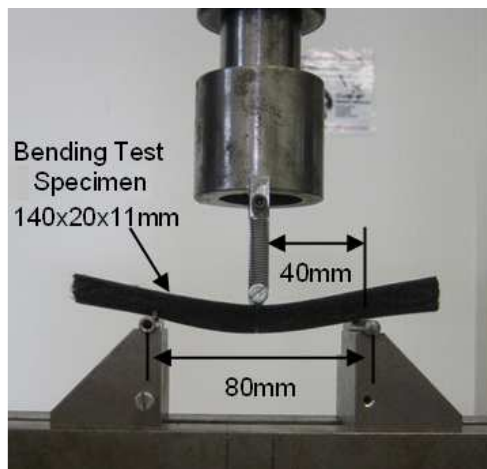


Figure 5.5 Test specimen between the three supports during 3 point bending test

For the analysis of a sandwich beam under three-point bending, consider a sandwich beam of width b and length l , comprising of two identical face sheets of thickness t_f and core of thickness t_c . Also h is the spacing of the mid plane of the face sheets ($h = t_c + t_f$), as shown in Figure 5.6.

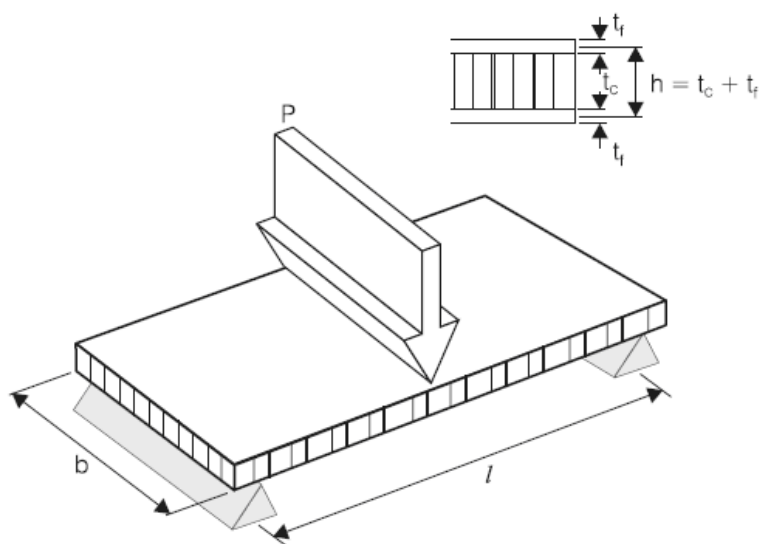


Figure 5.6 Schematic of a sandwich beam under three point bending showing geometrical parameters

The load P is applied at the centre of the beam. The maximum deflection of the beam is due to both flexural and shear deformations. The shear deformation is dominated in the core and hence, the approximate expression for the elastic deflection can be expressed as [128]:

$$\text{Maximum deflection, } \delta = \frac{Pl^3}{48D} + \frac{Pl}{4S} \quad (5.3)$$

The bending stiffness D and the shear stiffness S are given by

$$\text{Bending Stiffness, } D = \frac{E_s t_f h^2 b}{2} \quad (5.4)$$

$$\text{Shear Stiffness, } S = bhG_c \quad (5.5)$$

where E_s is the elastic modulus of the skins, G_c is the shear modulus of the core and t_f is the thickness of the skin. The maximum deflection δ is calculated experimentally by the three-point bending test, the only unknown is the shear modulus G_c which is calculated by putting Equation (5.5) in Equation (5.3). The obtained equation is only valid for the beginning of the bending tests when the deflection is relatively small and in fact is used only to evaluate the shear modulus.

The aim of the bending tests is to calculate the out of plane shear modulus G_c of the fiber entangled sandwich materials. It can be seen from the force-deflection curves in Fig 5.7 that despite the complex nature of the fabrication process, the results of the three heavy as well as the three light specimens show a relatively good correlation. In case of the heavy specimens, the first damage in the skin appears around the 4-5 mm mark, whereas for the lighter specimens the first damage signs are after 10 mm. In addition, lesser force is required in the case of the light specimens to crack the skin. The average shear modulus for the heavy specimens is 10 MPa, and for the light specimens is 4 MPa.

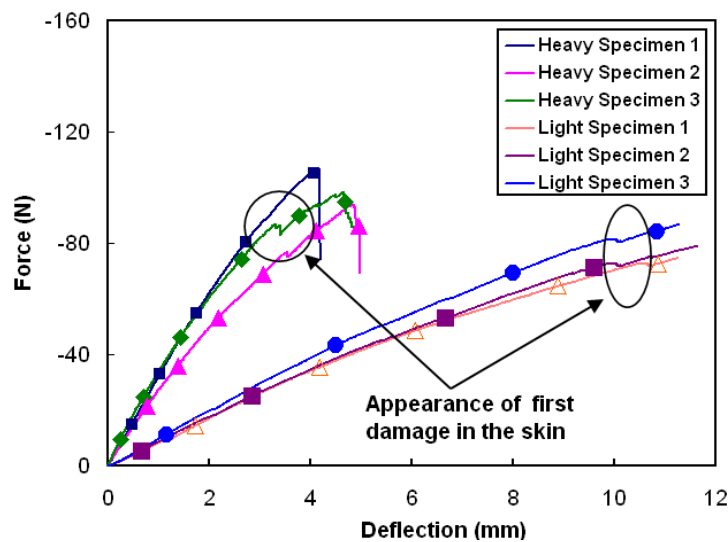


Figure 5.7 Force-deflection curves measured under three-point bending tests for the two types of fiber network sandwich specimens. The appearance of the first damage in the skins is indicated

The values of the elastic and shear moduli are considerably low from a structural strength point of view. It is important to underline here that the entangled sandwich beams are designed for specific applications only. The main idea behind the fabrication of these sandwich specimens is to have a material having good damping characteristics even if it does not possess high structural strength.

5.1.3 Dynamic Characterization of Long Carbon Entangled Sandwich Beams

Vibration Tests

Vibration tests are carried out on the carbon entangled sandwich beams by following the same procedure as of the composite laminate beams in Chapter 3 in Section 3.2.1. Vibration tests shall be carried out by only burst random excitation in case of carbon entangled sandwich beams because at the time of tests the Ideas B&K system was not available in order to perform vibration tests with sine-dwell excitation. The center of the carbon entangled sandwich beam is excited at Point 17 as shown in Fig 5.8.

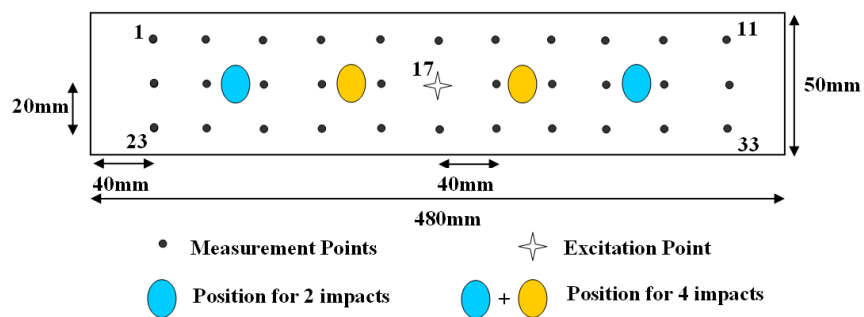


Figure 5.8 Entangled test beam with location of damage, excitation and measurement points

The modal parameters extracted from 33 high quality frequency response functions with the help of Polymax algorithm integrated in the LMS data acquisition system, are presented in Table 5.3.

Table 5.3 Modal parameters comparison for the light and heavy vibration test beams fabricated from the small and large mold (150 kg/m^3 fiber core density)

Type of Beam	Beam No	Beam Weight (g)	Natural Frequencies (Hz)				Damping Ratios (%)			
			1st Mode	2nd Mode	3rd Mode	4th Mode	1st Mode	2nd Mode	3rd Mode	4th Mode
Heavy (Large Mold)	1	124.1	222	652	1069	1550	0.33	0.38	0.62	1.23
	2	116.0	189	506	947	1493	0.46	0.69	1.20	1.26
	3	118.6	202	562	981	1428	0.55	0.64	1.03	1.12
	4	126.4	230	632	1107	1673	0.69	0.79	1.35	1.12
	5	98.0	160	349	701	1217	2.75	3.29	2.65	1.59
Light (Large Mold)	6	93.0	140	295	636	1160	3.31	2.18	3.98	1.25
	7	94.7	145	311	680	1179	3.63	2.98	2.53	0.93
	8	94.5	144	320	681	1171	3.62	2.59	2.28	1.10

As discussed before, the difference in weight between each of the four heavy and light beams is due to the fact that with the currently available fabrication technology it is difficult to spray the resin equally on the fibers. This difference in weight is also evident in the natural frequencies of these beams (Table 5.3). The heavy beam 4 and the light beam 5 have comparatively high natural frequencies due to them being relatively heavier in weight than the rest.

In case of the four heavy beams (Beams 1-4), the average natural frequency for the first mode is 211 Hz with a standard deviation of 18 Hz. The main reason for this dispersion is the uneven spray of resin on the fibers. So vibration tests have been used here as a diagnostic tool in order to verify the quality of the fabrication process.

On the other hand, the light beams (Beams 5-8) possess better damping characteristics because lesser amount of resin increases the friction between the carbon fibers in the sandwich core (weakening the cross-linking between the fibers), which leads to higher values of damping ratios (Table 5.3). It can be said that the vibration tests verify the results previously found by the compression and the bending tests, which also underline the softness of the light beams.

This observation can be further explained by studying the comparison of the sum of frequency response functions (FRF) for the heavy entangled beam 1 and the light beam 6 in Figure 5.9. The resonance peaks for the first four bending modes for each specimen are also highlighted.

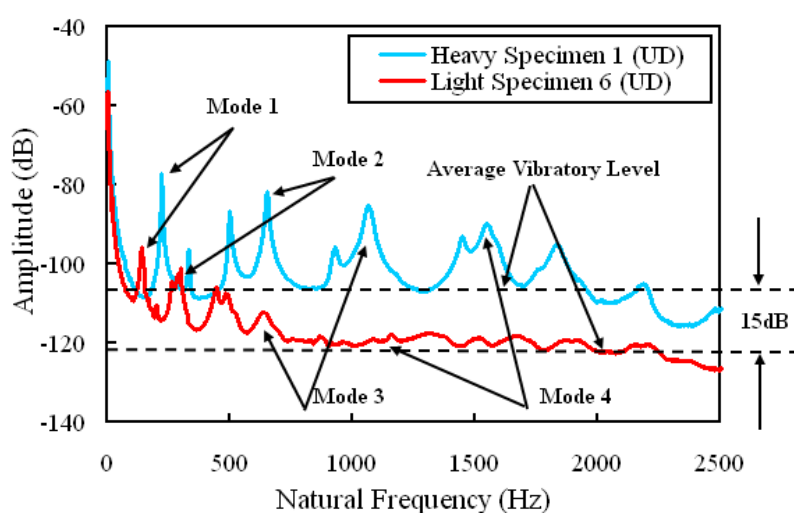


Figure 5.9 Comparison of the Sum of Frequency Response Function (FRF) for a light (EL1) and a heavy specimen (EH1) having 150 kg/m^3 fiber core density for the undamaged state (UD)

An interesting global approach is developed next in order to compare the average vibratory level of the specimens. The average vibratory level is calculated by taking the average of the amplitude (in dB) of the sum of the frequency response function for each specimen. The sum of the frequency response functions can be compared for all the vibration test specimens in this thesis, as same number of measurement points (33) has been chosen i.e. symmetry has been respected for all the specimens.

It can be seen in Figure 5.9, that the resonance peaks of the heavy specimen are more pointed and possess higher amplitude than the light specimen. The resonance peaks of the light specimens are comparatively rounded specially after 800Hz. The average vibratory level (AVL) is also compared for the two types of specimens, and it can be seen that the light specimens possess on average 15 dB lower amplitude than the heavy ones.

From Fig 5.9, it can be inferred that the difference in the natural frequencies between the heavy and light specimens signifies a loss in rigidity, whereas the change in vibratory level signifies a reduction in the amplitude of vibration. The percentage change in frequency and the change in vibrational level between the four heavy and four light vibration test specimens (150kg/m^3 fiber core density) for the first four bending modes are calculated with the help of Equations 5.6 and 5.7, and the resulting values are laid out in Table 5.4.

$$\text{Change in frequency } (\Delta f) = \frac{f_H(k) - f_L(k)}{f_H(k)} \quad (5.6)$$

where $f_H(k)$ is the average frequency for the four heavy beams (Beams 1-4) for the k_{th} mode and likewise $f_L(k)$ is the average frequency for the four light beams (Beams 5-8) for the k_{th} mode

$$\text{Change in vibratory level } (\Delta a) = a_H(k) - a_L(k) \quad (5.7)$$

where $a_H(k)$ is the average amplitude in dB for the four heavy beams for the k_{th} mode and $a_L(k)$ is the average amplitude in dB for the four light beams for the k_{th} mode

Table 5.4 Change in frequency and vibrational level for the light and heavy entangled sandwich beams for the first four modes

	Mode 1	Mode 2	Mode 3	Mode 4
% Change in Frequency (Δf)	30.1 %	45.7 %	34.3 %	23.1 %
Change in Vibratory Level (Δa)	10.1 dB	13.7 dB	17.9 dB	17 dB

Table 5.4 shows that the average change in frequency for the first four bending modes between the light and heavy specimens is approximately 33 %. As the decrease in natural frequency signifies a loss of rigidity, therefore it can be concluded that the lighter specimens are less rigid than the heavy ones.

5.1.4 Impact Parameters of Carbon Entangled Sandwich Beams

In case of the impact tests, the apparatus explained in Section 3.2.2 shall be employed. Impact tests shall only be done by clamping all four ends of the beam-type specimens. As impact tests are carried out the first time on entangled sandwich materials, so a simple case with symmetric impacts is chosen. These impact points are shown in Fig 5.8. The entangled sandwich specimens have three states. First one is the undamaged state (UD), the second is the damage state due to two impacts (D1) and the third is the damage state due to four impacts (D2). Vibration tests are carried out on the four entangled sandwich beams after each of these three states, which is the standard operating procedure of this thesis.

The carbon entangled sandwich beams like all other specimens in this thesis are impacted by taking into account the barely visible impact damage limit (BVID). Unfortunately, very little scientific literature can be found related to impact testing of entangled sandwich materials, so two test beams from each of the four heavy and four light specimens (Table 5.3) are used for trial impact tests, in order to determine the BVID levels. The impact energies are chosen in such a way that the heavy and light beams have the same level of damage. In general, two levels of damage are studied in this study

- Barely visible impact damage (0.6-0.8 mm of indentation measured just after the impact)
- Damage not apparent on the surface (0.1-0.2 mm of indentation measured just after the impact)

These trial impact tests revealed that in case of the heavy specimens, impact energy of 8 J corresponds to the BVID limit. However, in case of light specimens, they have to be impacted at 12 J in order to induce damage corresponding to the BVID limit. As discussed previously, that sometimes damage that is not visually apparent on the surface can prove quite detrimental to the load bearing capacities of sandwich structures. Therefore, during the trial impact tests on the heavy and light entangled sandwich specimens, an indentation depth of 0.1-0.2 mm is found to be undetectable through visual inspection. This indentation depth corresponds to impact energy of 6 J in case of heavy specimens and 8 J for the light ones.

After the trial impact tests, two remaining specimens of each heavy and light specimens are used for the real impact and vibration tests. These specimens with reference to Table 5.3 shall be referred to in the future discussions as follows:

- Heavy beam 4 shall be referred to as Entangled Heavy (EH1)
- Heavy beam 1 shall be referred to as Entangled Heavy (EH2)
- Light beam 7 shall be referred to as Entangled Light (EL1)
- Light beam 5 shall be referred to as Entangled Light (EL2)

Each specimen is impacted at four different points (Fig 5.8), but the impact energy level is kept the same for each of the specimens. The two heavy specimens are impacted at 6 J (0.1-0.2 mm indentation depth) and 8 J (BVID limit), whereas the two light specimens are impacted at 8 J (0.1-0.2 mm indentation depth) and 12 J (BVID limit). The impact parameters for the two heavy and two light entangled sandwich specimens studied in this section are listed in Table 5.5. The data obtained during the drop weight impact tests is shown in Fig 5.10.

Table 5.5 Impact test parameters for the carbon entangled sandwich beams

Beam Name	Energy of Impact (J)	Height (mm)	Indentation just after impact (mm)	Velocity of impact Measured (m/s)
Entangled Heavy 1 (EH 1)	6	331.8	0.1 - 0.2	2.49
Entangled Heavy 2 (EH 2)	8 (BVID)	442.3	0.6 - 0.8	2.83
Entangled Light 1 (EL 1)	8	442.3	0.1 - 0.2	2.83
Entangled Light 2 (EL 2)	12 (BVID)	663.5	0.6 - 0.8	3.52

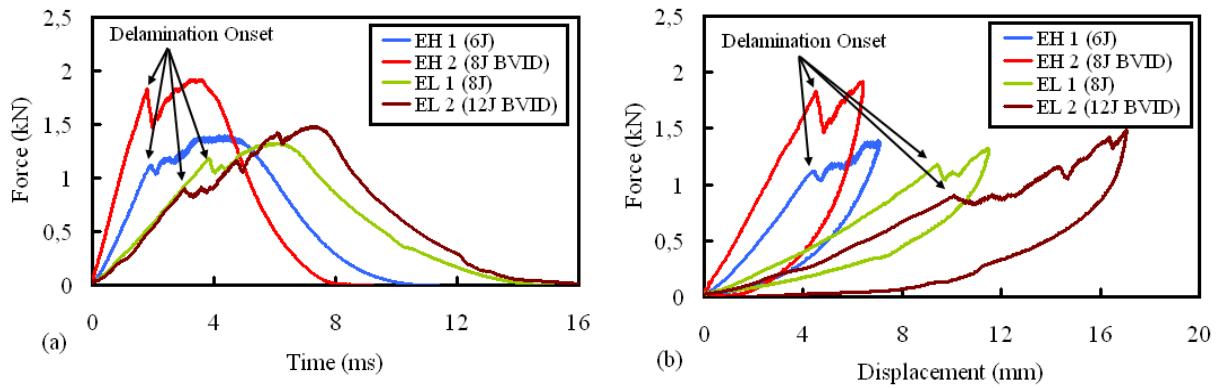


Figure 5.10 Impact test data (a) force-time (b) force-displacement

Four similar impacts have been performed on each specimen. However, in order to clarify these plots, only one impact test result for each specimen is plotted. As for the previous impact tests, all the impact curves presented in Fig 5.10 are filtered at 15 kHz. In Fig 5.10 a, the impact forces are drawn as a function of time during impact tests. These curves are globally smooth and almost sinusoidal at low impact energy, with little oscillation due to natural frequencies of the panel. They show an important force signal fall followed by oscillations which is characteristic of delamination onset. This phenomenon is more prominent for higher impact energies. The force-displacement plot (Fig 5.10 b) shows the same force signal peak as soon as the delamination begins. These curves also give us an indication about the static strength of the heavy and light entangled sandwich specimens. They underline the facts that as the light specimens are less dense having less resin as compared to the heavy ones, so in order to attain peak force or maximum energy, more time and displacement are required. The results of the static tests (compression and bending) carried out on the heavy and light specimens have been discussed in detail in the previous section.

5.1.5 Monitoring of Impact Damage in Long Carbon Entangled Sandwich Beams through Frequency and Damping Changes

Monitoring of the impact damage in the entangled sandwich specimens is carried out through frequency and damage changes as in case of the composite laminates and honeycomb sandwich beams. The impact toughness of entangled sandwich beams can also be evaluated by the decrease in natural frequency (global parameter of a structure) which signifies loss of rigidity. Frequency and damping are the global parameters of the entangled sandwich beams, and are extracted from the measurements carried out on the 33 measurement points. The frequency and damping changes are studied with the help of bending modes as they have the largest amplitudes for the type of test configuration presented in this thesis. For the first four bending modes, the variation of damped natural frequency as a function of the undamaged (UD) and the two damage states (D1 and D2) is presented in Fig 5.11.

Fig 5.11 shows a dispersion in the natural frequencies between the two heavy (EH 1 and 2) and the two light specimens (EL 1 and EL 2) at the undamaged state. Each of the two heavy and light entangled sandwich specimens is fabricated from the same mold. However, this dispersion is a result of the differences in weight (Tables 5.3 and 5.6) which as outlined previously, is due to the uneven distribution of the manually sprayed resin which highlights the complexity of the fabrication process.

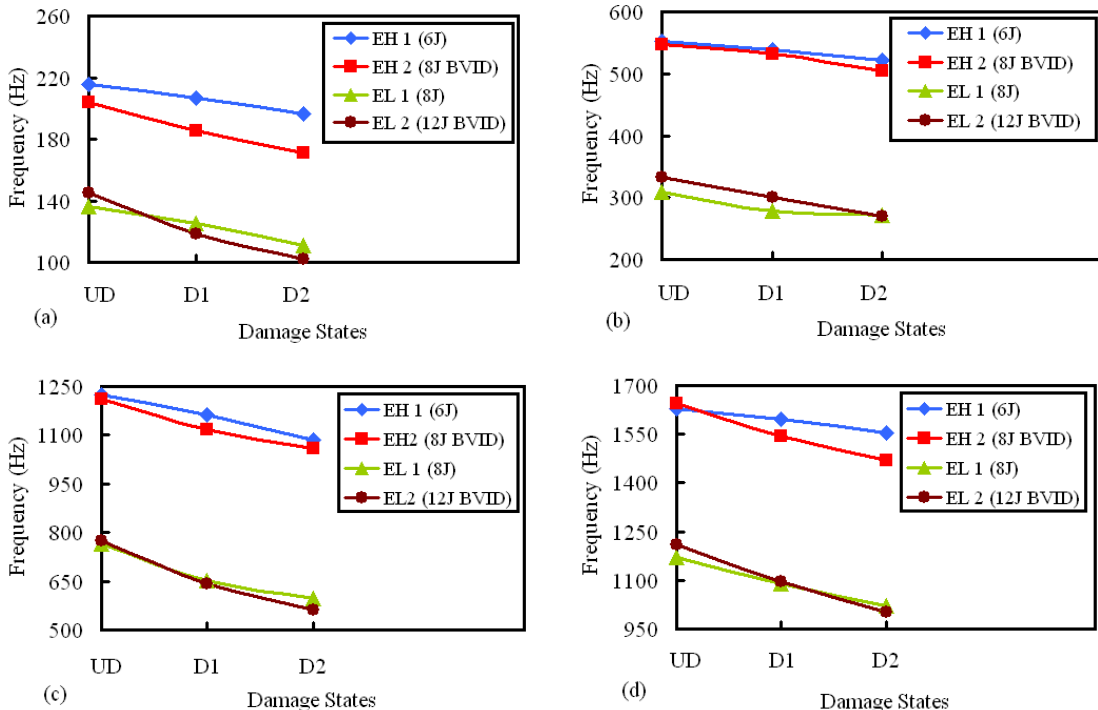


Figure 5.11 Variation of damped natural frequencies with damage states for (a) 1st bending mode, (b) 2nd bending mode, (c) 3rd bending mode and (d) 4th bending mode: UD is undamaged state, D1 is damaged at 2 points of impact and D2 is damaged at 4 points of impacts, for the four entangled sandwich specimens

As discussed previously, that damage in the entangled specimens prompts a decrease in natural frequencies. So from Fig 5.11, it is clear that the decrease in the natural frequencies for both the heavy and light specimens is more prominent in case of the higher impact energies i.e., 8 J in case of the heavy (EH 2) and 12 J in case of the light specimens (EL 2). But the interesting fact is that, for the heavy specimen (EH 1) impacted at 6 J which does not produce a visible damage on the surface, the average change in frequency for the first four bending modes between the undamaged and the damaged cases is 6 %. Similarly, for the light specimen (EL 1) impacted at 8 J this change in frequency ratio is 13 %. So it can be seen that the damage not visually apparent can affect the modal parameters resulting in a certain loss of rigidity. Therefore, vibration testing can be an effective tool to carry out non destructive tests for structural health monitoring purposes.

The shift in the natural frequencies between the undamaged and the damaged cases is more prominent at higher frequencies as was the case before the composite laminates and the composite sandwich beams. This is evident in Fig 5.12, which shows a comparison of the sum of the frequency response functions (FRF) for the entangled sandwich specimen EH 2 (impacted at 8 J) for the undamaged case (UD), damaged at 2 points (D1) and damaged at 4 points (D2). The sum of the FRF can be compared as for each entangled sandwich beam 33 symmetric measurement points have been chosen and the four impact points are also symmetric on both sides of the two major axes of symmetry. In Fig. 5.12, the peaks around 800 Hz between the 2nd and 3rd bending modes, correspond to the torsion mode.

Furthermore, the damping ratios estimated by Polymax algorithm for the two heavy and two light entangled sandwich specimens for the first four bending modes are shown in Fig 5.13.

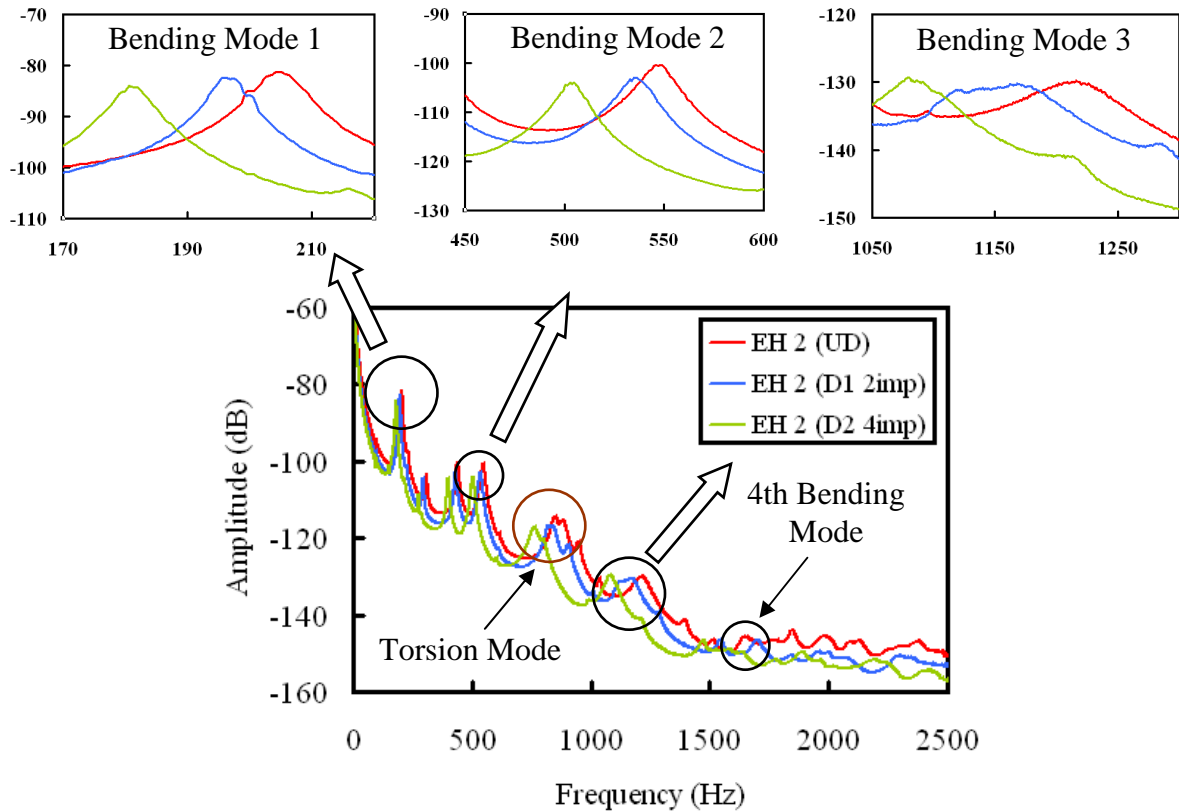


Figure 5.12 Comparison of the sum of the frequency response functions for EH 2 for the undamaged case (UD), damaged at 2 points (D1) and damaged at 4 points (D2)

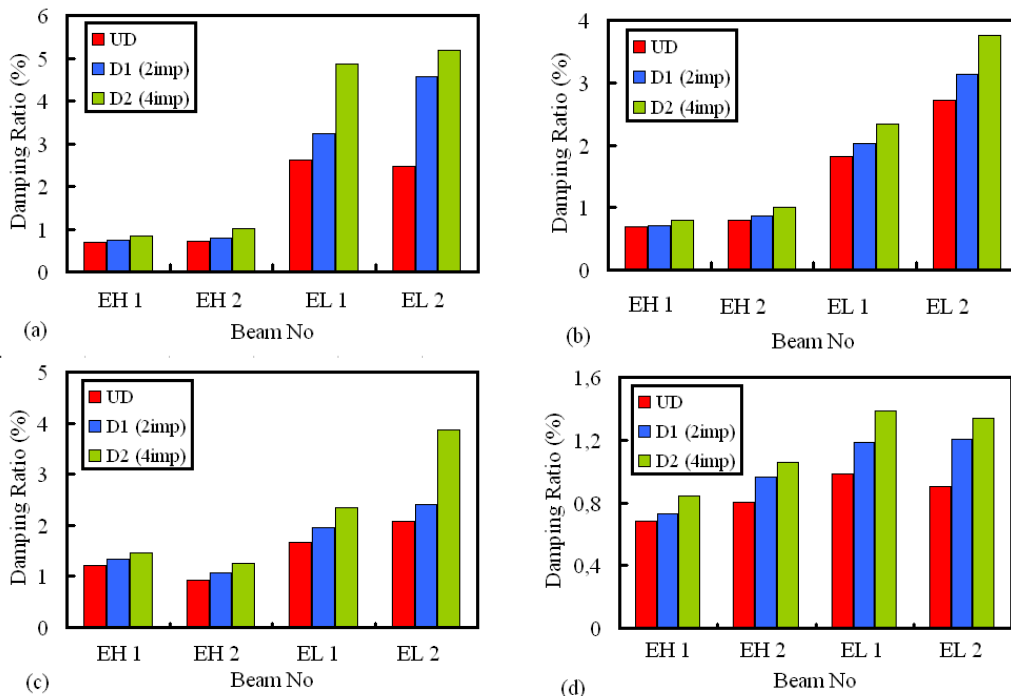


Figure 5.13 Variation of damping ratios for the three damage states for (a) 1st bending mode, (b) 2nd bending mode, (c) 3rd bending mode and (d) 4th bending mode: UD is undamaged state, D1 is damaged at 2 points of impact and D2 is damaged at 4 points of impacts, for the four entangled sandwich specimens

In case of damage, it can be inferred from Fig 5.13 that the damping increases with the increase in damage in the entangled sandwich beams. It can be noticed that with the exception of the 4th bending mode (Fig 5.13 d), the change in damping ratio between the undamaged and the damaged states for the two heavy specimens (EH 1 and EH 2) is smaller as compared to the two light specimens (EL 1 and EL 2), which shows that the light specimens are more sensitive to damage than the heavy ones.

The affect of damage on the frequencies and damping ratios can be further elaborated by studying the frequency and the damping change ratios between the undamaged (UD) and the damaged cases (D1 and D2) for the two heavy and the two light entangled sandwich specimens, presented in Table 5.6.

The percentage change in frequency and damping ratios between the undamaged and the damaged cases is calculated with the help of Equations 5.8 and 5.9:

$$\text{Change in frequency between UD and D1, } (\Delta f) = \frac{f_{UD}(k) - f_{D1}(k)}{f_{UD}(k)} \quad (5.8)$$

$$\text{Change in damping between UD and D1, } (\Delta f) = \frac{\zeta_{D1}(k) - \zeta_{UD}(k)}{\zeta_{UD}(k)} \quad (5.9)$$

where $f_{UD}(k)$ is the damped natural frequency for the undamaged specimen for the k_{th} mode and $f_{D1}(k)$ is the damped natural frequency for the specimen damaged at two impact points (D1) for the k_{th} mode. Nomenclature in case of Equation 5.9 is the same. Furthermore, in order to calculate the frequency and damping change ratios between UD and D2 the same procedure is used.

Table 5.6 Frequency and damping change ratios between the undamaged (UD) and the two damaged states (D1 and D2) for the two heavy (EH1 and EH2) and the two light (EL1 and EL2) entangled sandwich specimens

Type of Specimen	Specimen Weight (g)	Between States	Frequency Change Ratios (%)				Damping Change Ratios (%)			
			1st Mode	2nd Mode	3rd Mode	4th Mode	1st Mode	2nd Mode	3rd Mode	4th Mode
EH1 (6J)	127	UD and D1	4.2	2.4	4.8	2.0	7.0	2.2	9.5	31.3
		UD and D2	8.8	5.6	11.3	4.7	23.9	15.9	19.7	47.3
EH2 (8J)	124	UD and D1	9.1	2.9	7.6	6.1	10.1	9.2	14.1	19.6
		UD and D2	16.1	7.9	12.4	10.7	40.5	27.6	33.0	30.8
EL1 (8J)	95	UD and D1	7.9	9.7	14.6	7.0	24.1	11.4	16.1	20.7
		UD and D2	18.7	12.0	21.7	12.8	86.1	29.2	39.4	40.5
EL2 (12J)	98	UD and D1	18.2	9.9	17.2	9.3	85.1	15.3	15.9	32.8
		UD and D2	29.7	18.8	27.3	17.1	109.0	38.6	86.9	47.4

For all the four entangled sandwich beams studied, it can be seen from Table 5.6, that the damping change ratios are more prominent than the frequency change ratios, as it was found previously in case of composite laminate and honeycomb sandwich beams. The maximum

damping change ratio is 109.6 % and the maximum frequency change ratio is 29.7 % which occur in the case of EL 2 specimen impacted at 12J. It can be concluded from the above results that damping seems more sensitive to damage than the natural frequency variations even in the case of entangled sandwich materials. So it is reasonable to assume that damping may be used instead of natural frequency as a damage indicator tool for structural health monitoring purposes. However, the fact that damping is a parameter that is relatively difficult to estimate as compared to natural frequency has to be taken into account.

Furthermore, if the frequency and damping change ratios are compared for the two heavy and light specimens (EH 2 and EL 2) impacted at the BVID limits i.e., having the same damage (0.6 – 0.8 mm indentation depth), it can be seen from Table 5.6 that the change in modal parameters is more significant in case of the light entangled specimen. This shows that even if the same level of damage (BVID) is imparted to the two specimens, the lighter specimens seem to be more affected. Similarly, by comparing the heavy (EH 1) and the light entangled specimen (EL 1) having the same lower level of damage that is not visible (0.1 – 0.2 mm indentation depth) in Table 5.6, it is evident that again the light specimen (EL 1) is seen more sensitive to damage than the heavy one. The only exception is the damping change ratio for the 4th bending mode, which is higher in case of the heavy specimen.

So overall, it can be concluded that the light specimens having lesser amount of resin possess good damping capabilities as seen in Fig 5.13, but are more sensitive to impact damage than the heavy ones, even when they have the same amount of damage. Therefore, while selecting the application of these light entangled sandwich materials, their sensitivity to impact damage should be taken into consideration. The vibration results also prove that the damage is more localized in the heavy specimens as they are denser in nature as compared to the light specimens, which results in smaller variations of modal parameters in case of heavy specimens. Furthermore, the damage in light specimens is less restricted to a certain zone and thus the light specimens are more globally affected than the heavy specimens.

5.1.6 Drawbacks of the Study on Long Carbon Fiber Entangled Sandwiches and Proposed Modifications

The major drawbacks of relatively long entangled sandwich specimens (480mm length) studied in Section 5.1 are as follows:

- Due to the length of the beams (480 mm), distribution of fibers and the resin is not the same at every point along the length of the beam. With the current technology the resin is sprayed manually with the help of a spray gun, so if the volume of the beam is large so there is a possibility that all the fibers will not have the same quantity of resin.
- The second principal discrepancy of the study is that, carbon entangled sandwich specimens being a relatively new material, their static (compression and bending), dynamic (vibration and) and impact behavior is not compared with that of standard sandwiches e.g., with honeycomb and foam cores.
- The third drawback was that only carbon fibers are studied.

In the next section (Section 5.2), the above mentioned drawbacks shall be tried to be rectified as follows:

- Entangled sandwich beams of shorter length (250 mm instead of 480 mm) shall be fabricated with both carbon and glass fibers, in order to have beams with a more homogeneous distribution of fibers and resin.
- Honeycomb and foam core sandwiches of similar specifications shall be fabricated in order to compare the performance of entangled sandwich beams with existing sandwiches.

5.2 Damage Monitoring in Short Entangled Sandwich Beams by Modal Parameter Shifts

As discussed previously, in this section, relatively smaller entangled sandwich beams are fabricated and their performance compared with standard honeycomb and foam sandwiches. But one point needs clarification here, that the proposed entangled sandwich specimens are currently in the phase of research and are not a finished article as yet. Therefore the mechanical behavior of these sandwich materials are compared for now with standard sandwich beams with honeycomb and foam cores only. Once further expertise is developed in fabricating entangled sandwich specimens, their mechanical behavior especially damping capability and impact toughness shall be compared with innovative sandwich specimens such as multi-layered sandwiches with viscoelastic cores, 3D fabric sandwich structures including glass fibers in the thickness directions, thermoplastic cored sandwiches etc discussed previously in the literature review section 1.6.

5.2.1 Materials and Fabrication Procedure

Six types of sandwich beam specimens are studied in this section of shorter lengths (250 mm) as compared to carbon entangled beams in Section 5.1. The main emphasis however shall be on the two entangled sandwich beams with carbon and glass fibers as core materials. As discussed previously, the honeycomb and foam sandwich beams are only presented for comparison purposes, as the entangled sandwich material being a relatively new material is in the phase of extensive research at this moment. Therefore comparison with standard sandwich beams is essential in order to evaluate the performance of entangled sandwich materials. The six types of sandwich test beams are shown in Fig 5.14.

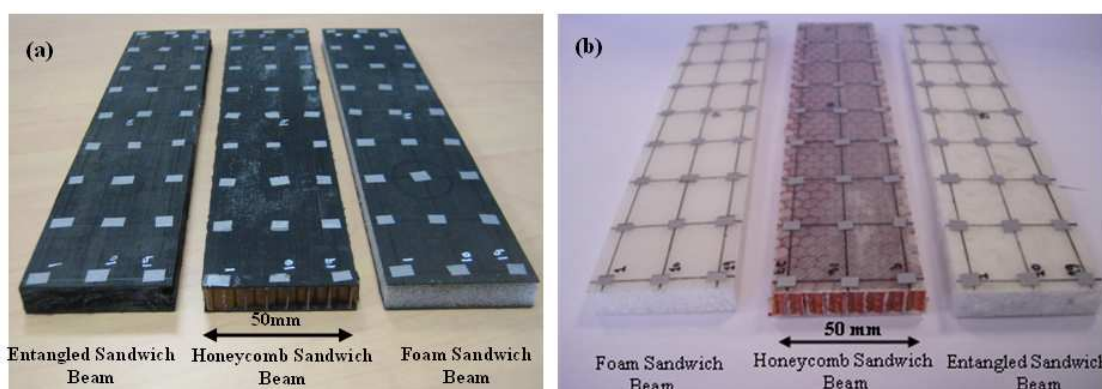


Figure 5.14 The six sandwich beams tested in this section with (a) carbon preps and (b) glass woven fabric as skin materials

Three of the six types of sandwich beams have entangled carbon fiber, honeycomb and foam as core materials. For the skin, carbon-fiber/epoxy preprints of T700/M21 are used as before in Sections 4.2.1 and 5.1.1 having similar thickness and stacking sequence.

The other three sandwich beams have entangled glass fibers, honeycomb and foam as core materials. The skins of these three sandwich beams are made of glass woven fabric 20823 supplied by Hexcel composites as well. The glass woven fabric is impregnated with the help of epoxy resin. The epoxy resin SR 8100 and injection hardener SD 8824 are used provided by Sicomin. The upper and lower skins consist of two plies each with a total thickness of 0.5 mm containing 50 % of resin. The thickness of the skins in case of glass woven fabric is kept similar to carbon fiber skins. The sandwich beam specimens are fabricated using an autoclave and an aluminum mold. The skin and the core are cured simultaneously in order to have an excellent bond. The physical properties of the glass woven fabric are set out in Table 5.7.

Table 5.7 Properties of glass woven fabric used as skin in glass sandwich beams

Properties	Value
Elastic modulus in the longitudinal direction (E_x)	23000 MPa
Elastic modulus in the transverse direction (E_y)	23000 MPa
Shear modulus (G)	2900 MPa
Poisson ratio	0.098

The honeycomb and foam cores can be selected from a wide range of metallic and non-metallic honeycomb cores and a variety of non-metallic foams. The honeycomb sandwich beams in this thesis are made of Nomex-aramid honeycomb core (HRH 10) supplied by Hexcel composites. The honeycomb core has a nominal cell size of 6.5 mm and a core thickness of 10 mm, similar to that used to fabricate the honeycomb sandwich beams in Section 4.2.1. The mechanical properties of the honeycomb core used are given in Table 4.2.

In case of the foam sandwich beams, the foam core has also a thickness of 10 mm and is provided by Rohacell (51 A). Mechanical properties of the foam core is given in Table 5.8.

Table 5.8 Properties of foam core (Rohacell 51A)

Properties	Value
Density	52 kg/m ³
Tensile strength	1.9 MPa
Compressive strength	0.9 MPa
Elastic modulus (traction)	70 MPa
Shear strength	0.8 MPa
Shear modulus	19 MPa
Elongation at break	3.0 %

The properties of the carbon and glass fibers used in the core of entangled sandwich beams are presented in Table 5.9. Same type of carbon fibers are used as before in Section 5.1.1 for the fabrication of long carbon fiber entangled sandwich beams.

Table 5.9 Properties of carbon and glass fibers used in the core of entangled sandwich beams

Properties	Value
Type of carbon fiber	HTS-5631
Length of glass fiber	10 mm
Diameter of carbon fiber	7 μm
Elastic modulus of carbon fiber	240 GPa
Type of glass fiber	Type E
Length of glass fiber	10 mm
Diameter of glass fiber	14 μm
Elastic modulus of glass fiber	73 GPa

The fabrication of honeycomb and foam sandwich beams shall not be explained as the fabrication process is simple and very well known. The fabrication of entangled sandwich beams is similar to that explained previously in this chapter. A fiber core density of approximately 150 kg/m^3 is chosen as previously for the entangled sandwich core in case of both carbon and glass fibers. In case of the glass sandwich beam, the core has 26 g of glass fiber and 17 g of epoxy resin approximately. For the carbon sandwich beam, the core has 30 g of glass fiber and 22 g of epoxy resin approximately. The final dimension for these six types of smaller sandwich beams is 250 x 50 x 11 mm.

This time the effect of fiber length in the entangled sandwich core shall also be studied. For this purpose, two types of glass fiber entangled sandwich beams are fabricated having glass fiber lengths of 10 mm and 15 mm for the core.

As discussed previously in Section 5.1, the entangled sandwich beams have to be characterized both statically and dynamically before further use. So for this purpose the glass entangled sandwich beams (10mm and 15mm core fiber length) and the honeycomb and foam sandwiches with glass skins (Fig 5.14 b) shall be first tested by compression and bending tests for the static characterization and then by vibration testing for dynamic characterization.

Furthermore the carbon fiber entangled sandwich beam and the honeycomb and foam sandwiches with carbon skins (Fig 5.14 a) shall only be studied for the impact toughness later on. As carbon entangled sandwiches have already been characterized statically and dynamically before in Section 5.1, so for the sake of clarity only glass fiber specimens (Fig 5.14 b) shall be studied for the static and dynamic characterization.

5.2.2 Static Characterization of Glass Sandwich Beams

Compression and Bending Tests

Same procedure is used for the compression and bending tests as in case of the long carbon entangled sandwich beams in Section 5.1.2. The result of the compression test carried out on the three types of glass sandwich beams is shown in Fig 5.15.

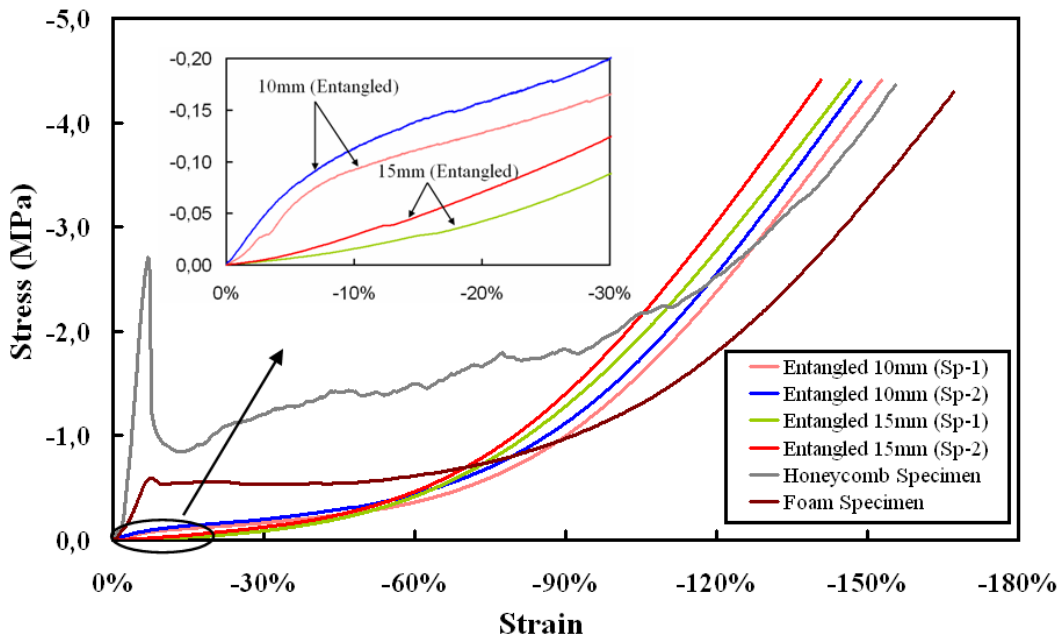


Figure 5.15 Compression stress/strain curves for the entangled (10 mm and 15 mm fiber core length), foam and honeycomb sandwich specimens. The zoomed view shows the linear-elastic phase used for calculating the elastic modulus

Fig 5.15 shows a typical stress-strain curve obtained from the quasi-static compression tests, carried out on the sandwich specimens with honeycomb, foam and entangled glass fiber cores (10 mm and 15 mm fiber length). Three specimens of each type of sandwich material are tested but for the sake of clarity, we only present results for a single specimen in case of honeycomb and foam sandwich materials, and two specimens each in case of the entangled sandwich materials with 10 mm and 15mm glass fiber lengths (Fig 5.15).

The compressive modulus is computed based on the linear-elastic phase by the method presented in [104,144]. In the case of honeycomb cores, the calculation of the compressive modulus is done without taking into account the open cells at the four ends of the 30 x 30 x 11 mm specimen. These open cells buckle under loading and do not contribute to the compressive modulus [143]. Thus the calculations are carried out based on an effective area of approximately 25 x 25 mm² instead of the original area 30 x 30 mm².

It can be seen that the overall behavior in compression is considerably identical for the two types of entangled sandwich specimens having glass fiber lengths of 10 mm and 15 mm. The densification for all the entangled specimens starts around the 60 % strain mark. However if the curves are analyzed more closely (zoomed view in Fig. 5.15), it can be seen that an elastic-linear part exists in case of the 10 mm fiber length entangled sandwich specimens, but this elastic-linear part is non-existent in the case of entangled sandwich specimens with 15mm length fibers in the core. The reason for this is the orientation of fibers in the specimen as shown in Fig 5.16.

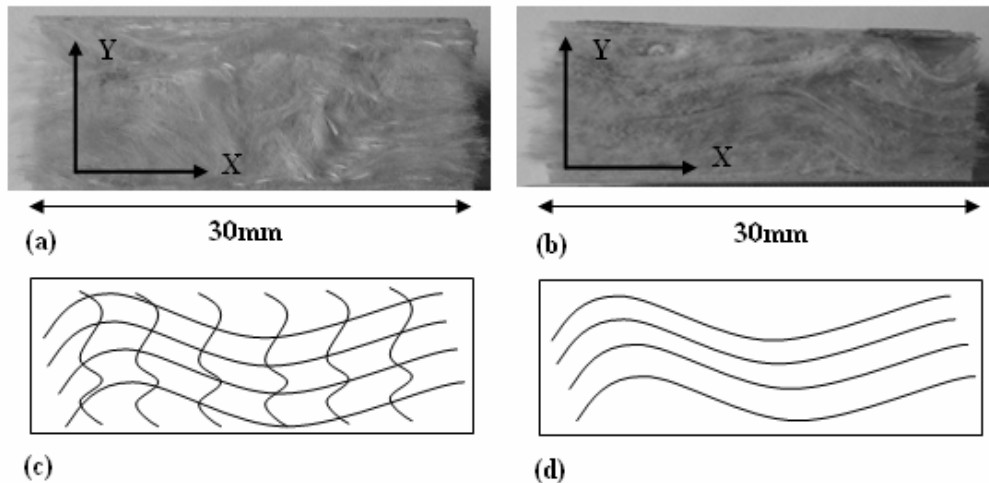


Figure 5.16 Cross-section view of specimen showing the orientation of fibers, (a) 10 mm fiber length entangled sandwich specimen, (b) 15 mm fiber length entangled sandwich specimen. Schematic view explaining the orientation of fibers (c) 10 mm fiber length entangled sandwich specimen, (d) 15 mm fiber length entangled sandwich specimen

For the 10 mm fiber length entangled specimens, the fibers are situated in both the x and y directions, but in case of the 15 mm fiber length entangled specimens, glass fibers in the y-direction are very sparse. The reason may be that in an entangled core better fiber orientation occurs if the length of the fibers is equal to or smaller than the thickness of the core, as discussed in reference [104]. This is the main reason why fibers in the entangled core have a more multi-direction orientation in case of 10 mm fiber lengths as compared to 15 mm fiber lengths. As the load during the compression tests is applied in the y direction, it is evident that the compressive modulus for the 15 mm fiber length specimens is very hard to calculate (absence of linear-elastic phase), as the specimens have very low resistance in the y direction due to lack of glass fibers.

The compressive modulus for the 10 mm fiber length entangled specimens calculated from the linear-elastic phase is 3 MPa. For the foam and honeycomb sandwich specimens, the linear-elastic phase is much more prominent when compared to the entangled sandwich specimens. The compressive moduli calculated from the compression tests are presented in Table 5.10. It can be seen that the compressive modulus for the entangled sandwich materials is much smaller than standard sandwich materials with honeycomb and foam cores.

Table 5.10 Compressive modulus of the honeycomb, foam and entangled material cores calculated from the compression tests

Properties	Value
Compressive modulus for honeycomb core	64 MPa
Compressive modulus for foam core	43 MPa
Compressive modulus for 10 mm glass fiber length entangled core	3.0 MPa
Compressive modulus for 15 mm glass fiber length entangled core	-

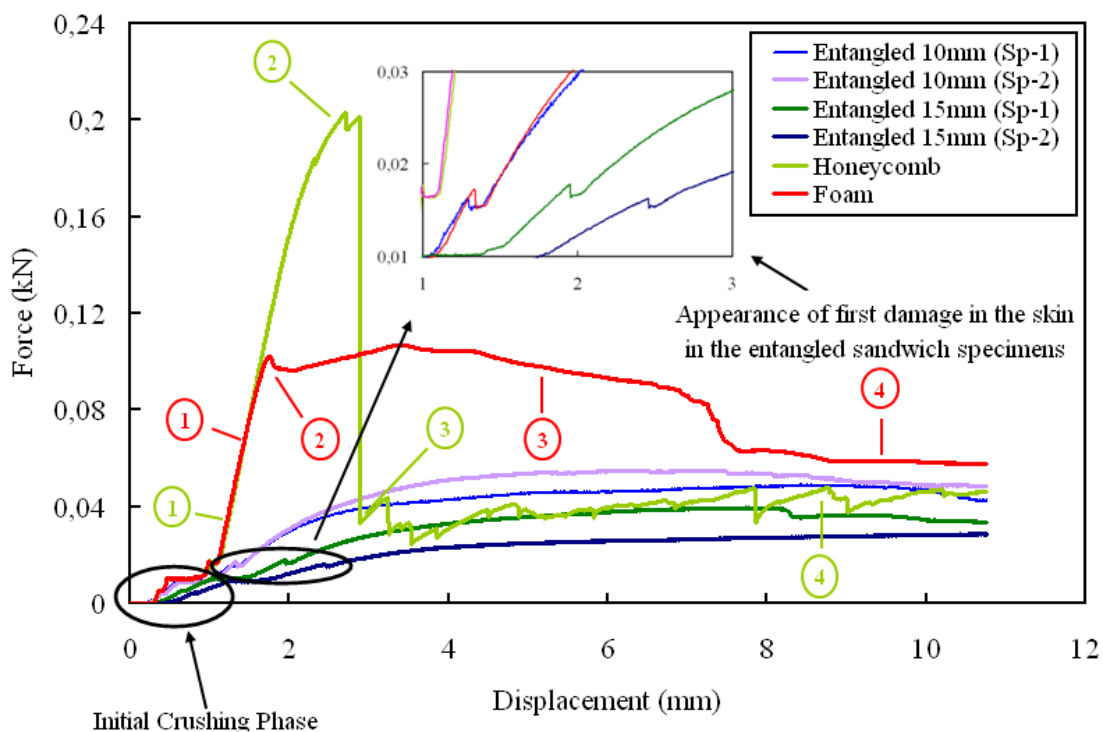


Figure 5.17 Force-deflection curves measured under three-point bending tests for the entangled (10 mm and 15 mm fiber core length), foam and honeycomb sandwich specimens. The appearance of the first damage in the skins is indicated

Fig 5.17 shows a typical load-deflection curve obtained under static three-point bending (support span of 80 mm), on the three types of sandwich materials studied in this section. In case of honeycomb and foam sandwich materials, load-deflection curve for a single specimen is presented whereas in the case of entangled sandwich specimens, results are presented for two specimens for each 10 mm and 15 mm fiber core length entangled sandwich materials. An initial crushing phase occurs for all specimens up to a deflection of 1mm due to skin thinness. In case of the foam sandwich specimen different key features can be clearly identified. The initial linear-elastic behavior (point ①) is followed by an elasto-plastic phase until a peak value is reached (point ②), after which the load decreases, initially markedly and then more smoothly (point ③ and ④); during this phase energy is mainly dissipated by indentation with the formation of hinges within the upper face adjacent to the indenter, and by compressive yielding of the underlying core.

For the honeycomb sandwich specimen, the load loss after the peak value (point ①) is much more evident (point ②) due to core shear failure. Afterward (point ③ and ④) the load remains almost constant. In case of the entangled materials, the behavior is a bit different. For the four entangled sandwich specimens (two 10 mm fiber length and the two 15 mm fiber length specimens), the first damage in the skin occurs around 18 N. After this phase, the load increases up to the 4mm deflection mark, and then it becomes constant due to the densification of the glass fibers in the core. The reason of this densification is the higher density of the glass fibers in the core of the entangled sandwich specimens (200 kg/m^3) as compared to that of honeycomb (30.5 kg/m^3) and foam (51.5 kg/m^3) sandwich cores. The shear moduli calculated from the three-point bending tests are presented in Table 5.11.

Table 5.11 Shear modulus of the honeycomb, foam and entangled material cores calculated from three point bending tests

Properties	Value
Shear modulus for honeycomb core (G_{yz})	12 MPa
Shear modulus for foam core	22 MPa
Shear modulus for 10mm glass fiber length entangled core	9 MPa
Shear modulus for 15mm glass fiber length entangled core	5 MPa

Table 5.11 shows that the standard sandwich specimens with honeycomb and foam core materials possess better shear strength when compared to the entangled sandwich specimens. In order to improve the shear modulus in case of the entangled specimens, a certain percentage of the glass fibers in the core should be placed in the $\pm 45^\circ$ direction, but unfortunately with the fabrication method proposed in the thesis, that is not possible. For the entangled sandwich specimens, we think that the shear modulus G is homogeneous in the plane (it remains to be verified), so we shall compare it with that of the honeycomb in the width direction only (G_{yz}) due to its smaller value (Table 4.2).

As in the case of compression tests, the computed values of the shear modulus for the honeycomb and foam sandwich specimens show a good correlation when compared with those presented in Tables 4.2 and 5.8, provided by the manufacturers. However, the difference in the shear moduli between the two types of entangled sandwich specimens is also due to the orientation of fibers as discussed above and shown in Fig 5.16.

5.2.3 Dynamic Characterization of Glass Sandwich Beams

Vibration Tests

The dynamic characterization of glass sandwich beams is carried out with the help of vibration tests. The aim is to find out the dynamic parameters (natural frequency and damping) in order to compare them with those of honeycomb and foam sandwiches. As before, the vibration tests are based on the experimental methodology previously explained in Section 3.2.1.

For the dynamic characterization, the vibration tests have been carried out on the three types of glass sandwich beams i.e., honeycomb, foam and glass fiber entangled materials with 10mm and 15mm fiber length as core, with burst random excitation only. The aim of using both the burst random and sine-dwell testing is when the beams are damaged, in order to compare the damping results. For the undamaged case, both burst random and sine dwell testing give the same damping results, therefore only burst random testing shall be used. In case of the shorter sandwich beams, the center is excited at Point 14 as shown in Fig 5.18.

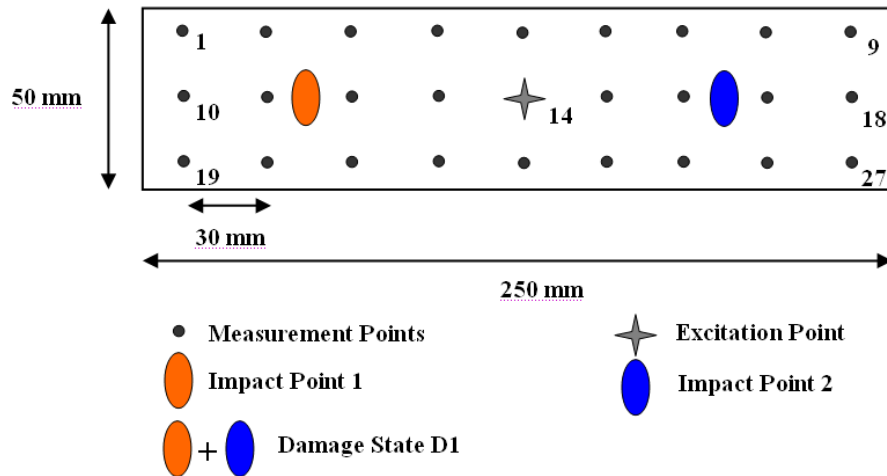


Figure 5.18 Sandwich test beams with location of the two impact points, 27 measurement points and one excitation point (Point 14)

Two specimens of each type of material are tested. The modal parameters extracted from 27 high quality frequency response functions with the help of Polymax algorithm integrated in the LMS data acquisition system, are presented in Table 5.12 along with the specimen weights. The difference in weights observed between the specimens is due to the uneven distribution of resin in skins and in the core (in case of the entangled specimens).

Table 5.12 Comparison of modal parameters for the honeycomb, foam and entangled sandwich specimens

Type of Beam	Beam. No	Weight (g)	Natural Frequency (Hz)			Damping Ratio (%)		
			1st Mode	2nd Mode	3rd Mode	1st Mode	2nd Mode	3rd Mode
Honeycomb	1	22.6	552	1092	1974	0.49	0.39	0.50
	2	23.4	560	1092	1994	0.52	0.44	0.62
Foam	1	26.2	540	1025	1970	0.36	0.55	0.40
	2	25.6	535	1023	1950	0.35	0.46	0.46
Entangled (10 mm)	1	49.7	403	1201	1799	0.54	0.72	0.95
	2	51.6	407	1240	1826	0.56	0.83	0.79
Entangled (15 mm)	1	50.7	308	1166	1622	0.81	1.75	1.77
	2	49	306	1199	1678	0.83	1.89	2.15

Table 5.12 shows that the natural frequencies and damping ratios for the honeycomb and foam sandwich specimens are quite similar; the only exception is the damping ratios for the 1st and 3rd bending modes. The compression and bending tests underlined that the 10 mm fiber length entangled sandwich specimens have higher compressive and shear moduli as compared to the 15 mm fiber length entangled sandwich specimens (Tables 5.10 and 5.11). The better strength of 10 mm fiber length entangled sandwich specimens can also be proved with the help of vibration test results by comparing the natural frequencies of the 10 mm and 15 mm fiber length entangled sandwich specimens in Table 5.12.

It can be seen that the 10 mm fiber length entangled sandwich specimens possess higher natural frequencies, thus proving that they are more rigid than the 15 mm fiber length entangled sandwich specimens. Furthermore, it can be observed from Table 5.12, that the

entangled sandwich specimens have higher damping ratios as compared to standard sandwiches with honeycomb and foam cores. However, it has to be clarified that enhanced sandwich structures with better damping characteristics exist as discussed previously, but this section deals only with the static and dynamic characterization of glass entangled sandwich specimens and their comparison with standard honeycomb and foam sandwiches. Comparison with enhanced sandwich structures e.g., honeycomb sandwiches with viscoelastic layer, etc is not in the scope of this work and shall be duly considered in future works.

The vibration test results can be further analyzed by studying the changes in the damping ratios, average vibratory levels (AVL) and specimen weights. These changes for the entangled sandwich specimens (10 mm fiber length) and the foam and honeycomb sandwich specimens are calculated with the help of Equations (5.10-5.12) and the resulting values are shown in Table 5.13. The comparison between the other materials is carried out in similar fashion.

$$\text{Change in damping ratio, } (\Delta\xi) = \frac{\bar{\xi}_{E10} - \bar{\xi}_{H,F}}{\bar{\xi}_{H,F}} \quad (5.10)$$

where $\bar{\xi}_{E10}$ is the average damping ratio in case of the two 10 mm fiber length entangled specimens for the first four bending modes and $\bar{\xi}_{H,F}$ is the average damping ratio in case of the two honeycomb and two foam sandwich specimens for the first four bending modes. The honeycomb and foam results are presented together in order to simplify the comparisons between the various types of materials presented in this section and also because their modal parameters and weights are quite similar (Table 4.23).

$$\text{Change in average vibratory level, } \Delta a = \bar{a}_{E10} - \bar{a}_{H,F} \quad (5.11)$$

where \bar{a}_{E10} is the average amplitude in dB of the sum of the frequency response functions for the two 10 mm fiber length entangled specimens and likewise, $\bar{a}_{H,F}$ is the average amplitude in dB of the sum of the frequency response functions for the two honeycomb and two foam sandwich specimens.

$$\text{Change in weight, } (\Delta W) = \frac{\bar{W}_{E10} - \bar{W}_{H,F}}{\bar{W}_{H,F}} \quad (5.12)$$

where \bar{W}_{E10} is the average weight (g) for the two 10 mm fiber length entangled specimens and likewise, $\bar{W}_{H,F}$ is the average weight (g) for the two honeycomb and two foam sandwich specimens.

Table 5.13 Comparison of the Vibrational levels, Damping ratios and weights between the sandwich specimens with honeycomb, foam and entangled glass fibers as cores (+ sign shows an increase, while – sign shows a decrease)

	Change in Damping Ratio	Change in Vibrational Level	Change in Weight
Entangled 10mm versus (Honeycomb, Foam)	+60 %	-16 dB	+96 %
Entangled 15mm versus (Honeycomb, Foam)	+215 %	-24 dB	+96 %
Entangled 15mm versus Entangled 10mm	+97 %	-8 dB	-

The entangled sandwich specimens with 10 mm fiber length have (in average for all modes) a 60 % higher damping ratio when compared to honeycomb and foam sandwich specimens. In the case of the 15 mm fiber length entangled specimens, this increase in damping ratio is around 215 % as shown in Table 5.13. On the other hand, the 15 mm fiber length entangled sandwich specimens have 97 % higher damping ratios than the 10 mm fiber length ones. So it can be concluded that entangled sandwich specimens with relatively shorter fiber length (10 mm) in the core possess higher structural strength but have lower damping ratios as compared to entangled sandwich cores with comparatively longer fiber lengths (15 mm). Therefore, the entangled sandwich specimens can be manufactured according to the choice of the type of application, i.e., possessing higher rigidity or better damping characteristics. The major disadvantage of the proposed entangled sandwich specimens is that they are nearly two times heavier as compared to sandwiches with honeycomb and foam cores.

The comparison of modal parameters between the sandwich specimens can be further explained by comparing their sum of frequency response functions (FRF) as shown in Fig 1.18 previously in Chapter 1. The sum of the frequency response functions can be compared for all vibration test specimens, as they have the same dimensions and the same number of measurement points (27) i.e. symmetry has been respected for all specimens. The average vibratory level for these sandwich specimens is also compared. The average vibratory level is computed by taking the average of the amplitude (in dB) of the sum of the frequency response function for each specimen.

It can be seen from Fig. 1.18 that the honeycomb and foam sandwich specimens have identical frequency response functions (FRF) which lead to relatively similar modal parameters as shown in Table 5.12. It can also be seen that the 10 mm fiber length entangled sandwich specimens have in average a 16 dB lower amplitude than the honeycomb or foam sandwich specimens. In case of the 15 mm fiber length entangled specimens, this difference in average vibratory level as compared to the honeycomb and foam specimens is 24 dB. Furthermore, Fig 1.18 shows that the entangled sandwich specimens with longer fiber length (15 mm) in the core have lower amplitudes than those with shorter fiber length (10 mm).

From the compression and bending tests, it is evident that the entangled materials have a low structural strength and are also heavier as compared to the standard sandwich materials (honeycomb or foam as core). But on the other hand, these materials possess higher damping ratios and low vibratory levels which make them suitable for damping suppression and sound absorption applications where structural strength is not the main requirement.

As previously discussed, enhanced sandwich structures with better damping characteristics exist, but this presented work deals only with the static and dynamic characterization of glass entangled sandwich specimens and their comparison with standard honeycomb and foam sandwiches. Comparison with enhanced sandwich structures e.g., honeycomb sandwiches with viscoelastic layer, etc is not in the scope of this work and shall be duly considered in future works.

5.2.4 Impact Parameters of Small Carbon and Glass Sandwich Beams

The impact tests are carried out by using the apparatus explained in Section 3.2.2 previously. Impact tests are done by clamping all four ends of the carbon and glass fiber sandwich beams shown in Fig 5.14. These beams are termed smaller as they have a length of 250mm as compared to the 480mm length in case of the composite laminate beams (Chapter 3), the honeycomb sandwich (Chapter 4) and carbon entangled beams (Sections 5.1). As the beams are smaller, so they are impacted at only two symmetric points as shown in Fig 5.18.

The small carbon and glass fiber sandwich beams (Fig 5.14) are also impacted by taking into account the barely visible impact damage limit (BVID). The idea behind the impact tests is to damage the specimens below the BVID limit, in order to detect by vibration testing the damage that is not visible through naked eye. However in case of honeycomb sandwich beams, it is difficult to induce the same amount of damage at different points in the same specimen, even if it is impacted with the same energy i.e., impacting at the honeycomb cell center and at the corner leads to different damages. Therefore, it is not possible to have the same density of damage in the honeycomb sandwich beams at the two impact points. This phenomenon is explained by taking the example of the carbon honeycomb sandwich beam impacted at 4 J shown in Fig 5.19. The indentation depth at the impact point 1 is 0.1 mm due to impact at the honeycomb cell corner. Whereas the indentation depth at the impact point 2 is 0.5 mm because the impactor head has induced severe damage due to impact at honeycomb cell center. This phenomenon was explained before as well in Section 4.2.2 (Fig 4.11).

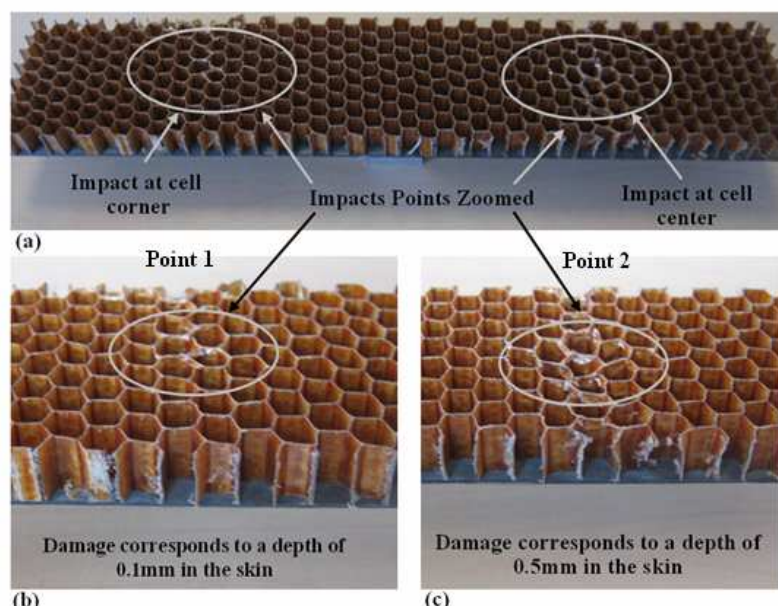


Figure 5.19 Dispersion of damage between the two impact points in case of honeycomb carbon beam, impacted at 4 J

This phenomenon introduces asymmetry in the beams and highlights the difficulty in inducing a global symmetric damage. The impact energy is chosen in such a way that each sandwich beam has approximately the same level of damage i.e., below the BVID limit which is nearly invisible on the surface. The impact parameters and the indentation depths measured for the six sandwich beams are listed in Table 5.14. It shall be noticed that the dispersion in damage between the two impact points is smaller in case of the entangled and foam sandwich beams as compared to the honeycomb sandwich beams due to the phenomenon explained above.

Table 5.14 Impact test parameters of the sandwich beams

Type of Specimen	Energy of Impact (J)	Height (mm)	Indentation just after impact (mm) Point 1	Indentation just after impact (mm) Point 2	Velocity of impact Measured (m/s)
Entangled Carbon	5	277	0.1	0.15	2.21
Honeycomb Carbon	4	222	0.1	0.5	1.98
Foam Carbon	4	222	0.1	0.2	1.98
Entangled Glass	6	332	0.2	0.15	2.49
Honeycomb Glass	4	222	0.2	0.4	1.98
Foam Glass	4	222	0.15	0.25	1.98

The data obtained during the drop weight impact tests carried out on the six sandwich beams is presented in Fig 5.20.

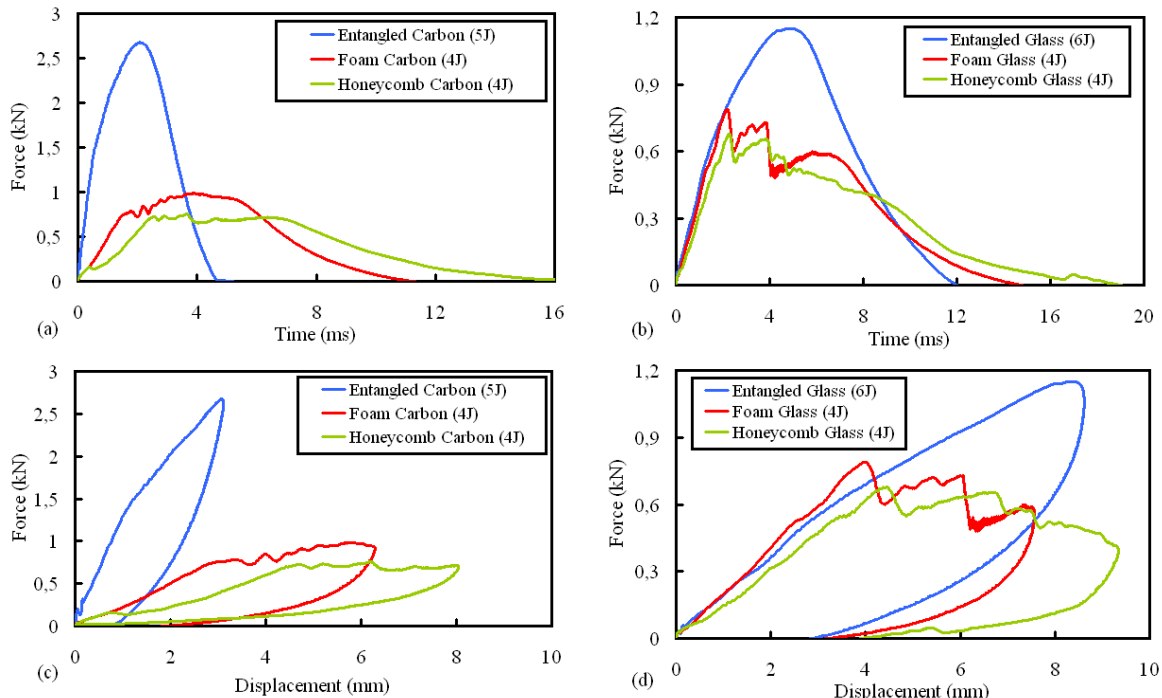


Figure 5.20 Impact test data (a,b) force-time (c,d) force-displacement for the carbon and glass sandwich beams

Two similar impacts have been performed on each sandwich beam. However, in order to clarify these plots, the three glass and three carbon sandwich beams are plotted separately and in addition, only one impact test result for each specimen is plotted. All the impact curves presented in Fig. 5.20 are filtered at 15 kHz to avoid a free frequency of the impactor at about

20 kHz. In Fig 5.20a and 5.20b, the impact forces are drawn as a function of time for the six sandwich beams. These curves are globally smooth and almost sinusoidal at low impact energy. It can also be seen, from the force-displacement plots of both the carbon and glass sandwich beams (Fig. 5.20c and 5.20d), that after the first damage in the classical sandwiches with honeycomb and foam cores there is a decrease in the force signal followed by oscillations which signifies damage and loss of rigidity in the material. But in case of both glass and carbon fiber entangled sandwich beams (Fig. 5.20c and 5.20d), after the appearance of first damage the material continues to rigidify which is shown by a progressive increase of force signal. If we speak in terms of energy dissipation, it can be observed from the force displacement curves of the honeycomb and foam core sandwiches (Fig. 5.20c and 5.20d) that the energy dissipation seems mostly due to the rupture mechanism. However in case of entangled sandwiches the behavior is different, it is possible that the energy dissipation might be predominantly due to damping as no oscillations or force signal loss is observed i.e., no apparent damage signs.

This behavior can also be seen on the stress-strain curves of compression tests which are very classical in scientific literature [106,107]. Compression test results in case of standard sandwiches with honeycomb and foam cores exhibit that there is a progressive decrease in the stress level once the maximum elastic limit is attained. However for the entangled sandwiches, normally there is a densification phase after the maximum elastic limit which explains the rigid nature of the entangled sandwiches as compared to the honeycomb and foam sandwich beams tested in this section. This rigid nature of entangled sandwich beams is also verified further ahead in this chapter when the monitoring of impact damage is carried out by changes in modal parameters.

As shown in Fig 5.18, the sandwich beams have two states. First one is the undamaged state (UD) and the second is the damage state due to two impacts (D1). Vibration tests are carried out on the six sandwich beams after each of these two states. As before the simple case of symmetrical impacts is studied as no literature is available regarding impact tests on entangled sandwich materials. If satisfactory results are obtained, then asymmetric damage shall be studied in the future.

5.2.5 Monitoring of Impact Damage and the Evaluation of the Impact Toughness of Small Carbon and Glass Sandwich Beams through Frequency and Damping Changes

Monitoring of impact damage of the small carbon and glass sandwich beams (Fig 5.14) is studied with the help of modal parameter shifts. This shall also give us an idea regarding the impact toughness (resistance against impact) of these materials. The impact toughness of entangled sandwich beams can also be evaluated by the decrease in natural frequency (global parameter of a structure) which signifies loss of rigidity. The author wants to clarify here, that impact toughness is only studied through vibration tests and the classical procedure used for determining the impact toughness i.e., compression after impact (CAI) has not been implemented as it is outside the scope of this work.

For the first three bending modes, the variation of damped natural frequency as a function of the undamaged (UD) and the damage state (D1) for the six sandwich beams for burst random (BR) and sine-dwell (SD) testing is presented in Fig 5.21.

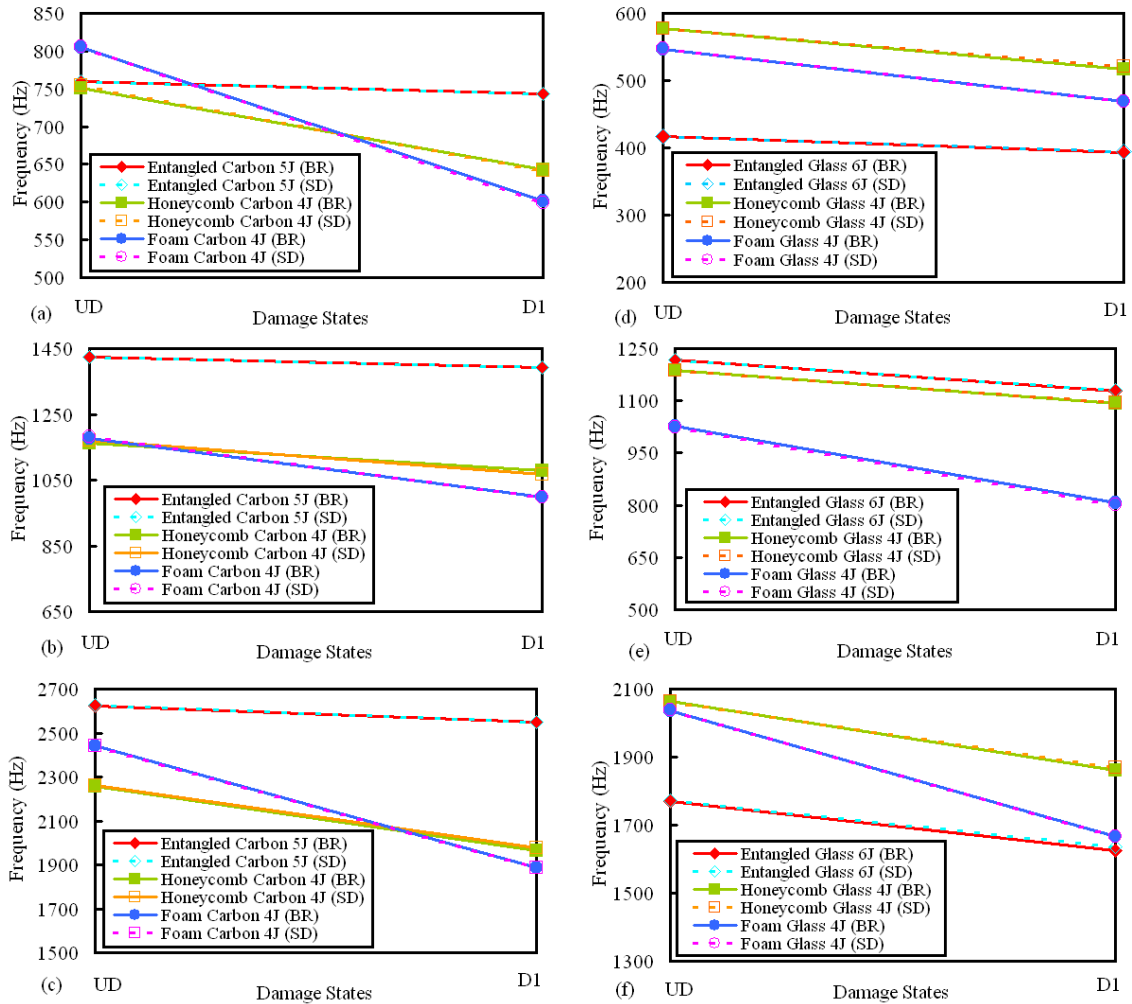


Figure 5.21 Variation of damped natural frequencies with damage states for (a) 1st bending mode, (b) 2nd bending mode and (c) 3rd bending mode for the carbon sandwich beams and (d) 1st bending mode, (e) 2nd bending mode and (f) 3rd bending mode for the glass sandwich beams: UD is undamaged state, D1 is damaged at 2 impact points for both burst random (BR) and sine-dwell (SD) testing

Fig 5.21 shows that as a result of impact damage, there is a decrease in the natural frequencies for the six sandwich beams. It can be noticed that this decrease is less prominent in case of both the carbon and glass entangled sandwich beams as compared to the honeycomb and foam sandwich beams. It is also evident from Fig 5.21 that in case of natural frequencies, both burst random and sine-dwell testing give similar results. But the interesting fact is that for all the sandwich beams, even as the impact damage does not produce a visible damage on the surface, the change in frequency between the undamaged and the damaged cases is quite noticeable. This proves that there is a notable loss of rigidity without any signs of damage on the surface (with the exception of some impact points in case of honeycomb sandwich beams as shown in Fig 5.19). It is particularly in these cases that vibration testing becomes a very useful tool for structural health monitoring.

The fact that the change in natural frequency between the damaged and the undamaged case is small in the entangled beams as compared to the foam and honeycomb beams can be seen in Fig 5.22, which presents a comparison between the frequency response functions of the undamaged and the damaged cases for the six sandwich beams for the 1st bending mode.

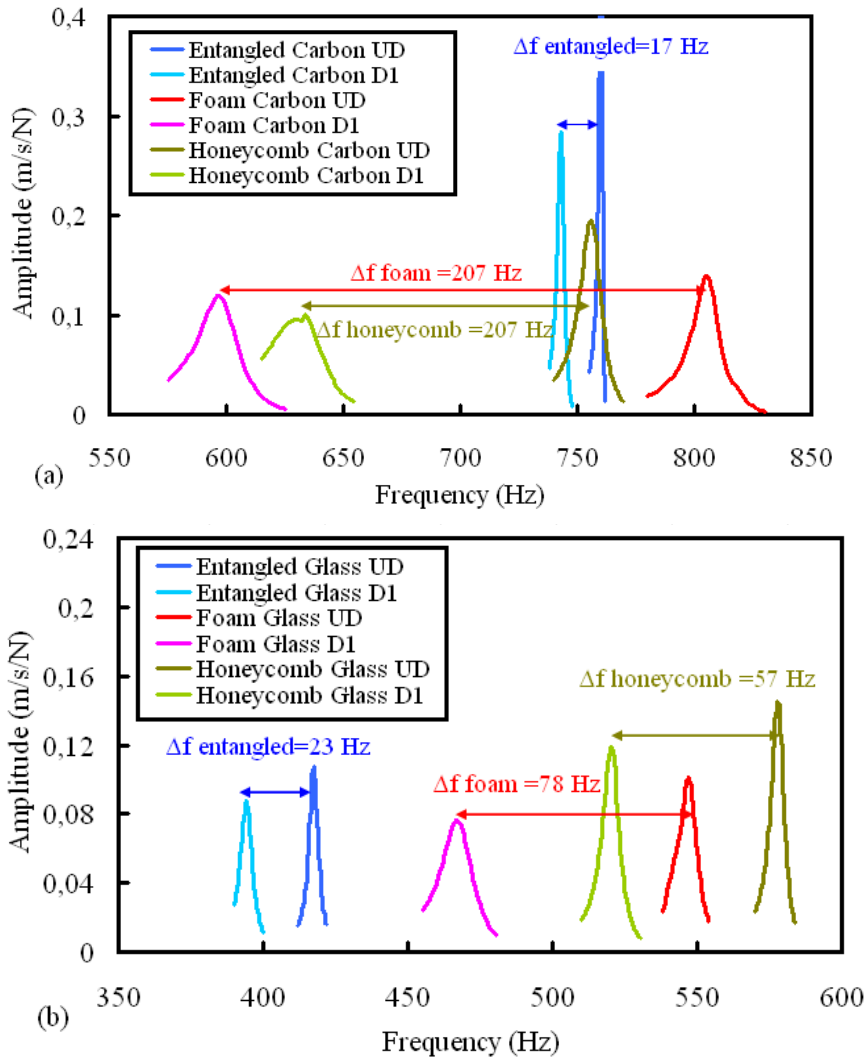


Figure 5.22 Comparison of the frequency response functions estimated by sine-dwell testing for the undamaged case (UD) and damaged at 2 points (D1) for the 1st bending mode for (a) Point 11 for the three carbon sandwich beams and for (b) Point 21 for the three glass sandwich beams

The frequency response functions presented in Fig 5.22 are obtained with the help of sine-dwell testing. For the six sandwich beams, it can be concluded that the shift in natural frequencies is slight in case of entangled sandwich beams proving that they have a loss of rigidity that is less pronounced as compared to the honeycomb and foam sandwich beams. Furthermore in case of the three carbon sandwich beams (Fig 5.22a), the frequency response functions of the carbon entangled sandwich beam are more acute (smaller in width) as compared to the honeycomb and foam sandwich beams. This phenomenon is less evident in case of the glass entangled sandwich beams (Fig 5.22b).

It is noticed that in case of honeycomb sandwich beams, the level of damage is not the same on both sides of the beams as discussed previously. So this asymmetric damage leads to distortion of the resonance peaks or the appearance of twin peaks instead of one. This is evident in Fig 5.23, which shows a comparison of the sum of the frequency response functions (FRF), estimated by burst random testing, for the six sandwich beams for the undamaged (UD) and the damaged cases (D1) for the 3rd bending mode. The sum of the FRF

can be compared as for each sandwich beam 27 symmetric measurement points have been chosen that are symmetric on both sides of the two major axes of symmetry.

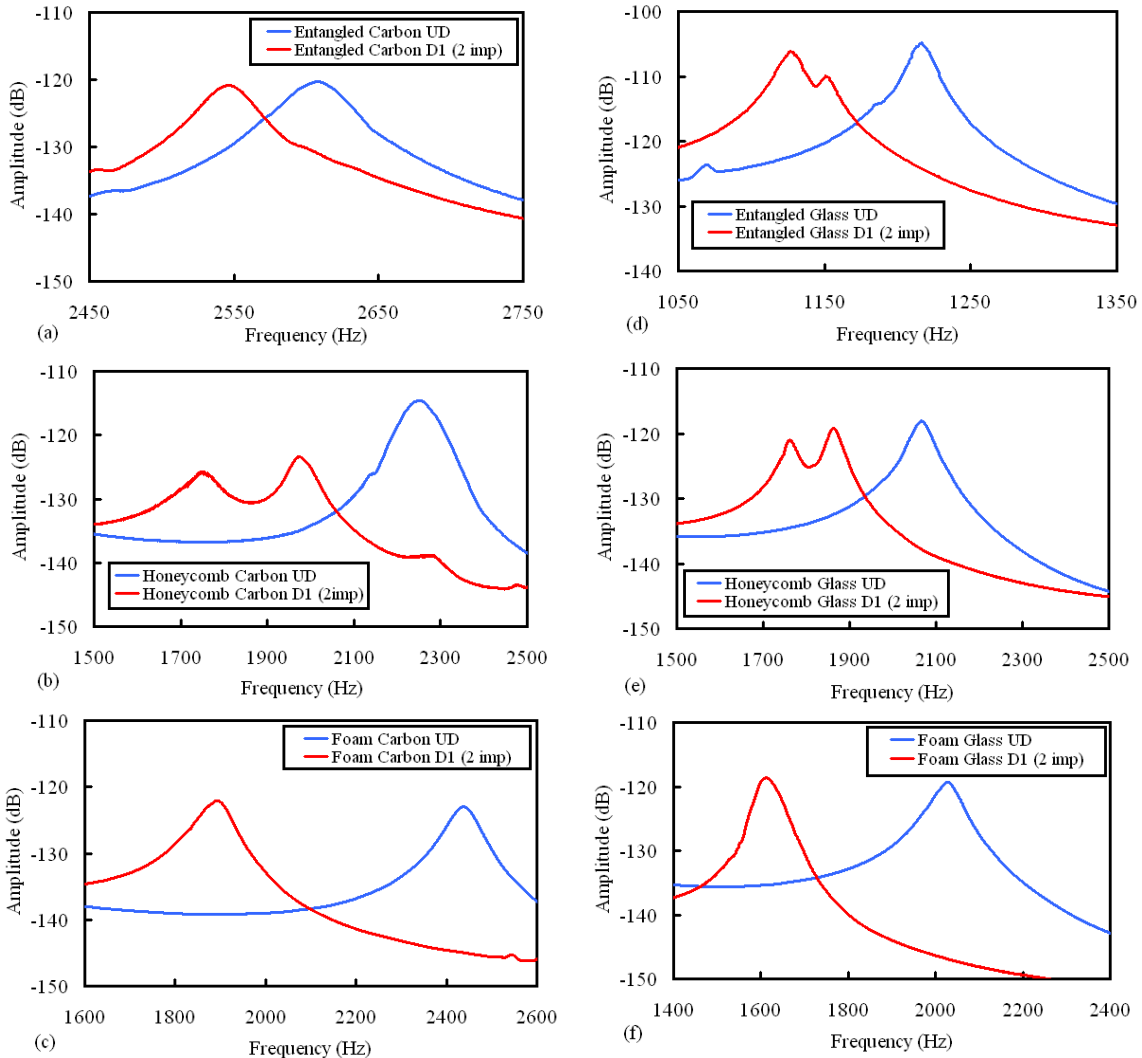


Figure 5.23 Comparison of the sum of the frequency response functions estimated by burst random testing for the undamaged case (UD) and damaged case (D1) for the 3rd bending mode for (a) entangled carbon (b) honeycomb carbon (c) foam carbon (d) entangled glass (e) honeycomb glass (f) foam glass sandwich beams

Fig 5.23 b and Fig 5.23 e show that in case of honeycomb sandwich beams due to asymmetric distribution of damage the shape of peaks become distorted. A slight distortion of peak is also observed in case of the entangled glass beam in Fig 5.23 d. But on the whole for the entangled and foam sandwich beams the damage is pretty much symmetric and peaks remain intact. Both burst random and sine-dwell testing give similar natural frequency results in the presence of damage. However, for the estimation of damping ratios for the damage state D1, there is a notable difference between the results of burst random and sine dwell testing as shown in Fig 5.24.

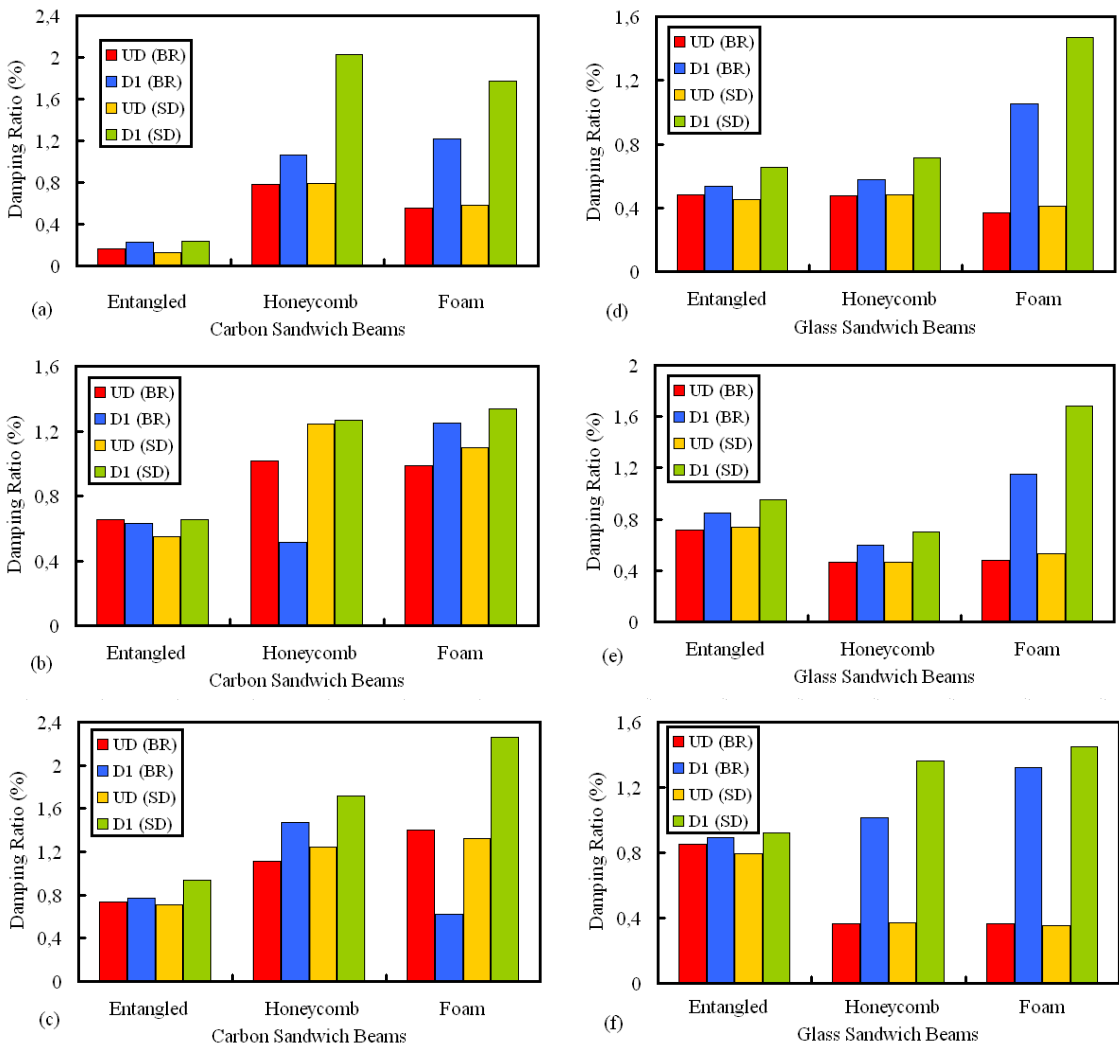


Figure 5.24 Variation of damping ratio with damage states (a) 1st bending mode, (b) 2nd bending mode and (c) 3rd bending mode for the carbon sandwich beams and (d) 1st bending mode, (e) 2nd bending mode and (f) 3rd bending mode for the glass sandwich beams: UD is undamaged state, D1 is damaged at 2 impact points for both burst random (BR) and sine-dwell (SD) testing

It can be seen in Fig 5.24 that in general the damping increases with the increase in damage in the sandwich beams as seen in previous sections. Nonetheless in case of burst random testing, for the carbon entangled and the carbon honeycomb sandwich beams (Fig 5.24 b) and for the carbon foam sandwich beam (Fig 5.24 c), the damping decreases with damage. However sine dwell testing shows a logical increase of damping for these beams. Furthermore, the estimation of damping by sine-dwell testing for the damage state (D1) is always notably higher as compared to burst random testing. It can be said that sine dwell testing is more capable of detecting non linear structural dynamic behavior (due to accumulation of damage as in state D1) unlike the broadband excitations.

Furthermore, the change in damping ratios between the undamaged and the damaged case is smaller again in case of entangled sandwich beams. So it can be concluded that the entangled sandwich beams show a better resistance to impact as compared to the honeycomb and foam sandwich beams, whereas all the beams have more or less the same level damage. So the entangled sandwich materials can replace the aluminum parts at the wing tips used to resist impact, as these aluminum parts are not load carriers. So the entangled materials can be used

in these types of specific applications where static strength is not required but the main objective is the resistance to impact.

The effect of impact damage on the natural frequencies and damping ratios can be further elaborated by studying the frequency and the damping change ratios between the undamaged (UD) and the damaged case (D1) for the six sandwich beams. The percentage change in frequency and damping ratios between the undamaged and the damaged cases is calculated with the help of Equations 5.13 and 5.14 and the results are presented in Tables 5.15 and 5.16.

$$\text{Change in frequency between UD and D1, } (\Delta f) = \frac{f_{UD}(k) - f_{D1}(k)}{f_{UD}(k)} \quad (5.13)$$

$$\text{Change in damping between UD and D1, } (\Delta \zeta) = \frac{\zeta_{D1}(k) - \zeta_{UD}(k)}{\zeta_{UD}(k)} \quad (5.14)$$

where $f_{UD}(k)$ is the damped natural frequency for the undamaged specimen for the k_{th} mode and $f_{D1}(k)$ is the damped natural frequency for the specimen damaged at two impact points (D1) for the k_{th} mode. Nomenclature in case of Equation 5.14 is the same.

Table 5.15 Frequency change ratios (%) between the undamaged (UD) and the two damaged states (D1 and D2) for the carbon and glass sandwich beams for both burst random (BR) and sine dwell (SD) testing

Type of Specimens	Between States	Mode 1		Mode 2		Mode 3	
		BR	SD	BR	SD	BR	SD
Foam Glass (4J)	UD and D1	14.1	14.2	21.4	21.6	18.0	18.2
Honeycomb Glass (4J)	UD and D1	10.4	9.8	8.0	7.9	9.7	9.4
Entangled Glass (6J)	UD and D1	5.8	5.5	7.2	7.1	8.2	7.6
Foam Carbon (4J)	UD and D1	25.2	25.6	15.3	15.5	22.6	22.7
Honeycomb Carbon (4J)	UD and D1	14.4	14.9	7.2	8.6	12.8	12.4
Entangled Carbon (5J)	UD and D1	2.2	2.2	2.1	2.2	2.8	2.9

Table 5.16 Damping change ratios (%) between the undamaged (UD) and the two damaged states (D1 and D2) for the carbon and glass sandwich beams for both burst random (BR) and sine dwell (SD) testing

Type of Specimens	Between States	Mode 1		Mode 2		Mode 3	
		BR	SD	BR	SD	BR	SD
Foam Glass (4J)	UD and D1	57.7	106.0	140.7	216.1	260.3	308.7
Honeycomb Glass (4J)	UD and D1	18.1	32.7	22.0	32.9	64.1	72.6
Entangled Glass (6J)	UD and D1	11.4	44.4	19.1	29.1	4.5	16.1
Foam Carbon (4J)	UD and D1	119.3	204.3	26.3	21.5	-55.9	70.8
Honeycomb Carbon (4J)	UD and D1	35.7	156.2	-49.4	2.01	32.3	37.5
Entangled Carbon (5J)	UD and D1	38.5	79.3	-3.53	19.0	4.1	31.1

Tables 5.15 and 5.16 prove that the shift in modal parameters is less in case of the entangled sandwich beams which signifies that they possess better impact toughness as compared to the standard sandwich beams with honeycomb and foam as core materials. It can also be noticed that the change in damping ratios is greater in case of sine dwell testing, because the damping ratio estimated by sine-dwell testing is always higher in case of the damaged state (D1) as compared to the burst random testing.

Furthermore, the results in Tables 5.15 and 5.16 underline the fact that the damping change ratios are more prominent than the frequency change ratios. The maximum damping change ratio is 310 % whereas the maximum frequency change ratio is 25 %. It can be concluded from the above results that damping seems more sensitive to damage than the natural frequency variations in case of honeycomb sandwich beams. So it is reasonable to assume that damping may be used instead of natural frequency as a damage indicator tool for structural health monitoring purposes. However, the fact that damping is a parameter that is relatively difficult to estimate as compared to natural frequency has to be taken into account.

5.2.6 Effect of Sine-Dwell Frequency Direction on Modal Parameters

The aim of carrying out sine dwell testing in both up and down frequency directions is to be able to detect structural non-linearities in the damaged sandwich beams. This type of study was carried out previously in case of long honeycomb sandwich beams in Section 4.2.7. A notable difference in the frequency response functions was observed when comparing the acquisition results in both upwards and downwards frequency directions for the 480 mm length honeycomb sandwich beams when damaged at four impact points. The reason for this difference in the FRF is the structural non-linearity in the beams due to high damage.

Now the aim of this section is to study the same effect of structural non-linearity in the smaller length sandwich beams, with entangled glass and carbon fibers, honeycomb and foam cores. As discussed previously, the smaller beams are damaged at only two points. So it shall be interesting to observe whether damage at two points induces a notable difference in the modal parameters or not. In this section, the effect of sine-dwell up and down directions is studied for all the six type of small sandwich beams (Fig 5.14) damaged at two points (D1). The resulting modal parameters for the carbon and glass sandwich beams are presented in Tables 5.17 and 5.18 respectively.

Table 5.17 Comparison of natural frequency and damping ratios for both up and down sine-dwell frequency directions for the carbon sandwich beams for the damage state (D1)

Type of Specimens	Sine Dwell Direction	Natural Frequency (Hz)			Damping ratio (%)		
		Mode1	Mode2	Mode3	Mode1	Mode2	Mode3
Foam Carbon (4J) D1 (2imp)	Up	599	997	1888	1.77	1.33	2.26
	Down	598	998	1891	1.45	1.27	2.06
Honeycomb Carbon(4J) D1 (2imp)	Up	642	1068	1978	2.02	1.26	1.71
	Down	643	1068	1978	1.87	1.12	1.69
Entangled Carbon (5J) D1 (2imp)	Up	743	1393	2547	0.23	0.65	0.93
	Down	743	1390	2548	0.22	0.53	0.77

Table 5.18 Comparison of natural frequency and damping ratios for both up and down sine-dwell frequency directions for the glass sandwich beams for the damage state (D1)

Type of Specimens	Sine Dwell Direction	Natural Frequency (Hz)			Damping ratio (%)		
		Mode1	Mod 2	Mode3	Mode1	Mode2	Mode3
Foam Glass (4J)	Up	469	802	1667	1.46	1.68	1.44
D1 (2imp)	Down	469	801	1671	1.39	1.64	1.73
Honeycomb Glass (4J)	Up	520	1094	1870	0.71	0.69	1.36
D1 (2imp)	Down	521	1094	1871	0.66	0.41	1.31
Entangled Glass (6J)	Up	394	1129	1635	0.65	0.95	0.92
D1 (2imp)	Down	395	1130	1635	0.64	0.95	0.73

Tables 5.17 and 5.18 show the presence of a slight nonlinear behavior in both the carbon and glass sandwich beams, as the natural frequencies and damping ratios have a small discrepancy when tested in the increasing and decreasing frequency order. This is also shown graphically in Fig 5.25 for each of the six sandwich beam by plotting the frequency response functions from sine-dwell sweeps upwards and downwards in frequency.

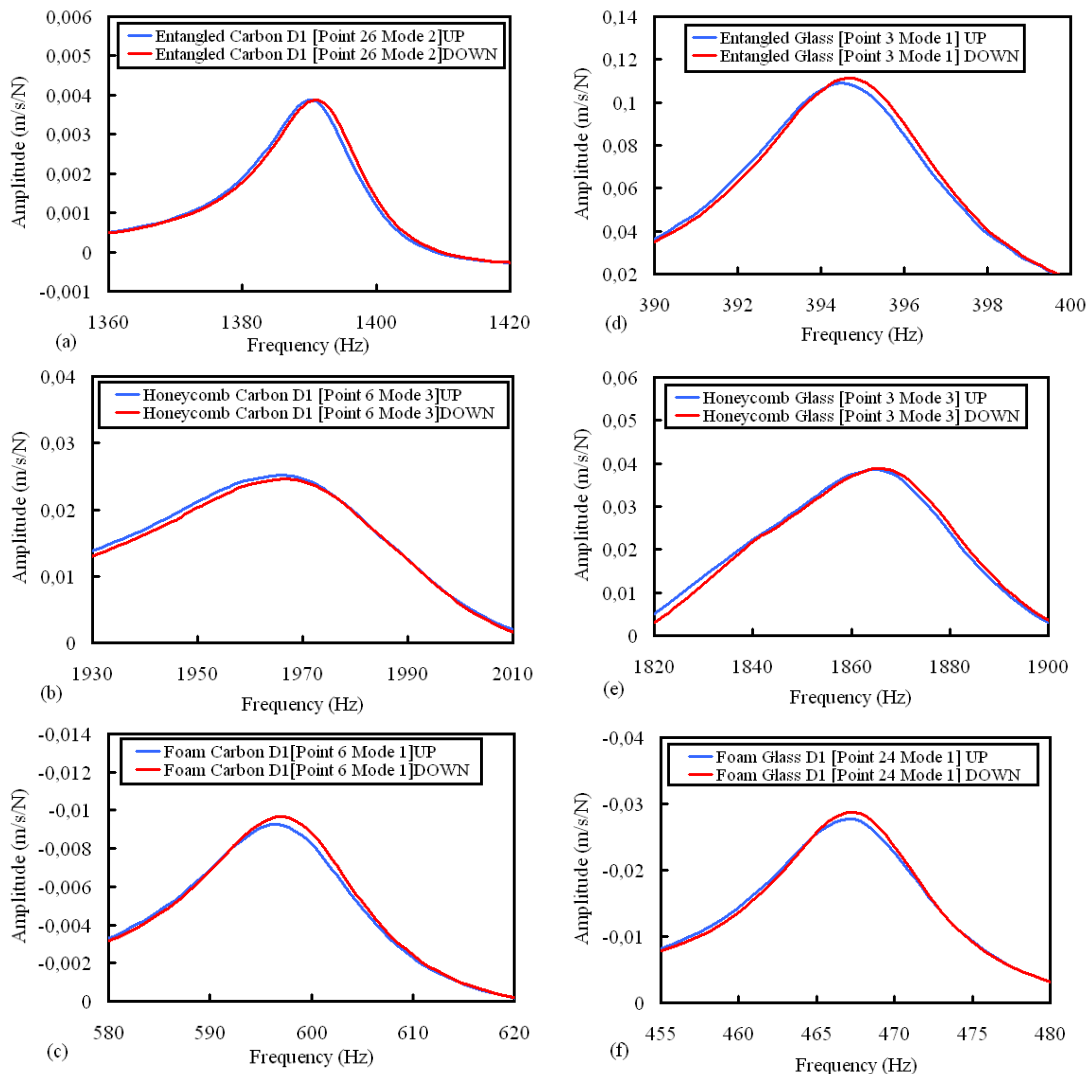


Figure 5.25 Frequency response functions (FRF) from sine-dwell sweeps upwards and downwards in frequency for the damaged case (D1) for (a) entangled carbon (b) honeycomb carbon (c) foam carbon (d) entangled glass (e) honeycomb glass (f) foam glass beams

As the level of damage in the six sandwich beams is relatively small as they have been impacted below the BVID limit, therefore these beams impacted at two points do not possess large structural non-linearities, as in case of long sandwich honeycomb beams damaged at four points (Fig 4.20). Fig 5.25 shows that in the presence of small non-linearities, there is a small change in amplitude coupled with a slight shift in frequencies.

5.2.7 Design of Experiments

Design of experiments (DOE) is carried out on the modal parameters (natural frequency and damping ratio) of the six small sandwich beams tested by both burst random and sine-dwell testing. Similar statistics based studies were carried out previously on long honeycomb sandwich beams (Section 4.2.8) and composite laminate beams (Sections 3.3.5 and 3.4.2). The aim as previously is to find out that which testing method gives a relatively better estimation of damping in the presence of damage. The design of experiments shall also identify the factors which have the most significant effect on these experimentally obtained modal parameters.

The three factors chosen for the design of experiments are the density of damage (DD), type of core materials (CM) and type of skin materials (SM). These design factors along with their respective levels are given in Table 5.19. The experimentally acquired natural frequencies and damping ratios are used as responses in the design of experiments that shall be carried out separately for the burst random and sine-dwell testing in order to compare their effectiveness for modal parameter estimation.

Table 5.19 Design parameters for the design of experiments and levels for each factor

Design Factors	Levels for each Factor		
Density of Damage (DD)	0 (Undamaged)	2 (Damage at 2 points)	
Type of Core Material (CM)	Entangled	Honeycomb	Foam
Type of Skin Material (SM)	Carbon	Glass	

By keeping in view the levels of the three factors, a full factorial design is chosen. The linear regression model associated with the full factorial design, based on the three variables discussed above is expressed as follows as in previous sections:

$$Y = a_0 + a_1.(DD) + a_2.(CM) + a_3.(SM) + E \quad (5.15)$$

In Equation 5.15, coefficients represent model constants (a_i) that are the contribution of independent variables on the response. E is the random error term representing the effects of uncontrolled variables, i.e., not included in the model. The second order interaction terms of the design factors are not taken into account in this study. The model constants (a_i) are determined by multi-linear regression analysis and are assumed to be normally distributed. The error is assumed to be random and normally distributed. These constants (a_i) are obtained with 90% confidence level. The significance of each variable on a given response (modal parameters in our case) is investigated using t test values based on Student's distribution. The t ratio is the ratio of the parameter estimate (constants) to its standard deviation. A t ratio greater than 2 in absolute value is a common rule of thumb for judging significance of the variable. The derived constants (a_i) and t ratios for the natural frequencies estimated by burst random and sine-dwell testing are presented separately in Tables 5.20 and 5.21. Negative values of the model constants and t ratios indicate that the response decreases with the

increase in the value of the parameter. In our case, this is most of the times true for the natural frequencies as they decrease with the increase in damage in the specimens.

Table 5.20 Coefficients and *t* ratios for the natural frequencies (Hz) by burst random testing

Design Factors	Mode 1		Mode 2		Mode 3	
	Constants (a_i)	<i>t</i> ratio	Constants (a_i)	<i>t</i> ratio	Constants (a_i)	<i>t</i> ratio
Density of Damage [0.2]	-40.9	-4.22	-58.2	-17.1	-136.2	-7.3
Type of Core Material [Entangled]	-23.8	-1.74	-49.3	-1.5	-79.3	3.0
Type of Core Material [Honeycomb]	-20.0	-1.46	-10.6	-2.2	-25.4	-0.9
Type of Core Material [Foam]	-3.7	-0.27	-38.7	-2.7	-53.9	-2.0
Type of Skin Material [Carbon]	-115.0	-11.8	-64.1	18.8	-225.1	-12.1
Type of Skin Material [Glass]	-115.0	-11.8	-64.1	-18.8	-225.1	-12.1

Table 5.21 Coefficients and *t* ratios for the natural frequencies (Hz) estimated by sine-dwell testing

Design Factors	Mode 1		Mode 2		Mode 3	
	Constants (a_i)	<i>t</i> ratio	Constants (a_i)	<i>t</i> ratio	Constants (a_i)	<i>t</i> ratio
Density of Damage [0.2]	-41.2	-4.2	-60.0	-12.9	-134.8	-7.6
Type of Core Material [Entangled]	-23.9	-1.7	-50.1	2.9	78.8	3.1
Type of Core Material [Honeycomb]	-21.1	-1.5	-10.6	-1.6	-22.5	-0.9
Type of Core Material [Foam]	-2.8	-0.2	-39.5	-1.2	-56.3	-2.2
Type of Skin Material [Carbon]	-114.9	-11.7	-64.9	14.0	224.6	12.7
Type of Skin Material [Glass]	-114.9	-11.7	-64.9	-14.0	-224.6	-12.7

Tables 5.20 and 5.21 indicate that the results of the design of experiments based on natural frequencies estimated by both burst random and sine-dwell testing show similar results as discussed previously in Figure 5.21. By comparing the *t* ratios of the design factors in Tables 5.20 and 5.21, it can be observed that for both burst random and sine-dwell testing the type of skin material is the factor having by far the most significant effect on the natural frequencies for the first three bending modes. The density of damage is the second most significant factor in case of natural frequencies for both burst random and sine-dwell testing. By following the same procedure, the design of experiment results based on the damping ratios estimated by both burst random and sine-dwell testing are laid out in Tables 5.22 and 5.23.

Table 5.22 Coefficients and *t* ratios for damping ratios (%) estimated by burst random testing

Design Factors	Mode 1		Mode 2		Mode 3	
	Constants (a_i)	<i>t</i> ratio	Constants (a_i)	<i>t</i> ratio	Constants (a_i)	<i>t</i> ratio
Density of Damage [0.2]	0.33	4.00	0.16	2.58	0.10	0.78
Type of Core Material [Entangled]	0.44	3.74	0.21	2.35	0.10	1.51
Type of Core Material [Honeycomb]	0.19	1.64	-0.17	-1.19	0.08	0.43
Type of Core Material [Foam]	0.25	2.10	0.06	1.32	-0.02	-0.08
Type of Skin Material [Carbon]	0.11	1.35	0.09	1.42	0.11	0.81
Type of Skin Material [Glass]	0.11	1.35	0.09	1.42	0.11	0.81

Table 5.23 Coefficients and t ratios for damping ratios (%) estimated by sine-dwell testing

Design Factors	Mode 1		Mode 2		Mode 3	
	Constants (a_i)	t ratio	Constants (a_i)	t ratio	Constants (a_i)	t ratio
Density of Damage [0.2]	0.15	9.94	0.06	1.64	0.32	7.16
Type of Core Material [Entangled]	0.27	12.53	0.19	3.93	0.28	4.45
Type of Core Material [Honeycomb]	0.10	4.59	0.13	2.61	0.05	0.85
Type of Core Material [Foam]	0.17	7.94	0.23	2.54	0.23	2.60
Type of Skin Material [Carbon]	0.04	2.76	0.07	1.90	0.25	5.51
Type of Skin Material [Glass]	0.04	2.76	0.07	1.90	0.25	5.51

As the estimation of damping ratio is different in case of the two types of testing as discussed in Section 5.2.5, therefore the design of experiment result are different as well unlike those in case of natural frequencies. By comparing the t ratios of the design factors in Tables 5.22 and 5.33, it can be seen that the density of damage (DD) is in most cases significant for the damping ratios estimated by the two types of testing, with the exception of Mode 3 in case of burst random testing and Mode 2 in case of sine-dwell testing as their t ratios are less than 2.

Furthermore, the type of skin material in case of damping ratios is only significant in case of sine-dwell testing. But the most interesting result is that in case of damping ratios unlike the natural frequencies, the type of core material becomes more significant. By comparing the t -ratios of the type of core material in Tables 5.22 and 5.23, it is clear that the entangled core material has a more significant effect on the damping ratios as compared to the honeycomb and foam cores. This fact is observed in both burst random and sine-dwell testing, which validates the vibration test results that underlined the presence of high damping in entangled sandwich materials [106,107].

Furthermore if a comparison is drawn out between the t ratios for the damping ratios estimated by burst random and sine-dwell testing in Tables 5.22 and 5.23, it can be seen that the design factors have higher t ratios in case of the damping ratios estimated by sine-dwell testing. So it can be concluded that sine-dwell testing gives relatively more reliable estimation of damping in the presence of damage as compared to burst random testing. This validates the results previously founded in Section 4.2.8 in case of long sandwich honeycomb beams.

Although the main disadvantage of sine-dwell testing is the lengthy acquisition times as compared to broadband excitations, but if quality damping estimations are required then sine-dwell excitation based vibration testing becomes indispensable. In future similar vibration tests shall be carried out with different excitation levels and asymmetric impacts in order to study their effects on modal parameters.

5.3 Conclusion of the Fifth Chapter

In this chapter static-dynamic characterization and damage monitoring has been carried out on entangled sandwich beams with carbon and glass fibers.

The first part of this chapter concerns the fabrication and mechanical testing of a new sandwich material with carbon fiber entangled core. It is seen that long entangled sandwich beams possesses **high damping characteristics** and can be used for specific applications like the inner paneling of a helicopter cabin as their structural strength is on the lower side. Monitoring of impact damage and evaluation of the impact toughness (uniquely based on

vibration test results) of these entangled sandwich materials is also carried out. Two types of long carbon fiber entangled sandwich beams (heavy and light) are tested. The light specimens have **2.5 times less resin** than the heavy ones. The impact energies are chosen in such a way that the heavy and light specimens have the same level of damage. Results show that with the accumulation of damage in the specimens, there is a decrease in natural frequency accompanied by an increase in the damping ratio. **Vibration test results prove that the light specimens having better damping characteristics are more sensitive to impact damage than the heavy ones.** Therefore, while selecting the application of these light entangled sandwich materials, their sensitivity to impact damage should be taken into consideration. In the heavy specimens, the damage seems to be more localized as compared to the light ones. It is proved again that damping is more sensitive to damage than the stiffness variations. The major drawback of this study is that no comparison is provided with standard sandwich materials.

In the second part of this chapter, shorter carbon and glass fiber entangled sandwich beams are fabricated and mechanically tested. Advantage of shorter entangled beams over longer ones is that **better distribution of fibers and resin is achieved** if the beams are shorter i.e., the current fabrication technology is more adapt to smaller size specimens. The aim as previously is to evaluate the damping capabilities and impact toughness of the entangled sandwich beams, but in addition this time a **comparison with standard honeycomb and foam sandwiches** is provided as well. Vibration tests show that entangled sandwich specimens possess on the average **150 % higher damping ratios and 20 dB lower vibratory levels** than the honeycomb and foam sandwich specimens. In order to evaluate the **impact toughness (uniquely based on vibration test results i.e., decrease in natural frequency which signifies loss of rigidity)**, a simple case of symmetrical impacts is studied and impacts are done below the BVID limit in order to detect damage by vibration testing that is hardly visible on the surface. Vibration tests have been carried out with both burst random and **sine dwell testing** in order to evaluate the damping estimation efficiency of these methods in the presence of damage. **Results prove that both carbon and glass fiber entangled sandwich beams have better impact toughness as compared to honeycomb and foam core sandwiches.** But it has to be remembered that the entangled sandwich beams are nearly two times heavier than the honeycomb and foam core beams of the same dimensions. Results again verify that **damping ratio is a more sensitive parameter** for damage detection than the natural frequency. Design of experiments (DOE) validated the experimental results by proving that sandwich beam with entangled fibers as core material have a more significant effect on the damping ratios and also proved that **sine dwell testing is more suitable for damping estimation** in the presence of damage as compared to burst random testing.

Chapter 6 : Updating and Damage Detection in Composite Beams using Finite Element Analysis

The Finite Element based updating and damage detection part of this thesis has the following two major objectives:

- Develop a Finite Element models that represent damaged composite beams in vibrations. Compare the numerical results with those obtained experimentally (Chapters 3 and 4) on the same beams. Update the damaged zone in the FE models by reducing the material properties in order to improve the experimental/numerical correlation of the frequency response functions. These simplified damage models give us a degradation factor that can serve as a warning regarding structure safety
- Develop damage localization tools in order to find the damage zone accurately in any material by using only vibration tests. The aim is to verify numerically the c-scan results carried out on the composite laminate beams. Material is removed in the precise zones of the FE model in order to minimize the error between the experimental and numerical frequency response functions (FRFs), this way an equivalent damage is modeled. Thus topology optimization is a diagnostic tool (for all types of materials) and requires only the undamaged state for localization of damages. Advantage of this tool is to give information about damage zone for materials for which C-Scan tests do not provide sufficiently accurate data e.g., composite sandwich materials.

6.1 Calculation of the Dynamic Response and Updating by Finite Element Methods

As highlighted previously, the aim of calculating the dynamic response of composite beams is not only to validate the experimental results but also to update with a simple tool the different damage states. A commercial Finite Element software Samcef is used for this purpose. Updating of the developed FE models of the composite beams is performed with the help of Boss Quattro software by carrying out a parametric study. A simple parametric study is used to update the material properties in the damaged zones.

6.1.1 Dynamic Response Calculation by Finite Elements

Basics of FEM

For simple structures, such as beams and plates, good analytical predictions using closed form solutions can be easily found in scientific literature [145]. Lumped parameter systems can also be used to model the dynamic behavior of the structure. However, for more complex structures more powerful tools are needed. Nowadays, two separate tools are used to model the dynamic behavior of the structures, namely numerical tools and experimental ones. The most widely used numerical tool is the Finite Element (FE) method, while the experimental counterparts are largely based on modal testing and analysis as discussed in detail in previous sections.

The main assumption in Finite Element Method (FEM) is that a continuous structure can be discretised by describing it as an assembly of finite (discrete) elements, each with a number of boundary points which are commonly referred to as nodes. For structural dynamic analysis, element mass, stiffness and damping matrices (proportional damping) are generated first and then assembled into global system matrices. Dynamic analysis of the produced model gives the modal properties; the natural frequencies and corresponding eigenvectors. The modal solution can subsequently be used to calculate forced vibration response levels for the structure under study. Further theoretical background and practical implementation of the FE method are given in various text books, such as those in the reference [146-148].

Modal Analysis in Samcef (Eigen value problem)

The DYNAM module in Samcef enables the classical computation of the frequencies and free vibration modes of a linear elastic structure. The available finite elements and material properties necessary for modeling such structures are described in detail in the Samcef User's Manuel [149]. The composite laminate beams presented in Chapter 3 have been modeled ply by ply in Samcef and no homogenization assumption is made. The eigen-value problem associated with this computation can be written formally as follows:

$$(K - \omega^2 M)X = 0 \quad (6.1)$$

where K represents the stiffness matrix, M the mass matrix, X is the displacement of the mass or the structure under consideration and ω^2 the circular frequency associated with this mode. The components of the vector X are the structure's degrees of freedom (DOF), usually displacements (translations and rotations).

The analyzed structures are assumed to be undamped and free from any external forces. In particular, the only permitted boundary conditions are the fixing of some degrees of freedom to zero. DOFs can however be interconnected by linear constraints. When a structure has rigid body modes or mechanisms, these are detected and can be displayed by post-processing. By considering a non-trivial solution of Equation 6.1, the resulting characteristic equation is given by:

$$\det(K - \lambda M) = 0 \quad (6.2)$$

The solutions of this equation are the n-eigen values for a system of n degrees of freedom, where each eigen-value λ_i corresponds to a natural angular frequency ω_i as shown in Equation in (6.3),

$$\lambda_i = \omega_i^2 \quad \text{with } i = 1, 2, \dots, n \quad (6.3)$$

The amplitude vector corresponding to an eigen-value is the eigen-vector or the modeshape vector ψ_i .

The algorithm used in DYNAM for solving eigen-value problems is the Lanczos Method which is based on an iterative scheme of the Equation 6.1 as follows.

$$Kq_{p+1} = Mq_p \quad (6.4)$$

The iterative process is initialized using trial vector q_0 whose components are randomly generated. Each iteration consists of solving a set of linear equations. With this in mind, the K matrix is triangularized before starting the iteration process. Triangularization is done by means of the frontal method. Further details on the Lanczos algorithm is presented in reference [149].

Frequency Response Analysis (Harmonic Analysis) in Samcef

The REPDYN module in Samcef calculates the dynamic response of linear elastic structures. It performs both time and frequency responses, taking into account the dissipating effects, in order to calculate the dynamic response of a system damping is essential and cannot be neglected. Whereas for the eigen-value calculation only, damping values are not required. The following solution techniques are available in Repdyn.

- Calculation by direct integration of a transient mechanical response
- Calculation by modal superposition of a transient mechanical response
- Calculation by modal superposition of a forced harmonic response (without calculation of residuals or reactions)
- **Calculation by modal superposition of a forced harmonic response (with calculation of residuals or reactions)**
- Direct calculation of a forced harmonic response

Choice of Solver

In this thesis, solution technique based on modal superposition approach using normal modes calculated previously by DYNAM module is implemented. The technique of modal superimposition is the most economical and gives excellent results if a few first eigen-modes are used to express the response. This method is coherent with linearity for non-dissipative terms of the structure i.e., stiffness [K] and mass [M].

Finally, it should be noted that each time a method of modal superposition is used, the truncation of the set of eigen-modes introduces an error in the spatial representation of the load which can be compensated for. This correction is systematically introduced in the REPDYN module which guarantees a statically accurate solution.

Choice of Excitation

Different types of loadings can be applied to the model in REPDYN i.e., point forces, distributed loads and ground motion. Differential accelerations may be imposed as well. The frequency response calculations in this thesis are performed by using a harmonic force. The amplitude of excitation is kept constant with the excitation frequency. By exciting this way a model, the response calculated at a point is directly the frequency response function of that point. The choice of the methodology is as such that the response is examined mode by mode. The aim is to compare the numerical (FEM) and the experimental FRFs.

Choice of Damping (Dissipation Mechanism)

Damping can be defined in a model by different ways in REPDYN. In our case, modal damping attached to each eigen-mode is used i.e., truncation is carried out locally for each mode. The experimentally obtained values of damping ratios associated with each type of

beam are used in the respective FE models. But as the damping values are relatively low so they do not affect the FRF amplitudes a lot. By giving an average damping value for all modes in the frequency spectrum gives relatively similar results to those obtained by giving a separate value for each mode.

Steps of Frequency Response Analysis

The main steps of frequency response analysis performed in a FE software are as follows:

The cornerstone of modal frequency analysis is the diagonalization of the system's matrices by modal transformation. In a separation approach, the primary variables are replaced by a linear combination of the modal coordinates and the mode shape vectors as shown in Equation 6.5, where Ψ is the modal matrix and q is the vector of modal coordinates.

$$x(t) = \psi_1 q_1(t) + \psi_2 q_2(t) + \dots + \psi_n q_n(t) = \Psi q(t) \quad (6.5)$$

Due to the orthogonality properties of the mode shape vectors, inserting Equation 6.5 into the characteristic dynamic equation and pre-multiplying by Ψ^T leads to Equation 6.6 which is the decoupled equation of motion of the analyzed system.

$$\Psi^T M \Psi \ddot{q}(t) + \Psi^T C \Psi \dot{q}(t) + \Psi^T K \Psi q(t) = \Psi^T f(t) \quad (6.6)$$

The system now consists of n equations of motion for single degree of freedom (SDOF) oscillators in form of Equation 6.7, where m_i is the modal mass, c_i a modal damping coefficient, k_i the modal stiffness and p_i a modal force.

$$m_i \Psi \ddot{q}_i(t) + c_i \Psi \dot{q}_i(t) + k_i q_i(t) = F_i(t) \text{ with } F_i(t) = \psi_i^T f \quad (6.7)$$

The equation can be normalized by the modal mass, so that the coefficients are expressed in terms of natural angular frequencies as shown in Equation 6.8 which then leads to Equation 6.9.

$$\omega_i^2 = \frac{k_i}{m_i} \text{ and } \zeta_i = \frac{1}{2} \frac{c_i}{\sqrt{k_i m_i}} \quad (6.8)$$

$$\ddot{q}_i(t) + 2\zeta_i \omega_i \dot{q}_i(t) + \omega_i^2 q_i(t) = \frac{F_i(t)}{m_i} \quad (6.9)$$

Equation 6.9 is an ordinary differential equation of second order that has the solution stated in Equation 6.10 that can be achieved by a complex approach, where Ω is the excitation frequency.

$$Q_i(\Omega) = \frac{1}{\omega_i^2 - \Omega^2 + 2j\zeta_i \omega_i \Omega} \cdot \frac{F_i}{m_i} \quad (6.10)$$

From Equation 6.10, the matrix of frequency response function (FRF) can be easily derived, since the frequency response functions are defined as the displacement response functions multiplied by the inverse of the excitation force vector as shown in Equation 6.11.

$$H(\Omega) = \hat{u}(\Omega) \hat{f}^{-1}(\Omega) = \sum_{i=1}^n \psi_i \hat{q}_i(\Omega) \hat{f}^{-1}(\Omega) = \sum_{i=1}^n \psi_i \frac{1}{\omega_i^2 - \Omega^2 + 2j\zeta_i \omega_i \Omega} \cdot \frac{\psi_i^T}{m_i} \quad (6.11)$$

The modal separation is based again on the partial linearity i.e., by the modal representation of the conservative terms $[M]$ and $[K]$ and the equivalent representation of dissipation by $[C]$, damping ratio (ζ) equivalent including eventual non-linearity in damping.

6.1.2 Updating of the FE models for Experimental/Numerical Correlation

Basics of Updating

One of the applications of the results of an experimental vibration test is the updating of an analytical model (FE model in our case). Model updating can be defined as adjustment (fit) of an existing FE model which represents the structure under study, using experimental data, so that it more accurately reflects the dynamic behavior of that structure. Model updating can be divided into three steps:

- comparison and correlation of two sets of data
- locating the errors
- correcting the errors

Correlation can be defined as the initial step to assess the quality of the FE model. If the difference between the FE model and experimental data is within some preset tolerances, the analytical model can be judged to be accurate and no updating is necessary. A good overview of updating of FE models in structural dynamics has been provided by Friswell and Mottershead in reference [152].

Most difficulties are encountered in the second step. The difficulties in locating the errors are mostly due to measurement process and can be summarized as:

- insufficient experimental modes
- insufficient experimental coordinates
- size and mesh incompatibility of the experimental and FE models
- experimental random and systematic errors
- absence of damping in the FE model

In spite of extensive research over the last two decades, model updating is still far from mature and no reliable and general applicable procedures have been formulated so far. As discussed before, the updating of the FE models by parametric studies developed in Samcef shall be carried out in Boss Quattro. The theoretical aspects of the methodology used can be found in the reference [150].

Modeling of Damage in FE Models of Composite Beams

The FEM modeling method of damaged structures used in this thesis is very commonly practiced and is found repeatedly in scientific literature as explained previously in Section 1.3.4. In many currently used commercial softwares for structural dynamic analysis, if a structure with small damage is directly meshed for establishing structural dynamics model, the following two problems are generally encountered:

- Excessive gridding number and extra large difference of gridding size (between damaged and undamaged zones) is time consuming for subsequent simulation calculations
- Difficulties for expressing different structural damage size in the same structure using direct meshing i.e., the errors due to different meshing may be greater than variations of structural dynamic characteristics caused by small structural damage.

As discussed previously several times in this thesis that local damage in a structure always causes reduction of local structural stiffness, so that these variations can be denoted by reduced material coefficients at the local damaged zone. Therefore in order to avoid the above mentioned problems due to direct meshing, dynamics model of a damaged structure can be established using the modified material elastic coefficients in local damage position of the structure. This way it may not be necessary to depict the geometry of small damage. This improved modeling method also described by Yan et al [65] has two steps

- Directly meshing structure and ignoring existence of structural damage
- Element stiffness matrices for those elements in the position of structural damage are adjusted to simulate damaged structure scenario

An example of the two ways of meshing is presented by Yan et al. [65] on a laminated composite vessel and shown in Fig 6.1.

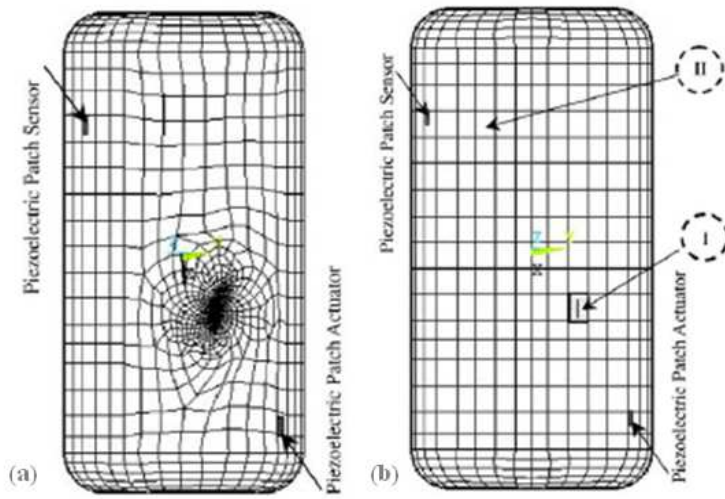


Figure 6.1 Model of a laminated composite vessel (a) Direct meshing of the crack damage (b) Reducing stiffness of elements in the position of damage [65]

The same procedure shall be followed to model the impact damage in case of the test-beams presented in Chapter 3 and Chapter 4. Instead of modeling directly the impact damage by direct meshing, the material properties in the impacted zone shall be reduced to find the modal parameters corresponding to the damaged cases. The impacted zones shall be approximated to a circle having an area that corresponds to the damage area found by C-scan testing.

A complete finite element model of the shell composite laminate beam with 3D end-masses and a 3D base block is shown in Fig 6.2 a. The circular damage zones approximated from the C-Scan results are also shown along with a close up of the mesh around the circular damage zone in Fig 6.2 c. Triangular elements have been avoided to minimize the risk of computation error due to twisting distortion, therefore only quadrangular elements are used for higher precision.

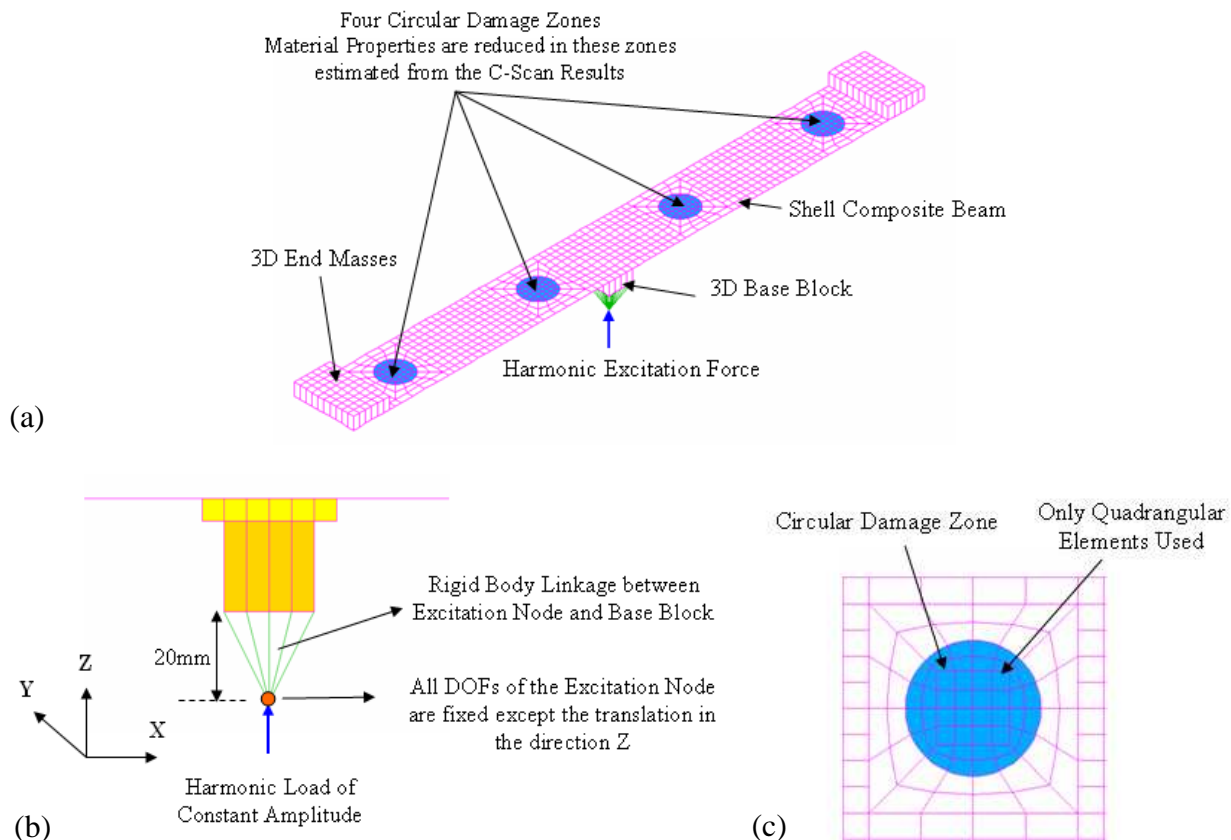


Figure 6.2 Modeling methodology of damage in Samcef (a) Composite laminate beam model with end masses and base block showing the damaged zones and the excitation (b) Application of harmonic load at the excitation node situated 20 mm beneath the center of the base block (c) Close-up of the mesh around the position of damage where the material properties shall be reduced to simulate the damaged case

For the elements in the damage zone (shown in blue in Fig 6.2a and 6.2c), their element stiffness matrixes (material properties) are adjusted to simulate damage in the following way:

$$K_0^e = \alpha \cdot K_d^e \text{ where } \alpha > 1 \quad (6.12)$$

where K_d^e is the stiffness matrix or material properties of elements in the impacted zone (shown in blue in Fig 6.2a and 6.2c) with some damage, K_0^e is the one for elements without damage and α is a damage modification coefficient. This way by reducing the material properties by the coefficient α in the impacted zones (based on c-scan results), damage can be simulated in structures relatively easily without facing the problems of excessive gridding number due to direct meshing. The change in mass due to damage is negligible; therefore it has not been taken into account.

As discussed previously, in order to calculate the dynamic response, the composite laminate beam models are excited by a harmonic force of constant amplitude. This excitation force is applied to a node situated 20mm below the center of the base block and is rigidly linked to the bottom nodes of the base block as shown in Fig 6.2 b. For the excitation node, all the degrees of freedom (DOFs) are fixed except the translation in Z direction, which signifies the direction of force generated by the shaker.

Procedure for Estimating the Damaged Area (Impacted Zone)

The circular shapes of the impact zones are estimated based on the results of the ultrasound (C-Scan) and radiographic results. The software which manipulates the ultrasound (C-scan) tests has the capability of estimating the damaged surface. The results of the ultrasound (C-Scan) and radiographic tests for the composite laminate Beam 4 impacted by clamping two ends for half beam length are shown in Fig 6.3. The calculated damaged area (conventional controlled area) is also indicated for each impact point.

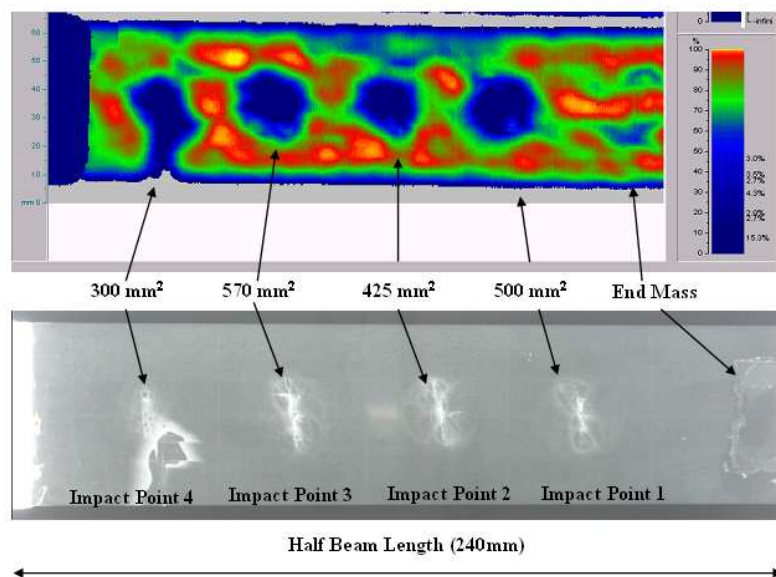


Figure 6.3 Calculation of the damaged surface for the composite laminate Beam 4 impacted by clamping two ends for half beam length at 7 J (a) Ultrasound (C-Scan) results (b) Radiographic results

As seen in Fig 6.3, that the calculated damaged area does not show a large dispersion between the four impacted points as they are impacted with the same energy. For all the test-beams, the ultrasound and radiographic tests have been carried out for half length of the test beams. As all the test-beams have been impacted with a same energy level, so it is assumed that the impact points for the other half of the test-beams have the same damaged surface. The procedure of estimating a circular shape zone from the ultrasound and radiographic test results is as follows:

- In the first step, average value of the damaged area is calculated by taking the mean of the damaged area for the four impact points shown in Fig 6.3.

$$\text{Average Damaged Area for Beam 10} = \frac{\text{Mean}}{4} = 595\text{mm}^2 \quad (6.13)$$

- Next this average damaged area is equated to the area of a circle as follows

$$595\text{mm}^2 = \pi(\text{radius})^2 \quad \text{where } \text{radius} \cong 14\text{mm} \quad (6.14)$$

- The circular shape impact zones are thus modeled representing the averaged impacted zones of the ultrasound results as shown in Fig 6.2 a.

Updating Procedure for a better Experimental/Numerical Correlation

An overview of the updating procedure is shown in the Flow Chart below by taking into account the damage modification coefficient α to simulate the damaged cases:

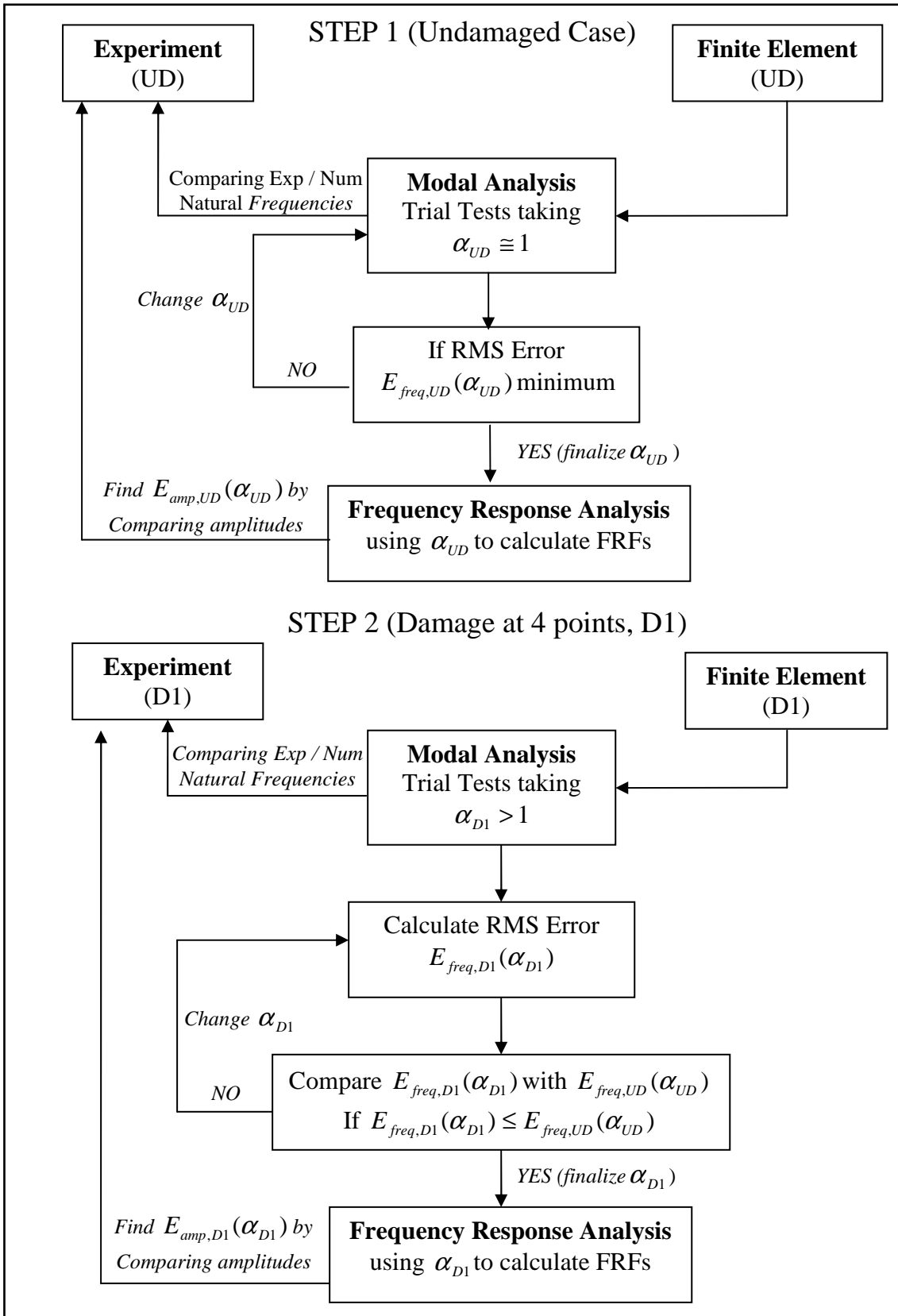


Figure 6.4 Flow chart of the experimental / numerical updating procedure

The aim of carrying out Finite Element modeling of the composite laminates and sandwich test-beams is to compare the modal parameters found experimentally (previously in Chapters 3 and 4) and numerically (FEM). When establishing a FE model for a damaged test-beam,

different values of coefficient α_{UD} are tried (by parametric study in Boss Quattro) until the smallest statistical (root mean square RMS) error is reached between the experimental and numerical results for the natural frequencies. The statistical error is defined in Equations 6.15 as follows:

$$E_{freq,UD}(\alpha_{UD}) = \sqrt{\frac{1}{N} \sum_{i=1}^N [f_{FEM,UD}^k(\alpha_{UD}) - f_{EXP,UD}^k]^2} \quad (6.15)$$

where $E_{freq,UD}(\alpha_{UD})$ is the statistical error (RMS) between the experimental based $f_{EXP,UD}^k$ and finite element based $f_{FEM,UD}^k$ natural frequencies for the undamaged case (UD) for the k_{th} mode and N is the total number of modes considered. $E_{freq,UD}(\alpha_{UD})$ has the units of Hz.

In our case, the first four bending modes are studied. A comparison between the experimentally obtained mode shapes of composite laminate beams estimated by the Polymax system and those obtained by FEM in Samcef are shown in Annex Fig 5.A. The corresponding mode shapes have the same shape which is very important to verify, to be sure that the similar things are compared. Usually the MAC (Modal Assurance Criterion) indicator tool is used to correlate the experimental / numerical mode shapes.

By using the same Equation 6.15 statistical error can be calculated between the natural frequencies for the damaged cases as well. In order to have a better experimental/numerical correlation, the following updating procedure shall be used:

- First of all FE models are built for the test-specimens for the undamaged case by considering $\alpha_{UD} \approx 1$ in Equation 6.12. For some test-beams, even at the undamaged case the modification coefficient α is not perfectly equal to 1 certainly due to aging of material i.e., $\alpha = 1.16$ for those composite beams where the material was expired which signifies a loss of rigidity (EI) of approximately 15 %.
- For the undamaged case, different values of α_{UD} close to 1 are tried and for each iteration result the statistical error $E_{freq,UD}(\alpha_{UD})$ is calculated.
- When the statistical error $E_{freq,UD}(\alpha_{UD})$ reaches a minimum value, the corresponding α_{UD} value can be taken as the required coefficient α_{UD} for simulating the undamaged case (UD).
- Once the modification coefficient α_{UD} is finalized by using the DYNAM module, the frequency response analysis is calculated by the REPDYN module by using the corresponding experimentally obtained damping ratios.
- The amplitudes of the experimentally and numerically (FE) obtained FRFs are compared and the statistical error (RMS) $E_{amp,UD}(\alpha_{UD})$ having dB as units between the amplitudes at the undamaged state is calculated as follows in the same way as Equation 6.13:

$$E_{amp,UD}(\alpha_{UD}) = \sqrt{\frac{1}{N} \sum_{i=1}^N [Amp_{FEM,UD}^k(\alpha_{UD}) - Amp_{EXP,UD}^k]^2} \quad (6.16)$$

- Once the undamaged state FE model is finalized, the same procedure is repeated again for the damaged case.
- Parametric studies are carried out to find the modification coefficient α_{D1} for the damaged state by comparing the natural frequencies between the FE model and the experimental ones.
- The statistical error $E_{freq,D1}(\alpha_{D1})$ for the damaged case (D1) is calculated for each iteration and compared with that of the undamaged case $E_{freq,UD}(\alpha_{UD})$.
- The aim is to find $E_{freq,D1}(\alpha_{D1})$ as close as possible to $E_{freq,UD}(\alpha_{UD})$.
- By finalizing the modification coefficient α for the damaged state, the FRFs are calculated and their amplitudes compared with the experimental FRFs for the damaged case by using experimentally obtained damping ratio values.
- The statistical error $E_{amp,D1}(\alpha_{D1})$ is calculated for the first four bending modes ($k=1,2,3,4$) and compared with $E_{amp,UD}(\alpha_{UD})$.
- If there is a further damage state (D2), the same value of the modification coefficient is used i.e., $\alpha_{D1} = \alpha_{D2}$. The difference is that the modification coefficient is applied to more impact zones.

6.1.3 Updating Procedure on Composite Laminate Beams Impacted by Clamping Two Ends

In this section, the modal response of the composite beams impacted by clamping two ends presented in Table 3.6 in Chapter 3, is modeled by Finite Elements by following the procedure explained in the preceding sections. Only 3.12 mm thick composite laminate beams shall be modeled by FE. The three parts of the composite laminate beams are modeled as follows:

- Composite beam is modeled (ply by ply) by using quadrangular Mindlin shell elements
- Steel End masses and aluminum base block (for fixing the beam on the shaker) are modeled with 3D brick elements

Trial FE tests have also been carried out by modeling the composite beam in 3D. No significant difference in result is observed by modeling the composite beam by shell or 3D elements. The main advantage of using Mindlin shell elements for the composite part is to reduce the calculation time.

Furthermore, Beams 2 and 3 (Table 3.6) impacted at 3 J and 4 J respectively cannot be modeled because due to very small damage, no conclusive image of the damaged area was obtained through the ultrasound tests (C-Scan) as shown in Annex Fig 5.B.

So for the lot of composite laminate beams impacted by clamping two ends, four test beams (Beams 4-7) having relatively larger damaged areas shall be modeled and updated with the experimental results. Average damaged area and the radius of the approximated circular zone depicting the damaged area based on the procedure explained previously, for the four composite laminate beams (Beams 4-7) is given in Table 6.1.

Table 6.1 FE parameters for the composite laminate beams impacted by clamping two ends; showing two groups of damage

Beam No	Impact Energy J	Average Damaged Area mm ²	Radius of the circular damage zone mm
4	7	448.8	11.95 ≈ 12 mm
5	8	475.0	12.30 ≈ 12 mm
6	9	631.3	14.18 ≈ 14 mm
7	10	595.0	13.76 ≈ 14 mm

From Table 6.1, it can be seen that there is a very small difference in the average damaged area between the beams 4 and 5 (7 J and 8 J) and beams 6 and 7 (9 J and 10 J). It can be said that the damage definition is coherent with the energy of impact. Furthermore, the radii of the approximated circular damage zones have been rounded off to facilitate the modeling and meshing processes.

The composite material (T300/914) used for fabricating the four composite beams shown in Table 6.1 was expired by a couple of years. This had a considerable effect on the material properties which were found to be reduced by approximately 15 %.

In order to model a composite laminate beam in a FE software the following three material properties are required:

- Longitudinal Elastic Modulus (E_L)
- Transverse Elastic Modulus (E_T)
- Shear Modulus (G)

By carrying out several trial tests by varying individually the above three material properties, it was found that the Longitudinal Elastic Modulus (E_L) is by far the material property which has the most profound effects on the natural frequencies. These trial tests are performed in the parametric module of Boss Quattro by using Samcef's DYNAM module.

Based on the trial test results, it was decided that in order to keep the damage modeling methodology simple, only the Longitudinal Elastic Modulus (E_L) shall be varied in case of the composite laminate beams. Trial tests also proved that the variations of Transverse Elastic Modulus (E_T) and the Shear modulus (G) have a very small effect on the natural frequencies.

Just to remind the readers that the composite laminate beams have three states, undamaged state (UD), damage at four impact points (D1) and damage at eight impact points (D2). The FE modeling at updating results shall be discussed separately for each case.

Modeling of the dynamic response and the updating procedure for Beam 4 is discussed below in detail, whereas similar results for the other beams can be found in the Annex.

Beam 4 (7 J)

The ultrasound and radiographic test results for Beam 4 impacted at 7 J are shown previously in Fig 6.3. The damage zones shown in Fig 6.3 for Beam 4 are modeled by approximating the shape of the real damaged surface to a circle of 12 mm radius as explained previously. For the elements in the damage zone (shown in blue in Fig 6.2 a and c), their element stiffness matrices (Longitudinal Elastic Modulus E_L) are adjusted to simulate damage.

Undamaged Case (UD) - Reference or Base Line Case

As discussed previously, the material properties of the composite beams in Table 6.1 are degraded a bit due to aging. This aging effect has to be taken into account in order to simulate properly the experimental results. Therefore in case of Beam 4 for undamaged case (UD), a E_L value of 1.24 E11 Pa instead of the original E_L value of 1.44 E11 Pa gives the minimum statistical error $E_{freq,UD}(\alpha_{UD})$ between the experimental and numerical (FE) natural frequencies based on Equation 6.15. Hence, the corresponding modification coefficient α_{UD} for the undamaged case corresponding to a minimum value of $E_{freq,UD}(\alpha_{UD})$ is calculated as follows:

$$\alpha_{UD} = \frac{E_L(\text{Original})}{E_L(\text{Aged})} = \frac{1.44E11}{1.24E11} = 1.16 \quad (6.17)$$

A comparison of the experimental and numerical (FE) natural frequencies for beam 4 for the undamaged state along with the statistical error $E_{freq,UD}(\alpha_{UD})$ and the modification coefficient α_{UD} is given in Table 6.2

Table 6.2 Comparison of experimental and numerical natural frequencies for Beam 4 impacted by clamping two ends for the undamaged state (UD) along with the statistical error and the modification coefficient

Natural Frequencies (Hz)			
Bending Modes No	Experimental (Hz)	Numerical (FE) (Hz)	Difference (%)
1	36.2	37.4	3.3
2	279.1	288.0	3.2
3	717.5	723.8	0.9
4	1408.4	1397.1	0.8
α_{UD}		1.16	
$E_{freq,UD}(\alpha_{UD})$		7.87 Hz	

In the next step, frequency response (harmonic) analysis is carried out by using the value of α_{UD} given by Equation 6.17 and using the experimental damping ratios values for each mode. A comparison of the experimental and numerical (FE) FRF amplitudes for the first four bending modes for Beam 4 for the undamaged state along with the statistical error

$E_{amp,UD}(\alpha_{UD})$ and the modification coefficient α_{UD} is given in Table 6.3. Furthermore a comparison of the experimental and numerical (FE) FRFs for Beam 4 for the measurement point 2 is shown in Fig 6.5.

Table 6.3 Comparison of experimental and numerical FRF amplitudes for Beam 4 impacted by clamping two ends for the undamaged state (UD) along with the statistical error and the modification coefficient

FRF Amplitudes (dB)			
Bending Modes No	Experimental (dB)	Numerical (FE) (dB)	Difference (%)
1	-61.5	-54.4	11.5
2	-75.4	-78.7	4.4
3	-106.5	-103.6	2.7
4	-102.5	-100.7	1.8
	α_{UD}	1.16	
	$E_{amp,UD}(\alpha_{UD})$	4.28 dB	

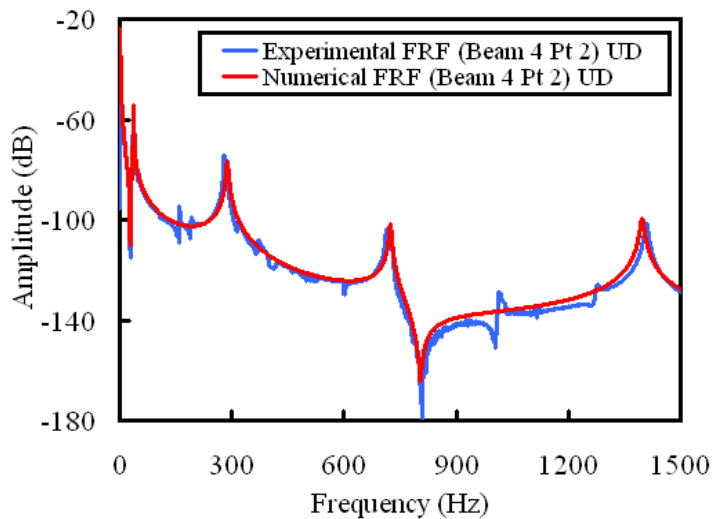


Figure 6.5 Comparison of experimental and numerical FRFs for Beam 4 impacted by clamping two ends for the undamaged case (UD) for the measurement point 2

Damage Case (D1)

The aim is to reduce the E_L in order to match the experimental frequencies of Beam 4 corresponding to the damage case (D1). This means calculating α_{D1} that corresponds to the minimum statistic error $E_{freq,D1}(\alpha_{D1})$ which should be as close as possible to $E_{freq,UD}(\alpha_{UD})$. The modification coefficient α_{D1} is then used for the frequency response analysis and the minimum statistic error for the FRF amplitudes $E_{amp,D1}(\alpha_{D1})$ is calculated. A comparison of the experimental and numerical natural frequencies and FRF amplitudes for the damage state D1 for the first four bending modes along with the modification coefficients and statistical errors are listed in Table 6.4.

Table 6.4 Comparison of experimental and numerical natural frequencies and FRF amplitudes for Beam 4 impacted by clamping two ends for the damaged state (D1) along with the statistical error and the modification coefficient

Bending Modes No	Natural Frequencies (Hz)			FRF Amplitudes (dB)		
	Experimental (Hz)	Numerical (FE) (Hz)	Diff (%)	Experimental (dB)	Numerical (FE) (dB)	Diff (%)
1	34.9	34.6	0.9	-44.8	-46.1	2.9
2	278.7	277.3	0.5	-72.8	-81.7	12.2
3	683.2	680	0.5	-84.9	-84.8	0.1
4	1337.7	1322.9	1.1	-99.8	-97.6	2.2
α_{D1}		5.96		α_{D1}	5.96	
$E_{freq,D1}(\alpha_{D1})$		7.61 Hz		$E_{amp,D1}(\alpha_{D1})$	4.63 dB	

Table 6.4 shows a good correlation between the experimental and numerical (FE) natural frequencies. The statistical error $E_{freq,D1}(\alpha_{D1})$ is slightly lesser than that for the undamaged case (Table 6.2). A comparison of the experimental and numerical (FE) FRFs for Beam 4 for the measurement point 30 for the state D1 is shown in Fig 6.6 which also shows a good correlation of the amplitudes.

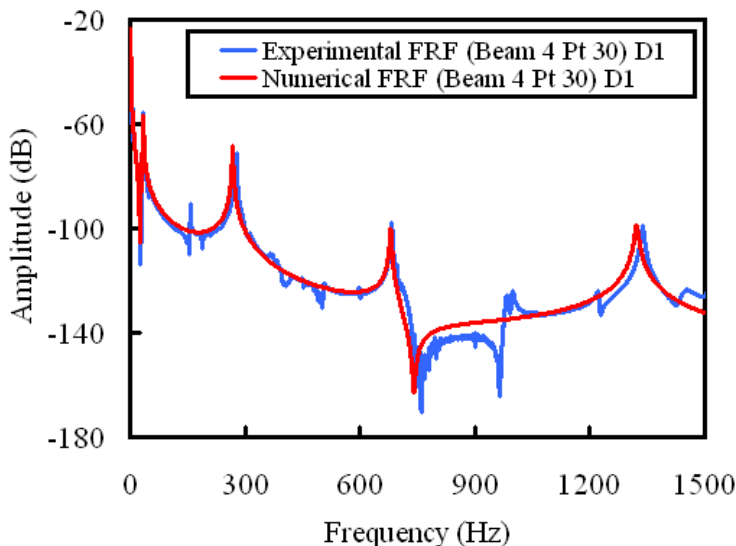


Figure 6.6 Comparison of experimental and numerical FRFs for Beam 4 impacted by clamping two ends for the damaged case (D1) for the measurement point 30

Damage Case (D2)

In case of damage state D2 with eight impact points, the same value of modification coefficient α_{D1} is used as the impact energy is the same for all the impact points i.e., density of damage remains the same. However the values of statistical errors are different as compared to the damage state D1 because the natural frequency and FRF amplitudes have different values. The experimental and numerical comparison is shown in Table 6.5 along with the FRF comparison at measurement point 18 in Fig 6.7.

Table 6.5 Comparison of experimental and numerical natural frequencies and FRF amplitudes for Beam 4 impacted by clamping two ends for the damaged state (D2) along with the statistical error and the modification coefficient

Bending Modes No	Natural Frequencies (Hz)			FRF Amplitudes (dB)		
	Experimental (Hz)	Numerical (FE) (Hz)	Diff (%)	Experimental (dB)	Numerical (FE) (dB)	Diff (%)
1	34.7	34.3	1.2	-61.2	-56.6	7.5
2	275	286.3	4.1	-79.8	-77	3.5
3	660.5	668.7	1.2	-103.5	-96.3	7.0
4	1300	1294.1	0.5	-103.2	-100.9	2.2
	$\alpha_{D2} = \alpha_{D1}$	5.96		α_{D1}	5.96	
	$E_{freq,D2}(\alpha_{D2})$	7.58 Hz		$E_{amp,D1}(\alpha_{D1})$	4.69 dB	

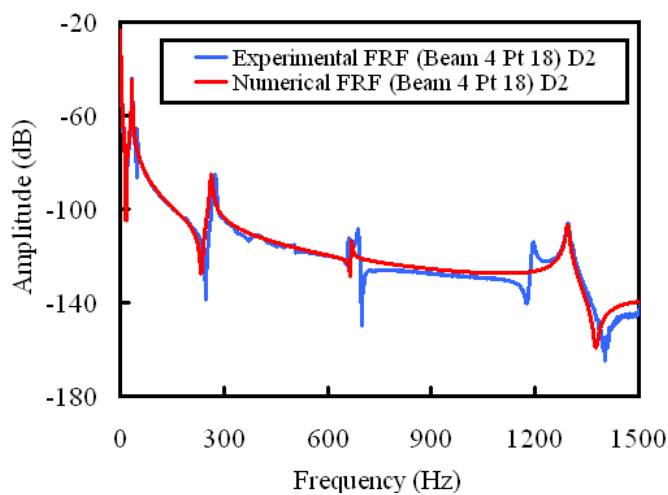


Figure 6.7 Comparison of experimental and numerical FRFs for Beam 4 impacted by clamping two ends for the damaged case (D2) for the measurement point 18

As the level of damage increases in the composite laminate beams i.e., damage state D2, signs of asymmetric behavior appear in the modal results. Even though, theoretically damage is same, effect of masses is same both ends of the beam etc. But the experimental curve in Fig 6.7 shows a double peak at the fourth bending mode around 1300 Hz which is due to the asymmetric nature of the damage. Numerically through finite element modeling, it is very difficult to simulate this phenomenon as everything is perfectly symmetric unlike in reality.

Due to shortage of space and for the sake of clarity, the comparison of FRFs is shown for one measurement point only. The comparison of the FRF amplitudes between the experimental and the FE results in case of all beams is done for one measurement point. The author compared the results for a few other measurement points and the difference in amplitudes remains pretty much the same. However the difference in the FRF amplitudes between the different measurement points is more than the difference in natural frequencies for each measurement point. As frequency is the global property of the structure so it remains the same at each point of the beam, but the amplitudes of the FRF are different, and depend on the position of the measurement point. But the difference between the amplitudes of the experimental and numerical FRFs remains nearly the same for all the 33 measurement points.

The FE modeling of the dynamic response and the updating procedure for the three remaining beams (Beams 5, 6 and 7) is provided in the Annex of Chapter 6.

6.1.4 Evaluation of the Degradation Factor with Impact Energy in Composite Laminate Beams Impacted by Clamping Two Ends

FE modeling of the dynamic response and updating of the four composite laminate beams (Beams 4-7) impacted by clamping two ends has been carried out in the previous sections. The main idea behind modeling the damage was to reduce the longitudinal elastic modulus E_L in the damaged zones by a modification coefficient α .

In order to have a better idea about the level of damage induced by impacting at different energies, it will be interesting to plot the variation of the modification coefficient α with the impact energies. However, the modification coefficient α cannot be plotted directly with the impact energies because it does not take into account the damaged area, and also all the beams do not have the same damaged area. To remedy this, a degradation factor is introduced which is a multiple of the modification coefficient α with the radius of the circular damage zone (R). This idea is further explained in Table 6.6.

Table 6.6 Calculation of the degradation factor for the composite laminate beams (Beams 4-7) impacted by clamping two ends

Beam. No	Impact Energy (J)	Radius (R) of the circular damage zone (mm)	Modification Coefficient $\alpha_{D1} = \alpha_{D2}$	Degradation Coefficient (mm) $\alpha_{D1} \cdot R$
4	7	12	5.96	71.5
5	8	12	6.56	78.7
6	9	14	6.63	92.8
7	10	14	7.05	98.7

The variation of the degradation coefficient $\alpha_{D1} \cdot R$ with the impact energy levels for the four composite beams (Table 6.6) impacted by clamping two ends is plotted in Fig 6.8.

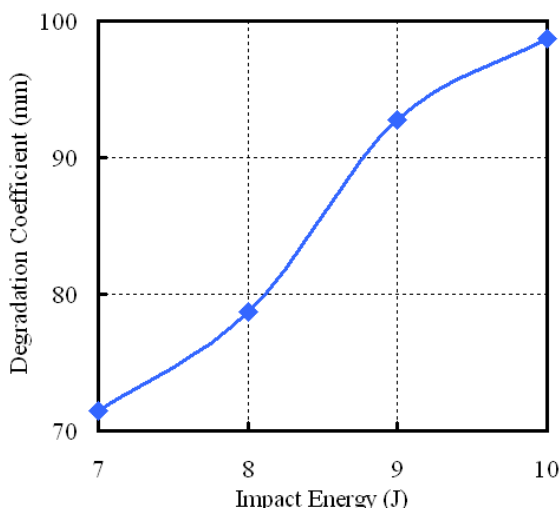


Figure 6.8 Variation of degradation factor ($\alpha_{D1} \cdot R$) with impact energy for the composite laminate beams (Beams 4-7) impacted by clamping two ends

Fig 6.8 shows a steady increase in the degradation coefficient. But it has to be noted that the difference between the damaged moduli corresponding to the impact energy levels from 7-10J is not very significant. Therefore the degradation coefficients shown in Fig 6.8 have to be considered close and their variation with impact energy has to be considered small as well. This reasoning can be verified by looking at the indentation depths caused by these impact energy levels which do not show a large difference. It was previously discussed in Section 3.2, that the indentation depths for the composite laminate beams (Beams 4-7) impacted by clamping two ends is approximately in the range of 0.15 to 0.35 mm.

6.1.5 Updating Procedure on Composite Laminate Beams Impacted by Clamping all Four Ends

The FE modeling of the modal response of the composite beams impacted by clamping all four ends (Table 3.7 in Chapter 3) is carried out by following exactly the same procedure as that of the composite laminate beams impacted by clamping two ends in the previous section. Average damaged area and the radius of the approximated circular zone depicting the damaged area based on the procedure as explained previously, for the five composite laminate beams (Beams 1-5) is given in Table 6.7.

Table 6.7 FE parameters for the five composite laminate beams impacted by clamping all four ends

Beam No	Impact Energy	Average Damaged Area	Radius of the circular damage zone
	J	mm ²	mm
1	6	545.0	13.17 ≈ 13 mm
2	8	567.5	13.44 ≈ 13 mm
3	10	900.1	16.93 ≈ 17 mm
4	12	976.3	17.63 ≈ 18 mm
5	14	1041.3	18.21 ≈ 18 mm

If the average damaged area of the composite beams given in Table 6.7 (impacted by clamping all four ends) are compared with those in Table 6.1 (impacted by clamping two ends), it can be clearly seen that by clamping all four ends at the time of end, more damage can be induced in the composite beams by impacting at the same energy.

The composite material (T300/914) used for fabricating this lot of five composite beams shown in Table 6.7 was not expired. Modeling of the dynamic response and the updating procedure for Beams 4 and 5 is discussed below, whereas the results for Beams 1, 2 and 3 are given in the Annex for Chapter 6.

Beam 4 (12 J)

The ultrasound (C-scan results) test results for Beam 4 impacted at 12 J are presented in Annex Fig 6.O. The experimental and numerical comparison of the natural frequencies for the three states (UD, D1 and D2) along with the modification coefficients and statistical errors is shown in Table 6.8. Likewise the comparison for the FRF amplitudes is shown in Annex Table 6.M. Furthermore, comparison of the experimental and numerical (FE) FRFs for Beam 4 for the damage states D1 and D2 is shown in Fig 6.9.

Table 6.8 Comparison of experimental and numerical natural frequencies for Beam 4 impacted by clamping all four ends for the undamaged state (UD) and the two damage states (D1 and D2) along with the statistical error and the modification coefficient

Bending Modes No	Natural Frequencies (Hz)						
	Undamaged (UD)		Damaged (D1)		Damaged (D2)		
	Exp	Num (FE)	Exp	Num (FE)	Exp	Num (FE)	
1	41.5	41.7	39.8	39.0	39.1	39.3	
2	319.0	319.4	308.2	303.1	305.1	301.5	
3	802.1	800.9	773.1	765.0	760.2	761.0	
4	1543.7	1537.8	1477.7	1480.4	1465.9	1478.4	
	α_{UD}	1.00	α_{D1}	2.63	α_{D2}	2.63	
	$E_{freq,UD}(\alpha_{UD})$	11.24	$E_{freq,D1}(\alpha_{D1})$	9.32	$E_{freq,D2}(\alpha_{D2})$	12.53	

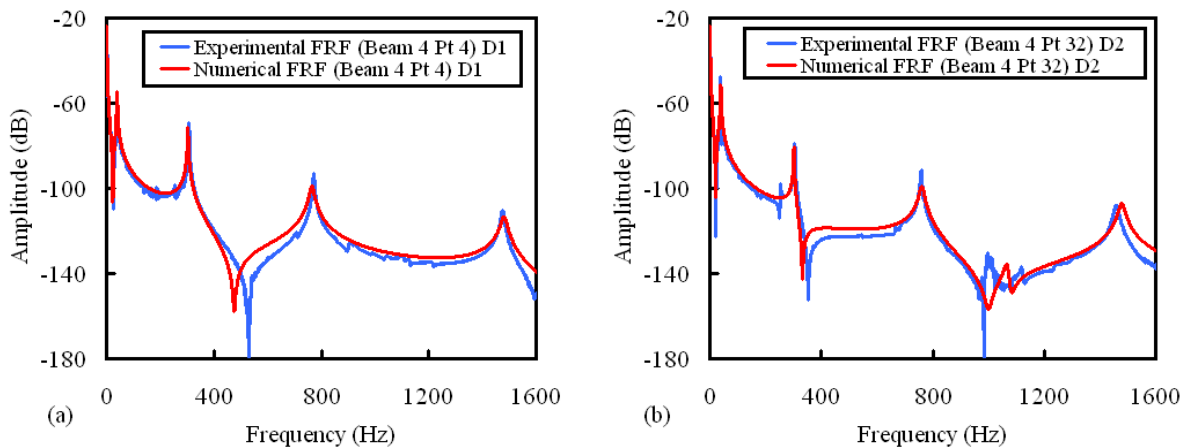


Figure 6.9 Comparison of experimental and numerical FRFs for Beam 4 impacted by clamping all four ends for the damaged states D1 and D2 for the measurement points 4 and 32 respectively

Up till now, due to the damage being relatively small and the behavior of the beam relatively linear, the decrease in natural frequencies of the four bending modes was proportional. So our approach of modeling the damage by reducing locally the elastic modulus E_L worked fine as shown by the experimental/numerical correlation results for all the previous beams. However, it shall be interesting to see the performance of our approach for the beams having significant damage.

Beam 5 (14 J)

The ultrasound (C-scan results) test results for Beam 5 impacted at 14 J are presented in Annex Fig 6.P. The experimental and numerical comparison of the natural frequencies for the three states (UD, D1 and D2) along with the modification coefficients and statistical errors is shown in Table 6.9. Likewise the comparison for the FRF amplitudes is shown in Annex Table 6.N. Furthermore, comparison of the experimental and numerical (FE) FRFs for Beam 5 for the undamaged state UD and the two damage states D1 and D2 is shown in Fig 6.10.

Table 6.9 Comparison of experimental and numerical natural frequencies for Beam 5 impacted by clamping all four ends for the undamaged state (UD) and the two damage states (D1 and D2) along with the statistical error and the modification coefficient

Bending Modes No	Natural Frequencies (Hz)					
	Undamaged (UD)		Damaged (D1)		Damaged (D2)	
	Exp	Num (FE)	Exp	Num (FE)	Exp	Num (FE)
1	41.2	41.5	40.5	38.2	38.5	37.7
2	318.1	318	301.2	295.1	287.8	293
3	799.5	797.5	707.1	748.4	698	734.8
4	1531.2	1531.2	1475.4	1452.7	1361.7	1394.2
	α_{UD}	1.00	α_{D1}	3.72	α_{D2}	3.72
	$E_{freq,UD}(\alpha_{UD})$	1.12	$E_{freq,D1}(\alpha_{D1})$	23.79	$E_{freq,D2}(\alpha_{D2})$	24.69

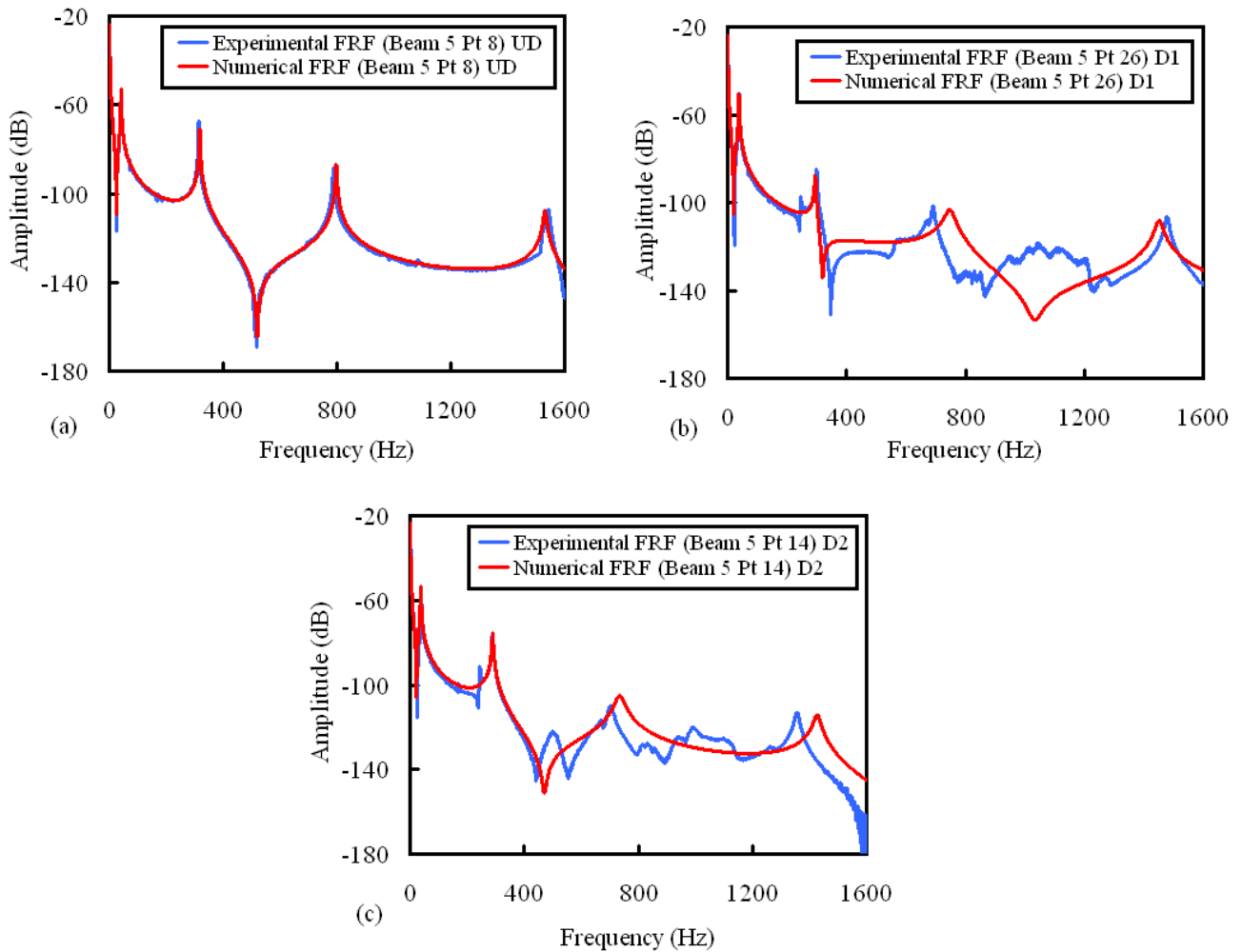


Figure 6.10 Comparison of experimental and numerical FRFs for Beam 5 impacted by clamping all four ends for the undamaged state UD and damaged states D1 and D2 for the measurement points 8, 26 and 14 respectively

Beam 5 impacted at 14 J has a relatively high damage level as compared to the rest. Beam 5 had an initial indentation depth of 1.1 mm which is nearly twice of the BVID limit. The

higher damage in this beam is also evident in the C-scan results in Annex Fig 6.I and in Table 6.10. But the real picture of the implications of high damage which introduces significant structural non-linearities is provided by the vibration test results. Table 6.9 shows that unlike previous beams, the decrease in natural frequencies for the four bending modes remains no longer proportional.

For example, in case of Beam 5, the frequency shift between the states UD and D1 for the third bending modes is 92 Hz, whereas the same for the fourth bending mode is 56 Hz. Logically the frequency shift for the higher modes is always greater as observed in case of all the other beams previously. Furthermore, as damage increases there is less possibility that it remains localized. The damage zones can get merged and there can be one big damage zone in place of several small ones.

This aberration can also be attributed to the increasing delamination size in Beam 5 which in turn increases the energy dissipation (damping). This effect can be observed in the FRFs in Fig 6.10 b and c, which show that in the presence of relatively higher damping the resonance peaks become considerably rounded at higher frequencies (above 400 Hz). High damping in Beam 5 especially for the damage state D2 was shown in the experimental results in Fig 3.16 in Chapter 3. The high statistical errors $E_{freq,D1}(\alpha_{D1})$ and $E_{freq,D2}(\alpha_{D2})$ in Table 6.9 are also due to the extraordinary decrease of the bending mode 3 which due to some unknown non-linear phenomenon is hard to simulate numerically.

It can be concluded that the damage modeling approach presented is limited to structures having small damage where the behavior remains more or less linear. Once the level of damage goes well beyond that corresponding to the BVID limit, this approach starts showing deficiencies. In order to model high damage successfully in composite laminates, an advanced material law has to be chosen and calculations have to be carried in FE softwares by using non-linear modules.

6.1.6 Evaluation of the Degradation Factor with Impact Energy in Composite Laminate Beams Impacted by Clamping all Four Ends

As previously for the case of composite laminate beams clamped at two ends, the variation of degradation factor with the impact energy shall be studied this time for the five composite beams (Beams 1-5) impacted by clamping all four ends. The degradation factor which is a multiple of the modification coefficient α with the radius of the circular damage zone (R) is given in Table 6.10 for the five beams.

Table 6.10 Calculation of the degradation factor for the composite laminate beams (Beams 1-5) impacted by clamping all four ends

Beam. No	Impact Energy (J)	Radius (R) of the circular damage zone (mm)	Modification Coefficient $\alpha_{D1} = \alpha_{D2}$	Degradation Coefficient (mm) $\alpha_{D1} \cdot R$
1	6	13	3.22	41.8
2	8	13	3.30	42.9
3	10	17	2.43	41.3
4	12	18	2.63	47.3
5	14	18	3.72	66.9

The variation of the degradation coefficient $\alpha_{D1} \cdot R$ with the impact energy levels for the five composite beams (Table 6.6) impacted by clamping all four ends is plotted in Fig 6.11.

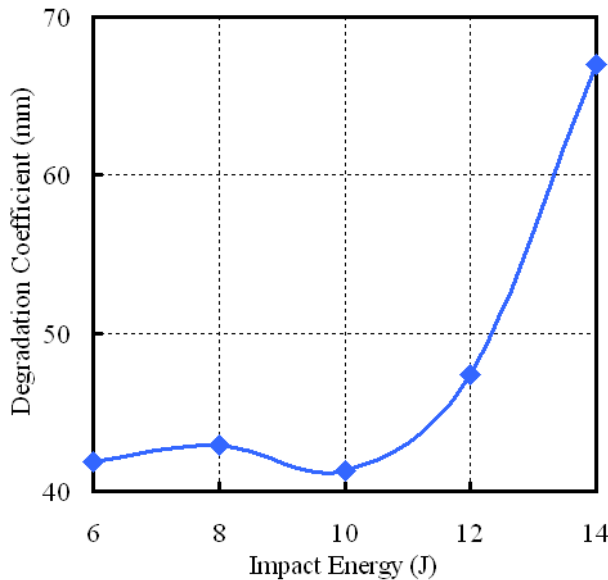


Figure 6.11 Variation of degradation factor ($\alpha_{D1} \cdot R$) with impact energy for the composite laminate beams (Beams 1-5) impacted by clamping all four ends

Fig 6.11 shows that up to the BVID limit (Beams 1-3) for the impact energies 6, 8 and 10J, the degradation coefficient varies very little. In case of Beam 4 (12 J), which is impacted slightly above the BVID limit the degradation coefficient is slightly bigger. But Beam 5 which showed considerable non-linear behavior as discussed previously possesses a remarkably high degradation coefficient.

6.1.7 Updating Procedure on Long Honeycomb Sandwich Beams

In this section, the FE modeling of the modal response is carried out on the long honeycomb sandwich beams vibration tested in Section 4.2 in Chapter 4. Only the three honeycomb beams (H2, H3 and H4) that are impacted shall be modeled.

In case of the honeycomb beams, the same modeling and updating procedure is followed as for the composite laminate beams. Reminding the readers that the honeycomb sandwich beams consists of four plies of composite laminate T700/M21 in the upper skin and four similar plies in the lower. So sandwich beam is modeled as follows

- The sandwich beam is modeled by nine plies. In which the middle ply (5th) is considered as the honeycomb core by changing its material properties and giving it a thickness of 10 mm. The sandwich beam is modeled by using quadrangular Mindlin shell elements
- Steel End masses and aluminum base block (for fixing the beam on the shaker) are modeled with 3D brick elements

One major drawback setback encountered when modeling sandwich beams was that the ultrasound results did not give reliable results on the details of the damage shape and surface as in the case of composite laminate beams. The ultrasound (C-Scan) results on the honeycomb beam H4 impacted at 8 J which induced significant damage is shown in Fig 6.12.

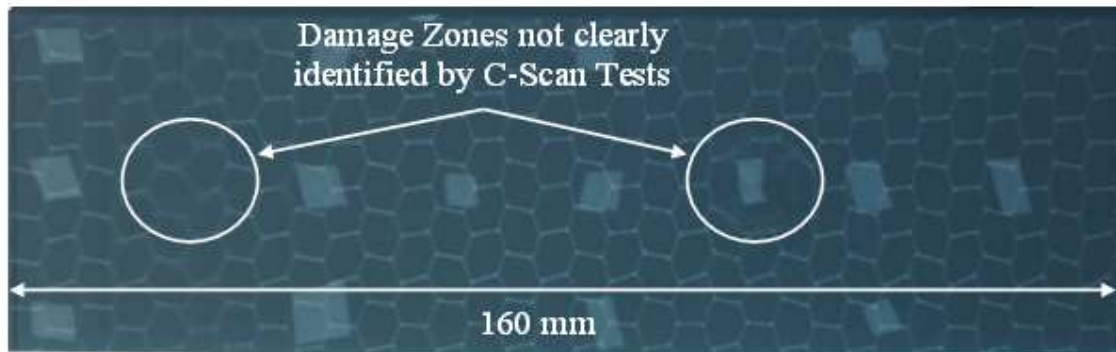


Figure 6.12 Ultrasound (C-Scan) results showing unclear calculation of the damaged surface for the long honeycomb beam H4 impacted at impact energy of 8 J

The C-scan results in Fig 6.12 underlines the vulnerability of this testing method for measuring the damage surface in thin skinned sandwich beams. To go ahead with the modeling the following assumptions are made:

- The damaged zones are considered circular and they are modeled in the same way as explained previously in Section 6.1.
- Hand tapping is carried out on the honeycomb skinned surface to estimate approximately the damaged area. The radius of the estimated circular damaged zone for the three honeycomb sandwich beams is presented in Table 6.11.
- Experimentally obtained damping values are used for each mode in the FE models.

Table 6.11 FE parameters for the three long honeycomb sandwich beams

Honeycomb Beam Name	Impact Energy J	Radius of the circular damage zone mm
H2	4	13 mm
H3	6	15 mm
H4	8	18 mm

The location of impact points in the 480 mm long honeycomb sandwich beams is shown in Fig 4.9 in Chapter 4. Generally in the sandwich beams, the shear forces normal to the panel will be carried by the honeycomb core. Bending moments and in-plane forces on the panel will be carried as membrane forces in the facing skins (composites in our case). For many practical cases, where the span of the panel is large compared to its thickness, the shear deflection will be negligible. In these cases, it may be possible to obtain reasonable results by modeling the structure using composite shell elements [139]. It should be noted that the in-plane stiffness of the honeycomb is negligible compared to that of the facing skins. The honeycomb sandwich beams (directions shown in Fig 6.13) is modeled by defining the following properties

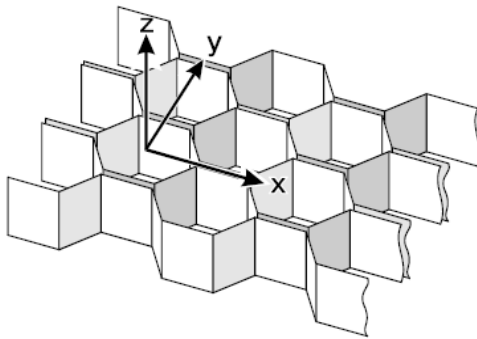


Figure 6.13 Material property directions for sandwich honeycomb beams

Skin Properties

In order to model a composite laminate beam in FE software the following three material properties are required:

- $E_L = E_X$ = Longitudinal elastic modulus
- $E_T = E_Y$ = Transverse elastic modulus
- G = Shear modulus

Core Properties

When defining the properties of honeycomb core (Table 4.2) the following points should be taken into consideration:

- $E_L = E_X = 0$ (Longitudinal and transverse elastic modulus)
- $E_T = E_Y$ = Transverse elastic modulus
- $\mu_{XY} = \mu_{XZ} = \mu_{YZ} = 0$ (Poisson ratio)
- $G_{XZ} = G_L$ = shear modulus in longitudinal (ribbon) direction = 29 MPa
- $G_{YZ} = G_T$ = shear modulus in transverse direction = 13.8 MPa
- $G_{XY} = 0$ (In-plane shear modulus)
- $E_Z = E_C$ = compressive modulus of core material = 75.8 MPa

By carrying out several trial tests by varying individually the above skin and core material properties, it is found that the skin properties have very little effect on the modal properties due to its small thickness. Among the core properties the shear modulus G_{XZ} is by far the material property which has the most profound effects on the natural frequencies. These trial tests are performed in the parametric module of Boss Quattro by using Samcef's DYNAM module. Based on these trial test results, it was decided that in order to keep the damage modeling methodology simple, only the Shear Modulus (G_{XZ}) shall be varied in case of the honeycomb sandwich beams. Modeling of the dynamic response and the updating procedure for Honeycomb Beam H2 is discussed below, whereas results for the Honeycomb Beams H3 and H4 are given in Annex for the sake of clarity.

Another difference with the composite laminate beams is that only the first three bending modes shall be studied, because very large dispersion and high statistical errors are obtained if the fourth bending mode is considered as well.

Beam H2 (4 J)

The four impact points are modeled by a circle of 13 mm radius. Due to unavailability of accurate C-Scan results the damage surface is approximated. The experimental/numerical correlation procedure is the same as that used for the composite laminate beams. The experimental and numerical comparison of the natural frequencies for the three states (UD, D1 and D2) along with the modification coefficients and statistical errors is shown in Table 6.12. Likewise the comparison for the FRF amplitudes is shown in Annex Table 6.O. Furthermore, comparison of the experimental and numerical (FE) FRFs for Beam H2 for the undamaged state UD and the two damage states D1 and D2 is shown in Fig 6.14.

Table 6.12 Comparison of experimental and numerical natural frequencies for Honeycomb Beam H2 (4J) for the undamaged state (UD) and the two damage states (D1 and D2) along with the statistical error and the modification coefficient

Bending Modes No	Natural Frequencies (Hz)						
	Undamaged (UD)		Damaged (D1)		Damaged (D2)		
	Exp	Num (FE)	Exp	Num (FE)	Exp	Num (FE)	
1	144.0	147.8	132.0	136.8	124.3	129.2	
2	763.9	764.5	691.3	702.0	614.3	639.3	
3	1360.4	1360.7	1244.4	1243.1	1141.5	1135.4	
	α_{UD}	1.00	α_{D1}	350	α_{D2}	350	
	$E_{freq,UD}(\alpha_{UD})$	2.23	$E_{freq,D1}(\alpha_{D1})$	6.81	$E_{freq,D2}(\alpha_{D2})$	15.12	

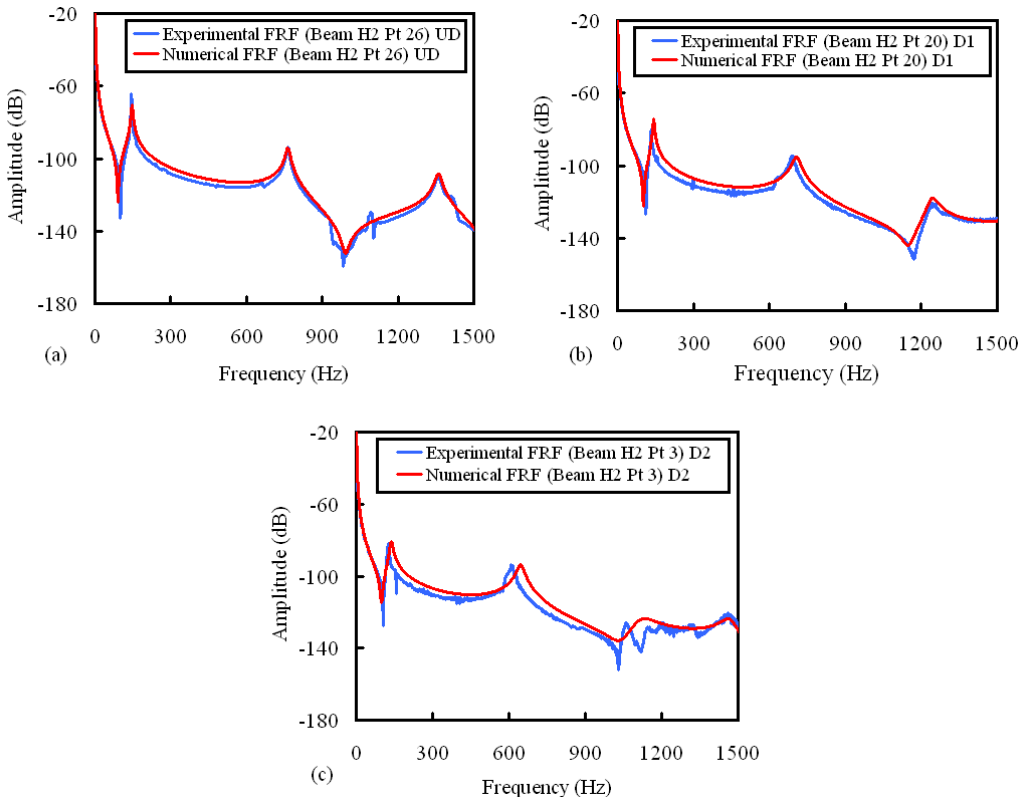


Figure 6.14 Comparison of experimental and numerical FRFs for Long Honeycomb Beam H2 for the undamaged state UD and the two damaged states D1 and D2 for the measurement points 26, 20 and 3 respectively

Table 6.12 and Fig 6.14a shows a good correlation between the natural frequencies and FRFs at the undamaged state (UD), which is proved by the very small statistical error. But for the damaged cases (D1 and D2), this error increases and is relatively high for the damaged case (D2). Fig 6.14c also shows a considerable dispersion in the FRFs. In case of honeycomb beams, it can be said with authority that this dispersion in the FRFs and the high statistical errors $E_{freq,D2}(\alpha_{D2})$ are due to the asymmetric nature of damage in the sandwich honeycomb beams i.e., impacting at the honeycomb cell center and at the corner leads to different damages.

The FE results of the dynamic response and updating for the other two honeycomb beams H3 and H4 impacted at 6 J and 8 J respectively are presented in Annex.

Generally the experimental/numerical correlation gives better results in case of the composite laminate beams because damage area was modeled based on accurate C-Scan results.

But still from the results on the three honeycomb sandwich beams (H2, H3 and H4), a good correlation is obtained certainly for the undamaged case (UD) and also to some extent for the damaged case (D1). But in case of the damaged state (D2) which is the damage at 4 points, unsatisfactory correlation results are obtained because due to the nature of the honeycomb (cell or corner), the damage density varies a lot. With the current methodology where the material properties are reduced by the same factor at each damage point, it is not a very good idea to model asymmetric damage. This can be one reason for the shift in the experimental and FE results.

As discussed previously, due to the unavailability of the C-scan results, damage surface was approximated by hand tapping. The circular damage shape was also a big approximation for the sandwich beams, because in case of the composite laminate beams C-Scan results showed the damage surface to be nearly circular. Therefore the circular shape assumption worked relatively well in the FE models for the composite laminates. However for the sandwich beams, this unavailability of data regarding damage shape and extent leads to errors while updating the FE model.

In the FE modeling methodology presented in this thesis, one major assumption that is made is that, the material properties have been reduced in the damage zones by taking into account the total thickness of the specimen. The C-scan results do not indicate clearly the location of damage in the thickness for the composite laminates. Therefore, the material properties have been reduced for all the thickness. This hypothesis works well in case of composite laminates as we have the same material in all the thickness.

However, for the sandwich beams having two skins and a core this hypothesis is a bit far fetched. Therefore, this can also be the reason why the FE modeling results are less good in honeycomb sandwich beams as compared to the composite laminates, because we assumed that the damage is the same in the two skins and the core. However in reality this might not be true. The skin that is impacted is more damaged in reality than the lower one, as shown in Fig 6.15. So our hypothesis of constant damage in thickness can be misleading in case of sandwich beams.

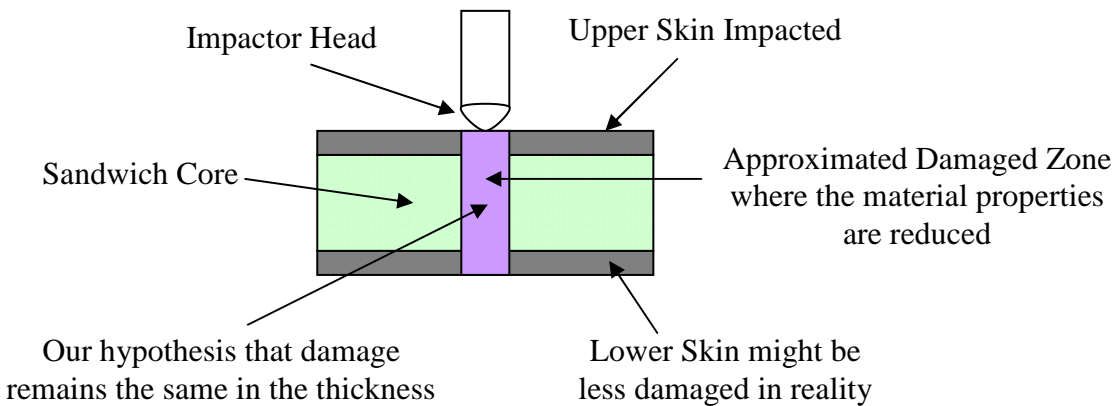


Figure 6.15 Schematic of a sandwich beam showing the approximated damaged zone where the material properties are reduced – In sandwich beams lower skin might be less damaged in reality, so our hypothesis can be misleading

Therefore in future, the impact points shall be modeled in such a way that material properties can be varied separately at each impact point. The honeycomb beams shall be cut around the damaged area and will be observed by a Scanning Electron Microscope (SEM). The aim shall be to obtain information regarding the shape and surface of the damage surface.

As in the case of honeycomb sandwich beams the FE results are less reliable therefore the variation of the degradation factor $\alpha_{D_1} \cdot R$ with the impact energy levels is not studied.

6.1.8 Updating of Long Carbon Entangled Sandwich Beams

In this section, modeling of the modal response of the long carbon entangled sandwich beams is tried. The aim is to model the entangled sandwich beam with measured core properties (Static Tests in Section 5.1.2) in order to calculate the natural frequencies to compare with the experimental test results (Table 5.3 in Chapter 5). As entangled sandwiches are a new brand of sandwich materials, therefore such comparisons will provide a verification of the measured core properties. The procedure of modeling the entangled sandwich beam is similar to that of the honeycomb sandwich beams in the previous section.

- The sandwich beam is modeled by nine plies. In which the middle ply (5th) is considered as the entangled core by changing its material properties based on the static test results and giving it a thickness of 10 mm. The sandwich beam is modeled by using quadrangular Mindlin shell elements
- Aluminum base block (for fixing the beam on the shaker) is modeled with 3D brick elements (no end-masses are attached)

As in the case of sandwich honeycomb beams, the ultrasound (C-Scan) results are incapable of measuring the damaged surface for the entangled sandwich beams as well, as shown in Fig 6.16.

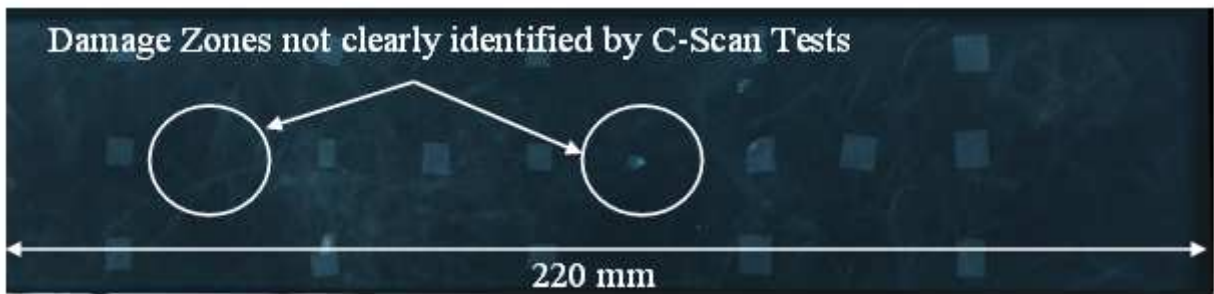


Figure 6.16 Ultrasound (C-Scan) results showing unclear calculation of the damaged surface for the long carbon entangled beam (EL2) impacted at impact energy of 12 J

The entangled sandwich beams (directions shown in Fig 6.13) is modeled by defining the following properties:

Skin Properties

In order to model a composite laminate beam in FE software the following three material properties are required:

- $E_L = E_X$ = Longitudinal elastic modulus
- $E_T = E_Y$ = Transverse elastic modulus
- G = Shear modulus

Core Properties

When defining the properties of honeycomb core (Table 4.2) the following points should be taken into consideration:

- $E_X = E_Y = E_Z = 1.4 \text{ MPa}$ (Section 4.3.2)
- $\mu_{XY} = \mu_{XZ} = \mu_{YZ} = 0$ (Poisson ratio)
- $G_{XY} = G_{XZ} = G_{YZ} = 10 \text{ MPa}$ (Section 4.3.2)

From the core material properties it can be seen that our entangled sandwich core is isotropic in nature. First of all the FE model for the undamaged case (UD) is built and if a satisfactory comparison is obtained with the experimental results, only then shall the damaged scenarios be modeled.

A comparison of the experimental and numerical FRF of the Long Carbon Entangled Sandwich Beam EH1, for the undamaged state UD at the measurement points 2 is shown in Fig 6.17 below.

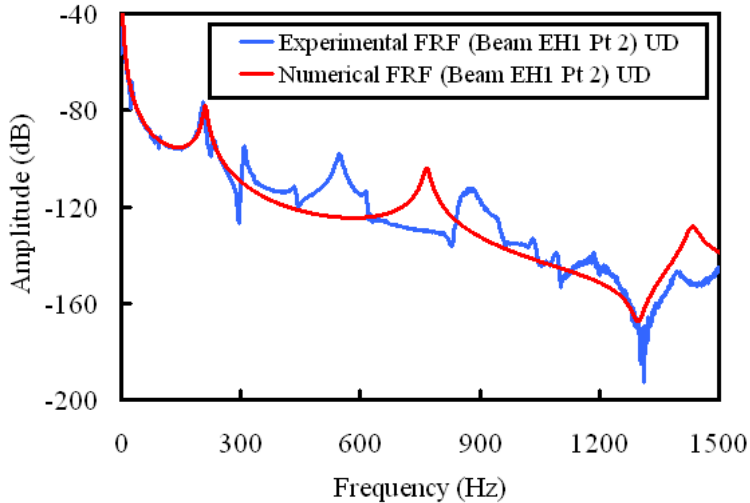


Figure 6.17 Comparison of experimental and numerical FRFs for the Long Carbon Entangled Sandwich Beam EH1 for the undamaged state UD for the measurement points 2

The numerical FRF shown in Fig 6.17 is obtained by varying the experimentally calculated elastic modulus ($E = 1.4 \text{ MPa}$) and shear modulus ($G = 10 \text{ MPa}$) for the carbon entangled core by approximately 5 %. By doing so a very good correlation is found for the first bending mode which is around 220 Hz. However after the first bending mode a large dispersion is seen between the experimental and numerical FRFs. Whereas the question of the verification of the measured core properties is concerned, they are reliable because the first bending mode gives a good correlation between the experimental and FE results. As the frequency of the first bending mode is directly proportional to the material properties so it can be said that the experimentally obtained elastic and shear modulus are considerably reliable.

By observing the experimentally obtained FRF for the entangled sandwich beam (EH1) in Fig 6.17, it can be seen that there are multiple modes that are not to be seen in the numerical results. This leads us to the following conclusions:

In the FE model for the entangled beam, the fiber entangled core is considered completely homogeneous and isotropic i.e., having the same properties in all directions. Due to this homogeneous nature of the entangled beam only three modes are obtained in the (0-1500 Hz) bandwidth.

However in reality the nature of the carbon fiber entangled sandwich core is different. As discussed in Chapter 4, if the volume of the beam is considerably large, with the current manufacturing technology i.e., by manually spraying the resin on the fibers by a spray paint gun it, it is not possible in our case to obtain a homogeneous distribution of fibers and resin in the entangled core. The multiple peaks in the experimentally obtained FRF shown in Fig 6.17 are due to the non-homogeneous distribution of the resin. Furthermore, due to this reason the FE modeling for the damaged cases in case of the entangled sandwich beams shall not be performed.

Therefore the aspect of spraying resin in the manufacturing process of the entangled materials has to be improved in future in order to obtain homogeneous sandwich materials like those with honeycomb and foam cores.

In future FE models, in a similar way (reducing the material properties in the damaged zone) shall be developed for the glass fiber entangled sandwich beams but as these have also been

fabricated by the same methodology, therefore the author thinks that similar additional peaks shall be encountered due to non-symmetric nature. Therefore before taking into consideration seriously FE modeling for entangled beams, the fabrication methodology has to be upgraded.

6.2 Damage Localization by Topology Optimization

Up till now in this thesis, damage detection in various types of composite beams has been performed. The stake here is not only to update the model, but to go one step further in the diagnostics and try and localize the damage, without prior knowledge of its position.

In this section, damage detection and localization is carried out on the composite laminate beams (previously tested in Chapter 3) through topology optimization. By the topology optimization approach, a numerical model is updated towards a similar structure with embedded damages using only mass penalization and the experimentally obtained modal parameters as objectives. The aim of this technique is just to localize damage in any type of material either isotropic (aluminum) or quasi-isotropic (composites), and not to provide the exact damaged surface like C-scan tests.

Topology optimization has been carried out in MSC Nastran as this option was not available in Samcef. First of all a brief theoretical background about the topology optimization methodology is presented.

6.2.1 Optimization Problem Formulation for damage Localization

For formulating general optimization statements suitable for computation, some general definitions have to be established. In the beginning, an objective of the optimization has to be identified that is a function of the design variables that are changed in the course of the optimization. As the main objective of the performed optimizations is the matching of a set of modal parameters, any kind of matching function (e.g. least square formulations) can be considered. In the case of the presented work, a pseudo objective function is chosen, considering the parameters that are to be matched only as constraints. Furthermore, the number of parameters can be dynamically adapted during the optimization depending on the fulfilment or non-fulfilment of the constraints. This means that each constraint has principally to be matched to itself and not to a least-square of all of them together. In preliminary tests, this formulation gave the most promising results, whereas other formulations more often led to wrong local optima. The mentioned approach has also already been proposed in the recent article by Lee [75].

An exemplary pseudo objective function is shown in Equation 6.18, where f is the original objective function and P a penalty function consisting of a set of inequality or equality constraints, which are g and h respectively. The parameter r_p is a further penalization coefficient that can be applied to the constraints.

$$\min : \Phi(x) = f(x) + P(r_p, h(x), g(x)) \quad (6.18)$$

The vector of design variables x consists of the Topology design variables corresponding to the Power Law approach [71]. These design variables are principally an additional element property that can be understood as a relative density of each element e as stated in Equation 6.19.

$$x_e = \frac{\rho_e}{\rho_0} \text{ subject to } 0 \leq x_{\min} \leq x \leq 1 \quad (6.19)$$

Since the variable is normalized by the original densities, it can only assume values between 0 and 1, as stated in the side constraints. Due to numerical reasons, 0 is replaced by a minimum threshold. This design variable is then multiplied by the corresponding element's stiffness and mass and thereby alters the properties of the element (Equation 6.20).

$$E_e = x_e^p E_0 \text{ and } m_e = x_e^q m_0 \quad (6.20)$$

The design variable is also being penalized, which is supposed to help in getting a clearer solid-void solution by making intermediate design variables more "costly". The values of the penalization exponents p and q are problem-dependent, but a penalization factor of about 3 is generally proposed in common literature [72].

In the following, the constraints consisting of modal parameters are defined, where the primed value always denotes the reference data of the damaged structure, and the plain value corresponds to the current data of the optimized model. Since the goal is to minimize the difference between these values, a proximity ε_ω is usually defined. The first set of constraint equations g^ω requires the n_ω chosen angular resonance frequencies to be within the proximity of corresponding resonance frequencies of the damaged structure (Equation 6.21).

$$g_i^\omega = (\omega_i^2 - \bar{\omega}_i^2)^2 < \varepsilon_\omega \text{ for } i = 1, 2, \dots, n_\omega \quad (6.21)$$

This formulation has a global character, since the resonant frequencies are global parameters for the structure. In [17], it has however been shown that local modal data is necessary for achieving better results, which is why the use of anti-resonances is proposed. Whereas resonances can be found at the peaks of the frequency response functions, their local minima are called anti-resonances (Fig 6.18). These minima result from the additional contribution of two neighboring modes with a 180 degree phase shifts [122]. Anti-resonances are unique for any point on the structure and therefore considered as local data.

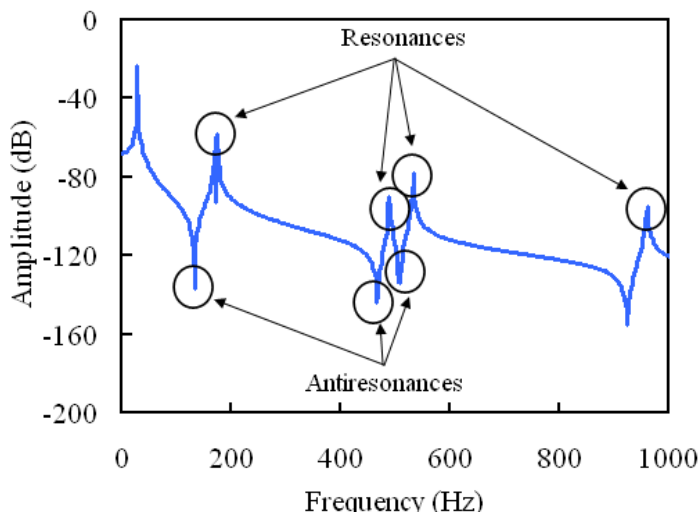


Figure 6.18 Resonances and anti-resonances in frequency response functions

It is important to underline the fact that dissipation (damping) modifies resonance and anti-resonance peaks, and furthermore, non-linearity induces a shift and distortion in both the resonance and anti-resonance peaks.

Due to limitations in Nastran, anti-resonances could not directly be considered as constraints, but the nodal frequency response functions, so that anti-resonances can still be included in the optimization by evaluating the FRFs at the corresponding frequency. Thus, the second used set of constraint equations g^H requires that the magnitude value of the nodal FRF (FRF of an FE node) at a certain excitation frequency Ω_j to be within the proximity ε_H of that of the damaged structure at the same frequency.

$$g_j^H = \left\{ \left| H_{kl}(\Omega_j) \right| - \left| \bar{H}_{kl}(\Omega_j) \right| \right\} < \varepsilon_H \text{ for } i = 1, 2, \dots, n_H \quad (6.22)$$

where the suffix k is the excitation and l is the measurement DOF.

As objective function, further penalization functions have been used that are not necessary but showed to improve results in preliminary tests. These functions can be understood as a penalization for the structural mass. Since the fibre composites do not lose mass due to the impacts, it is desired to keep the structural mass close to the original mass.

Since the design variables are the elements' fractional densities, it is more practical to use also fractional masses for the objective functions, as defined in Equation 6.23, where m_0 is the mass when all design variables are at 1 (solid).

$$m_{fractional} = \sum_{ne} \frac{m_e}{m_0} \quad (6.23)$$

Here, n_e is the number of elements in the design domain. Due to the constant design volume, this fractional mass is equal to the sum of all fractional densities as shown in Equation 6.24.

$$m_{fractional} = \sum_{ne} \frac{V_0 \rho_e}{V_0 \rho_0} = \sum_{ne} x_e \quad (6.24)$$

Several objective functions have been tested, which are shown in Table 6.13, whereas Fig 6.19 depicts these objective functions.

Table 6.13 Objective functions for fractional mass penalization

Number	Function	Derivative
1	$L = m_{frac} (1 - m_{frac})$	$L' = 1 - 2m_{frac}$
2	$L = 1 - m_{frac} $	$L' = -1 \text{ for } m_{frac} < 1$
3	$L = (1 - m_{frac})^2$	$L' = -1 + 2m_{frac}$

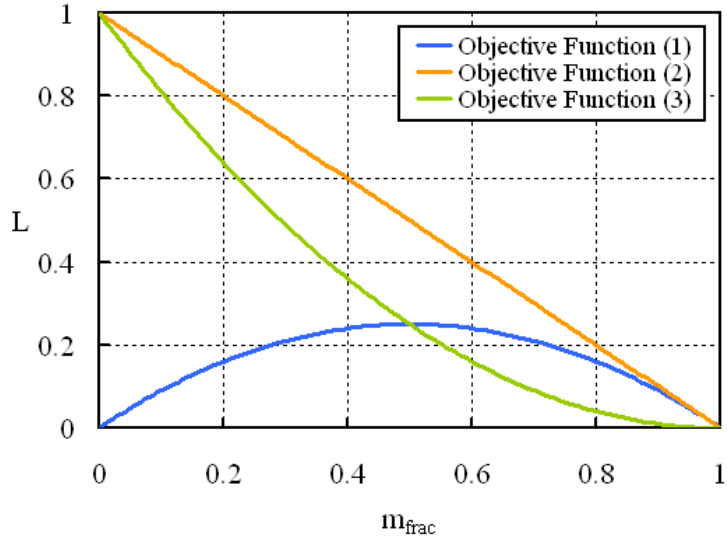


Figure 6.19 Objective functions for fractional mass penalization

In the displayed figure it can be seen that all functions show a relative minimum at the right border of the domain where all fractional densities are 1, but they possess different derivatives, which are important for the sensitivity analysis and basically characterize the penalization. The derivative of function (2) is constant over the whole domain ($[0;1]$), the derivatives of the other functions are variable with the fractional mass. Whereas the derivative value of function (1) approaches the value of the derivative of function (2) close to the right border, the derivative of function (3) approaches zero. Therefore, similar results have been obtained using functions (1) and (2) during the simulations. Also, they generally gave better results than function (3).

Sensitivity Analysis

Since mathematical programming methods usually involve the calculation of gradients of the objectives for the sensitivity analysis, the derivatives of the constraints with respect to the design variables are presented in this section. Equation 6.25 shows the gradients of the resonance frequencies as derived in [27], where ψ_{ie} are the components of the corresponding eigenvector with respect to the nodal degrees of freedom of the element e .

$$\frac{\partial \omega_i^2}{\partial x_e} = \boldsymbol{\psi}_{ie}^T \left(\frac{\partial E_e}{\partial x_e} - \omega_i^2 \frac{\partial M_e}{\partial x_e} \right) \boldsymbol{\psi}_{je} \quad (6.25)$$

The partial derivatives of the frequency response functions have been derived in [73]. Based on Equation 6.12 the frequency response function can be written as Equation 6.26.

$$H(\Omega) = \Psi \hat{q}(\Omega) \hat{f}^{-1}(\Omega) \quad (6.26)$$

Then, the gradients of the frequency response functions with respect to the element density fraction x_e are calculated as in Equation 6.27.

$$\frac{\partial H(\Omega)}{\partial x_e} = \Psi S \hat{q}(\Omega) \hat{f}^{-1}(\Omega) \quad (6.27)$$

Here, S is the sensitivity matrix as defined in Equation 6.28, where ω_i is the i th natural frequency and ζ_i the corresponding damping ratio. As before, Ω is the exciting frequency.

$$S_{ij} = \frac{-1}{\omega_i^2 - \Omega^2 + i2\zeta_i\omega_i\Omega} \psi_{ie}^T \cdot \left(\frac{\partial E_e}{\partial x_e} - \Omega^2 \frac{\partial E_e}{\partial x_e} \right) \psi_{je} \quad (6.28)$$

In both cases the gradients of the stiffness and mass matrices can be calculated as in Equations 6.29 and 6.30.

$$\frac{\partial K_e}{\partial x_e} = \int_{V_e} (DN)^T \frac{\partial E_e}{\partial X_e} DN dV \quad (6.29)$$

$$\frac{\partial M_e}{\partial x_e} = \int_{V_e} N^T \frac{\partial \rho_e}{\partial X_e} NdV \quad (6.30)$$

Set-up of Topology Optimization Formulation for Damage Localization in Nastran

In the following Nastran input file parameters for the damage localization approach are presented. Also, the models that are used for a numerical validation of this method, as well as the modeling of the specimens described in the previous sections are explained. The latter models are supposed for an experimental validation of the damage localization method.

MD Nastran seemed therefore suitable for this kind of job, since, with the release of the version MSC Nastran 2005 r2, the embedded optimization libraries were enhanced by a topology optimization capability and the introduction of the BIGDOT optimizer. Especially this new optimization library provided the capability to deliver practical results dealing with the large amount of design variables that are common in topology optimization. Thus, only Nastran was available for an "all at once" implementation of the described method, combined with low calculation time.

For the optimization of the structure, several new cards had to be added to the input file. At first, the design variable has to be defined. In the case of topology optimization, this is explicitly done by the command TOPVAR. The structure of this command is exemplary shown in Table 6.14 with the corresponding symbols from the previously derived equations.

Table 6.14 Definition of topology optimization variable in Nastran

Command	ID	Label	Type of property	x_0	x_{min}	Δx	P	Property ID
TOPVAR	1	DREGION	PSHELL	0.99	0.0001	0.2	3	4

Here, type of property characterizes the elements, that are included in the optimization, concerning their deformation behavior. This definition has to be in accordance with the elements of the defined design region, which is called by the Property ID that has been assigned prior to the corresponding elements

Then, the chosen modal parameters of the structure that build up the constraints and objectives have to be included in the calculations. In Nastran these parameters are referred to design responses and they are accessed by the DRESP*i* entries. For each desired structural response, such a DRESP*i* entry has to be defined, where the index *i* denotes the type design response formulation.

The design responses can then be constrained by referencing the corresponding DRESP*i* entry in a DCONSTR command and by defining the boundaries there. All the responses and constraints can be called, either by themselves or as a linear combination, by the global objective function (DESOBJ) or the global constraint command DESGLB in the case control section, or, as sub-case dependent constraints, by a DESSUB command for each sub-case. Fig 6.20 shows how responses, constraint and objectives can principally be connected. More precise definitions of each of the commands are given in reference [74]. In each optimization cycle, two sub-cases have to be evaluated: the modal analysis and the modal frequency response analysis. Each sub-case thereby calls its own set of design constraints via the DESSUB command. An exemplary input file can be found in the appendix A, where the design constraints and corresponding design responses, like the model itself, are sourced out into external files to keep input file mostly model-independent.

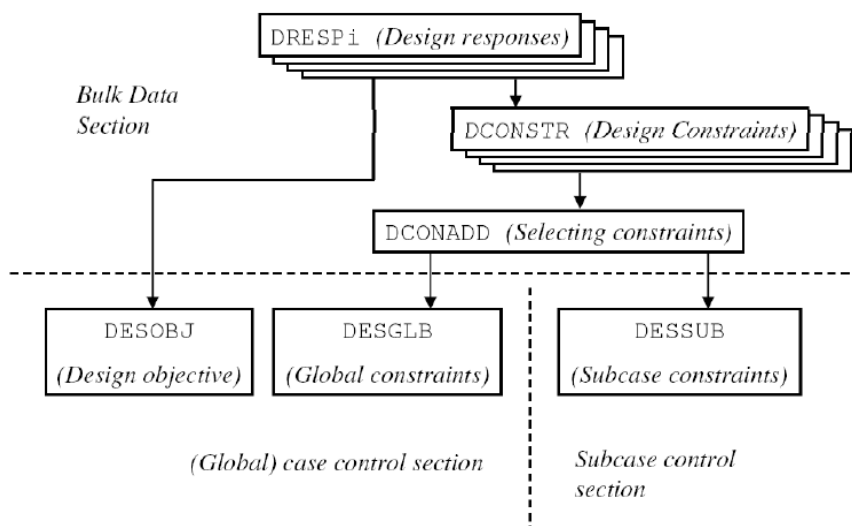


Figure 6.20 Constructions of objective functions and global or sub-case design constraints in Nastran input files

The composite laminate beams in Nastran are modeled in the same way as they were modeled in Samcef. The composite beam is modeled by shell elements and the steel masses and the aluminum fixation system is modeled by 3D elements. A harmonic load with constant amplitude of 1 N is applied at a node situated 20 mm below the bottom of the base block as shown previously in Fig 6.2b.

Before undertaking the case of composites, this topology optimization technique has been validated with success for various aluminum beams with cracks.

6.2.2 Experimental Validation of Topology Optimization in Composites

The optimization algorithm is applied on the composite laminate beam (Beam 4) impacted by clamping two ends with an impact energy of 7 J (vibration tests on this beam are carried out in Section 3.3). If reliable results are obtained then this study shall be carried out on the other composite laminate beams as well in future. Here, the data used for the constraints are the natural frequencies and the FRFs that have been obtained by vibration tests on Beam 4 for the two damage states D1 (4 impact points) and D2 (4 impact points).

It has to be reminded, that as the ultrasound results are only available for half length of the beam so the topology optimization results are also shown for one half as well. As the beams are considered to be symmetrical, thus each side of the beam has undergone two and four impacts, respectively. The topology optimization results for the damage state D1 (2 impacts on half beam length) in comparison with the ultrasound results are shown in Fig 6.21.

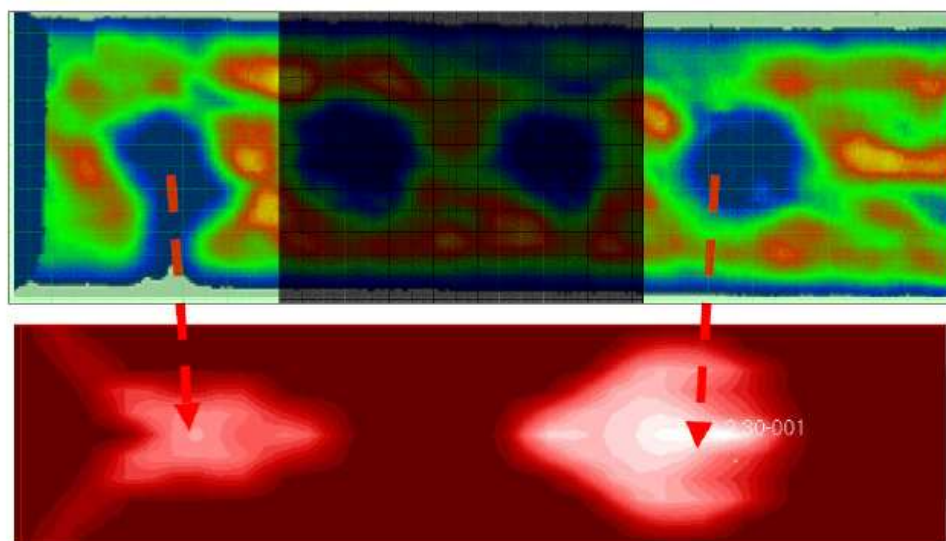


Figure 6.21 Comparison between C-Scan results (top) and topology optimization (bottom) for the damage state D1 - The two middle impact points are blackened as they correspond to the damage state D2

Fig 6.21 show that for the first two impacts, the right locations have been found effectively with similar sizes as in the ultrasound images that have been produced after vibration testing i.e., the outer two impact damage points have been introduced first (D1) and the two inner impacts later (D2) as shown in Fig 6.21. Ultrasonic tests are only performed after all other testing has been completed.

Similarly, the topology optimization results for the damage state D2 (4 impacts on half beam length) in comparison with the ultrasound results are shown in Fig 6.22.

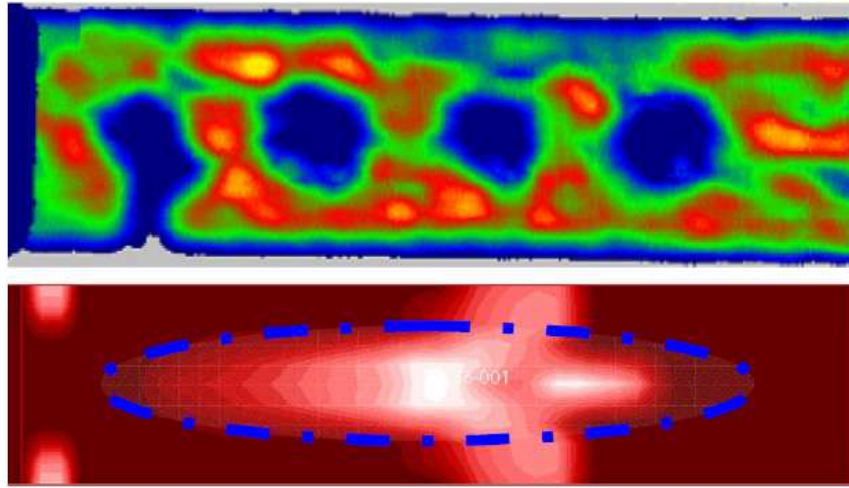


Figure 6.22 Comparison between C-Scan results (top) and topology optimization (bottom) for the damage state D2, the blue zone shows the optimization results – algorithm is not able to distinguish separately the four damages

In case of the damaged state D2 with four impact sites for half-beam length (Fig 6.22), only a rather uncertain region of damage with lower densities is located, but not the discrete impact points as shown in the ultrasound result. However, the displayed region of lower densities is still close to a damage region if the delamination regions due to the impacts (Fig 6.22) are merged. However, the optimized FRFs show a good match with those obtained experimentally for both the damaged cases as shown in Fig 6.23

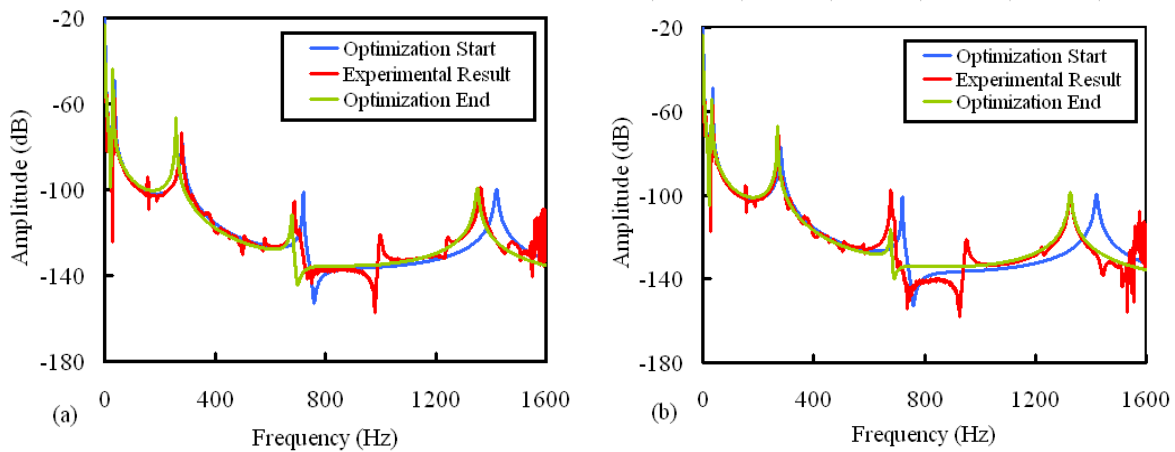


Figure 6.23 Experimentally obtained FRF for Beam 4 impacted by clamping two ends and calculated FRF of the FEM model at the same point, before and after optimization using only resonance frequency constraints (a) for damage state D1 (4 impacts) (b) for damage state D2 (8 impacts)

To clarify further the results, a comparison of the natural frequencies between the experimental and the topology optimized results for Beam 4 are laid out in Table 6.15. It can be seen that better matching is obtained for higher frequencies.

Table 6.15 Experimental (vibration tests) and optimized (Topology optimization) natural frequencies for Beam 4 impacted by clamping two ends

Bending Modes No	Natural Frequency (Hz)				
	Damaged State (D1)		Damaged State (D2)		
	Experimental (Target)	Numerical (Optimized)	Experimental (Target)	Numerical (Optimized)	
1	37	30	-44.8	-46.1	
2	278	270	-72.8	-81.7	
3	687	679	-84.9	-84.8	
4	1363	1351	-99.8	-97.6	

From the obtained results it can be concluded that their quality depended vastly on the choice of the optimization parameters. These optimization sensitive parameters can be divided in two main groups. The first one consists of the parameters related to the optimization process i.e., penalization exponents and objective functions, and the other depends upon the quality of the experimental results. Since higher resonance frequencies usually show a higher shift when damaged, therefore vibration tests should be carried out with a larger bandwidth if possible. But with higher frequencies the necessary modal identification becomes more difficult as higher modes are more susceptible to noise and furthermore the higher modes participate less and less in the actual dynamic response.

The presented topology optimization approach is also limited to modal parameter shifts due to loss of stiffness and mass, and does not take into account damping which as proved by the experimental results is more sensitive to damage than stiffness changes. In the current formulation it is not possible to consider changes in damping as constraints in the optimization, since no response for damping is available so far in Nastran.

So in the future, the changes in damping will be considered as a matching parameter, and in addition, the frequency bandwidth will be increased as well while performing experimental modal analysis to take into account higher modes that are more sensitive to damage.

6.3 Conclusion of the Sixth Chapter

The numerical part of this thesis consisted of two major parts. The first part is to develop Finite Element models that represent damaged composite beams in vibrations. Finite Element models in Samcef are used to calculate the modal parameters and dynamic response of the composite laminate and the composite sandwich beams. These simplified damage models give us a degradation factor that can serve as a warning regarding structure safety. **Compare the numerical results with those obtained experimentally** (Chapters 3, 4 and 5) on the same beams. Then **update** the Finite Element models in order to **improve the experimental/numerical correlation**. The methodology used to model damage in the test-beams is a simple one. Instead of modeling the damage as it is by directly meshing the structure, the **material properties of the elements in the damage zones are modified**. This way the problems of excessive gridding number and small mesh sizes are avoided.

The size of the circular damage zones is estimated based on the fairly accurate C-Scan results. The **longitudinal Elastic Modulus (E_L)** is varied in the circular damage zones for the composite laminate beams, because trial tests highlighted (E_L) as the material property which has the most profound effects on the natural frequencies. For the process of updating, the

FEM model corresponding to the undamaged case (UD) is established by trying different values of **coefficient** α_{UD} (by a Parametric study in Boss Quattro), until the smallest statistical error is reached between the experimental and numerical results for the natural frequencies based on the following equation.

$$E_{freq,UD}(\alpha_{UD}) = \sqrt{\frac{1}{N} \sum_{i=1}^N [f_{FEM,UD}^k(\alpha_{UD}) - f_{EXP,UD}^k]^2}$$

The same procedure is followed for the damaged cases (D1 and D2). The statistical error $E_{freq,D1}(\alpha_{D1})$ for the damaged case (D1) is calculated for each iteration and compared with that of the undamaged case $E_{freq,UD}(\alpha_{D1})$. The aim is to find $E_{freq,D1}(\alpha_{D1})$ as close as possible to $E_{freq,UD}(\alpha_{UD})$. The same procedure is followed for updating the FRF amplitudes.

By following the above mentioned procedures, the dynamic response of the composite laminate beams has been successfully modeled and a very good experimental/numerical correlation is obtained. However, it needs to be highlighted that **our methodology only stands** for the cases where the **damage is small** i.e., around the BVID limit where the behavior of the structure remains more or less linear. Once the level of damage goes well beyond that corresponding to the BVID limit (Example of Beam 5, impacted by clamping all four ends), this approach starts showing deficiencies. In order to model high damage successfully in composite laminates, an advanced material law has to be chosen and calculations have to be carried in FE softwares by using non-linear modules (solvers).

In case of the honeycomb beams, the same modeling and updating procedure is followed as for the composite laminate beams. Generally the experimental/numerical correlation gives better results in case of the composite laminate beams because damage area was modeled based on accurate C-Scan results. However for the honeycomb beams due to the **unavailability of the C-scan results**, damage surface was approximated by tapping. The material property varied in the damage zones in case of the honeycomb sandwich beams is the **shear modulus (Gxz)**, which seems to have the most significant effect on the modal parameters.

But still from the results on the three honeycomb sandwich beams (H2, H3 and H4), a good correlation is obtained certainly for the undamaged case (UD) and also to some extent for the damaged case (D1). But in **case of the damaged state (D2)** which is the damage at 4 points, **unsatisfactory correlation results** are obtained because due to the nature of the honeycomb (cell or corner) the damage density varies a lot. With the current methodology where the material properties are reduced by the same factor at each damage point, it is not a very good idea to model asymmetric damage. Therefore in future, the impact points shall be modeled in such a way that material properties can be varied separately at each impact point. The honeycomb beams shall be cut around the damaged area and will be observed by a Scanning Electron Microscope (SEM). The aim shall be to obtain information regarding the shape and surface of the damage surface.

The author has also tried to model the dynamic response of the carbon fiber entangled sandwich beams. **The experimental/numerical correlation was less than satisfactory due to multiple peaks in the experimentally obtained FRF due to the non-homogeneous distribution of the resin.** This asymmetric behavior due to random distribution of fibers and resin is not possible to simulate numerically, because in the FE model the fiber entangled core

is considered completely homogeneous and isotropic i.e., having the same properties in all directions. Therefore the aspect of spraying resin in the manufacturing process of the entangled materials has to be improved in future in order to obtain homogeneous sandwich materials like those with honeycomb and foam cores, and only then shall the FE modeling be carried out. Furthermore modeling numerically or analytically an entangled material is a complete thesis in itself.

The second part of the numerical work concerns **damage localization** and its validation in composite laminate beams through topology optimization in Nastran using the experimentally obtained modal parameters (Chapter 3). The damage localization approach can be divided into two sub-problems, the optimization routine using Topology Optimization, and the experimental estimation of modal parameters with the correct numerical modeling. Results on composite laminate beams (Beam 4) showed that with topology optimization the **right damage locations** have been found rather efficiently **only for the lower damage state D1**.

The topology optimization approach presented in this thesis is a **preliminary study**, and it was observed during trial tests while comparing with the experimental results (C-Scan), that sometimes the results were less clear and the optimization got stuck in wrong local optima more often. But it can be assumed that this anomaly is mostly due to the simplicity of the approach, the lack of constraint data and for not taking into account damping that controls the FRF amplitudes. Still, with a suitable choice of parameters, for composite beams some good results with correct localization of the impacts is achieved. Damage localization by topology optimization turns out to be a rather promising method but it is not the core of this thesis.

Chapter 7 : Conclusion and Future Work

7.1 Overall Conclusion

The thesis presents an experimental study on the effects of multi-site impact damage on the vibration response of composite laminate and composite sandwich beam-type specimens. Finite element based models are also developed to simulate the dynamic response of these damaged composite beams, in order to find a good experimental/numerical correlation with the help of updating. A preliminary study on damage localization in composites based on topology optimization is also carried out.

Impact damage in composites may lead to severe degradation of the mechanical behavior due to the loss of structural integrity. Therefore structural health monitoring (SHM) based on vibration testing is useful in detecting this damage caused by impact because damage generally effects the vibration characteristics of a structure i.e., natural frequency, damping and mode shapes change in detectable manner due to the loss of stiffness and mass. Structural health monitoring is a very vast domain and consists of five major steps:

- detection of damage in a structure
- localization of damage
- classification of the damage type
- quantification of damage severity
- prediction of the remaining service life of the structure

Due to the vastness of this subject, it is very difficult in a thesis to work on all the above mentioned five aspects. The scope of the work presented in this thesis concerns the first two steps of SHM i.e., detection and localization of damage. However, identification of the type of damage and its quantification can be achieved by updating of reliable FE models.

At the start of this thesis, shift in modal parameters due to low impact damage was studied in various types of specimens. It appeared clearly that the pertinent way to proceed was to study the effects of impact damage through changes in natural frequency and damping by experiments and FE models which help in the identification of damage in composites. Whereas topology optimization based on experimental results was used to localize damage only in composite laminate beams.

The monitoring of impact damage in this thesis is carried mainly on beam-type specimens of the following type. One thing needs to be highlighted here that all the test specimens used in this thesis have been fabricated personally by the author.

- Composite laminate beams
- Honeycomb Sandwich beams
- Entangled Sandwich beams

The conclusion of the experimental results for each of the above type of beams shall be discussed separately for the sake of clarity.

Composite Laminate Beams

- The vibration test results on pristine and damaged composite laminate beams show that with the accumulation of damage in the specimens, there is a decrease in natural frequency accompanied by an increase in damping ratio.
- An interesting new feature developed in our study is that the vibration tests are carried out by placing steel masses at the two ends of the test-beams in order to enhance the shift between the modal parameters between the undamaged and the damaged cases.
- Results show that damping ratio is a more sensitive parameter for damage detection than the natural frequency.
- Better and noise free vibration test results are obtained by gluing reflecting stickers on the measurement points. The noise free measurements by gluing the stickers enhance the quality of damping results, which as compared to natural frequency is a property that is far less stable and should be therefore estimated with extra care. High quality measurements are done by using a Laser Vibrometer.
- For the composite laminate beams, the Ideas Test Lab system with Polyreference curve fitting algorithm was not available to validate the damping results by sine-dwell testing, as damping is a parameter that is difficult to estimate with confidence. Therefore a novel parameter by the name of damage index is introduced based on the integral of the amplitude of the frequency response functions, in order to verify the damping ratio results estimated by Polymax which are not stable for certain specimens. For the test-beams where damping decreases with damage, damage index shows an increase validating the theoretical reasoning.
- Energy of impact is highlighted as the factor having the most significant effect on the modal parameters by carrying out design of experiments on the experimental data. Furthermore, the Half Bandwidth Method is found unsuitable for damping estimation in the presence of damage.

Honeycomb Sandwich Beams

- In a case of honeycomb sandwich beams, similar vibration tests have been carried out on pristine and damaged honeycomb sandwich beams. This time vibration tests have been carried out using both burst random (LMS Test Lab) and sine dwell excitations (Ideas Test Lab) in order to compare that which testing method gives a more logical estimation of damping in the presence of damage.
- The modal parameters show similar tendency as previously in case of composite laminates i.e., damage prompts a decrease in natural frequency accompanied by an increase in damping ratio.
- End steel masses also enhance the shift in modal parameters in sandwich beams but this shift is very less prominent as compared to the composite laminate beams.

- Again, damping seems to be more sensitive to damage than the natural frequency. So it is reasonable to assume that damping may be used instead of natural frequency as a damage indicator tool for structural health monitoring purposes.
- Presence of non-linearity in the impacted sandwich beams is proved by carrying out sine-dwell testing upwards and downwards in frequency which unfortunately could not be done incase of the composite laminate beams, it is observed that in the presence of non-linearity, there is always a change in amplitude coupled with a slight shift in frequencies in the FRFs.
- The aim of using design of experiments is to improve the understanding of impact damage in composites. Design of experiments carried out on the extracted modal parameters show highlighted density of damage as the factor having the most significant effect on the modal parameters and give an indication that sine-dwell excitation based modal testing gives more reliable estimation of damping in the presence of damage as compared to burst random testing. This is an interesting result because similar design of experiments carried out on the modal parameter results in case of composite laminate beams highlighted energy of impact as the most significant parameter, but in the case of honeycomb sandwich beams it is the density of damage that is the most significant parameter.

Entangled Sandwich Beams

- An important and novel aspect of this thesis concerns the fabrication and mechanical testing of a new sandwich material with carbon fiber entangled core. Entangled sandwich materials possess high damping characteristics and can be used for specific applications like the inner paneling of a helicopter cabin as their structural strength is considerably low.
- Studies have been carried out by varying the quantity of resin in the entangled core. It was concluded that entangled sandwich specimens with lesser resin have better damping characteristics, better resistance against impact but on the other hand, their static strength is low.
- Furthermore, the effect of varying the fiber length in the entangled core has also been studied. If the fiber length is equal to the core thickness (10 mm in our case), a better fiber orientation is obtained. However for fiber length greater than the thickness of the core a relatively poor orientation is obtained which reduces considerably the static strength.
- The damping capabilities and impact toughness of the entangled sandwich beams has also been compared with standard sandwiches having honeycomb and foam cores.
- Vibration tests show that entangled sandwich specimens possess on the average 150 % higher damping ratios and 20 dB lower vibratory levels than the honeycomb and foam sandwich specimens.
- Results prove that both carbon and glass fiber entangled sandwich beams have better impact toughness as compared to honeycomb and foam core sandwiches. But it has to

be remembered that the entangled sandwich beams are nearly two times heavier than the honeycomb and foam core beams of the same dimensions.

- In case of entangled sandwich beams too it is again observed that damping ratio is a more sensitive parameter for damage detection than the natural frequency.
- Design of experiments (DOE) validated the experimental results by proving that sandwich beam with entangled fibers as core material have a more significant effect on the damping ratios and also proved that sine dwell testing is more suitable for damping estimation in the presence of damage as compared to burst random testing.

Finite Element Modeling and Updating of the Experimental/Numerical Correlation

- Simplified Finite element models are developed that represent damaged composite beams in vibrations. These simplified damage models give us a degradation factor that can serve as a warning regarding structure safety.
- The methodology used to model damage in the test-beams is a simple one. Instead of modeling the damage as it is by directly meshing the structure, the material properties of the elements in the damage zones are modified by a coefficient α . This way the problems of excessive gridding number and small mesh sizes are avoided.
- The size and shape of the approximated damage zones in case of composite laminate beams depends on the fairly accurate C-Scan results. The damage zones are circular shaped which is the closest approximation to reality and gives a very good experimental/numerical correlation.
- However for the honeycomb beams due to the unavailability of the C-scan results, damage surface was approximated by tapping. Consequently the results were less accurate as compared to the composite laminates.
- The longitudinal Elastic Modulus (E_L) is varied in the circular damage zones for the composite laminate beams, because trial tests highlighted (E_L) as the material property which has the most profound effects on the natural frequencies. The material property varied in the damage zones in case of the honeycomb sandwich beams is the shear modulus (G_{xz}), which seems to have the most significant effect on the modal parameters.
- A statistical error is defined, and that value of the modification coefficient α is chosen that gives the minimum statistical error between the experimental and numerical results. This process is first done for the undamaged case and then for the damaged cases. The statistical error for the natural frequencies and FRF amplitudes should match that for the previous case whether it is an undamaged or a damaged case.
- In the case of composite laminate beams generally a very good experimental/numerical correlation is obtained. However, it needs to be highlighted that our methodology only stands for the cases where the damage is small i.e., around the BVID limit where the behavior of the structure remains more or less linear. Once the level of damage goes well beyond that corresponding to the BVID limit (Example of Beam 5, impacted by clamping all four ends), this approach starts showing

deficiencies. In order to model high damage successfully in composite laminates, an advanced material law has to be chosen and calculations have to be carried in FE softwares by using non-linear modules (solvers).

- For the honeycomb sandwich beams, a good correlation is obtained certainly for the undamaged case (UD) and also to some extent for the damaged case (D1). But in case of the damaged state (D2) which is the damage at 4 points, unsatisfactory correlation results are obtained, because due to the nature of the honeycomb (cell or corner) the damage density varies a lot. With the current methodology where the material properties are reduced by the same factor at each damage point, it is not a very good idea to model asymmetric damage.
- Finite element modeling of the dynamic response of the carbon fiber entangled sandwich beams has also been performed. The experimental/numerical correlation was less than satisfactory due to multiple peaks in the experimentally obtained FRF due to the non-homogeneous distribution of the resin. This asymmetric behavior due to random distribution of fibers and resin is not possible to simulate numerically in this thesis, because in the FE model the fiber entangled core is considered completely homogeneous and isotropic i.e., having the same properties in all directions. Therefore the aspect of spraying resin in the manufacturing process of the entangled materials has to be improved in future in order to obtain homogeneous sandwich materials like those with honeycomb and foam cores, and only then shall the FE modeling can be successfully carried out.

Damage Localization by Topology Optimization

- The second part of the numerical work concerns the application of a damage localization tool developed by H. Niemann, J. Morlier and A. Shahdin, based on topology optimization in Nastran using the experimentally obtained modal parameters (Chapter 3). Material is removed in the precise zones of the FE model in order to minimize the error between the experimental and numerical frequency response functions (FRFs), this way an equivalent damage is modeled. Thus topology optimization is a diagnostic tool (for all types of materials) and requires only the undamaged state for localization of damages.
- From the obtained results it can be concluded that their quality depended vastly on the choice of the optimization parameters. These optimization sensitive parameters can be divided in two main groups. The first one consists of the parameters related to the optimization process i.e., penalization exponents and objective functions, and the other depends upon the quality of the experimental results. Since higher resonance frequencies usually show a higher shift when damaged, therefore vibration tests should be carried out with a larger bandwidth if possible. But with higher frequencies the necessary modal identification becomes more difficult as higher modes are more susceptible to noise and furthermore the higher modes participate less and less in the actual dynamic response.
- Results on composite laminate beams (Beam 4) showed that with topology optimization the right damage locations have been found rather efficiently at lower damage levels (D1) i.e., first state of damage in our case.

- However during trial tests, while comparing with the experimental results (C-Scan) sometimes the results were less clear and the optimization got stuck in wrong local optima more often. But it can be assumed that this anomaly is mostly due to the simplistic approach taken and the lack of constraint data and for not taking into account damping that controls the FRF amplitudes. Still, with a suitable choice of parameters, for composite beams some good results with correct localization of the impacts is achieved.

7.2 Overall Comparison

In the last section, an overall comparison between the different types of beams tested in this thesis is provided. Different experimental parameters are compared which give an idea regarding the efficiency of these types of materials regarding impact toughness and damage detectability etc. In order to compare efficiently the different types of test beams, the comparison is carried out at the same level of damage i.e., 0.1-0.3 mm indentation depth which is below the BVID limit, as the aim of vibration based damage detection methods is to detect damages that are not visible on the surface, but can be quite harmful. The following points are helpful in understanding the overall comparison:

- The shift in modal parameters presented in this table, is between the undamaged state and the damage state with 4 impacts
- Damage detection is based on the average shift in damping ratio, as experimentally damping was proved more sensitive to damage than the frequency ('+' sign shows significance of damage detection, increase in '+' signs signifies better detectability)
- Impact toughness is based on the average shift in natural frequencies in our case, as decrease in natural frequency signifies loss of rigidity which gives a measure of resistance against impact ('+' sign shows significance of impact toughness, increase in '+' signs signifies better impact toughness)

Type of Test Beams	Damage Level (Indentation depth)	Method of Excitation	Significant Parameter (DOE)	Damage Detectability (Shift in Damping)	Impact Toughness (Decrease in Frequency)
Composite Laminate	0.1-0.3 mm	Burst Random	Impact Energy (IE)	+++ 66 %	++++ 4 %
Long Honeycomb Sandwich	0.1-0.3 mm	Burst Random & Sine-Dwell	Density of Damage (DD)	++ + + 221 %	+ 27 %
Long Carbon Entangled Sandwich	Heavy	0.1-0.3 mm	Burst Random	Density of Damage (DD)	++ + 8 %
	Light	0.1-0.3 mm	Burst Random	Density of Damage (DD)	++ 16 %

7.3 Future Works and Perspectives

The author has succeeded in achieving a few things during the three year thesis, but as it is true for every other thesis and research work, there remains still a lot that could not be achieved due to the lack of time and sometimes due to unavailability of equipment, technical support and material. All these aspects which the author did not develop which could have shed more light on principal idea of the thesis, the author has laid them out in the future work. It needs to be highlighted that work on a few of these aspects discussed below has already been started with help of undergraduate and master students, and if a few of them are finished in time, these results shall be presented at the time of the thesis defense.

- In this thesis, a simple case of symmetric impacts has been chosen on all the test-beams in order to have a globally homogeneous density of damage. Work has been started on asymmetric impacts on composite laminate beams. The procedure will be that one composite laminate beam shall be impacted at three random positions on each side with the same impact energy e.g., 10 J. Another similar beam shall be impacted with the same impact energy but at five positions on one side and one position on the other. The shift in modal parameters as a result of damage for both these cases shall be compared to a reference composite laminate beam with three symmetric impacts on each ends. So this way, by keeping the same impact energy and only changing the positions of impact, the effect of asymmetric impacts on the modal parameters shall be evaluated. If a significant difference is observed as compared to the symmetric case, then this study shall also be carried out on the honeycomb sandwich beams.
- In case of the composite laminate beams, only one lay-up of the plies has been used $[0/90/45/-45]_{3s}$, which was proposed by Saravos and Hopkins [52] in which the delamination is said to have a more profound effect on the dynamic characteristics. Other commonly used lay-ups e.g., $[90/45/-45/0]_{3s}$, $[45/-45/90/0]_{3s}$ shall be used to fabricate similar composite laminate beams, which shall be impacted with the same energy in order to study the effect of modal parameter shifts on the lay-up of composite laminate plies.
- All the test-beams in this thesis have been tested by burst random and sine-dwell excitations with the exception of a few that have only been tested by burst random. However, the excitation level has always been kept 1 N. In the future, it is envisaged to vary this excitation level for the same damaged beam in order see whether by changing the excitation level the damping ratios are effected are not.
- In the presented work, all the impacts have been carried out with a hemispherical head of 12.7 mm. It would be interesting to impact similar test-beams with the same energy, by changing only the shape and size of impact heads. Again the aim shall be to study the shift in modal parameters. It is important to note that in all these studies, only one parameter shall be varied at a time for the sake of clarity.
- All the above mentioned studies shall enrich our knowledge in the domain of impacts on composite laminate beams and a better statistical analysis can be carried out by design of experiments. Based on this information damage detection algorithms shall be built in future to monitor damage in composite specimens.

- As it has been found in this thesis, that the damping ratios shifts are far more significant than the stiffness changes. Therefore in future based on the works of Montalvao et al. [53], a method shall be developed that uses the modal damping factor variation from a reference state to a damaged state as feature. It will also make use of the modal strain shapes, described by what is called a plane shape function (PSF), as a tool to spatially describe the local sensitivity to damage.
- When modeling impact damage in honeycomb sandwich beams, detailed information on the shape and extent of the damage could not be obtained by ultrasound (C-scan) results. This lack of knowledge made us assume the damaged surface which consequently resulted in less satisfactory experimental/numerical correlation. To rectify this problem, the honeycomb beams shall be cut around the damaged area and the beams shall be observed by a Scanning Electron Microscope (SEM). The aim shall be to obtain accurate information regarding the shape and surface of the damage surface. Furthermore, the impact points shall be modeled in such a way that material properties can be varied separately at each impact point, because in the sandwich beams the density of damage varies a lot and depends on the point of impact (cell corner or center).
- Precise modelling of the damage phenomenon (delamination, matrix cracking etc) in composite laminates. This will help in damage identification step of SHM
- As the entangled sandwich specimens are in the phase of development and extensive research, so there are certain modifications that have to be carried out in future to improve the manufacturing process, which will enhance the quality and performance of these novel sandwiches. First of all, the aspect of spraying resin on the fibers in the manufacturing process of the entangled materials has to be improved, so that homogeneous sandwich materials like those with honeycomb and foam cores can be developed.
- Once entangled sandwiches with a homogeneous core are fabricated, only then shall the finite element modeling be undertaken seriously. Furthermore, with these enhanced entangled sandwich beams, comparison with enhanced sandwich structures e.g., honeycomb sandwiches with viscoelastic layers, rubber-type cores made of butyl rubber, integrated core sandwich composites etc shall be fabricated in order to compare the damping characteristics and impact toughness of entangled sandwich beams with other enhanced sandwiches available in the market.
- Topology optimization approach for damage localization is only validated for few numerical examples (2D, 3D) and one composite laminate beam. So in the near future, this study shall be extended to all the other composite laminate and sandwich beams presented in this thesis. As C-scan testing is incapable of detecting damage in composite sandwiches, so the main interest of localizing damage in sandwiches by topology optimization will be to locate damage that can be achieved by C-Scan tests. Prospects of this work also could be the implementation of further design responses like directly addressing the mentioned anti-resonances or mode shapes by referencing to the imaginary part of the FRFs and by increasing the frequency bandwidth to take in to account higher modes that are more sensitive to damage. Also, changes in damping shall be considered as matching parameters.

Annex for Chapter 3

Table 3.A Frequency change ratios (%) between the undamaged (UD) and the two damaged states (D1 and D2) for the six Type-2 composite beams impacted by clamping two ends (-ve sign indicate increase in frequency with the increase in damage)

Beam No	Between States	Mode 1	Mode 2	Mode 3	Mode 4
Beam 2	UD & D1	0.5	0.9	1.0	1.4
3J	UD & D2	3.2	1.5	1.7	2.1
Beam 3	UD & D1	1.2	1.1	1.2	1.9
4J	UD & D2	2.6	2.2	2.1	2.3
Beam 4	UD & D1	3.4	1.6	4.1	5.0
7J	UD & D2	4.1	3.4	7.3	8.0
Beam 5	UD & D1	-1.2	1.7	4.0	3.7
8J	UD & D2	-0.4	4.7	5.3	6.3
Beam 6	UD & D1	3.9	1.6	5.1	3.3
9J	UD & D2	-2.5	3.9	6.5	5.5
Beam 7	UD & D1	-1.8	2.8	3.9	3.7
10J	UD & D2	5.1	4.0	5.2	5.8

Table 3.B Damping change ratios (%) between the undamaged (UD) and the two damaged states (D1 and D2) for the six Type-2 composite beams impacted by clamping two ends (-ve sign indicate decrease in damping with the increase in damage)

Beam No	Between States	Mode 1	Mode 2	Mode 3	Mode 4
Beam 2	UD & D1	179.5	-42.6	69.8	-14.4
3J	UD & D2	313.1	137.9	272.2	-9.0
Beam 3	UD & D1	1.3	35.3	152.5	16.7
4J	UD & D2	5.63	68.3	61.0	-35.5
Beam 4	UD & D1	12.9	19.5	40.3	-12.2
7J	UD & D2	19.9	53.5	47.2	14.6
Beam 5	UD & D1	44.6	-20.5	73.4	-6.9
8J	UD & D2	22.7	-87.2	348.6	2.0
Beam 6	UD & D1	5.9	3.0	5.3	68.8
9J	UD & D2	49.2	7.1	11.9	33.2
Beam 7	UD & D1	4.9	26.3	840.9	-2.9
10J	UD & D2	45.5	-103.4	-125.0	5.8

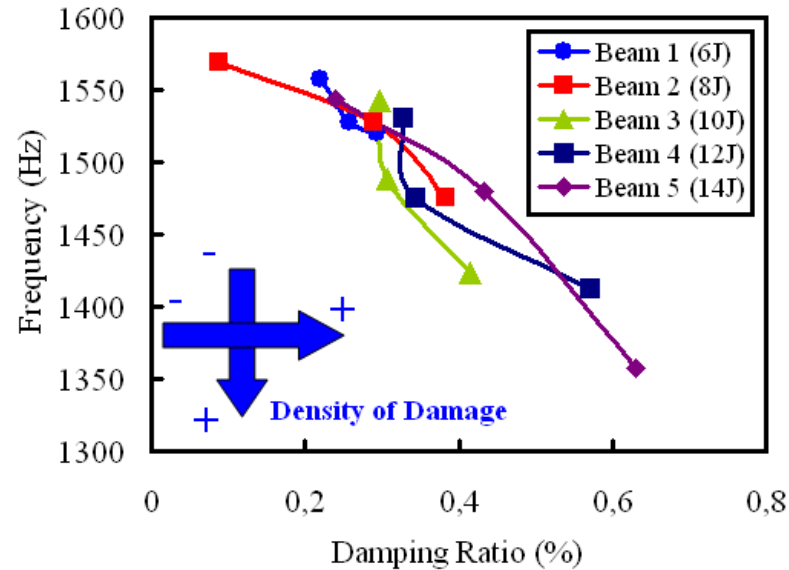


Figure 3.A Variation of natural frequencies with damping ratio for an increase in density of damage for (a) 2nd bending mode and (b) 3rd bending mode for Composite Beam 1 (6J), Beam 2 (8J), Beam 3 (10J), Beam 4 (12J) and Beam 5 (14J) impacted by clamping all four ends, where (UD) is undamaged state, (D1) damaged at 4 impact points and (D2) damaged at 8 impact points

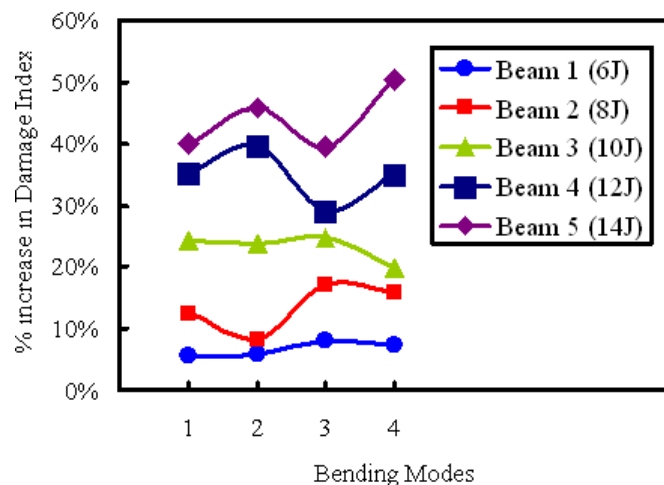


Figure 3.B Variation of percentage of increase in Damage Index as a function of modes for the five Type-2 composite beams impacted by clamping all four ends

Annex for Chapter 6

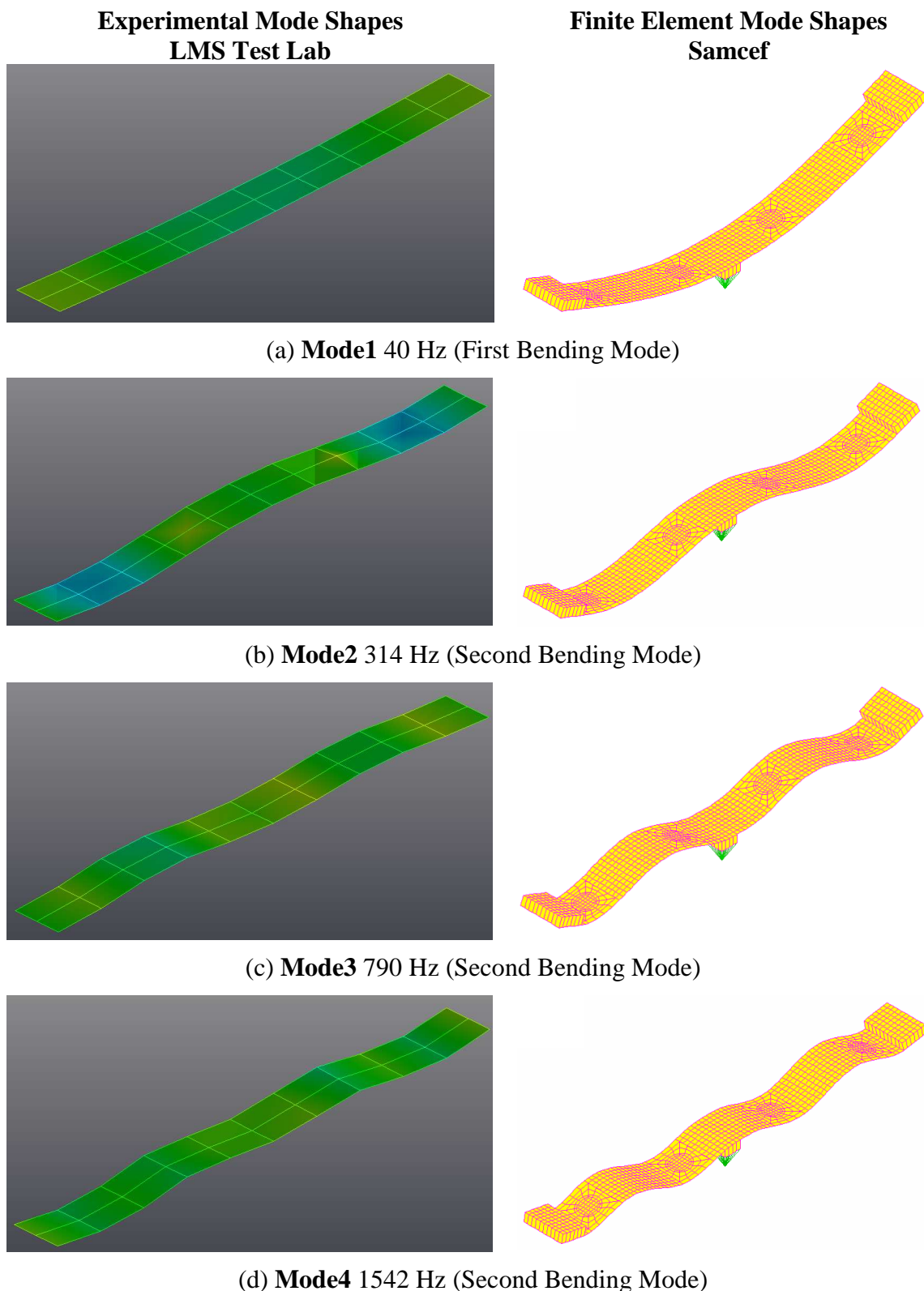


Figure 6.A Comparison of the first four experimental and numerical (FE) bending modes
Inconclusive results of the ultrasound tests (C-Scan) on Beam 3 impacted at 4 J by clamping two ends

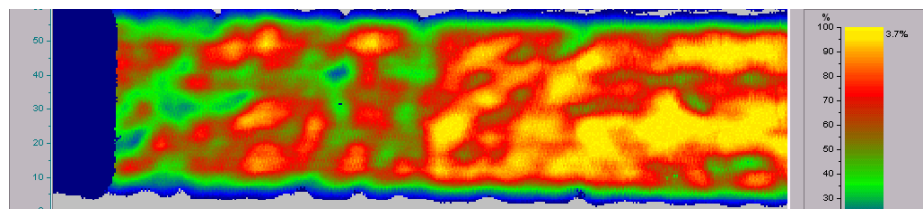


Figure 6.B Inconclusive results of the ultrasound tests (C-Scan) on Beam 3 impacted at 4 J by clamping two ends

Beam 5 (8 J) (two ends clamped)

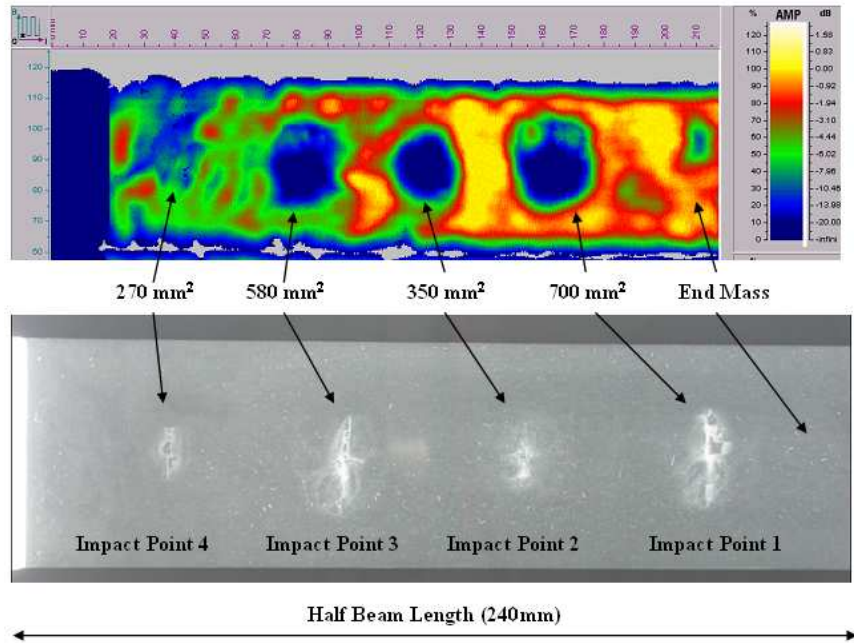


Figure 6.C Calculation of the damaged surface for the composite laminate Beam 5 impacted by clamping two ends for half beam length at 8 J (a) Ultrasound (C-Scan) results (b) Radiographic results

Table 6.A Comparison of experimental and numerical natural frequencies for Beam 5 impacted by clamping two ends, for the undamaged state (UD) and the two damage states (D1 and D2) along with the statistical error and the modification coefficient

Bending Modes No	Natural Frequencies (Hz)						
	Undamaged (UD)		Damaged (D1)		Damaged (D2)		
	Exp	Num (FE)	Exp	Num (FE)	Exp	Num (FE)	
1	37.1	37.6	36.3	35.8	36	34.8	
2	284.2	289.5	279.2	280.2	270.7	279.3	
3	716.9	727.5	687.9	700.1	678.7	680.3	
4	1416.8	1403.9	1363.3	1360.8	1326.5	1327.2	
	α_{UD}	1.15	α_{D1}	6.58	α_{D2}	6.58	
	$E_{freq,UD}(\alpha_{UD})$	8.76	$E_{freq,D1}(\alpha_{D1})$	6.25	$E_{freq,D2}(\alpha_{D2})$	4.43	

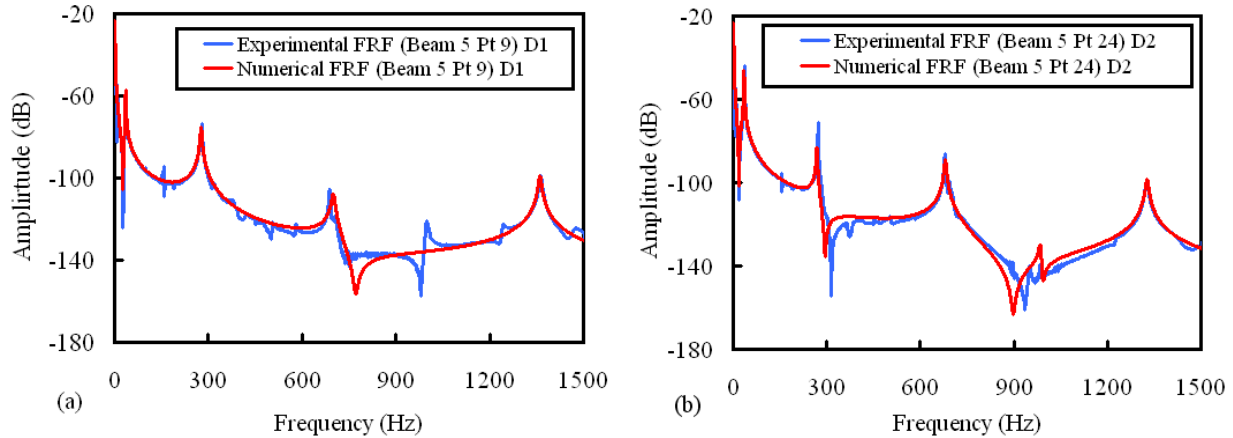


Figure 6.D Comparison of experimental and numerical FRFs for Beam 5 impacted by clamping two ends for the damaged states D1 and D2 for the measurement points 5 and 24 respectively

Table 6.B Comparison of experimental and numerical FRF amplitudes for Beam 5 impacted by clamping two ends, for the undamaged state (UD) and the two damage states (D1 and D2) along with the statistical error and the modification coefficient

Bending Modes No	FRF Amplitudes (dB)					
	Undamaged (UD)		Damaged (D1)		Damaged (D2)	
	Exp	Num (FE)	Exp	Num (FE)	Exp	Num (FE)
1	-47.4	-44.1	-58.8	-57.4	-56.8	-56.1
2	-87.2	-88.5	-73.4	-75.9	-67.8	-72.1
3	-79.7	-85	-104.9	-109.7	-99.2	-104.3
4	-100.6	-99.7	-100.8	-98.1	-102.4	-100.6
	α_{UD}	1.15	α_{D1}	6.58	α_{D2}	6.58
	$E_{amp,UD}(\alpha_{UD})$	3.22	$E_{amp,D1}(\alpha_{D1})$	3.10	$E_{amp,D2}(\alpha_{D2})$	3.48

Beam 6 (9 J) (two ends clamped)

Table 6.C Comparison of experimental and numerical natural frequencies for Beam 6 impacted by clamping two ends, for the undamaged state (UD) and the two damage states (D1 and D2) along with the statistical error and the modification coefficient

Bending Modes No	Natural Frequencies (Hz)					
	Undamaged (UD)		Damaged (D1)		Damaged (D2)	
	Exp	Num (FE)	Exp	Num (FE)	Exp	Num (FE)
1	36.3	37.6	34.9	36.5	37.3	34.9
2	285.2	289.5	280.5	283.2	275.01	282.9
3	713	727.5	690.6	706.6	683.5	683.4
4	1410.5	1404.1	1359.13	1360.5	1347.2	1332.5
	α_{UD}	1.15	α_{D1}	6.63	α_{D2}	6.63
	$E_{freq,UD}(\alpha_{UD})$	8.24	$E_{freq,D1}(\alpha_{D1})$	8.18	$E_{freq,D2}(\alpha_{D2})$	8.43

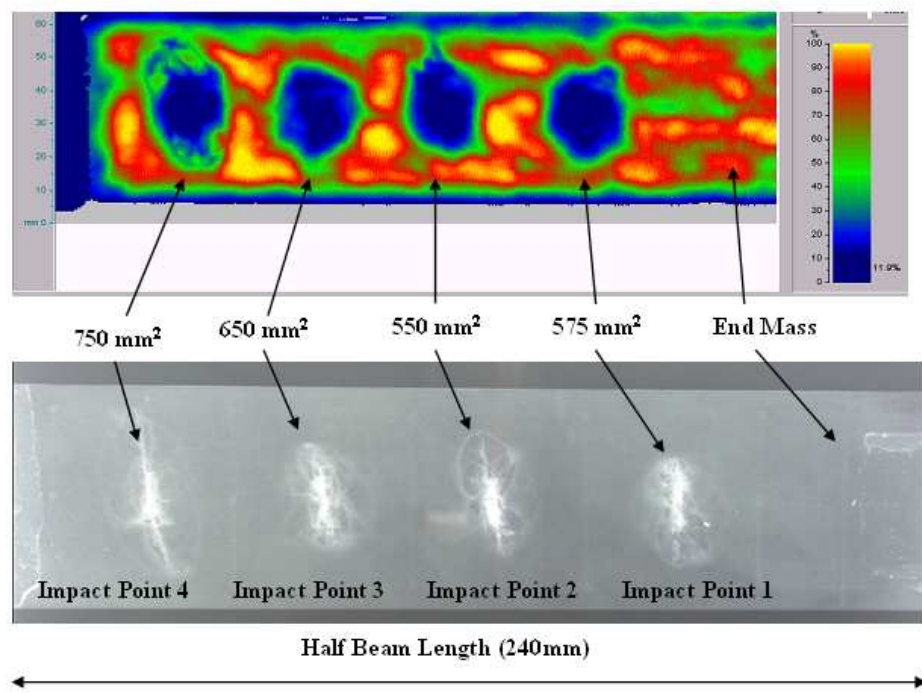


Figure 6.E Calculation of the damaged surface for the composite laminate Beam 6 impacted by clamping two ends for half beam length at 9 J (a) Ultrasound (C-Scan) results (b) Radiographic results

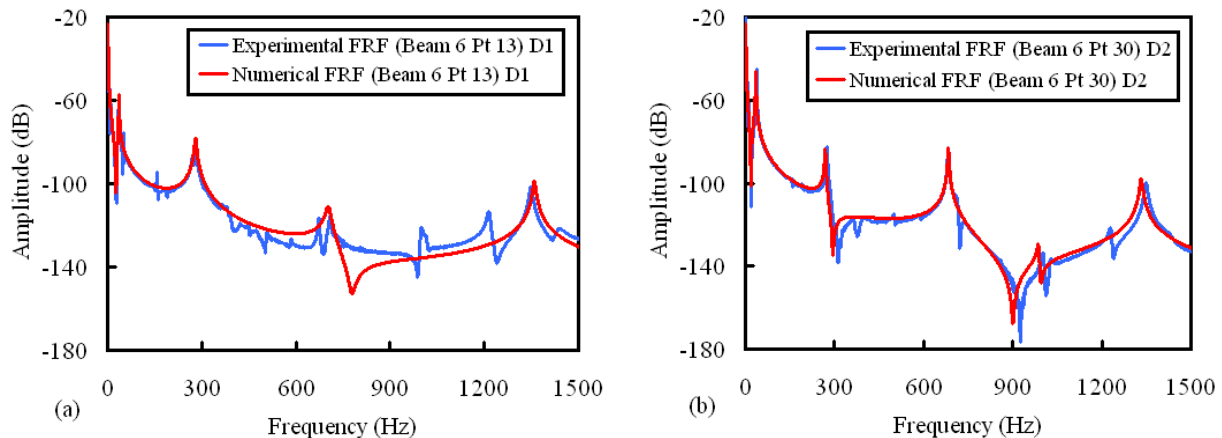


Figure 6.F Comparison of experimental and numerical FRFs for Beam 6 impacted by clamping two ends for the damaged states D1 and D2 for the measurement points 13 and 30 respectively

Table 6.D Comparison of experimental and numerical FRF amplitudes for Beam 6 impacted by clamping two ends. for the undamaged state (UD) and the two damage states (D1 and D2) along with the statistical error and the modification coefficient

Bending Modes No	FRF Amplitudes (dB)					
	Undamaged (UD)		Damaged (D1)		Damaged (D2)	
Exp	Num (FE)	Exp	Num (FE)	Exp	Num (FE)	
1	-68.4	-59.2	-44.7	-47.1	-45.3	-52.2
2	-74.2	-77.9	-87.8	-91.3	-83.8	-89.2
3	-111.1	-108.8	-95.3	-98.8	-85.8	-81.8
4	-99.8	-101.4	-102.7	-106.4	-101.8	-98.6
α_{UD}	1.15	α_{D1}	6.63	α_{D2}	6.63	
$E_{amp,UD}(\alpha_{UD})$	5.15	$E_{amp,D1}(\alpha_{D1})$	3.31	$E_{amp,D2}(\alpha_{D2})$	5.07	

Beam 7 (10 J) (two ends clamped)

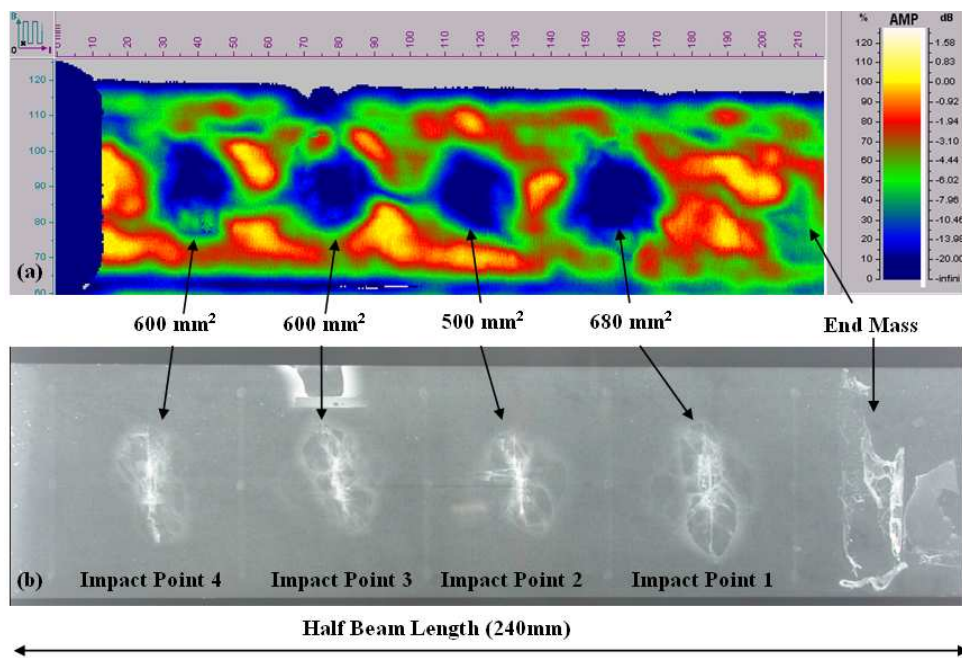


Figure 6.G Calculation of the damaged surface for the composite laminate Beam 7 impacted by clamping two ends for half beam length at 10 J (a) Ultrasound (C-Scan) results (b) Radiographic results

Table 6.E Comparison of experimental and numerical natural frequencies for Beam 7 impacted by clamping two ends, for the undamaged state (UD) and the two damage states (D1 and D2) along with the statistical error and the modification coefficient

Bending Modes No	Natural Frequencies (Hz)						
	Undamaged (UD)		Damaged (D1)		Damaged (D2)		
Exp	Num (FE)	Exp	Num (FE)	Exp	Num (FE)	Exp	Num (FE)
1	36.4	37.6	37.1	35.4	34.5	34.5	
2	284.3	289.6	276.3	278.6	272.8	283.1	
3	717.2	727.5	686.8	693.6	677.7	677.7	
4	1414.7	1404.1	1362.3	1349.5	1331.5	1320.6	
	α_{UD}	1.15	α_{D1}	7.05	α_{D2}	7.05	
	$E_{freq,UD}(\alpha_{UD})$	7.87	$E_{freq,D1}(\alpha_{D1})$	7.39	$E_{freq,D2}(\alpha_{D2})$	7.50	

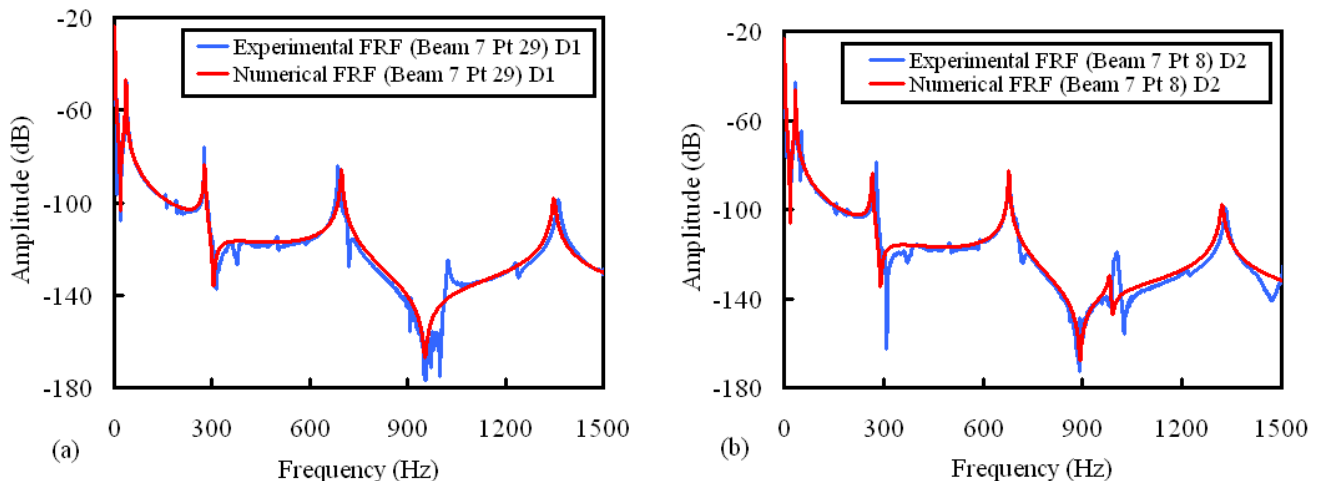


Figure 6.H Comparison of experimental and numerical FRFs for Beam 7 impacted by clamping two ends for the damaged states D1 and D2 for the measurement points 29 and 8 respectively

Table 6.F Comparison of experimental and numerical FRF amplitudes for Beam 7 impacted by clamping two ends. for the undamaged state (UD) and the two damage states (D1 and D2) along with the statistical error and the modification coefficient

Bending Modes No	FRF Amplitudes (dB)						
	Undamaged (UD)		Damaged (D1)		Damaged (D2)		
Exp	Num (FE)	Exp	Num (FE)	Exp	Num (FE)	Exp	Num (FE)
1	-47.9	-48.9	-48.2	-46.8	-42.8	-46.1	
2	-78.4	-85.1	-77	-85.1	-79.9	-85.1	
3	-74.9	-85.2	-85.1	-89	-85.5	-84.3	
4	-101.6	-100.9	-99.9	-100.1	-101.4	-97.3	
	α_{UD}	1.15	α_{D1}	7.05	α_{D2}	7.05	
	$E_{amp,UD}(\alpha_{UD})$	6.17	$E_{amp,D1}(\alpha_{D1})$	4.55	$E_{amp,D2}(\alpha_{D2})$	3.75	

Beam 1 (6 J) (four ends clamped)

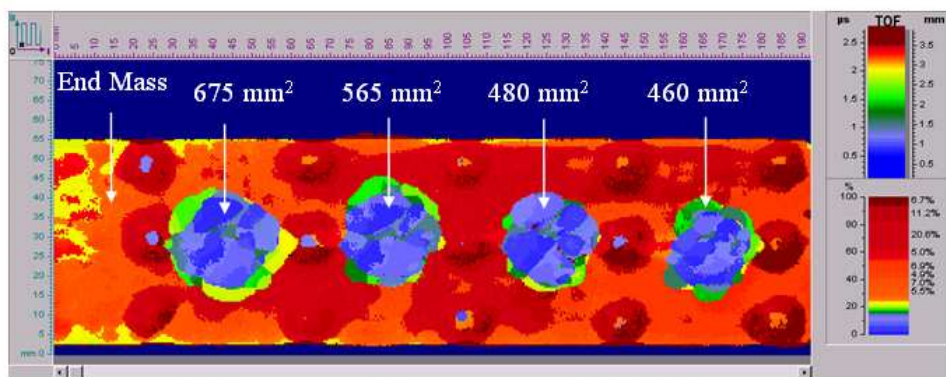


Figure 6.I Ultrasound (C-Scan) results showing the calculated damaged surface for the composite laminate Beam 1 impacted at 6 J by clamping all four ends for half beam length

Table 6.G Comparison of experimental and numerical natural frequencies for Beam 1 impacted by clamping all four ends for the undamaged state (UD) and the two damage states (D1 and D2) along with the statistical error and the modification coefficient

Bending Modes No	Natural Frequencies (Hz)					
	Undamaged (UD)		Damaged (D1)		Damaged (D2)	
	Exp	Num (FE)	Exp	Num (FE)	Exp	Num (FE)
1	40.8	41.3	39.3	40.1	38.9	39.9
2	316.2	316.5	307.9	308.9	306.7	308.6
3	796.9	793.7	781	781.2	779.7	786.7
4	1557.2	1534.2	1527.5	1509.8	1520.5	1529.8
	α_{UD}	1.02	α_{D1}	3.22	α_{D2}	3.22
	$E_{freq,UD}(\alpha_{UD})$	8.76	$E_{freq,D1}(\alpha_{D1})$	6.25	$E_{freq,D2}(\alpha_{D2})$	4.43

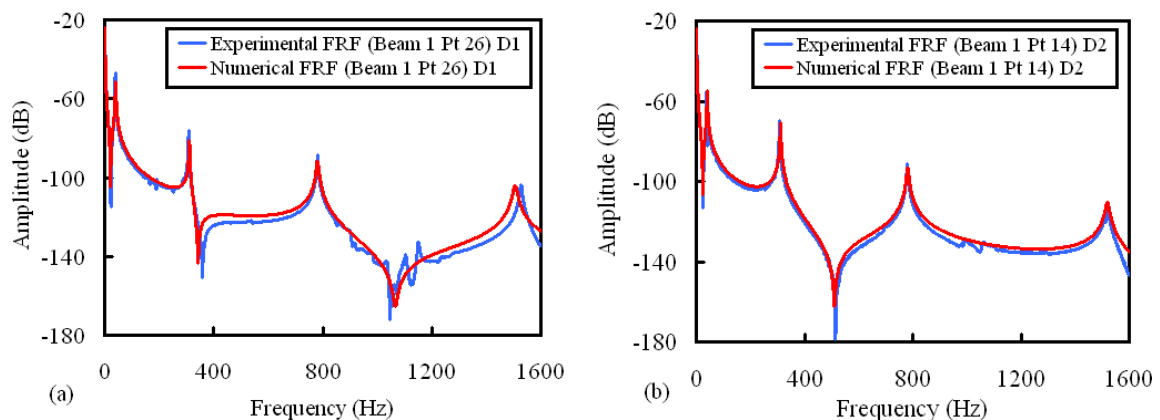


Figure 6.J Comparison of experimental and numerical FRFs for Beam 1 impacted by clamping all four ends for the damaged states D1 and D2 for the measurement points 26 and 14 respectively

Table 6.H Comparison of experimental and numerical FRF amplitudes for Beam 1 impacted by clamping all four ends for the undamaged state (UD) and the two damage states (D1 and D2) along with the statistical error and the modification coefficient

Bending Modes No	FRF Amplitudes (dB)						
	Undamaged (UD)		Damaged (D1)		Damaged (D2)		
Exp	Num (FE)	Exp	Num (FE)	Exp	Num (FE)	Exp	Num (FE)
1	-47	-52.6	-46.7	-52.8	-52.8	-55.3	
2	-78.5	-82.8	-76.1	-81.8	-68.1	-71.1	
3	-89.6	-87.3	-90.8	-92.2	-91.8	-95.1	
4	-105.3	-103.5	-106.1	-105.5	-109.5	-111.9	
α_{UD}	1.00		α_{D1}	3.22		α_{D2}	3.22
$E_{amp,UD}(\alpha_{UD})$	3.82		$E_{amp,D1}(\alpha_{D1})$	4.24		$E_{amp,D2}(\alpha_{D2})$	2.55

Beam 2 (8 J) (four ends clamped)

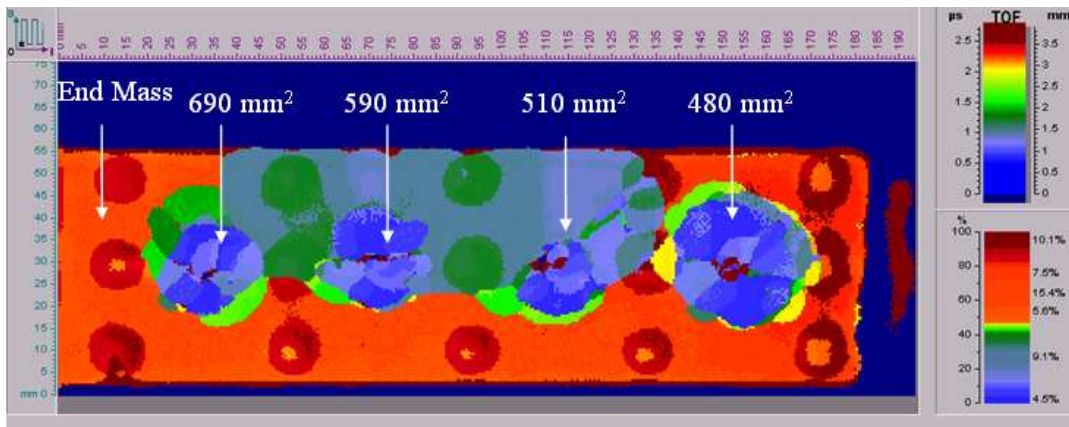


Figure 6.K Ultrasound (C-Scan) results showing the calculated damaged surface for the composite laminate Beam 2 impacted at 8 J by clamping all four ends for half beam length

Table 6.I Comparison of experimental and numerical natural frequencies for Beam 2 impacted by clamping all four ends for the undamaged state (UD) and the two damage states (D1 and D2) along with the statistical error and the modification coefficient

Bending Modes No	Natural Frequencies (Hz)						
	Undamaged (UD)		Damaged (D1)		Damaged (D2)		
Exp	Num (FE)	Exp	Num (FE)	Exp	Num (FE)	Exp	Num (FE)
1	42.1	41.8	39.5	40.2	38.3	39.1	
2	319.1	320.3	310.5	309.6	307.2	306.3	
3	803.1	803.1	779.5	779.3	766.1	767.3	
4	1568.7	1546.6	1527.3	1507	1475.6	1496.1	
α_{UD}	1.00		α_{D1}	3.30		α_{D2}	3.30
$E_{freq,UD}(\alpha_{UD})$	11.07		$E_{freq,D1}(\alpha_{D1})$	10.17		$E_{freq,D2}(\alpha_{D2})$	10.29

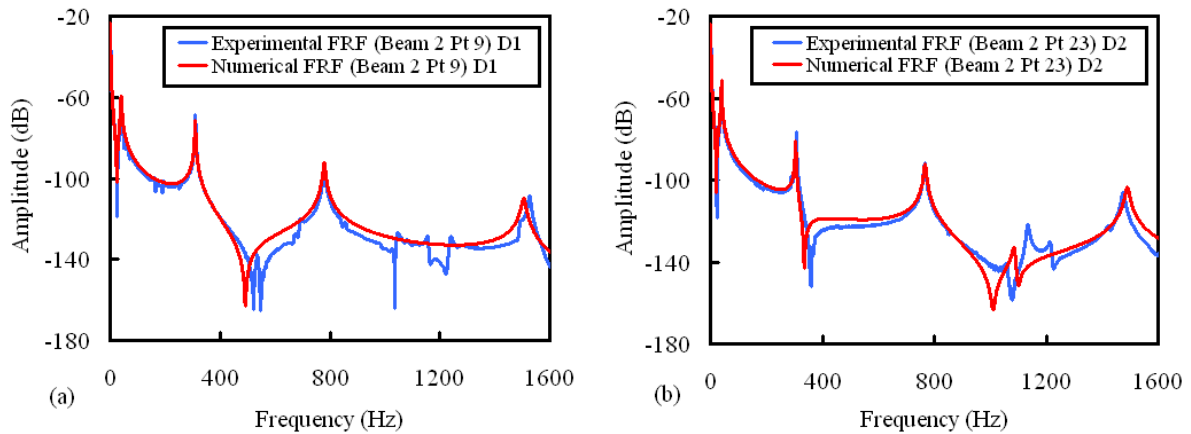


Figure 6.L Comparison of experimental and numerical FRFs for Beam 2 impacted by clamping all four ends for the damaged states D1 and D2 for the measurement points 9 and 23 respectively

Table 6.J Comparison of experimental and numerical FRF amplitudes for Beam 2 impacted by clamping all four ends for the undamaged state (UD) and the two damage states (D1 and D2) along with the statistical error and the modification coefficient

Bending Modes No	FRF Amplitudes (dB)						
	Undamaged (UD)		Damaged (D1)		Damaged (D2)		α_{UD}
	Exp	Num (FE)	Exp	Num (FE)	Exp	Num (FE)	
1	-48.3	-50.1	-68.8	-60.5	-54.5	-51.8	
2	-69.7	-72.7	-69.3	-71.5	-70.2	-74.3	
3	-89	-86.7	-93.3	-93.5	-93.3	-96.7	
4	-103.8	-109.4	-110.1	-112.1	-105.8	-110	
	α_{UD}	1.00	α_{D1}	3.30	α_{D2}	3.30	
	$E_{amp,UD}(\alpha_{UD})$	3.50	$E_{amp,D1}(\alpha_{D1})$	4.42	$E_{amp,D2}(\alpha_{D2})$	3.65	

Beam 3 (10 J) (four ends clamped)

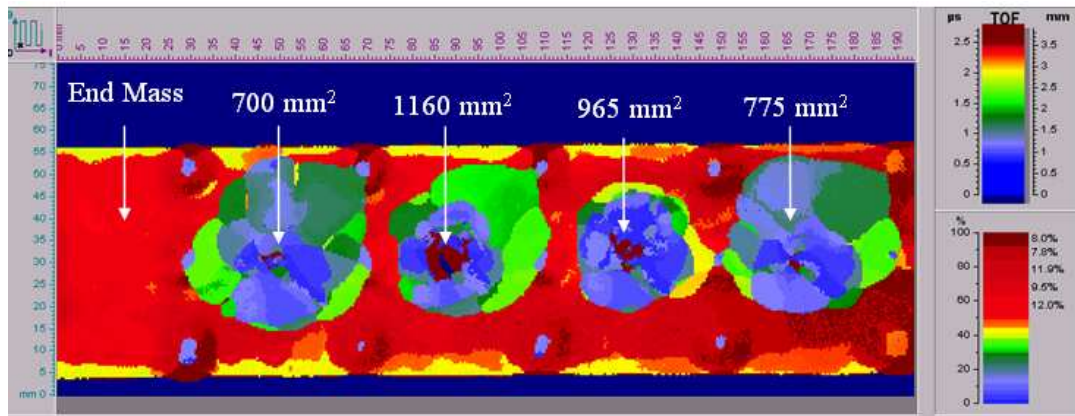


Figure 6.M Ultrasound (C-Scan) results showing the calculated damaged surface for the composite laminate Beam 3 impacted at 10 J by clamping all four ends for half beam length

Table 6.K Comparison of experimental and numerical natural frequencies for Beam 3 impacted by clamping all four ends for the undamaged state (UD) and the two damage states (D1 and D2) along with the statistical error and the modification coefficient

Bending Modes No	Natural Frequencies (Hz)						
	Undamaged (UD)		Damaged (D1)		Damaged (D2)		
	Exp	Num (FE)	Exp	Num (FE)	Exp	Num (FE)	
1	41.5	41.2	39.5	39.6	39.2	38	
2	314.5	315.5	306.2	304.8	305.6	293.3	
3	789.8	791.4	761	767.6	755.6	738.4	
4	1542.5	1520.1	1485.2	1482.9	1423.8	1434.8	
	α_{UD}	1.00	α_{D1}	2.43	α_{D2}	2.43	
	$E_{freq,UD}(\alpha_{UD})$	11.24	$E_{freq,D1}(\alpha_{D1})$	9.32	$E_{freq,D2}(\alpha_{D2})$	12.53	

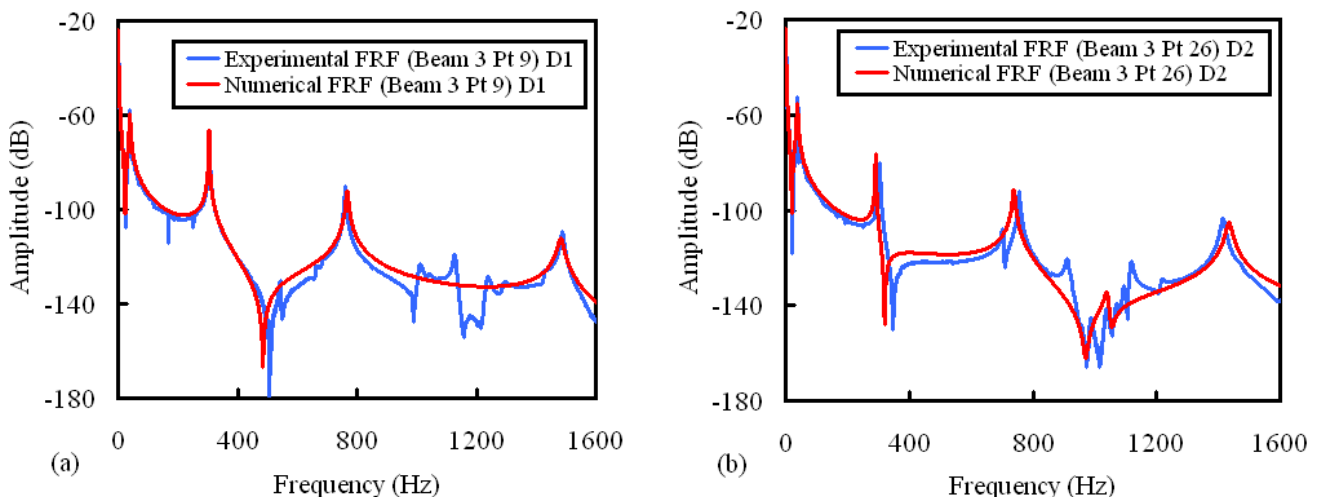


Figure 6.N Comparison of experimental and numerical FRFs for Beam 3 impacted by clamping all four ends for the damaged states D1 and D2 for the measurement points 9 and 26 respectively

Table 6.L Comparison of experimental and numerical FRF amplitudes for Beam 3 impacted by clamping all four ends for the undamaged state (UD) and the two damage states (D1 and D2) along with the statistical error and the modification coefficient

Bending Modes No	FRF Amplitudes (dB)						
	Undamaged (UD)		Damaged (D1)		Damaged (D2)		
	Exp	Num (FE)	Exp	Num (FE)	Exp	Num (FE)	
1	-48.9	-53.4	-55	-57.4	-54.3	-60.2	
2	-70.2	-72.8	-69.3	-79.2	-72.8	-65.3	
3	-88.7	-88.1	-91.2	-92.9	-94.3	-93.3	
4	-112.5	-109.3	-120.5	-117.5	-113.2	-112.4	
	α_{UD}	1.00	α_{D1}	2.43	α_{D2}	2.43	
	$E_{amp,UD}(\alpha_{UD})$	3.07	$E_{amp,D1}(\alpha_{D1})$	5.38	$E_{amp,D2}(\alpha_{D2})$	4.81	

Beam 4 (12 J) (four ends clamped)

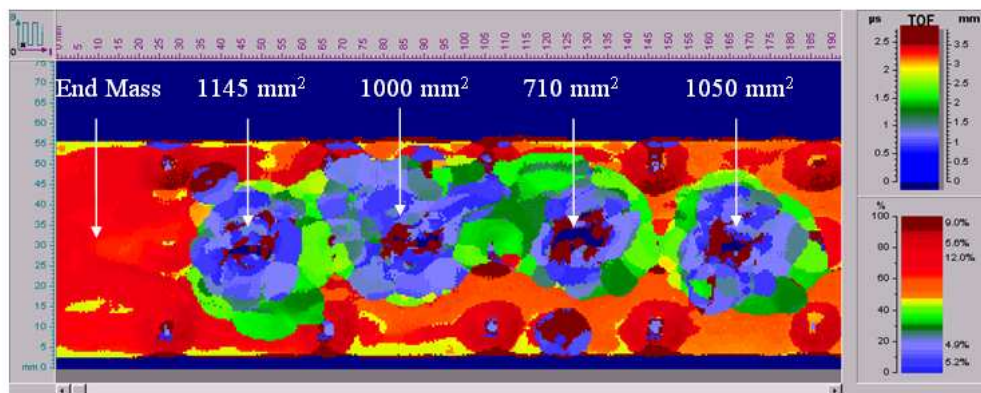


Figure 6.O Ultrasound (C-Scan) results showing the calculated damaged surface for the composite laminate Beam 4 impacted at 12 J by clamping all four ends for half beam length

Table 6.M Comparison of experimental and numerical FRF amplitudes for Beam 4 impacted by clamping all four ends for the undamaged state (UD) and the two damage states (D1 and D2) along with the statistical error and the modification coefficient

Bending Modes No	Undamaged (UD)		FRF Amplitudes (dB)		Damaged (D2)	
	Exp	Num (FE)	Exp	Num (FE)	Exp	Num (FE)
1	-49.2	-51.4	-57.6	-54.4	-54.8	-54.3
2	-69.1	-72.5	-70.1	-71.5	-71.3	-70.9
3	-90.1	-85.7	-92.9	-100.3	-96.1	-100.5
4	-101.9	-106.4	-111.1	-114.4	-116.1	-114.5
	α_{UD}	1.00	α_{D1}	2.63	α_{D2}	2.63
	$E_{amp,UD}(\alpha_{UD})$	4.32	$E_{amp,D1}(\alpha_{D1})$	4.41	$E_{amp,D2}(\alpha_{D2})$	3.36

Beam 5 (14 J) (four ends clamped)

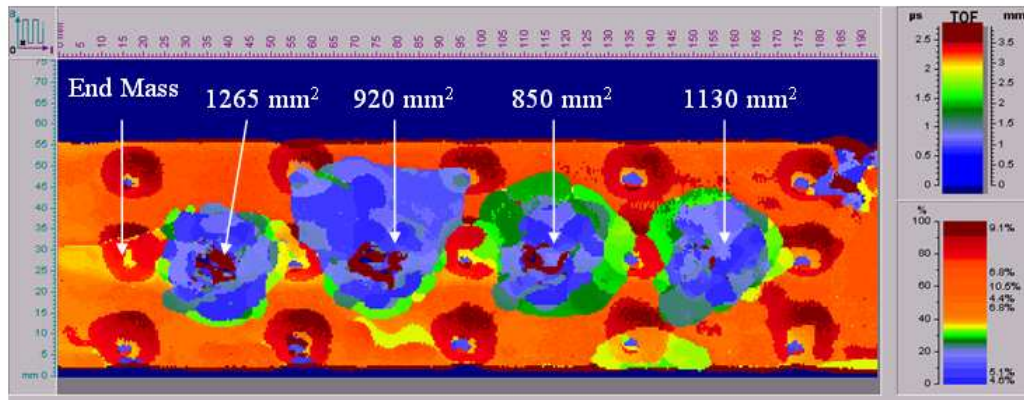


Figure 6.P Ultrasound (C-Scan) results showing the calculated damaged surface for the composite laminate Beam 5 impacted at 14 J by clamping all four ends for half beam length

Table 6.N Comparison of experimental and numerical FRF amplitudes for Beam 5 impacted by clamping all four ends for the undamaged state (UD) and the two damage states (D1 and D2) along with the statistical error and the modification coefficient

Bending Modes No	FRF Amplitudes (dB)						
	Undamaged (UD)		Damaged (D1)		Damaged (D2)		
Exp	Num (FE)	Exp	Num (FE)	Exp	Num (FE)	Exp	Num (FE)
1	-52.8	-52.7	-50.2	-54.7	-50.6	-50.7	
2	-67.5	-71.8	-76.7	-78.7	-85.9	-86.3	
3	-90.8	-87.3	-108	-105.8	-106.6	-105.3	
4	-108	-108.8	-114.4	-116.1	-106.2	-109.7	
α_{UD}	1.00	α_{D1}	3.72	α_{D2}	3.72		
$E_{amp,UD}(\alpha_{UD})$	2.80	$E_{amp,D1}(\alpha_{D1})$	2.83	$E_{amp,D2}(\alpha_{D2})$	1.88		

Beam H2 (4 J) (Honeycomb Sandwich)

Table 6.O Comparison of experimental and numerical FRF amplitudes Honeycomb Beam H2 (4J) for the undamaged state (UD) and the two damage states (D1 and D2) along with the statistical error and the modification coefficient

Bending Modes No	FRF Amplitudes (dB)						
	Undamaged (UD)		Damaged (D1)		Damaged (D2)		
Exp	Num (FE)	Exp	Num (FE)	Exp	Num (FE)	Exp	Num (FE)
1	-73.4	-75.2	-76.3	-71.9	-92.6	-89.3	
2	-92.8	-96.8	-101.5	-100.6	-99.6	-91.2	
3	-118.6	-113.1	-114.3	-111.2	-120.2	-126.3	
α_{UD}	1.00	α_{D1}	350	α_{D2}	350		
$E_{amp,UD}(\alpha_{UD})$	4.06	$E_{amp,D1}(\alpha_{D1})$	3.15	$E_{amp,D2}(\alpha_{D2})$	5.45		

Beam H3 (6 J) (Honeycomb Sandwich)

Table 6.P Comparison of experimental and numerical natural frequencies for Honeycomb Beam H3 (6J) for the undamaged state (UD) and the two damage states (D1 and D2) along with the statistical error and the modification coefficient

Bending Modes No	Natural Frequencies (Hz)						
	Undamaged (UD)		Damaged (D1)		Damaged (D2)		
Exp	Num (FE)	Exp	Num (FE)	Exp	Num (FE)	Exp	Num (FE)
1	143.9	147.2	128.1	135.4	106.0	138.0	
2	756.1	751.3	676.7	661.6	522.7	535.7	
3	1334.7	1332.9	1152.6	1148.6	1006.5	978.2	
α_{UD}	1.00	α_{D1}	560	α_{D2}	560		
$E_{freq,UD}(\alpha_{UD})$	3.52	$E_{freq,D1}(\alpha_{D1})$	9.95	$E_{freq,D2}(\alpha_{D2})$	25.78		

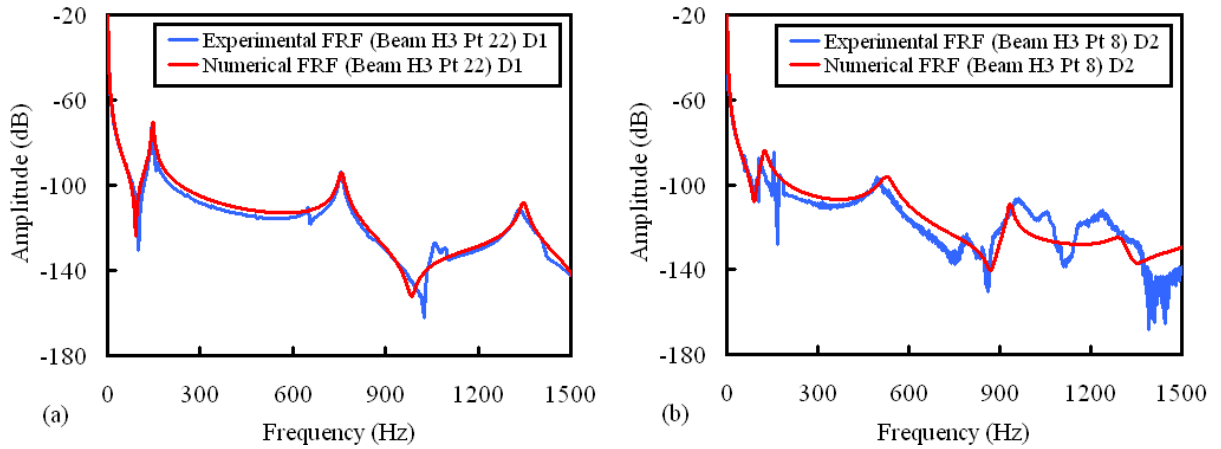


Figure 6.Q Comparison of experimental and numerical FRFs for Long Honeycomb Beam H3 for the two damaged states D1 and D2 for the measurement points 22 and 8 respectively

Table 6.Q Comparison of experimental and numerical FRF amplitudes Honeycomb Beam H3 (6J) for the undamaged state (UD) and the two damage states (D1 and D2) along with the statistical error and the modification coefficient

Bending Modes No	Undamaged (UD)		FRF Amplitudes (dB)		Damaged (D2)	
	Exp	Num (FE)	Exp	Num (FE)	Exp	Num (FE)
1	-77.8	-76.2	-84	-80.5	-76.7	-77.5
2	-91.9	-93.5	-94.8	-97.7	-100.2	-98.9
3	-116.3	-112.2	-124.3	-120.4	-122.6	-113.2
α_{UD}	1.00		α_{D1}	560	α_{D2}	560
$E_{amp,UD}(\alpha_{UD})$	2.70		$E_{amp,D1}(\alpha_{D1})$	3.46	$E_{amp,D2}(\alpha_{D2})$	5.50

Beam H4 (8 J) (Honeycomb Sandwich)

Table 6.R Comparison of experimental and numerical natural frequencies for Honeycomb Beam H4 (8J) for the undamaged state (UD) and the two damage states (D1 and D2) along with the statistical error and the modification coefficient

Bending Modes No	Undamaged (UD)		Natural Frequencies (Hz)		Damaged (D2)	
	Exp	Num (FE)	Exp	Num (FE)	Exp	Num (FE)
1	144.2	147.2	116.2	123.2	99.7	108.1
2	752.7	750.0	605.8	603.4	475.9	482.2
3	1327.6	1330.1	1084.3	1081.5	862.8	842.4
α_{UD}	1.00		α_{D1}	756	α_{D2}	756
$E_{freq,UD}(\alpha_{UD})$	2.74		$E_{freq,D1}(\alpha_{D1})$	4.57	$E_{freq,D2}(\alpha_{D2})$	13.25

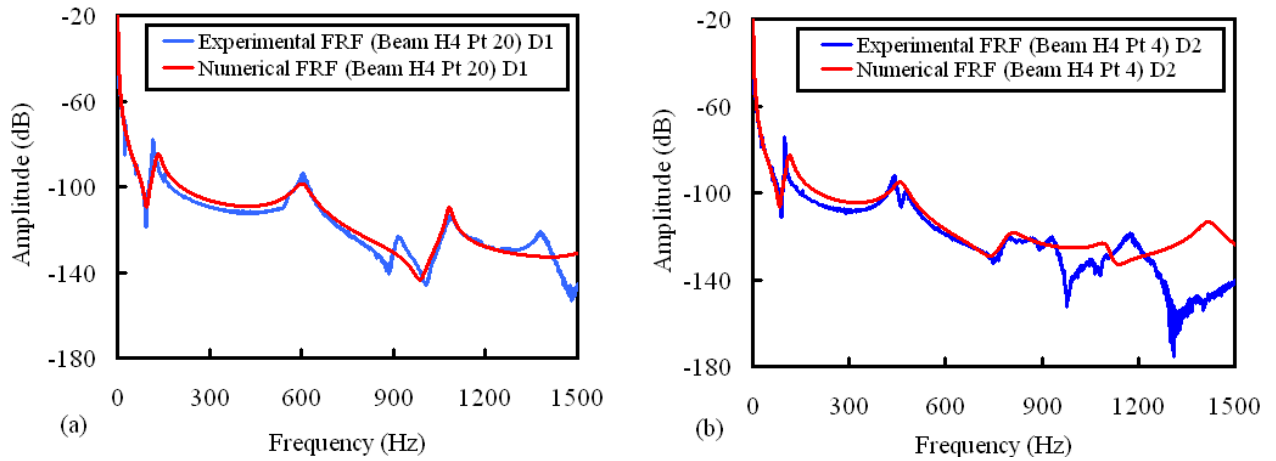


Figure 6.R Comparison of experimental and numerical FRFs for Long Honeycomb Beam H4 for the two damaged states D1 and D2 for the measurement points 20 and 4 respectively

Table 6.S Comparison of experimental and numerical FRF amplitudes Honeycomb Beam H4 (8J) for the undamaged state (UD) and the two damage states (D1 and D2) along with the statistical error and the modification coefficient

Bending Modes No	FRF Amplitudes (dB)						
	Undamaged (UD)		Damaged (D1)		Damaged (D2)		
	Exp	Num (FE)	Exp	Num (FE)	Exp	Num (FE)	
1	-67.6	-77.7	-78.9	-86.2	-76.7	-83.8	
2	-92.5	-92.6	-95.2	-100.6	-92.8	-96.6	
3	-120.8	-117.2	-115.2	-111.4	-118.2	-120.16	
	α_{UD}	1.00	α_{D1}	756	α_{D2}	756	
	$E_{amp,UD}(\alpha_{UD})$	6.19	$E_{amp,D1}(\alpha_{D1})$	5.68	$E_{amp,D2}(\alpha_{D2})$	4.79	

References

- [1] Farrar CR, Worden K. An introduction to structural health monitoring. *Philosophical Transactions of the Royal Society A* 2007;365:303-315.
- [2] Farrar CR, Lieven AJ. Damage prognosis: the future of structural health monitoring. *Philosophical Transactions of the Royal Society A* 2007;365:623-632.
- [3] Van der Auweraer H. International research projects on structural damage detection. *Key Engineering Materials* 2001;204(2):97–112.
- [4] Zou Y, Tong L, Steven GB. Vibration-based model-dependent damage (delamination) identification and health monitoring for composite structures. A review. *Journal of Sound and Vibration* 2000;230:357-378.
- [5] Yan YJ, Cheng L, Wu ZY, Yam LH. Development in vibration-based structural damage detection technique. *Mechanical Systems and Signal Processing* 2007;21:2198-2211.
- [6] Doebling SW, Farrar CR, Prime MB, Shevitz DW. Damage identification and health monitoring of structural and mechanical systems from changes in their vibration characteristics: a literature review. Research Report LA-13070-MS ESA-EA Los Alamos National Laboratory (1996).
- [7] Sohn H, Farrar CR, Hemez FM, Shunk D, Stinemates DW, Nadler BR. A review of structural health monitoring literature: 1996-2001. Los Alamos National Laboratory Report LA-13976-MS
- [8] Carden EP, Fanning P. Vibration based condition monitoring: A review, *Structural Health Monitoring* 2004;3(4):355–377.
- [9] Schwarz BJ, Richardson MH. Experimental modal analysis. CSI Reliability week Orlando FL (1999).
- [10] Gloth G, Sinapius M. Influence and characterisation of weak non-linearities in swept-sine modal testing. *Aerospace Science and Technology* 2004;8:111-120.
- [11] Fugate ML, Sohn H, Farrar CR. Vibration-based damage detection using statistical process control. *Mechanical Systems and Signal Processing* 2001;15(4):707-721.
- [12] Waldron K, Ghoshal A, Schulz MJ, Sundaresan MJ, Ferguson F, Pai PF, Chung JH. Damage detection using finite elements and laser operational deflection shapes. *Journal of Finite Elements in Analysis and Design* 2002;38:193-226.
- [13] Sundaresan MJ, Pai PF, Ghoshal A, Schulz MJ, Ferguson F, Chung J. Methods of distributed sensing for health monitoring of composite material structures. *Composites A Journal* 2001;32:1357-1374.
- [14] LeClerc JR, Worden K, Staszewski WJ, Haywood J. Impact detection in an aircraft composite panel – a neural network approach. *Journal of Sound and Vibration* 2007;299(3): 672-682.
- [15] Banks HT, Inman DJ, Leo DJ, Wang Y. An experimentally validated damage detection theory in smart structures. *Journal of Sound and Vibration* 1996;191:859–880.
- [16] Garesci F, Catalano L, Petrone F. Experimental results of a damage detection methodology using variations in modal parameters. *Experimental Mechanics* 2006;4:441-451.
- [17] Yan YJ, Yam LH. Online detection of crack damage in composite plates using embedded piezoelectric actuators/sensors and wavelet analysis. *Composite Structures* 2002; 58(1):29–38.
- [18] Kao CY, Hung SL. Detection of structural damage via free vibration responses generated by approximating artificial neural networks. *Computers & Structures* 2003;81(28–29):2631–2644.
- [19] Wojtowicki JL, Jaouen L. New approach for the measurements of damping properties of materials using oberst beam. *Review of Scientific Instruments* 2004;75(8):2569-2574.

- [20] Vanhoenacker K, Schoukens J, Guillaume P, Vanlanduit S. The use of multisine excitations to characterise damage in structures. *Mechanical Systems and Signal Processing* 2004;18:43-57.
- [21] Cheraghi N, Riley MJ. A novel approach for detection of damage in adhesively bonded joints in plastic pipes based on vibration method using piezoelectric sensors. *Systems, Man and Cybernetics, IEEE International Conference* 2005;4:3472- 3478.
- [22] Yam LH, Yan YJ, Wei Z. Vibration-based non-destructive structural damage detection, *Advances in Non-destructive Evaluation, PT 1-3. Key Engineering Materials* 2004;270-273(Part 1-3):446-1453.
- [23] Yan YJ, Hao HN, Yam LH. Vibration-based construction and extraction of structural damage feature index. *International Journal of Solids and Structures* 2004;41(24-25):6661-6676.
- [24] Yan YJ, Yam LH, Cheng L, Yu L. FEM modeling method of damage structures for structural damage detection. *Composite Structures* 2006;72(2):193-199.
- [25] Schubel PM, Luo JJ, Daniel IM. Impact and post impact behaviour of composite sandwich panels. *Composites Part A* 2007;38:1051-1057.
- [26] Dear JP, Lee H, Brown SA. Impact damage processes in composite sheet and sandwich honeycomb materials. *International Journal of Impact Engineering* 2005;32:130-154.
- [27] Petit S, Bouvet C, Bergerot A, Barrau JJ. Impact and compression after impact experimental study of a composite laminate with a cork thermal shield. *Composites Science and Technology* 2007;67:3286-3299.
- [28] Bull PH, Edgren F. Compressive strength after impact of CFRP-foam core sandwich panels in marine applications. *Composites Part B* 2004;35(6-8):535-41.
- [29] Abrate S. Impact on composite structures. Cambridge University Press 1988.
- [30] Sierakowski RL, Chaturvedi SH. Dynamic loading and characterization of fiber-reinforced composites. A Wiley-Interscience Publication (1997).
- [31] Sierakowski RL, Newaz GM. Damage tolerance in advanced composites. Technomic Publication (1995).
- [32] Zagainov GI, Lozino-Lozinski GE. Composite materials in aerospace design. Soviet Advanced Composite Technologies Series (1996).
- [33] Abi Abdallah E, Bouvet C, Broll B, Barrau JJ. Experimental analysis of damage creation and permanent indentation on highly oriented plates. *Composites Science and Technology* doi:10.1016/j.compscitech.2009.02.029
- [34] Kessler SS, Spearing SM, J. Attala M, Cesnik CES, Soutis C. Damage detection in composite materials using frequency response. *Composites Part B* 2002;33:87-95.
- [35] Della CN, Shu D. Vibration of delaminated composite laminates: A Review. *Applied Mechanics Reviews* 2007;60:1-20.
- [36] Yam LH, Cheng L, Wei Z, Yan YJ. Damage detection of composite structures using dynamic analysis. *Key Engineering Materials* 2005;295-296:33-39.
- [37] Montalvao D, Maia NMM, Ribeiro AMR. A review of vibration-based structural health monitoring with special emphasis on composite materials. *The Shock and Vibration Digest* (2006) doi:10.1177/0583102406065898
- [38] Adams RD, Cawley P. The localisation of defects in structures from measurements of natural frequencies. *Journal of Strain Analysis* 1979;14:49-57.
- [39] Kim HY, Hwang W. Effect of debonding on natural frequencies and frequency response functions of honeycomb sandwich beams. *Composite Structures* 2002;55:51-62.
- [40] Lestari W, Qiao P. Damage detection of fiber-reinforced polymer honeycomb sandwich beams. *Composite Structures* 2005;67:365-373.
- [41] Yam LH, Cheng L. Damage detection of composite structures using dynamic analysis. *Key Engineering Materials* 2005;295-296:33-39.

- [42] Arkaduiz JZ. Non-linear vibration of a delaminated composite beam. *Key Engineering Materials* 2005;293-294:607-614.
- [43] Giannocaro NI, Messina A. Fatigue damage evaluation of notched specimens through resonance and anti-resonance data. *Engineering Failure Analysis* 2005;13:340-352.
- [44] Tracy JJ, Pardoen GC. Effect of delamination on the natural frequencies of composite laminates. *Journal of Composite Materials* 1989;23(12):1200-1215.
- [45] Khoo LM, Mantena PR, Jadhav P. Structural damage assessment using vibration modal analysis. *Structural Health Monitoring* 2004;3(2):177-194.
- [46] Mattson SG, Pandit SM. Damage detection and localization based on outlying residuals. *Smart Materials and Structures* 2006;15:1801-1810.
- [47] Salawu OS. Detection of structural damage through changes in frequency: a review. *Engineering Structures* 1996;19(9):718-23.
- [48] Shahdin A, Morlier J, Gourinat Y. Significance of low energy impact damage on modal parameters of composite beams by design of experiments. Open access on-line Journal of Physics Conference Series (MPSVA 2009).
- [49] Adams RD. Damping in composites. *Material Science Forum* 1993;119-121:3-16.
- [50] Nelson DJ, Hancock JW. Interfacial slip and damping in fiber-reinforced composites. *Journal of Material Science* 1978;13:2429-2440.
- [51] Chandra R. A study of dynamic behavior of fiber-reinforced composites. *Proceedings of Workshop on Solid Mechanics*, University of Roorkee, India, 1985:59-63.
- [52] Saravanos DA, Hopkins DA. Effects of delaminations on the damped dynamic characteristics of composites. *Journal of Sound and Vibration* 1995;192:977-993.
- [53] Montalvao D, Ribeiro AM, Duarte-Silva J. A method for the localization of damage in a CFRP plate using damping. *Mechanical Systems and signal Processing* (2008) doi:10.1016/j.ymssp.2008.08.011.
- [54] Gibson RF. Modal vibration response measurements for characterization of composite materials and structures, *Composites Science and Technology* 2000;60:2769-2780.
- [55] Kyriazoglou C, Le Page BH. Vibration Damping for crack detection in composite laminates. *Composites Part A* 2004;35:945-953.
- [56] Colakoglu M. Description of fatigue damage using a damping monitoring technique. *Turkish Journal of Engineering and Environmental Sciences* 2003;27:125-130.
- [57] Zhang Z, Hartwig G. Relation of damping and fatigue damage of unidirectional fibre composites. *International Journal of Fatigue* 2004;24:713-738.
- [58] Richardson MH, Mannan MA. Correlating minute structural faults with changes in modal parameters. *Proceedings of SPIE, International Society for Optical Engineering* 1993;1923(2):893-898.
- [59] Shahdin A, Morlier J, Gourinat Y. Correlating low energy impact damage with changes in modal parameters: A preliminary study on composite beams. *Structural Health Monitoring* 2009, doi:10.1177/1475921709341007.
- [60] Shahdin A, Morlier J, Gourinat Y. Damage monitoring in sandwich beams by modal parameter shifts: A comparative study of burst random and sine-dwell testing. Submitted February 2009 in *Journal of Sound and Vibration*
- [61] Pandey AK, Biswas M, Samman MM. Damage detection from changes in curvature mode shapes. *Journal of Sound and Vibration* 1991;145:321-332.
- [62] Kim JT, Ryu YS, Cho HS, Stubbs N. Damage identification in beam-type structures: frequency-based method vs. mode-shape based method. *Engineering Structures* 2003;25(1):57-67.
- [63] Salawu OS, Williams C. Damage location using vibration mode shapes. *Proceedings of the 12th International Modal Analysis Conference*, Honolulu, Hawaii 1994:933-939.

- [64] Dong C, Zhang P, Feng W, Huang T. The sensitivity study of the modal parameters of a cracked beam. Proceedings of the 12th International Modal Analysis Conference, Honolulu, Hawaii 1994:98-104.
- [65] Yam LH, Wei Z, Cheng L. Non-destructive detection of internal delamination by vibration-based method for composite plates. *Journal of Composite Materials* 2004;38(24):2183-2198.
- [66] Yan YJ, Lam LH. FEM modeling method of damage structures for structural damage detection. *Composite Structures* 2004;72:193-199.
- [67] Yang S, Gibson RF, Gu L, Chen WH. Modal parameter evaluation of degraded adhesively bonded composite beams *Composite Structures* 1998;43:79-91.
- [68] Hou JP, Jeronimidis G. Vibration of delaminated thin plates. *Composites Part A* 1999;30:989-995.
- [69] Teughels A, De Roeck G, Suykens JAK. Global optimization by coupled local minimizers and its application to FE model updating. *Computers & Structures* 2003;81:2337-2351.
- [70] Bendsoe MP, Kikuchi N. Generating optimal topologies in structural design using a homogenization method. *Computer Methods in Applied Mechanics in Engineering* 1992;35:1487–1502.
- [71] Bendsoe MP. Optimal shape design as a material distribution problem. *Structural Optimization* 1989;1:193–202.
- [72] Bendsoe MP, Sigmund O. *Topology Optimization-Theory, Methods and Applications*. Springer Verlag, 2003.
- [73] Ma ZD, Kikuchi N, Hagiwara I. Structural topology and shape optimization for a frequency response problem. *Computational Mechanics* 1993;13:157–174.
- [74] MSC. Software Corporation. *Users Guide for Topology Optimization* (2007).
- [75] Lee JS, Kim JE, Kim YY. Damage detection by the topology design formulation using modal parameters. *International Journal for Numerical Methods in Engineering* 2007;69:1480–1498.
- [76] Wang B, Yang M. Damping of Honeycomb Sandwich Beams, *Journal of Materials Processing Technology* 2000;105:67-72.
- [77] Berthelot JM, Assarar M, Sefrani Y, El Mahi A. Damping analysis of composite materials and structures. *Composite Structures* 2008;85:189-204.
- [78] Li Z, Crocker MJ. Effects of thickness and delamination on the damping in honeycomb-foam sandwich beams. *Journal of Sound and Vibration* 2006;294:473–485.
- [79] Chandra R, Singh SP, Gupta K. Damping studies in fiber-reinforced composites – a review. *Composite Structures* 1999;46:41-51.
- [80] Hao M, Rao MD. Vibration and damping analysis of a sandwich beam containing a viscoelastic constraining layer. *Journal of Composite Materials* 2005;39:1621-1643.
- [81] Rao MD, He S. Dynamic analysis and design of laminated composite beams with multiple damping layers. *AIAA Journal* 1993;31(4):736-745.
- [82] Mead DJ. The measurements of the loss factors of beams and plates with constrained and unconstrained damping layers: A critical assessment. *Journal of Sound and Vibration* 2006;300:744-762.
- [83] Yim JH, Cho SY, Seo YJ, Jang BZ. A study on material damping of 0° laminated composite sandwich cantilever beams with a viscoelastic layer. *Composite Structures* 2003;60(4):367–74.
- [84] Gacem H, Chevalier Y, Dion JL, Soula M, Rezgui B. Nonlinear dynamic behavior of a preload thin sandwich plate incorporating visco-hyperelastic layers. *Journal of Sound and Vibration* 2009, doi:10.1016/j.jsv.2008.11.040.

- [85] Ramkumar K, Ganesan N. Vibration and damping of composite sandwich box column with viscoelastic/electrorheological fluid core and performance comparison. *Materials and Design* 2009, doi:10.1016/j.matdes.2008.12.023.
- [86] Yeh JY, Chen LW. Vibration of a sandwich plate with a constrained layer and electrorheological fluid core. *Composite Structures* 2004;65:251–258.
- [87] Jung WJ, Aref AJ. A combined honeycomb and solid viscoelastic material for structural damping application. *Mechanics and Materials* 2003;53(8):831–844.
- [88] Aref AJ, Jung WJ. Advanced composite panels for seismic and vibration mitigation of existing structures. *Journal of Engineering Materials and Technology* 2006;128(4):618–623.
- [89] Bronowicki AJ, Kaplan A. Viscoelastic damping structures and related manufacturing method. United States Patent 5-342-465, 30 August 1994.
- [90] Lapp CK, Grund PD. Method of making a composite laminate having an internally damped constraining layer. United States Patent 5-250-132, 05 October 1993.
- [91] Obeshaw DF. Structural members containing vibration damping mechanisms and methods for making the same. Patent (wo/2002/004826), 17 January 2002.
- [92] Garai M, Pompoli F. A Simple empirical model of polyester fiber materials for acoustic applications. *Applied Acoustics* 2005;66:1383-1398.
- [93] Golosnoy LO, Cockburn A, Clyne TW. Optimisation of metallic fiber network materials for compact heat exchangers. *Advanced Engineering Materials* 2008;10(3):210-218.
- [94] Zhang BM, Zhao SY, He XD. Experimental and theoretical studies on high-temperature thermal properties of fibrous insulation. *Journal of Quantitative Spectroscopy & Radiative Transfer* 2008;109:1309–1324.
- [95] Gustavsson R. Formable sandwich construction material and use of the material as construction material in vehicles, refrigerators, boats, etc. Patent WO 98/01295, 15th January 1998, AB Volvo.
- [96] Markaki AE, Clyne TW. Ultra light stainless steel sheet material. US patent 10/000117, filed 31st October 2001, Cambridge University.
- [97] Markaki AE, Clyne TW. Mechanics of thin ultra-light stainless steel sandwich sheet material, part i. stiffness. *Acta Mater* 2003;51:1341–1350.
- [98] Dean J, Fallah AS, Brown PM, Louca LA, Clyne TW. Energy absorption during projectile perforation of lightweight panels with metallic fibre cores. 8th International Conference on Sandwich Structures (ICSS 8), Porto, 2008.
- [99] Zhou D, Stronge WJ. Mechanical properties of fibrous core sandwich panels. *International Journal of Mechanical Sciences* 2005;47:775-798.
- [100] Mezeix L, Bouvet C, Castanié B, Poquillon D. A new sandwich structured composite with entangled carbon fibers as core material. *Processing and Mechanical Properties*, 8th International Conference on Sandwich Structures (ICSS 8), Porto, 2008.
- [101] Mezeix L, Bouvet C, Poquillon D. Mechanical behavior of entangled fibers and entangled cross-linked fibers during compression. *Journal of Material Science* 2009;44(14):3652-3661.
- [102] Castéra P. Comportement physico-mecanique des matériaux fibreux cellulosiques considérés comme des milieux aléatoires. Proceeding of Materiaux 2002, Tours, France.
- [103] Baudequin M. Identification des mécanismes physiques mis en jeu lors de la reprise d'épaisseur de la laine de verre. PhD Thesis, Université Pierre et Marie Curie Paris VI, France, 2002.
- [104] Poquillon D, Viguier B, Andrieu E. Experimental data about mechanical behavior during compression tests for various matted fibres. *Journal of Materials Science* 2005;40(22):5963 - 5970.
- [105] Faessel M, Delisée C, F. Bos F, Castéra P. (2005). 3D Modelling of random cellulosic fibrous networks based on x-ray tomography and image analysis. *Composites Science and Technology* 2005;65:1931-1940.

- [106] Shahdin A, Mezeix L, Bouvet C, Morlier J, Gourinat Y. Fabrication and mechanical testing of a new sandwich structure with carbon fiber network core. *Journal of Sandwich Structures and Materials* 2009, doi: 10.1177/1099636208106070
- [107] Shahdin A, Mezeix L, Bouvet C, Morlier J, Gourinat Y. Fabrication and mechanical testing of glass fiber entangled sandwich beams: A comparison with honeycomb and foam sandwich beams. *Composite Structures* 2009;90(4):404-412.
- [108] Wang D. Impact behavior and energy absorption of paper honeycomb sandwich panels. *International Journal of Impact Engineering* 2009;36:110-114.
- [109] Yoo SH, Chang SH. An experimental study on energy absorbing structures made of fabric composites. *Composite Structures* 2008;86:211-219.
- [110] Li G, Jones N. Development of rubberized syntactic foam. *Composite Part A* 2007;38(6):1483-1492.
- [111] Li G, John M. A crumb rubber modified syntactic foam. *Materials Science and Engineering A* 2008;1-2:390-399.
- [112] Torre L, Kenny JM. Impact testing and simulation of composite sandwich structures for civil transportation. *Composite Structures* 2000;50:257-267.
- [113] Huybrechts S, Tsai SW. Analysis and behavior of grid structures. *Composites Science and Technology* 1996;56(9):1001-1015.
- [114] Hosur MV, Abdullah M, Jeelani S. Manufacturing and low-velocity impact characterization of foam filled 3-D integrated core sandwich composites with hybrid face sheets. *Composite Structures* 2005;69(2):167-181.
- [115] Vaidya UK, Hosur MV, Earl D, Jeelani S. Impact response of integrated hollow core sandwich composite panels. *Composites Part A* 2000;31(8):761-772.
- [116] Shahdin A, Mezeix L, Bouvet C, Morlier J, Gourinat Y. Monitoring the effects of impact damages in carbon fiber entangled sandwich beams. *Engineering Structures* 2009, doi:10.1016/j.engstruct.2009.07.008
- [117] De Silva CW. *Vibrations fundamentals and practice*. CRC Press (2000).
- [118] Fundamentals of modal testing. Agilent Technologies, Application Note 243-3.
- [119] Technical review to advance techniques in acoustical, electrical and mechanical measurement. Dual channel FFT analysis. Brüel & Kjaer.
- [120] Fundamentals of modal testing. Agilent Technologies, Application Note 243-3.
- [121] Ahlin K, Brandt A. Experimental modal analysis in practice. Saven EduTech AB, Sweden (2001).
- [122] Avitabile P. Twenty years of structural dynamic modification – A review. *Sound and Vibration Magazine*, January 2003.
- [123] Balmes E. : Modèles expérimentaux complets et modèles analytiques réduits en dynamique des structures. Mémoire de H.D.R, Université Pierre et Marie Curie - Paris VI, 1997.
- [124] Balmes E. Methods for vibration design and validation (2005).
- [125] Gay D, Hua SV. *Composite Materials: Designs and Applications* (2nd edition). CRC Press (2007).
- [126] Steeves CA, Fleck NA. Material selection in sandwich beam construction. *Scripta Materialia* 2004;50:1335–9.
- [127] Allen HG. *Analysis and design of structural sandwich panels*. Pergamon Press, Oxford 1969.
- [128] Zenkert D. *The handbook of sandwich construction*. 442 pages, Chameleon Press Ltd. London, United Kingdom 1997.
- [129] Vinson JR. *The behaviour of sandwich structures of isotropic and composite materials*, Technomic Publishing Co.INC 1999.

- [130] Hayman B, Berggreen C, Jenstrup C, Karlsen K. Advanced mechanical testing of sandwich structures. 8th International Conference on Sandwich Structures (ICSS 8), Porto, 2008. p. 417-427.
- [131] ISO 844:2007, edition 5. Determination of compression properties, International Organization for Standardization 2007.
- [132] ASTM C 393-62. Standard test method for flexural properties of flat sandwich constructions, 1988.
- [133] Sendlein LS, Carlsson LA, Merry LA. Characterization of face sheet/core shear fracture of composite sandwich beams. *Journal of Composite Materials* 1991;25:101-116.
- [134] Frosting Y, Brauch M. Bending of sandwich beams with transversely flexible core. *AIAA Journal* 1990;28(3):523-531.
- [135] Lingaiah K, Suryanarayana BG. Strength and stiffness of sandwich beams in bending. *Experimental Mechanics* 1989;1-9.
- [136] Soares B, Reis L, Silva A. Testing of Sandwich Structures with Cork Agglomerate Cores, 8th International Conference on Sandwich Structures (ICSS 8), Porto, 2008. p. 447-458.
- [137] HexPly 914. Data Sheet, Hexcel Composites, F.R.
- [138] HexPly M21. Data Sheet, Hexcel Composites, F.R.
- [139] HexWeb™, Honeycomb attributes and properties, Hexcel Composites, F.R.
- [140] Meyers RH, Montgomery DC. Response surface methodology, Wiley 1995.
- [141] Yin HP. A new theoretical basis for the bandwidth method and optimal power ratios for the damping estimation. *Mechanical Systems and Signal Processing* 2008; 22(8):1869-1881.
- [142] Morlier J, Chermann B, Gourinat Y. Original statistical approach for the reliability in modal parameters. Proceedings of the International Modal Analysis Conference, IMAC XXVII 2009.
- [143] Aminanda Y, Castanié B, Barrau JJ, Thevenet P. Experimental analysis and modelling of the crushing of honeycomb cores. *Applied Composite Materials* 2005;12(3):213-227.
- [144] ASTM E111-04. (2004). Standard test method for Young's Modulus, Tangent Modulus, and Chord Modulus.
- [145] Timoshenko S. Vibration problems in engineering, John Wiley and Sons, 5th edition, 1990.
- [146] Cook RD. Concepts and applications of finite element analysis, John Wiley and Sons, 2nd edition, 1981.
- [147] Bathe KL. Finite element procedures in engineering analysis. Prentice- Hall, 1982.
- [148] Zienkiewicz OC, Taylor RL. The Finite Element Method. MacGraw-Hill 4th edition, 1986.
- [149] SAMCEF User Manuel 12.1.
- [150] Remouchamps A, Radovcic Y. Theoretical aspects about optimization methods and algorithms. Boss Quattro V5, SAMTECH. (2003).
- [151] Gourinat Y, Belloeil V. A truncated low approach of intrinsic linear and nonlinear damping in thin structures. *Journal of Vibrations and Acoustics* 2007;129:32-38.
- [152] Friswell MI, Mottershead JE. Finite element model updating in structural dynamics Springer 1995.
- [153] Zhang XY, Yang CH. Recent developments in finite element analysis for laminated composite plates. *Composite Structures* 2009;88:147-157.
- [154] Shin K, Hammond J. Fundamentals of signal processing for sound and vibration engineers, John Wiley and Sons, 2008.
- [155] B. Peeters, H. V. Auweraer, P. Guillaume, J. Leuridan. The PolyMAX frequency-domain method: a new standard for modal parameter estimation, *Shock and Vibrations* 11 (2004) 395-409.

Surveillance vibratoire de l'endommagement dû à l'impact sur poutres en matériaux composites stratifiés, sandwiches et matériaux enchevêtrés par variations des paramètres modaux

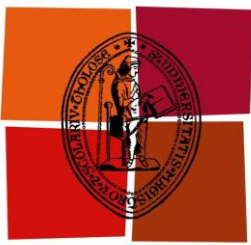
La Surveillance de la Santé des Structures (SSS) s'effectue par la mesure de réponses pertinentes sous sollicitations extérieures. L'identification a pour but de détecter, de localiser et de quantifier ces défauts. La thèse porte sur les deux premiers niveaux de SSS, la détection et la localisation de dommage. Le but est d'étudier les effets d'impacts symétriques par variations des paramètres modaux en faisant un nombre important d'expériences. Une validation par recalage de modèles éléments finis est effectuée sur différents matériaux composites dédiés à l'aéronautique. Pour tous les spécimens (poutres), il a été observé que, avec l'accumulation de l'endommagement (impact), il y a une diminution de la fréquence propre (flexion) accompagnée par une augmentation du taux d'amortissement. Un aspect nouveau de cette thèse concerne la fabrication et les essais mécaniques (statique et dynamique) d'un matériau innovant (sandwich avec âme en fibre de carbones enchevêtrés) possédant des taux d'amortissements élevés ainsi qu'une meilleure résistance à l'impact. La modélisation par éléments finis (Samcef) est utilisée pour calculer la réponse dynamique de ces poutres. Ces modèles recalés permettent de donner un indicateur de taux de dégradation et peuvent servir d'outils diagnostic (et d'alarme) pour la surveillance de l'intégrité des structures. Une partie innovante de cette thèse concerne la localisation de l'endommagement et sa validation sur les poutres composites stratifiées par optimisation topologique (Nastran), en utilisant les paramètres modaux obtenus expérimentalement. Ainsi on estime avec succès les zones d'endommagement pour des défauts isolés.

Mots clés : Structures composites, Vibrations, Surveillance de la santé des structures, Endommagement dû à l'impact

Monitoring of impact damage in composite laminate, honeycomb sandwich and entangled sandwich beams by modal parameter shifts

Impact damage in composite structures may lead to severe degradation of the mechanical behavior due to the loss of structural integrity. Therefore Structural Health Monitoring (SHM) based on vibration testing is useful in detecting this damage caused by impact because damage generally affects the vibration characteristics of a structure. The scope of this thesis concerns the first two steps of SHM i.e., detection and localization of damage. The vibration test results on pristine and damaged composite laminate and composite sandwich beams show that with the accumulation of damage there is a decrease in natural frequency and an increase in the damping ratio. Results show that damping ratio is a more sensitive parameter for damage detection than the natural frequency. An important and novel aspect of this thesis concerns the fabrication and mechanical testing of a new sandwich material with carbon fiber entangled core. Entangled sandwich materials possess high damping characteristics and better impact toughness as compared to standard sandwiches with honeycomb and foam cores and can be used for specific applications like the inner panelling of a helicopter cabin as their structural strength is considerably low. Simplified Finite element models are developed that represent damaged composite beams in vibrations. These simplified damage models give us a degradation factor that can serve as a warning regarding structure safety. The localization of damage is carried out by topology optimization. Results on composite laminate beams showed that with topology optimization the right damage locations have been found rather efficiently at lower damage levels.

Keywords : Composite structures, Vibrations, Structural health monitoring, Impact damage



Université
de Toulouse

THÈSE

En vue de l'obtention du

DOCTORAT DE L'UNIVERSITÉ DE TOULOUSE

Délivré par **l'Institut Supérieur de l'Aéronautique et de l'Espace**
Spécialité : Génie mécanique

Présentée et soutenue par **Amir SHAHDIN**
le 23 juillet 2009

Surveillance vibratoire de l'endommagement dû à l'impact sur poutres en matériaux composites stratifiés, sandwiches et matériaux enchevêtrés par variations des paramètres modaux

Monitoring of impact damage in composite laminate, honeycomb sandwich and entangled sandwich beams by modal parameter shifts

Résumé

JURY

M. Ménad Sidahmed, président
M. Frédéric Bos, rapporteur
M. Paul Cranga
M. Olivier Dorvaux
M. Yves Gourinat, directeur de thèse
M. Joseph Morlier, co-directeur de thèse
M. Hui-Ji Shi, rapporteur

École doctorale : **Mécanique, énergétique, génie civil et procédés**

Unité de recherche : **Équipe d'accueil ISAE DMSM**

Directeur de thèse : **M. Yves Gourinat**
Co-directeur de thèse : **M. Joseph Morlier**



Université
de Toulouse

THÈSE

en vue de l'obtention du

DOCTORAT DE L'UNIVERSITÉ DE TOULOUSE

Délivré par l'**Institut Supérieur de l'Aéronautique et de l'Espace**

Discipline ou Spécialité : Génie Mécanique

Présentée et soutenue par **Amir SHAHDIN**

Le 23 juillet 2009

Surveillance vibratoire de l'endommagement dû à l'impact sur
poutres en matériaux composites stratifiées, sandwiches et
matériaux enchevêtrés par variations des paramètres modaux
(Résumé)

JURY

M. Ménad SIDAHMED
M. Yves GOURINAT
M. Frederic BOS
M. Hui-Ji SHI
M. Olivier DARVAUX
M. Paul CRANGA
M. Joseph MORLIER

Président du jury
Directeur de thèse
Rapporteur
Rapporteur
Examinateur
Examinateur
Co-directeur de thèse

Ecole doctorale : **Mécanique, énergétique, génie civil et procédés**

Unité de recherche : **Equipe d'accueil ISAE DMSM**

Directeur(s) de Thèse : **M. Yves GOURINAT**
Co-directeur de thèse : **M. Joseph MORLIER**

Tables des matières

Chapitre 1 : Etat de l'art sur la surveillance de l'intégrité des structures en matériaux composites	5
Chapitre 2 : Principes d'Analyse modale	11
Chapitre 3 : Surveillance d'endommagements dû à l'impact sur poutres composites stratifiées par variations des paramètres modaux.....	15
Chapitre 4 : Influence du type d'endommagement sur poutres sandwiches en nid d'abeille par diagnostic vibratoire.....	23
Chapitre 5 : Caractérisation statique-dynamique et surveillance d'endommagement dû à l'impact sur poutres sandwiches en fibres enchevêtrées	23
Chapitre 6 : Recalage de modèle Eléments Finis pour la détection, localisation et quantification des défauts.....	27
Chapitre 7 : Conclusion et perspectives	31

Introduction Générale

La surveillance de la santé (SHM) des structures s'effectue par la mesure des réponses pertinentes sous sollicitations environnementales. Elle permet de suivre et d'évaluer les incidents et les anomalies qui peuvent affecter la structure. L'indentification de défauts a pour but de les détecter, de les localiser et de les quantifier. C'est donc une subdivision de la Surveillance de la Santé des Structures (Structural Health Monitoring). Normalement, on utilise cinq niveaux d'identification de défauts :

Niveau 1, la détection : La structure est elle endommagée ou non ?

Niveau 2, la localisation : Où est le défaut sur la structure ?

Niveau 3, la classification : Quel est le type de défaut ?

Niveau 4, la quantification : Quelle est l'importance du défaut ?

Niveau 5, la prédiction : Combien de temps la structure peut elle être utilisée ?

En raison de l'immensité de ce sujet, il est très difficile dans une thèse de travailler sur tous les niveaux d'identification de défauts. L'objectif du travail présenté dans cette thèse porte sur les deux premiers niveaux du SHM c'est-à-dire, l'identification et la localisation de dommage tout en essayant de relier par la variation des paramètres modaux, le phénomène d'endommagement d'une structure avec le phénomène de dissipation. Ainsi, l'objectif de cette thèse est d'étudier les effets d'impacts symétriques par variations des paramètres modaux (fréquences propres, taux d'amortissements et déformées) par un nombre important d'expériences, validées par un recalage de modèles éléments finis sur différents matériaux composites dédiés à l'aéronautique.

Chapitre 1 : Etat de l'art sur la surveillance de l'intégrité des structures en matériaux composites

Les différents mécanismes de dommages dans les matériaux composites, sont classés comme suit :

- Fissuration de la matrice : comprend la rupture de fibres/matrice dans le sens transverse des stratifié
- Délaminage: apparaît à l'interface et est dû au cisaillement inter-laminaire
- Rupture de la fibre: La rupture standard se produit en traction et la rupture en flambage se produit en compression

Les méthodes de détection d'endommagement sont principalement basés sur variations des fréquences propres, amortissements et déformées. Quelqu'une affinent sur la méthode des éléments finis pour identifier les défauts par recalage des paramètres dynamiques.

Le changement des fréquences propres (variation locale de raideur) est le paramètre le plus utilisé dans la littérature pour l'identification des défauts dédiée à l'endommagement dans les matériaux composites. Mais on peut noter que la mesure seule de la fréquence propre ne peut pas fournir suffisamment d'informations sur la détection d'endommagements structurels. En outre, la fréquence propre n'est souvent pas assez sensible des défauts initiaux. Cette méthode ne peut ainsi que vérifier l'existence de grands défauts, mais n'est pas capable d'indiquer la position de l'endommagement (Un endommagement structurel aux deux endroits différents peut provoquer le même changement en fréquence).

Dans des structures composites, il y a une tendance à utiliser l'amortissement comme un outil d'indication d'endommagement, car il est en général plus sensible aux dommages que les variations de fréquence, surtout quand le défaut est le délaminage. Une partie de notre travail dans cette thèse est de justifier cette tendance. L'introduction d'un défaut cause une augmentation d'amortissement (par frottement), qui est liée à la dissipation d'énergie lors que la structure est excitée. On peut d'ailleurs constater que un endommagement localisé dans

une structure correspond la perte de la rigidité d'une structure correspond à une diminution de la fréquence propre combinée avec une augmentation de l'amortissement.

Une autre façon d'établir une corrélation entre l'endommagement et le changement des paramètres dynamiques est d'utiliser la variation des déformées. Dans nos travaux, la surveillance d'endommagement est basée principalement sur les variations de fréquence propre et de l'amortissement. Par exemple, des changements dans la courbure des déformées permettent de repérer des endommagements. Cette information peut être utilisée pour obtenir la quantité d'endommagement dans la structure, car la déformée contient des informations locales, mais on est dépendant (plus on a de capteurs, plus l'estimation est précise)

Les simulations numériques par Eléments finis sont utilisées dans beaucoup de travaux. Certains travaux montrent que sur des structures simple (de type poutres et plaques) et aussi sur des structures complexes les Eléments finis sont utilisés pour prédire l'effet dynamique des types, tailles et emplacements des défauts (analyse paramétriques) en vue d'une diagnostique d'une structure inconnue. Ces prédictions sont validées expérimentalement et on peut noter que :

- les fréquences propres d'une structure endommagée diminuent à cause de la perte de rigidité en présence d'endommagement
- les modes propres et les déformées à hautes fréquences sont plus sensibles aux dommages que ceux aux basses fréquences

Une nouvelle approche a été développée au cours de cette thèse. Elle utilise l'optimisation topologique pour localiser des endommagements. Les entrées du processus d'optimisation sont les résonances (FRF). L'idée et de réduire progressivement la rigidité des éléments pour obtenir un défaut équivalent en terme de comportement dynamique. La méthode d'optimisation topologique décrite dans cette thèse est basée sur une nouvelle formulation des contraintes afin de localiser des endommagements sur les poutres composites avec une précision proche aux résultats ultrasons (C-Scan).

Le cœur de cette thèse repère sur la détection d'endommagement sur les composites stratifiés et sandwiches. Les sandwiches standards en l'âme nid d'abeille et mousse ont été testés pour

comparer avec un nouveau matériau sandwich en fibres de carbones orientées d'une manière aléatoire (enchevêtrés). Le but est de fabriquer/diagnostiquer le processus de ce nouveau matériau sandwich et d'étudier ces caractéristiques dynamique notamment l'amortissement et la résistance à l'impact par rapport aux sandwiches en nid d'abeille et mousse.

Chapitre 2 : Principes d'Analyse modale

Aujourd'hui, les ingénieurs sont confrontés aux complexes problèmes du bruit et des vibrations associés à la conception et au diagnostique des structures. En raison des contraintes de coût, durée de vie,..... les structures actuelles sont généralement plus complexes en termes de conception et de matériaux. Par conséquent, la conception doit prendre en compte les aspects dynamiques des structures ou vibrations.

Récemment, des outils ont été développés pour aider l'ingénieur dans ces domaines. L'analyste utilise désormais des logiciels d'éléments finis pour aider à la compréhension et la conception de structures. L'expérimentateur a à sa disposition des équipements sophistiqués d'analyse et de traitement vibratoire des signaux qui l'aide dans la compréhension du comportement dynamique d'une structure. La méthodologie consacrée pour étudier expérimentalement le comportement dynamique d'une structure est appelée analyse modale expérimentale (EMA).

Le but principal de ce chapitre est de montrer comment à partir des entrées (force) et sorties (accélération ou déplacement) on peut calculer les fonctions de réponse en fréquence (FRF) qui permettent à extraire sont liées aux modes propres et déformées d'une structure. Cet objectif général sera atteint par la construction d'une base mathématique aussi bien du point de vue expérimental et numérique. Ce chapitre est divisé en trois sections principales:

L'identification du système nous permet de caractériser un processus physique (structures). L'objectif de cette quantification est de donner des informations sur le système et de permettre de prédire son comportement quelque soit les excitations futurs. Ou identifier donc la structure comme un système linéaire et invariant dans le temps. La définition d'outils tel que la transformée de Fourier ou l'opération de convolution est expliquée et nous aide à caractériser le système par sa fonction de la réponse en fréquence $H(f)$.

On illustre par un exemple simple d'un système SDOF afin de fournir et pratiquer les aspects théoriques de l'analyse modale. L'extraction des fréquences propres et des amortissements modaux est introduit par la méthode d'indentification de FRF par une fonction rationnelle (en

p , variable de Laplace), les poles de cette fonction contiennent l'information modale (Figure 2.1).

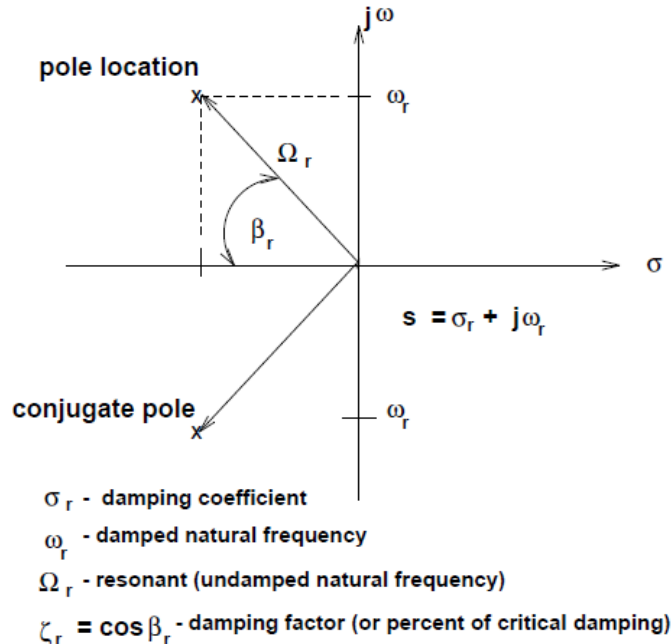


Figure 2.1 *s*-plane (le plan de Laplace), position de pôle

La troisième partie de ce chapitre traite de l'analyse modale expérimentale, outils de détermination des paramètres modaux (la fréquence propre, l'amortissement et la déformée). Tout d'abord, les deux principaux types d'essais modaux sont examinés, par exemple l'essai avec un marteau d'impact ou l'essai avec pot vibrant. Les essais de vibrations dans cette thèse sont basés sur des tests vibratoires avec un pot vibrant. Différents types de signaux d'excitation utilisés comme le bruit blanc et le sinus pas à pas. L'estimation de paramètres modaux par la méthode « Polyreference » est aussi expliquée et permet d'extraire les paramètres modaux. En général par la pratique le processus d'estimation nécessite trois étapes:

- Déterminer combien de modes k sont représentés dans les données spectrales
- Estimer un pôle $\lambda_i = \sigma_i + j\omega_i$ pour chaque mode, pour obtenir la pulsation propre amortie ω_i et le taux d'amortissement σ_i
- Estimer des résidus A_i pour chaque mode afin de calculer les déformées

En toute fin de chapitre, la variation des fréquences propres et des taux amortissements dans le plan de Laplace (s-plane) en fonction d'un endommagement est discutée pour mettre en relation la théorie mathématique avec l'objectif principal de cette thèse : l'identification de défauts. On peut constater que, avec une augmentation de l'endommagement dans un matériau, généralement, il y a une diminution de la fréquence propre (ω) suivie d'une augmentation de l'amortissement modal (σ).

Chapitre 3 : Surveillance d'endommagements dû à l'impact sur poutres composites stratifiées par variations des paramètres modaux

Ce chapitre explique la corrélation entre le changement des paramètres modaux et les niveaux de l'endommagement (dû à l'impact) dans les poutres composites stratifiés. Des rouleaux carbones-époxy pré-imprégnés de T300/914 sont utilisés pour fabriquer les échantillons de type poutre avec un drapage de $[(0/90/45/-45)_3]s$. Les essais vibratoires ont été effectués sur deux lots de six poutres composites stratifiés non endommagés et après chaque niveau d'endommagement (diagnostique est effectué à chaque étape).

Les poutres composites ont été impactées selon deux conditions limites c'est-à-dire, en encastrant deux côtés ou les quatre côtés (système de bridage), en prenant en compte à chaque fois la limite BVID. Le but n'est pas de faire une comparaison entre les variations des paramètres modaux pour les deux conditions limites de l'impact. Au départ, les moyens d'essais disponibles nous permettaient d'impacter seulement un encastrement sur deux côtés. Il a été constaté que les poutres ne sont pas bien bridées, et donc pour le prochain lot de poutres composites stratifiées, le système de fixation a été modifié de manière à nous permettre de faire les impacts en encastrant les quatre côtés. Toutefois, il a été observé que, si l'on impacte à la même énergie, les poutres impactées en encastrant tous les quatre côtés sont plus endommagées par rapport aux poutres impactées en encastrant seulement deux côtés. Les résultats pour les deux lots de poutres sont présentés afin d'obtenir une meilleure compréhension des variations de paramètres modaux en fonction du dommage à l'impact dans les poutres composites stratifiés.

De plus les masses sont placées aux extrémités des poutres afin d'augmenter l'effort tranchant et donc d'agrandir le spectre (différence entre les paramètres modaux) d'abord pour le cas sain et puis pour le cas endommagé. Les résultats d'essais vibratoires montrent que la différence dans les fréquences propres avant et après l'impact est plus grande pour la poutre avec des masses (Figure 3.1).

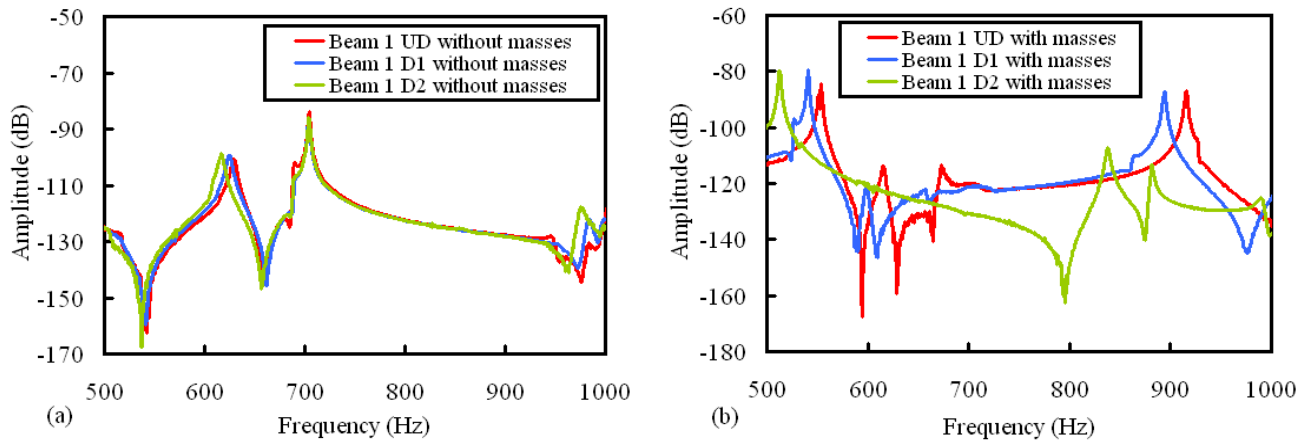


Figure 3.1 Comparaison des FRFs de la poutre 1 à point de mesure 5 pour les états UD (non endommagé), D1 (endommagé à 4 points d'impacts) and D2 (endommagé à 8 points d'impacts) pour (a) Poutre 1 sans masses aux extrémités (b) Poutre 1 avec masses aux extrémités

On observe que les défauts dans les spécimens provoquent une diminution de la fréquence propre qui est logique avec le niveau d'endommagement. De même le changement en fréquences est plus important en hautes fréquences. De plus les décalages des pôles dus à l'endommagement montrent que le changement du taux d'amortissement est plus important que le changement de fréquence. Dans le cas de la poutre impactée à 14 J, la variation moyenne de la fréquence propre (entre les cas sain et endommagé) pour les quatre premiers modes de flexion est de 8%, alors que dans le cas d'amortissement ce taux de variation moyen est de l'ordre de 78%. Il est donc raisonnable de supposer que l'amortissement peut être utilisé en lien et place de la fréquence propre comme un indicateur d'endommagement pour la surveillance des structures. On se pose dès lors la question cruciale de la fiabilité d'estimation de l'amortissement, paramètre relativement difficile à estimer, par rapport à la fréquence propre.

Les changements des paramètres modaux en fonction des endommagements peuvent être expliqués à l'aide d'un indice d'endommagement (Damage Index). La première étape consiste à calculer l'intégrale (I_X) de l'amplitude des fonctions de réponse en fréquence (FRF) sur une plage de fréquences définies. Pour notre travail, un intervalle de fréquence de ± 20 Hz est choisi pour le calcul de l'intégrale des pics de résonance de la FRF. Les résultats montrent clairement une augmentation de l'indice d'endommagement avec l'augmentation de niveau d'énergie d'impact qui correspond à l'accumulation d'endommagement dans les poutres composites (Figure 3.2). Comme le taux d'amortissement et l'indice d'endommagement (basé

sur l'intégrale I_x) expliquent le même phénomène, alors l'introduction de l'indice d'endommagement (DI) permet de vérifier les résultats d'amortissement estimés par Polymax. Donc, en utilisant DI, un outil supplémentaire est introduit à la compréhension du comportement de l'amortissement dans les poutres composites endommagées.

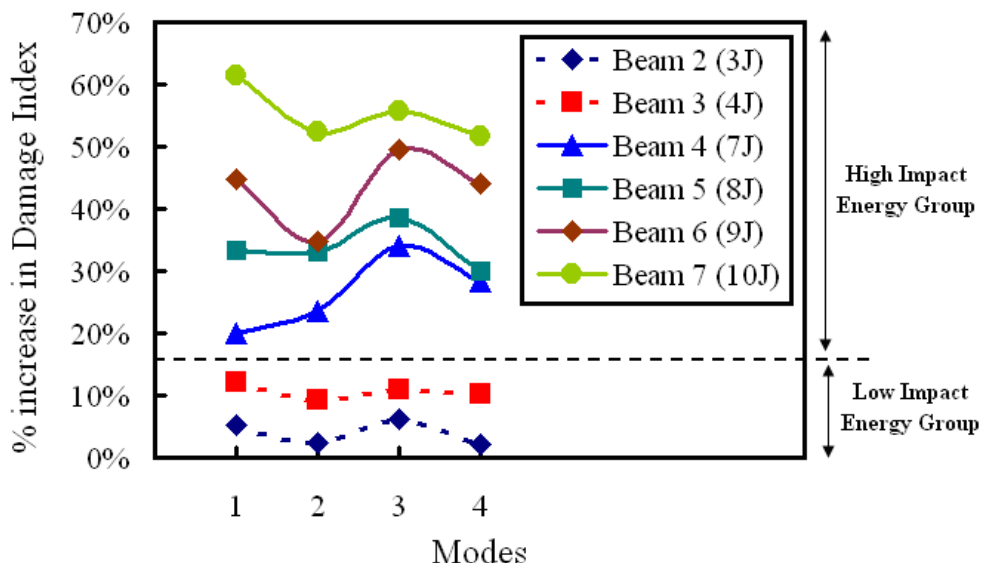


Figure 3.2 Variation de l'indice d'endommagement avec l'augmentation de niveau d'énergie d'impact en fonctions des modes pour des six poutres composites

Pour certains points de mesure, l'endommagement dans les poutres composites déforme les pics de résonance et, parfois, il y a une apparition de doubles pics au lieu d'un seul dans les fonctions de réponse en fréquence (Figure 3.3).

Une meilleure qualité de résultats d'essais vibratoires est obtenue par collage d'autocollants réfléchissants sur les points de mesure. L'énergie d'impact est soulignée comme le facteur ayant l'effet le plus significatif sur les paramètres modaux en effectuant des études statistiques (plan d'expérience) sur des données expérimentales.

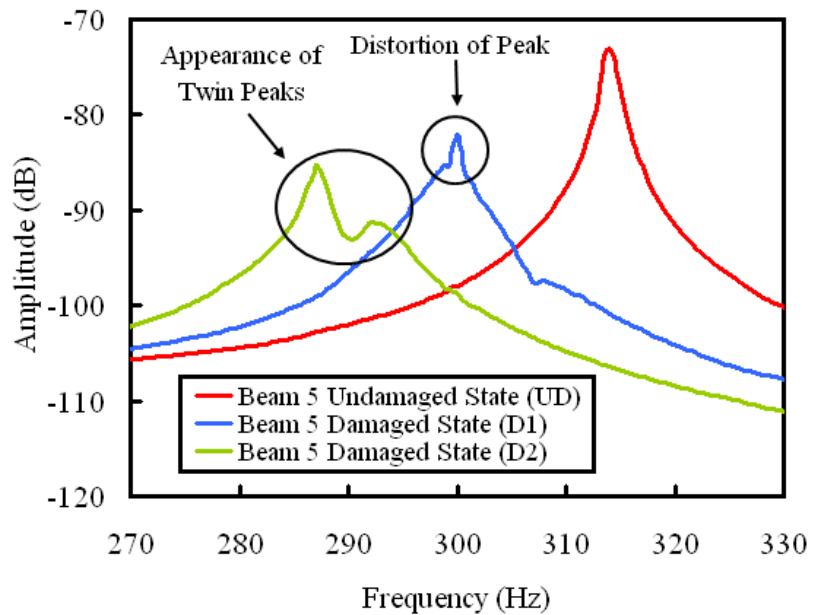


Figure 3.3 Comparaison des formes des FRFs de la poutre 5 à point de mesure 2 pour les états UD (non endommagé), D1 (endommagé à 4 points d'impacts) et D2 (endommagé à 8 points d'impacts)

Chapitre 4 : Influence du type d'endommagement sur poutres sandwiches en nid d'abeille par diagnostic vibratoire

Dans ce chapitre, la surveillance d'endommagement a été effectuée sur les différents types de poutres sandwiches en nid d'abeille avec l'aide de changements des paramètres modaux toujours de manière expérimentale.

Dans la première partie de chapitre, les essais de vibrations ont été effectués sur des poutres sandwiches longues en nid d'abeille, dans les états sains et endommagées, en utilisant les excitations bruit blanc et sinus pas à pas. Ils ont permis de déterminer quelle méthode d'essai donne une estimation plus « logique » de l'amortissement au regard de la théorie dans la présence d'endommagement. Les essais vibratoires sont effectués en plaçant des masses d'acier aux deux extrémités, sur les poutres sandwiches en nid d'abeille afin d'augmenter le décalage dans les paramètres modaux entre les cas sain et endommagé. Les six poutres sandwiches longues en nid d'abeille testées dans ce chapitre sont endommagées de deux manières différentes. Les quatre premières poutres sont endommagées par des impacts à basses vitesses autour de la limite BVID (Barely Visible Impact Damage). Les deux autres poutres sont endommagées par un trou, percé dans la largeur de l'âme en nid d'abeille avec une perceuse (endommagement uniquement dans l'âme, Figure 4.1).

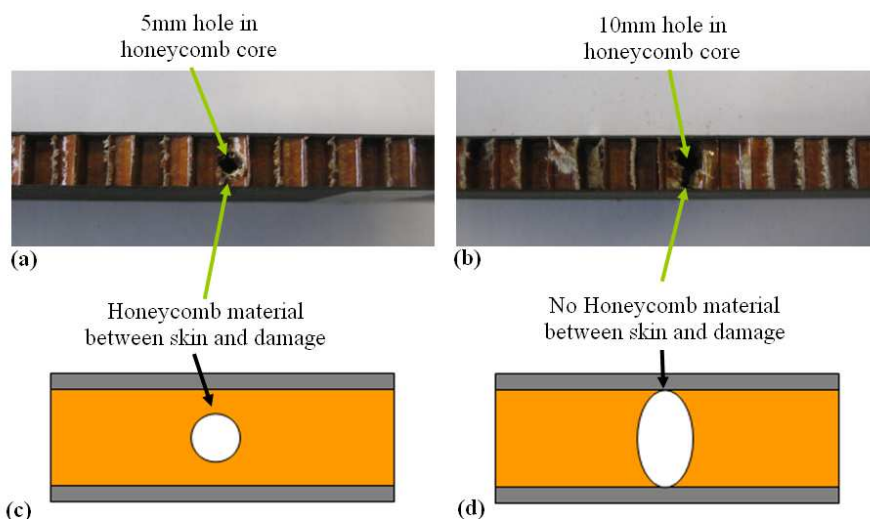


Figure 4.1 Vue transversale poutres sont endommagées par un trou, percé dans la largeur de l'âme en nid d'abeille avec une perceuse

Les résultats montrent qu'avec l'accumulation d'endommagement dans les échantillons, il y a une diminution de la fréquence propre accompagnée d'une augmentation du taux d'amortissement.

Les effets d'endommagement sur les paramètres modaux uniquement dans l'âme semblent faibles, par rapport aux endommagements dus aux impacts. En outre, l'amortissement semble plus sensible à l'endommagement que la fréquence propre. Il est donc raisonnable de supposer que l'amortissement peut être utilisé comme un indicateur d'endommagement pour la surveillance des structures car elle est beaucoup plus sensible à la présence d'un défaut.

La présence de non linéarité dans les poutres sandwiches en nid d'abeille est démontrée par des essais en sinus pas à pas, dans les sens croissants et décroissants. Il est constaté qu'en la présence de non linéarité, il y a toujours un changement dans l'amplitude accompagné par un léger décalage dans les fréquences propres de FRF (Figure 4.2).

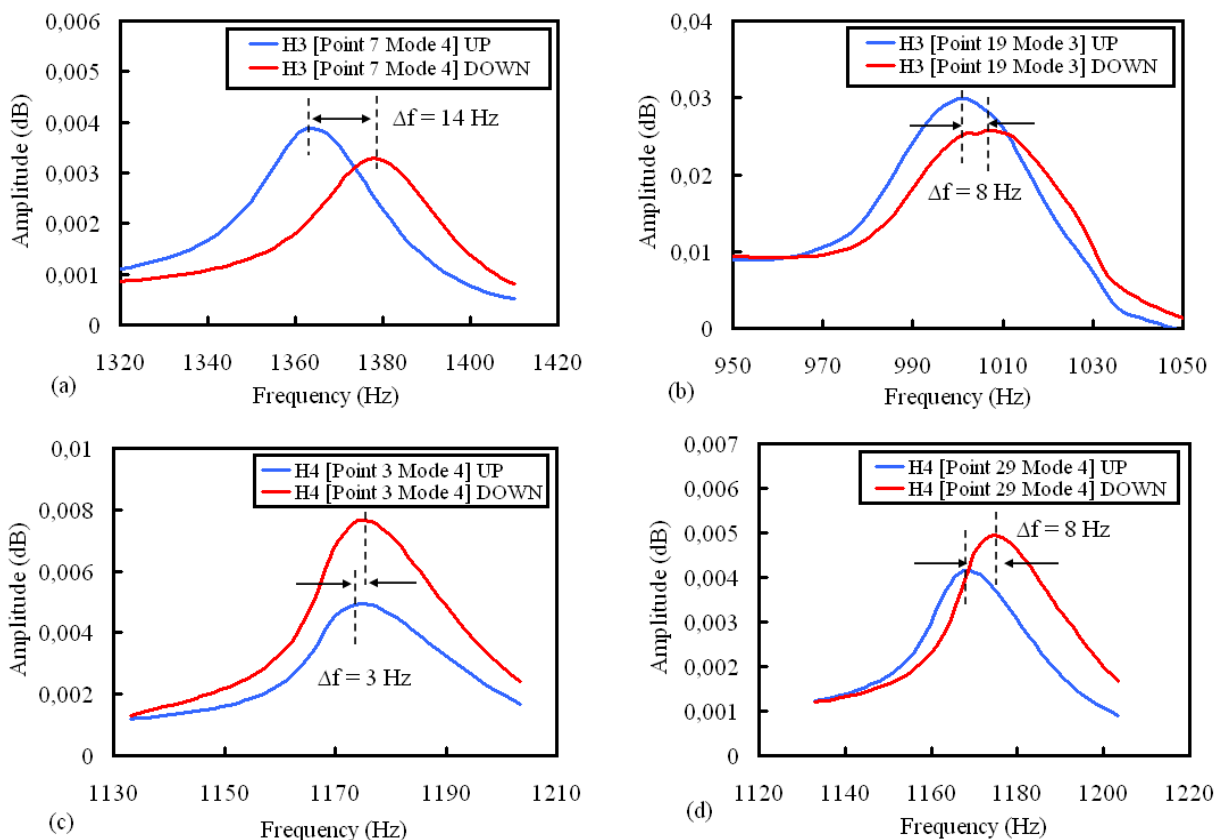


Figure 4.2 FRFs des essais en sinus pas à pas, dans les sens croissants et décroissants dans les poutres sandwiches en nid d'abeille

Le plan d'expériences effectuées sur les paramètres modaux déterminés expérimentalement souligne que la densité d'endommagement est le facteur ayant l'effet le plus significatif sur les paramètres modaux. Il montre que l'essai modal basé sur l'excitation sinus pas à pas, donne une estimation relativement plus fiable de l'amortissement en présence d'endommagement par rapport aux essais en bruit blanc.

Chapitre 5 : Caractérisation statique-dynamique et surveillance d'endommagement dû à l'impact sur poutres sandwiches en fibres enchevêtrées

Dans ce chapitre, nous parlons de la fabrication et des essais mécaniques d'un matériau amortissant : sandwich avec âme en fibres de carbone enchevêtrées. Les sandwiches en fibres enchevêtrées possédant des caractéristiques d'amortissement élevées peuvent être utilisés pour des applications spécifiques comme dans les panneaux intérieurs de la cabine d'un hélicoptère (leur rigidité structurale étant faible). La résistance à l'impact de ces matériaux est aussi étudiée. Deux types de poutres sandwiches longues en fibres enchevêtrées (lourdes et légères) sont testés. Les spécimens légers ont 2,5 fois moins de résine par rapport aux spécimens lourds (Figure 5.1).

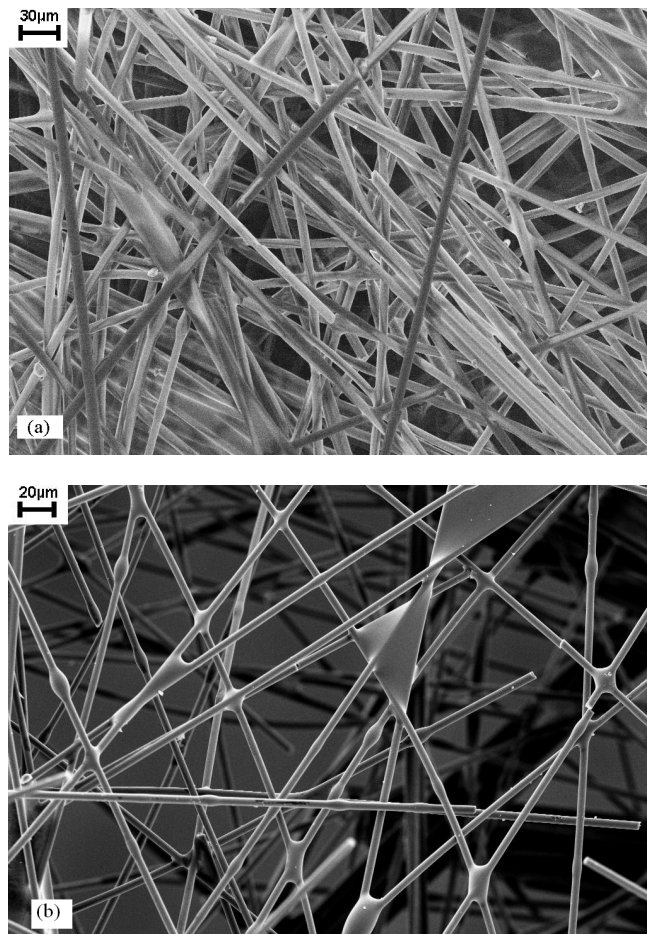


Figure 5.1 Observations sous microscope SEM (a) spécimens lourds (b) spécimens légers

Les énergies d'impacts sont choisies de telle manière que les deux types des spécimens aient le même niveau d'endommagement. Les résultats montrent qu'avec l'accumulation de l'endommagement dans les échantillons, il y a une diminution de la fréquence propre accompagnée par une augmentation du taux d'amortissement pour quatre premiers modes de flexion. Les résultats d'essais vibratoires montrent que les spécimens légers ont de meilleures caractéristiques d'amortissement, et qu'ils possèdent une meilleure résistance à l'impact que les spécimens lourds. Par conséquent, avant de choisir l'application de ces matériaux sandwiches légers, leur sensibilité à l'impact doit être prise en considération. Dans les spécimens lourds, l'endommagement semble être plus localisé par rapport aux spécimens légers. On a aussi démontré expérimentalement que l'amortissement est plus sensible aux endommagements que la variation de la fréquence. L'inconvénient majeur de cette étude est qu'aucune comparaison n'est fournie avec des matériaux sandwiches standards.

Dans la deuxième partie de ce chapitre, des poutres sandwiches en fibres enchevêtrées courtes de carbone et de verre sont fabriquées et testées (Figure 5.2). L'avantage de ces poutres en fibres enchevêtrées courtes sur les poutres longues est une meilleure distribution des fibres et de la résine est obtenue lorsque les poutres sont plus courtes c'est-à-dire que le procès de fabrication actuel est mieux adapté à une taille de spécimen plus faible.

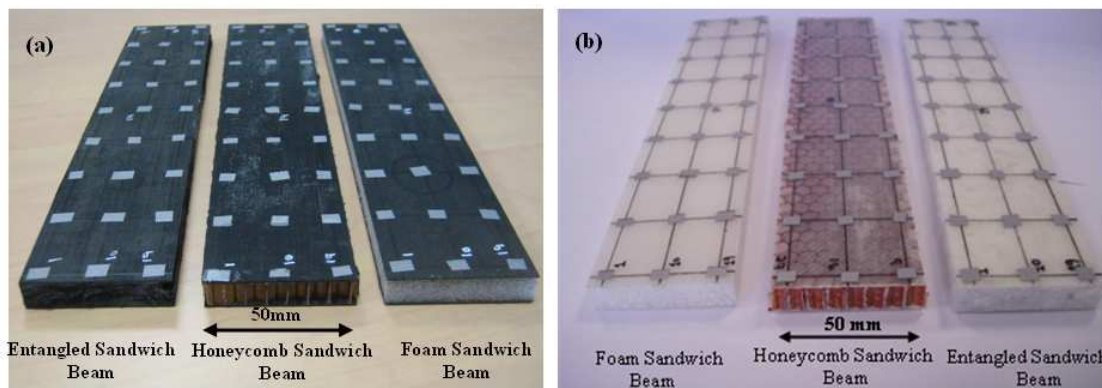


Figure 5.2 Les six poutres sandwiches (a) en carbone et (b) en verre

Comme précédemment, le but est d'évaluer les capacités amortissant et de résistance à l'impact des poutres enchevêtrées sandwich, mais cette fois, avec une comparaison avec des sandwiches standards l'âme en nid d'abeille et mousse. Les essais vibratoires montrent que les spécimens sandwiches en fibres enchevêtrées possèdent en moyenne un taux d'amortissement 150 % plus élevé, et des niveaux vibratoires 20 dB plus faible par rapport

aux sandwiches standards. Afin d'évaluer la résistance à l'impact, un cas simple d'impacts symétriques effectués en dessous de la limite BVID est étudié, afin de détecter ces dommages par les essais de vibration. Les essais de vibrations ont été effectués sur ces poutres sandwiches en fibres enchevêtrées en utilisant les excitations bruit blanc et sinus pas à pas. On compare aussi la méthode d'essai, en comparant les estimations en termes de logique avec la théorie. Les résultats montrent que les deux poutres sandwiches en fibres enchevêtrées courtes de carbone et de verre ont une meilleure résistance à l'impact par rapport aux sandwiches standards de mêmes dimensions (Figure 5.3).

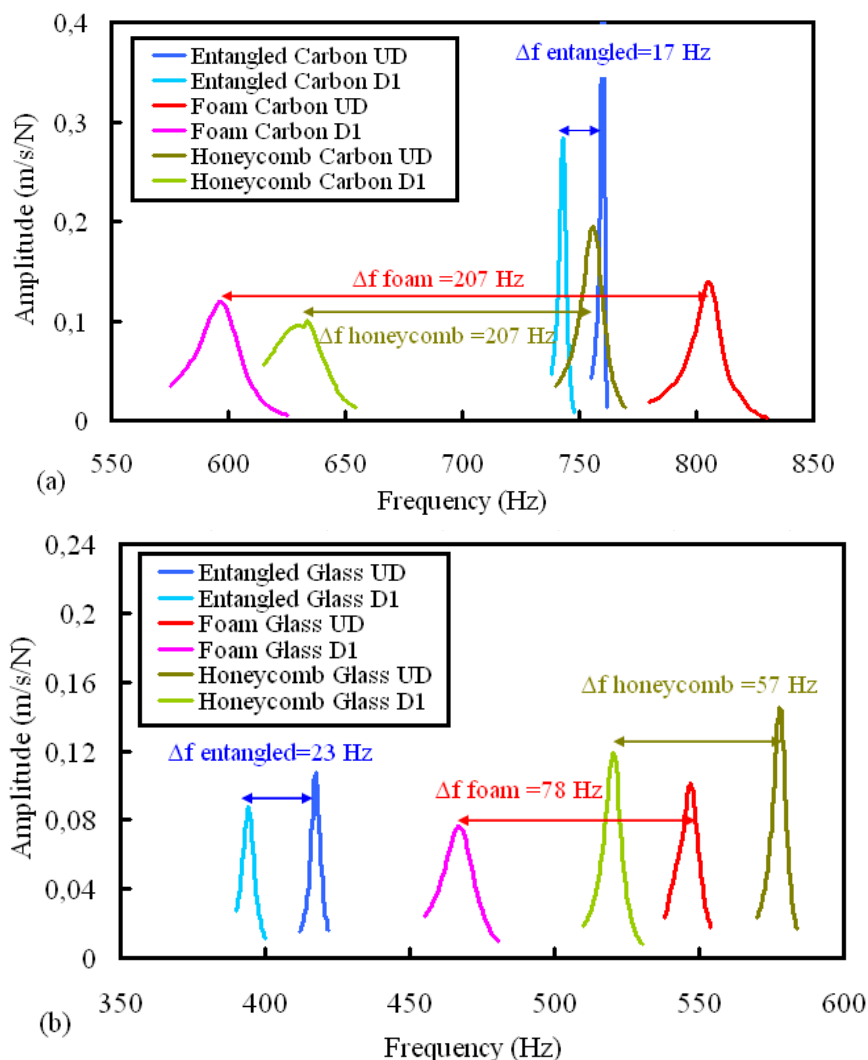


Figure 5.3 Comparaison des FRFs estimée par sinus pas à pas pour les états UD (non endommagé) et D1 (endommagé à 2 points d'impacts) pour le premier mode de flexion pour (a) le point de mesure 11 pour les trois poutres sandwiches en fibres de carbone (b) le point de mesure 21 pour les trois poutres sandwiches en fibres de verre

De plus, dans ces spécimens on trouve la même tendance à savoir que le taux d'amortissement est un paramètre plus sensible pour la détection des dommages que la fréquence propre. Un plan d'expériences montre de manière satisfaisante que le meilleur indicateur est le taux d'amortissement.

Chapitre 6 : Recalage de modèle Eléments Finis pour la détection, localisation et quantification des défauts

La partie numérique de cette thèse se compose de deux sous chapitres. La première partie est la mise au point des modèles éléments finis (SAMCEF) pour calculer les paramètres modaux et la réponse dynamique des composites stratifiés et les composites sandwiches en nid d'abeille. Le but est de comparer les résultats numériques (FRFs) avec ceux obtenus expérimentalement (chapitres 3 et 4) sur les mêmes poutres. Ensuite, les modèles éléments finis sont recalés par une analyse paramétrique afin d'améliorer la corrélation expérimental/numérique. La méthodologie utilisée pour modéliser l'endommagement dans l'échantillon d'essai est simple. Au lieu de modéliser l'endommagement tel qu'il est en réalité, les propriétés des matériaux des éléments dans la zone endommagée sont modifiées localement.

La taille de la zone circulaire de dommage est estimée basée sur les résultats d'ultrason (C-Scan), on fait varier le module d'élasticité longitudinal (E_L) dans les zones circulaires d'endommagement (pour les poutres composite stratifié). Parce que les essais numériques soulignent le fait que (E_L) est la propriété matériau ayant les effets les plus significatifs sur les fréquences propres (Figure 6.1).

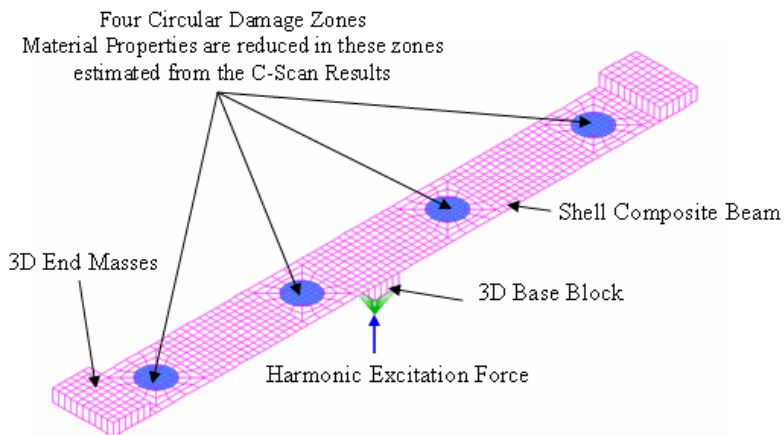


Figure 6.2 Méthodologie de modélisation d'endommagement en SAMCEF- modèle éléments finis des poutres en composites stratifiés avec de masses à l'extrémités ainsi que les zones endommagés et le chargement à la centre

Pour le processus de recalage, le modèle éléments finis correspondant au cas sain (non endommagé) est établi en essayant différentes valeurs du coefficient α_{UD} (par une étude paramétrique en BOSS Quattro), jusqu'à ce que la plus petite erreur statistique soit atteinte entre les résultats expérimentaux et numériques pour les fréquences propres, basées sur l'équation suivante :

$$E_{freq,UD}(\alpha_{UD}) = \sqrt{\frac{1}{N} \sum_{i=1}^N [f_{FEM,UD}^k(\alpha_{UD}) - f_{EXP,UD}^k]^2}$$

La même procédure est suivie pour les cas endommagés (D1 et D2). L'erreur statistique $E_{freq,D1}(\alpha_{D1})$ pour le cas endommagé (D1) est calculée pour chaque itération de (α_{D1}) , et est comparée avec l'erreur correspondant au cas sain (UD). Le but est de trouver $E_{freq,D1}(\alpha_{D1})$ aussi près que $E_{freq,UD}(\alpha_{UD})$. La même procédure est suivie pour le recalage des amplitudes de FRF.

En suivant cette procédure du recalage, la réponse dynamique des poutres composites stratifiés a été modélisée, et une bonne corrélation expérimental / numérique est obtenue (Figure 6.2).

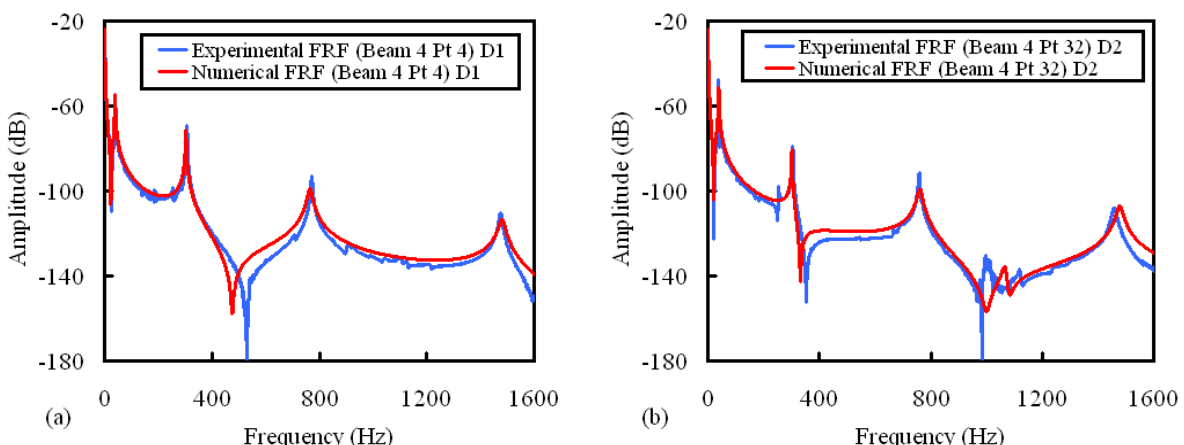


Figure 6.2 Comparaison des FRFs expérimentaux et numériques de la poutre 4 pour les états D1 (endommagé à 4 points d'impacts) et D2 (endommagé à 8 points d'impacts)

Pourtant, il faut mettre en évidence que notre méthode s'applique lorsque l'endommagement reste faible c'est-à-dire, autour de la limite BVID où le comportement de la structure reste plus ou moins linéaire. Une fois que le niveau d'endommagement devient plus important que la

limite BVID, cette approche ne fonctionne plus aussi bien. Afin de modéliser avec précision les endommagements plus importants dans notre modèle de composites stratifiés, il faut choisir une modélisation de l'endommagement plus avancée, et les calculs éléments finis devraient être menés par les modules non-linéaires.

Pour les cas des poutres sandwiches en nid d'abeille, la même procédure est suivie pour la modélisation et le recalage. Généralement, la corrélation expérimentale/numérique donne des meilleurs résultats pour les poutres composites stratifiés, parce que la surface endommagée a été modélisée à partir des résultats précis de C-Scan. En effet, pour les poutres sandwiches en nid d'abeille, en raison de l'indisponibilité de résultats, la surface endommagée a été estimée par *tapping*. De plus on a trouvé que le module du cisaillement (G_{XZ}), qui semble avoir l'effet le plus significatif sur le recalage des paramètres modaux (changements locale de G_{XZ} sur les zones détectées).

Les résultats sur les trois poutres en sandwiches en nid d'abeille (H2, H3 et H4) montrent une bonne corrélation pour le cas sain (UD), mais aussi dans une certaine mesure pour le cas endommagé (D1). Pour le cas avec plus d'endommagement (D2) en revanche les résultats sont insatisfaisants parce qu'à cause de la nature du nid d'abeilles (impact au milieu de la cellule ou sur le coin), la densité d'endommagement varie beaucoup (Figure 6.3).

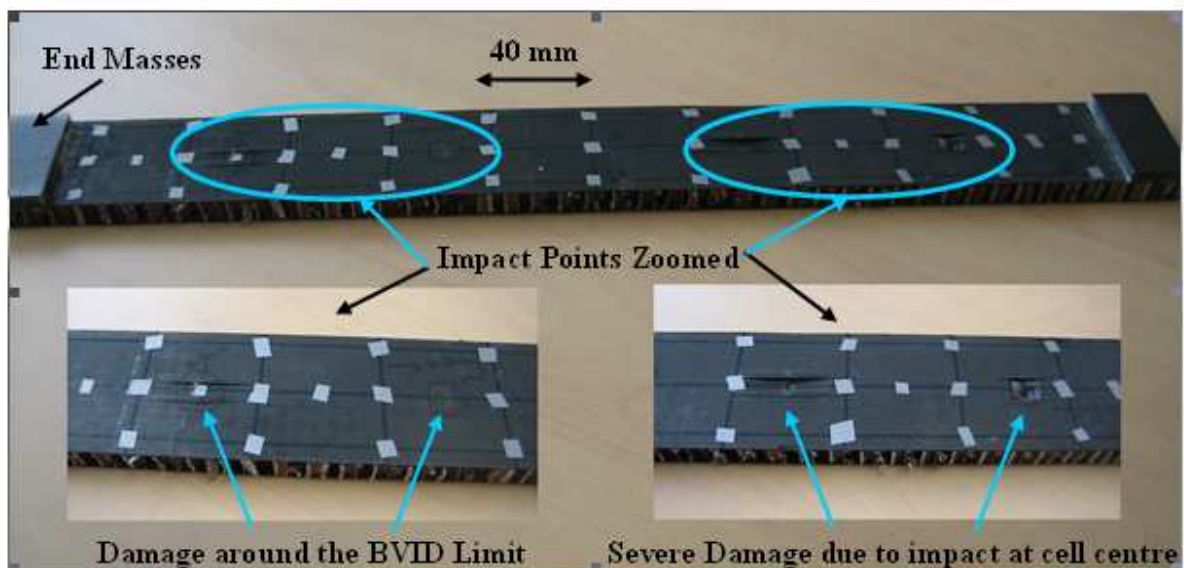


Figure 6.3 Variation la densité d'endommagement à cause de la nature du nid d'abeilles (impact au milieu de la cellule ou sur le coin) pour la poutre sandwich H4 impacté à 8J

Dans le futur, les points d'impact seront modélisés de telle façon que les propriétés du matériau peuvent être modifiées séparément à chaque point d'impact. Les poutres sandwiches en nid d'abeille seront coupées près de la zone endommagée, et seront observées par un microscope électronique précis. L'objectif sera d'obtenir des informations concernant la forme et la surface d'endommagement.

La deuxième partie du travail numérique concerne la localisation d'endommagement et sa validation sur les poutres composites stratifiées par l'optimisation topologique dans Nastran, en utilisant les paramètres modaux obtenus expérimentalement (chapitre 3). La localisation d'endommagement étant résolue par un problème d'optimisation topologique. Les résultats sur les poutres composites stratifiés démontrent qu'en utilisant l'optimisation topologique, on peut trouver efficacement les zones endommagées pour le cas D1 (zones bien isolés) et pas pour le cas D2 (défaut globale). On enlève de la matière dans les zones précise pour minimiser l'erreur entre FRF expérimentaux et FRF numérique. On modélise aussi un défaut équivalent, c'est donc un outil global de diagnostic (pour tous matériaux) ne nécessite qu'un état non endommagé.

Chapitre 7 : Conclusion et perspectives

La surveillance de l'endommagement a été effectué sur des spécimens de type poutre :

- composites stratifiées
- sandwiches en nid d'abeille
- sandwiches en fibres enchevêtrées

Pour toutes les poutres d'essai, il a été observé que, avec l'accumulation de l'endommagement dans les spécimens, il y a une diminution de la fréquence propre de flexion accompagnée par une augmentation du taux d'amortissement.

Comme attendu par la théorie, les résultats montrent que le taux d'amortissement est un paramètre plus sensible pour la détection de l'endommagement que la fréquence propre.

Les deux masses d'acier aux extrémités des poutres augmentent le décalage dans les paramètres modaux pour les trois types de spécimens. Par contre, ce changement est plus important en cas de poutres composites stratifiées par rapport aux poutres sandwiches.

En cas des poutres composites stratifiées, l'énergie d'impact peut être soulignée comme le facteur ayant l'effet le plus significatif sur les paramètres modaux (en effectuant des études statistiques sur des données expérimentales). Par contre, dans le cas des poutres sandwiches, le plan d'expérience montre que la densité d'endommagement est le facteur le plus significatif.

Un aspect nouveau et important de cette thèse concerne la fabrication et les essais mécaniques d'un matériau sandwich avec âme en fibre de carbone enchevêtrés. Les sandwiches en fibres enchevêtrées possédant des caractéristiques d'amortissement élevées et une meilleure résistance à l'impact peuvent être utilisés pour des applications spécifiques comme dans les panneaux intérieurs de la cabine d'un hélicoptère, étant donné leur faible résistance structurale. Mais il faut rappeler aussi que les poutres sandwiches en fibres enchevêtrées sont presque deux fois plus lourdes que les sandwiches standards avec le nid d'abeille et la mousse de mêmes dimensions.

La modélisation par éléments finis est utilisée pour calculer les paramètres modaux et la réponse dynamique des poutres composites stratifiées et des poutres sandwiches. Ensuite, les modèles éléments finis sont recalés afin d'améliorer la corrélation expérimental/numérique.

La méthodologie utilisée pour modéliser l'endommagement dans l'échantillon d'essai est simple. Au lieu de modéliser le dommage tel qu'il est en réalité, les propriétés des matériaux des éléments dans la zone endommagée sont modifiées. La taille de la zone circulaire de dommage est basée sur les résultats d'ultrason (C-Scan). On fait varier le module d'élasticité longitudinal (E_L) dans les zones circulaires d'endommagement pour les poutres en composites stratifiés, et le module du cisaillement (G_{XZ}) pour les poutres sandwiches en nid d'abeille.

En suivant cette procédure de recalage, la réponse dynamique des poutres composites stratifiées a été modélisée, et une bonne corrélation expérimentale / numérique est obtenue pour l'état sain et les deux états endommagés. Par contre, pour les poutres sandwichs en nid d'abeille, en raison de l'indisponibilité des résultats d'ultrasons (C-scan), les résultats de la corrélation sont moins bons par rapport aux poutres stratifiées (zones d'endommagement moins précis).

De même, la modélisation par éléments finis de la réponse dynamique des poutres sandwiches en fibres enchevêtrées a également été effectuée. La corrélation expérimentale / numérique est moins bonne à cause de plusieurs pics dans les fonctions de réponse en fréquence (FRF) obtenues expérimentalement. La distribution non-homogène de la résine n'est pas prise en compte dans le modèle.

La deuxième partie du travail numérique concerne la localisation de l'endommagement et sa validation sur les poutres composites stratifiées par l'optimisation topologique dans Nastran, en utilisant les paramètres modaux obtenus expérimentalement ou en modèle sain. Pour des défauts isolés (cas D1), on estime avec succès les zones d'endommagement.

Dans cette thèse, le cas simple des impacts symétrique a été choisi pour toutes les poutres d'essai afin d'avoir une densité homogène d'endommagement. Dans le futur, les impacts asymétriques seront effectués sur des poutres composites stratifiés afin, d'étudier leur effet sur les paramètres modaux. Jusqu'à présent, dans cette thèse, on a toujours gardé 1N comme niveau d'excitation pour les essais de vibration. Donc dans les prochains essais, on fera varier

le niveau d'excitation afin de vérifier si la linéarité des paramètres modaux est effectuée. Dans l'avenir, le processus de fabrication des poutres sandwiches en fibres enchevêtrées sera modifié pour améliorer la qualité et la performance de ces nouveaux sandwiches.

Enfin l'approche détection/localisation par l'optimisation topologique sera validée pour toutes les autres poutres d'essai présenté dans cette thèse. La bande passante sera aussi augmentée afin de prendre en compte l'influence des modes plus élevés, qui sont considérés plus sensibles à l'endommagement.

Surveillance vibratoire de l'endommagement dû à l'impact sur poutres en matériaux composites stratifiés, sandwiches et matériaux enchevêtrés par variations des paramètres modaux

La Surveillance de la Santé des Structures (SSS) s'effectue par la mesure de réponses pertinentes sous sollicitations extérieures. L'identification a pour but de détecter, de localiser et de quantifier ces défauts. La thèse porte sur les deux premiers niveaux de SSS, la détection et la localisation de dommage. Le but est d'étudier les effets d'impacts symétriques par variations des paramètres modaux en faisant un nombre important d'expériences. Une validation par recalage de modèles éléments finis est effectuée sur différents matériaux composites dédiés à l'aéronautique. Pour tous les spécimens (poutres), il a été observé que, avec l'accumulation de l'endommagement (impact), il y a une diminution de la fréquence propre (flexion) accompagnée par une augmentation du taux d'amortissement. Un aspect nouveau de cette thèse concerne la fabrication et les essais mécaniques (statique et dynamique) d'un matériau innovant (sandwich avec âme en fibre de carbones enchevêtrés) possédant des taux d'amortissements élevés ainsi qu'une meilleure résistance à l'impact. La modélisation par éléments finis (Samcef) est utilisée pour calculer la réponse dynamique de ces poutres. Ces modèles recalés permettent de donner un indicateur de taux de dégradation et peuvent servir d'outils diagnostic (et d'alarme) pour la surveillance de l'intégrité des structures. Une partie innovante de cette thèse concerne la localisation de l'endommagement et sa validation sur les poutres composites stratifiées par optimisation topologique (Nastran), en utilisant les paramètres modaux obtenus expérimentalement. Ainsi on estime avec succès les zones d'endommagement pour des défauts isolés.

Mots clés : Structures composites, Vibrations, Surveillance de la santé des structures, Endommagement dû à l'impact

Monitoring of impact damage in composite laminate, honeycomb sandwich and entangled sandwich beams by modal parameter shifts

Impact damage in composite structures may lead to severe degradation of the mechanical behavior due to the loss of structural integrity. Therefore Structural Health Monitoring (SHM) based on vibration testing is useful in detecting this damage caused by impact because damage generally affects the vibration characteristics of a structure. The scope of this thesis concerns the first two steps of SHM i.e., detection and localization of damage. The vibration test results on pristine and damaged composite laminate and composite sandwich beams show that with the accumulation of damage there is a decrease in natural frequency and an increase in the damping ratio. Results show that damping ratio is a more sensitive parameter for damage detection than the natural frequency. An important and novel aspect of this thesis concerns the fabrication and mechanical testing of a new sandwich material with carbon fiber entangled core. Entangled sandwich materials possess high damping characteristics and better impact toughness as compared to standard sandwiches with honeycomb and foam cores and can be used for specific applications like the inner panelling of a helicopter cabin as their structural strength is considerably low. Simplified Finite element models are developed that represent damaged composite beams in vibrations. These simplified damage models give us a degradation factor that can serve as a warning regarding structure safety. The localization of damage is carried out by topology optimization. Results on composite laminate beams showed that with topology optimization the right damage locations have been found rather efficiently at lower damage levels.

Keywords : Composite structures, Vibrations, Structural health monitoring, Impact damage